Straining of Small Particles in Porous Media

by

Elena Rodríguez, B.S.

Thesis

Presented to the Faculty of the Graduate School of

The University of Texas at Austin

in Partial Fulfillment

of the Requirements

for the Degree of

Master of Science in Engineering

The University of Texas at Austin

December 2006

Straining of Small Particles in Porous Media

Approved by
Supervising Committee:

Steven L. Bryant

Mukul M. Sharma

Acknowledgements

I would like to thank my supervisor Dr. Steven L. Bryant for his support, patience and encouragement throughout this research. I am grateful to Dr. Sharma for being in my supervising committee and provide useful comments in my thesis. Thanks to Professor J.L. Finney for access to the coordinates of his famous packing of spheres.

Special thanks to my colleagues Cynthia Thane and Siyavash Motealleh who also provided me useful data for this thesis.

I express my gratitude to the faculty and staff of the Petroleum and Geosystems Engineering Department. And last, but not least, I would like to thank my friends and fellow graduate students at The University of Texas who made my time at Austin even more enjoyable.

This thesis would have not been possible without the support of the U.S. Department of Agriculture.

December 8th, 2006

Abstract

Straining of Small Particles in Porous Media

Elena Rodríguez, M.S.E.

The University of Texas at Austin, 2006

Supervisor: Steven L. Bryant

Modeling the retention of colloidal particles in soils is important to understanding water contamination from viruses, bacteria or contaminants adsorbed on colloids. Particles transported by fluid remain in the soil when they arrive at constrictions in the pore space too small to admit them. This phenomenon, called "straining", depends on the size and shape of constrictions in pore space. An analogy can be made between the retention of colloidal particles in soils and the trapping of fine particles within reservoir formations. Fine particles of clay or quartz are naturally present in the porous media. They may also enter the reservoir from external sources, like completion fluids. Once in the reservoir, fine particles can be mobilized by a chemical composition of the water in contact with the formation or simply by the shear forces during production. In their movement through the reservoir, fines can get trapped at small pore constrictions,

reducing flow through the porous medium and causing a decline in reservoir productivity. The terms *colloid* and *fine particle* are interchangeable in this thesis.

While theories of straining predict that dilute concentrations of particles smaller than the smallest nominal pore throats should migrate without being strained, experiments show that such particles are nevertheless retained in the porous medium. This thesis tests the hypothesis that particles are strained not just in throats between three grains, but also in gaps between pairs of grains. To test that hypothesis the number, width and distribution of such gaps has been quantified in model soils. The Finney packing (a widely used model for ideal soils) and ten new computer generated packings have been used for this purpose. All of them are dense random packings of mono-disperse spheres. The characterization of gaps in these ideal soils has confirmed that their occurrence in the packings is large enough to trap a considerable number of particles. The statistics of gap widths and point contacts in the Finney packing are comparable to the statistics from the computer generated packings, making the latter packings acceptable models of ideal soils. A range of gap widths of interest has been defined according to the size of the particles that show non-classical straining behavior in experiments. This range includes gap widths between 0.03 and 0.1 times the radius of the soil grains.

The flow velocity through the gap, necessary to evaluate theories of particle straining, has been estimated assuming that the gap is a slit of width equal to the gap width. The range of capture specific to each gap width and particle size has been calculated in order to compute the volumetric flow appropriate to the particle being strained. This range of capture indicates the distance from the minimum constriction at which a particle approaching the gap can be strained. The calculated volumetric flows in gaps were between two and three orders of magnitude smaller than the flows in adjacent pore throats, obtained from a steady-state single–phase flow calculation.

The distribution of gap widths and the volumetric flow through gaps in the Finney pack have been combined into a flow-rate-weighted distribution of gap widths. This distribution has been used in the theory of particle straining developed by Sharma and Yortsos (1987, a, c) in order to predict the probability of particle trapping in gaps. The theoretical rate constant for straining has been determined for several particle sizes and its scaling with particle size has been evaluated. This result has been compared to an empirical correlation reported by Bradford (2002). There was no concordance between the scaling correlation calculated in this work using a flow-weighted distribution of gap widths and the one reported in the literature. The data suggest a much weaker dependence of the straining rate on the volumetric flow through gaps than postulated in the theory. Another evaluation of the theory was made, this time assuming that straining rate is independent of flow rate through the gap. In this case, the predicted scaling exponent was smaller than the experimental value. The two evaluations of the straining theory yielded two relationships for straining rate constant that bound the observations. These evaluations represent two limiting cases when studying the dependence of straining with particle size. This suggests that the gap geometry obtained here, combined with a more refined evaluation of flow in the vicinity of gaps, could account for the experimental observations.

Table of contents

List of Tables

Table of figures

Chapter 1: Overview

1.1 STATEMENT OF THE PROBLEM

Water quality is one of the most basic concerns confronting agriculture in the U.S. Nowadays, there is an increasing interest in the non-point sources of water contamination, i.e., rainfall, snowmelt, or irrigation that runs over land or through the ground, collects pollutants, and deposits them into rivers, lakes, and coastal waters or introduces them into ground water. Agricultural activities make up the majority of non-point sources. On the other hand, water quality is an important issue since agricultural practices usually need water as an input. In both cases, water quality is strongly influenced by the transport of colloidal particles through soils. The colloids themselves can be contaminants or, in other cases, contaminants can adsorb onto colloids and consequently get the same mobility as the colloids (see section 1.2). Being able to model the transport of colloidal particles is necessary for evaluating risk and for designing remediation.

Another face of the colloid transport problem is fines migration in oil reservoirs. Fines migration refers to the movement of fine particles of clay, quartz or similar materials within the reservoir formation due to drag forces during oil and gas production. This phenomenon often occurs in an unconsolidated formation, or when an incompatible completion fluid releases fine particles. The mobilized particles should be produced to prevent near-wellbore damage.

The terms *colloids* and *fines* are considered interchangeable in this thesis, although for brevity it will be referred simply to colloids.

The long term objective of this thesis is a quantitative, predictive basis for evaluating the retention of colloids in soils and fines in reservoirs by straining. Only single phase flow will be considered for this purpose. Straining is a conceptually simple mechanism that primarily depends on the grain scale geometry of constrictions in pore space; even so, the understanding of the phenomenon is still inadequate (see section 1.4). This project focuses on developing a more complete description of pore space geometry and incorporating it into a model of colloid transport in saturated media.

1.2 COLLOIDS

Colloids are particles with effective diameters between 0.01 and 10 microns. According to their composition, their nature can be organic, for example humic materials; inorganic, for example silicate clays and mineral precipitates; or biologic, like the case of microorganisms such as viruses and bacteria. All of these colloids exist in natural subsurface systems associated with geological matrices; hence, their occurrence in groundwater is expected. They can be released into soil and groundwater through a variety of processes such as dissolution of minerals and surface coatings (Ryan & Gschwend, 1990), precipitation from solution (Gschwend & Reynolds, 1987) and deflocculation of aggregates. On the other hand, organic and inorganic contaminants, like polycyclic aromatic hydrocarbons (PAHs) and heavy metals, can be attached to the colloids due to the high surface area of the latter. Therefore, colloids in groundwater can be contaminants themselves or act as a mobile solid phase that accelerates the transport of attached contaminants. Magee et al. (1991) showed that when colloids are present, contaminants could migrate farther than predicted by conventional transport models.

Concentration, composition, structure, and size of colloids will depend on a combination of physical, chemical, and biological factors. A typical value for the concentration of natural colloids in groundwater ranges from 10^8 to 10^{17} particles per liter (Kim, 1991).

Knowledge of the processes controlling colloid transport is essential in order to efficiently remediate environmental contaminants. For example, an accurate description of colloid transport is required to assess contamination potential and to safeguard sources of drinking water from pathogenic microorganisms (Bitton and Harvey, 1992). Other processes like the microbially enhanced oil recovery (MacLeod et al., 1988) also need a description of colloid transport.

1.3 FINES

Fines are small particles of clay, quartz or similar materials that are present in most naturally occurring porous media. The migration of fine particles includes their release from the porous media, their motion with the flow of permeate, and finally their capture at some pore sites or their passage out of the porous medium. Kaolinite and illite are the most common migrating clays.

Like colloids, fines generally have a size of the order 1 μm and a net surface charge. They may come from external sources or may originate within the porous medium itself. During the flow of a permeating liquid through a porous medium, a change in the chemical composition of the fluid or the shear forces applied by the moving fluid can mobilize fine particles attached to pore surfaces. The fines moving with the permeating fluid can get retained at other locations in the porous medium (pore constrictions, crevices, caverns and regular pore surfaces) eventually plugging the porous

medium and causing a reduction in permeability and therefore reducing well productivity. Fines can also exit the porous medium causing erosion, and thus increasing the porosity, which results in structural failure in the porous medium.

Formation damage in sandstone oil reservoirs is often caused by the dispersion of fine clay particles when the salinity of the interstitial water is reduced or the ionic composition is changed. This phenomenon is known as water sensitivity of sandstones and it can cause a strong reduction in permeability resulting in drastic decline in oil migration. This phenomenon depends on the cations present in the brine, the pH, and the rate of salinity change and can be observed in a core flood experiment with Berea sandstone, known as a water shock experiment (Khilar and Fogler, 1983). Thus any fluids which may encounter the producing formation (drilling fluid filtrate, completion fluids, stimulation fluids, etc.) should have a non damaging ionic composition. Commonly used criteria to prevent damage are for brines to contain at least 2 wt% of KCl or that at least one-tenth of the cations are divalent cations (Schechter, 1992).

1.4 FILTRATION AND STRAINING

There are two controlling mechanisms of colloid retention according to McCarthy and Zachara (1989): filtration and straining.

Filtration is a physicochemical mechanism controlled by electrostatic, chemical and van der Waals forces which lead to the attachment/detachment (sorption/desorption) of particles to the filter media. Classical filtration theories use irreversible first order kinetic attachment of colloids that predicts an exponential decrease in colloid concentration with distance in porous media. Logan et al. (1995) showed that:

$$\frac{C}{C_0} = \exp\left[-\frac{3}{2}\frac{(1-\theta)^{1/3}}{d_c}\alpha\eta L\right] \qquad \text{Eqn. 1.1}$$

where C and C_0 are the effluent and influent particle concentration respectively, θ is the packed bed porosity, d_c is the diameter of a spherical collector in the packed bed, α is a sticking coefficient (defined as the ratio of the particles that stick to collector to the particles that strike the collector) η is the collector collision efficiency and L is the length of the column.

Traditional theories also predict an optimum particle size for transport (Tobiason and O'Melia, 1988). Bigger particles would be removed by sedimentation and interception while smaller particles are predicted to be removed more efficiently by diffusive transport at the interface between pores and the flowing water.

Straining is a geometric mechanism. Particles are retained by straining when they arrive at constrictions in pore space too small to allow passage. When particles are much bigger than soil's pores, they are physically excluded from the medium and the process is called complete straining or mechanical filtration. This simple phenomenon of straining is still not well understood. For example, several studies by Elimelech et al. (1994) and Ryan and Elimelech (1996) regarding the transport of microorganisms have shown discrepancies with the unique value of the attachment coefficient predicted by classical filtration theories. The removal trends observed by Bradford et al. (2002) were not in agreement with the traditional first order attachment and detachment model. They found that, in packed column experiments, the majority of the colloid mass was deposited near the column inlet, and the spatial distribution was not exponential. The lack of consistency in these filtration studies may be because classical theories do not account for straining (Bradford, 2003).

1.5 PREVIOUS WORK IN STRAINING

Experiments reported in the literature have shown that surprisingly small particles can be strained. The behavior of these particles does not fit clearly into the filtration versus straining classification. Hall (1957) observed retention of particles 3 to 9 times smaller than pore throats in sand filters. Colloids between 0.3 to 3 microns were removed more efficiently than predicted from filtration theory in the clean-bed experiment of Yao et al. (1971). Gruesbeck (1982) reported retention of colloids three to six times smaller than estimated pore throat diameters in their sand pack. Baghdikian (1989) observed significant retention of particles an order of magnitude smaller than pore throats. Marlow et al. (1991) observed retention of colloids sixteen times smaller than pore throats. When throat size was reduced by a third by reducing grain size, the retention of the same size particles was almost complete. This sensitivity to grain size is much greater than theoretically expected for filtration. Bradford et al. (2002) observed strong dependence on retention on colloid size in a glass bead pack under conditions in which filtration would have been relatively insignificant, and then demonstrated similar behavior in sand packs. They showed that a consistent application of filtration theory could not account for their observations and concluded that straining must have contributed to retention, though the colloids were much smaller than the various theoretical thresholds. The experiments of Tufenkji et al. (2004), conducted under conditions in which physicochemical filtration is negligible, indicated straining as an important capture mechanism of bacteria. Foppen et al. (2005) demonstrated that straining in dead end pores dominates bacteria breakthrough in fine grained sediment (0.06-0.2 mm). Hence, these experiments show that particles too small to be strained according to classical theory, and too large to be filtered, are nevertheless retained.

Straining models correlate particle size (d) and grain size (D). Hall (1957) studied straining in the crevice between two spheres in point contact and estimated a constant for straining rate (k_{str}) based only in geometric considerations:

$$k_{str} \sim \left(\frac{d}{D}\right)^{3/2} \qquad \text{Eqn. 1.2}$$

Herzig et al. (1970) used a threshold of d/D > 0.15 for straining a single particle in a pore throat and d/D > 0.08 for straining four particles in the same throat. Matthess (1985) uses a semi-empirical relation between these two parameters.

Bradford et al. (2003) quantified straining by using an irreversible first order factor that depends on depth. Four different sized fluorescent colloids with negatively charged surface and columns of various sieve sizes of Ottawa sand were used in the experiments. The aqueous phase chemistry was chosen to create a stabilized suspension with the selected colloids. Two models were run assuming that colloid retention occurs by both attachment and straining, and another two assuming that retention occurs exclusively by attachment or straining, respectively. A dependence of straining on d/D very similar to the one from Hall was found after these experiments:

$$k_{str} = 269.7\left(\frac{d}{D}\right)^{1.42} \qquad \text{Eqn. 1.3}$$

Recently, Bradford et al. (2006) modified the previous equation by adding an inverse dependence in porosity (ε). This indicates greater straining at smaller porosity:

$$k_{str} = 3.32\left(\frac{d}{D}\right)^{1.23} \varepsilon^{-3.46} \qquad \text{Eqn.1.4}$$

Foppen et al. (2005) experiments indicated that straining in dead end pores (DEP) is an important process that dominates bacteria breakthrough in fine grained sediment (0.06-0.2 mm). They suggest a modification of equation 1.3 to account for pore water flow velocity (v), namely:

$$k_{DEP} = a\left(\frac{d}{D}\right)^{b} v \qquad \text{Eqn.1.5}$$

where k_{DEP} is the straining constant in the dead end pores and a and b are fitting parameters. The value of k_{DEP} calculated with equation 1.5 and Bradford's values for parameters a and b is twice the value of k_{DEP} observed in an experiment with fine sand.

Straining will likely depend on other factors not included in these correlations, such as the uniformity of the soil grain size, the colloid surface charge, the water content and also the experimental scale. Additional experimental studies are needed to asses the influence of these factors in straining.

1.6 GAPS AND PORE THROATS

It is important to clearly differentiate these two parts of the porous media. Pore throats are the small constrictions between triplets of *nearest neighbor* grains and they connect two larger pore volumes. A set of nearest neighbors, also known as a *grain ensemble*, can be defined for each grain in the soil. The centers of four grains define a circumsphere on whose surface the four points lie. Four grains are nearest neighbors, relative to all the other grains in the soil, if no center of any other grain lies inside this circumsphere.

Gaps are the void spaces between the centers of two neighboring spheres and they are the smallest constrictions within a pore throat (Figure 1.1 a). Although gaps are part of pore throats, they are not counted when calculating throat dimensions. Pore throat size is usually measured as the diameter of the biggest circumference that can be inscribed in a pore throat (Figure 1.1.b). Gap widths (w_{gap}) are given by the distance between the centers of the pair of grains less the spheres' radii (Figure 1.1.b).

Another method for calculating the dimensions of pore throats is described by Bryant and Blunt (1992) after studying the geometry of the pore space. The throat is characterized by the radius of the largest circumference that can be inscribed in the void space between grains (r_c), and the radius of the circle whose area is equal to the area of the cross section (r_{eq}) (Figure 1.1.c). The effective radius (R_{ef}) of the pore throat is then estimated as:

$$R_{ef} = \frac{r_c + r_{eq}}{2} \qquad \text{Eqn.1.6}$$

giving a good estimate of the true hydrodynamic radius of the pore throat.

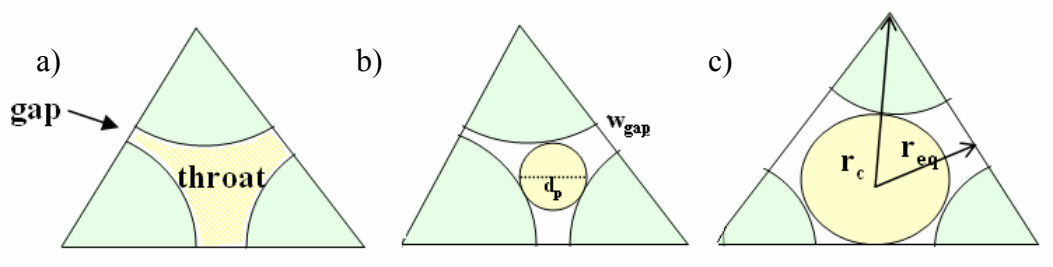

Figure 1.1: a) Cross section of a pore throat; b) & c) Methods to calculate pore throat size.

1.7 HYPOTHESIS AND OBJECTIVE

Existent experimental works suggest that filtration theory underestimates the extent of retention. They also suggest that the assumption that straining occurs only at pore throats is too restrictive.

The hypothesis in this project is that straining occurs in small gaps between pairs of grains in addition to the pore throats between triplets of nearest neighbor's grains (Figure 1.1). This hypothesis would explain why geometric criteria and theories based only on pore throats do not account for observed behavior.

The objective in this thesis is to determine if the retention of particles in the small constrictions in granular media (gaps) can explain the differences between theories based only on pore throats and experiments. This mode of particle straining will be examined without consideration of any other mechanism for the trapping of particles. The geometric analysis of a dense random packing of equal spheres will be key to reach this objective. The theory of Sharma and Yortsos (1987a) will be used to predict straining rates. The input to that theory is the frequency distribution of throat sizes, which will be extended in this work to include gaps.

Application of the current theories for straining requires an independent determination of the pore size distribution of the granular medium and of the local flow velocities. This project will test the theories quantitatively with realistic pore-scale data.

Chapter 2: Geometry of Sphere Packings

The base for this project is an analysis of the geometry of a simple model soil: a dense random packing of equal spheres. Random sphere packings are used as models for ideal soils in columns packed with glass beads, in laboratory studies of flow and transport through sands. Two kinds of sphere packings will be used in this thesis, one real and several computer-generated packings of random monodispered spheres. The characteristics of these packings are discussed next (sections 2.1 and 2.2) followed a method to identify pore throats in packings (section 2.3). The range of gap widths of interest to strain particles in the packings is discussed in section 2.4. Finally, section 2.5 defines the concept of range of capture which is dependent on the gap width and the size of the strained particle.

2.1 FINNEY PACKING

In 1968, J. L. Finney built a random dense spherical packing of 25,000 precision ball bearings and measured the Cartesian coordinates of the centers of 8,000 of them (Finney, 1968). In order to do that, the ball bearings were confined within a rubber bladder that was kneaded afterwards to obtain a denser packing. The ball bearings were locked in place by pouring hot wax into the bladder and finally their position was determined using a traveling microscope. This was the first physically representative model for a soil with a complete description of the geometry of both grain and void space.

Even if these smooth monodispersed spheres are a simplification of the natural grains occurring in soils, they capture the random spatial arrangement of grains which is

a physical feature of the actual soils. Therefore, an ideal soil is a powerful method to study phenomena that depend in pore geometry. In fact, columns packed with smooth glass beads are routinely used in laboratory studies of flow and transport.

The porosity of the Finney packing is 36.2%. Figure 2.1 shows the Finney packing used in this thesis. The dimensions are relative to radius R equal to 1.

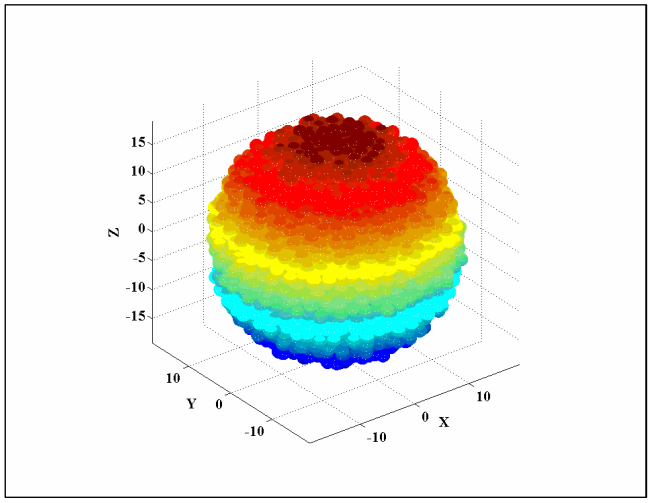

Figure 2.1: Finney pack (4021 spheres).

2.2 COMPUTER GENERATED PACKINGS

Ten different computer generated packings were used to estimate the uncertainty in the density of point contacts and near contacts computed for the Finney packing. These packings were created by Thane (2006) implementing a version of the cooperative rearrangement method (Cargill, 1984) which allows the use of periodic boundary conditions at the packing edges to eliminate edge effects. The spheres in the front (top) are virtually in contact with the spheres at the back (bottom), eliminating edge effects and thus possible non-randomness in the packing. They contain approximately 4,000 equal

spheres (mono-dispersed) and their porosities range from 36% to 38%. For convenience, the original sphere radius of these packings has been normalized to one. Figure 2.1 shows a computer generated packing of 1,000 spheres.

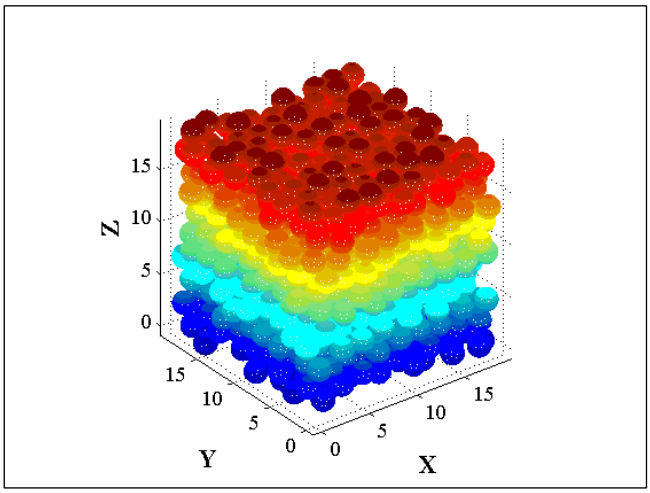

Figure 2.2: Dense random pack of 1000 equal spheres generated by cooperative rearrangement

The Finney packing can be used as form of validation for these random mono-dispersed computer-generated packings

2.3 DELAUNAY TESSELLATION

A tessellation is a computational geometric structure created by dividing space into convex polygonal regions. In the Voronoi tessellation, the decomposition of the space is determined by distances to a specified discrete set of points. This tessellation identifies the regions of space nearest each point.

The Delaunay tessellation is the dual of the Voronoi. Given sets of points in space, the Delaunay tessellation is created by joining all neighboring points in the Voronoi tessellation, i.e., pair of points whose Voronoi cells share an edge. Applying the

Delaunay tessellation to the sphere centers of the Finney and computer generated packings allows the identification of groups of nearest neighbor spheres.

Since in 3D space there are four points in each group of nearest neighbors, the Delaunay cells in the packings are tetrahedra as shown in Figure 2.3. Making an analogy of one of these packings with an ideal soil, the faces of the tetrahedra would correspond to the pore throats and the interior corresponds to the pore bodies. The Delaunay tessellation will be used to identify and quantify geometric features of pore space.

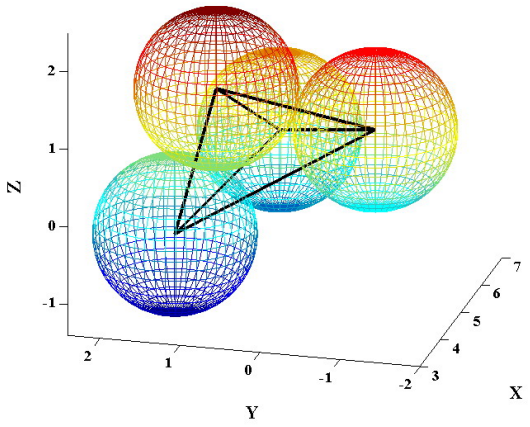

Figure 2.3: Four spheres and their corresponding Delaunay cell

Figure 2.4 shows the trapping of particles in a Delaunay cell. Figure 2.5 is a sketch of the pore space in a soil represented by equal spheres and it shows the retention of particles between grains by straining. It is the cut of a three dimensional figure, like the one presented in Figure 2.4.

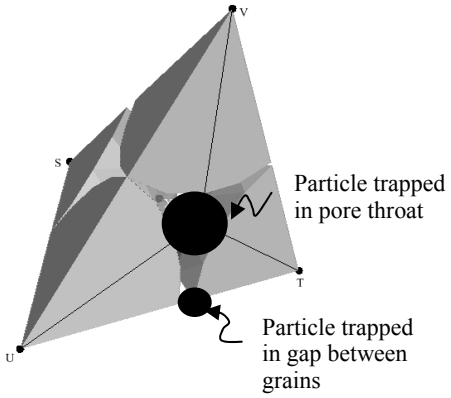

Figure 2.4: Retention of particles in a Delaunay cell by straining.

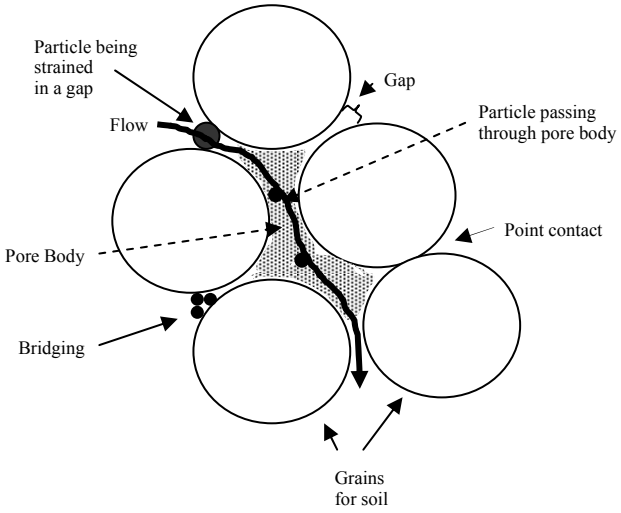

Figure 2.5: Sketch of retention in pore space. In this work, only the straining of single particles will be considered.

2.4 RANGE OF INTEREST FOR PARTICLE STRAINING

The minimum pore throat size in an ideal packing of random mono-dispersed spheres, measured as the diameter of the biggest circumference that can be inscribed in a pore throat, is $0.3R$, R being the grain radius. It occurs when the three spheres are in point contact (touching) and it sets a lower bound in the size of particles that can be trapped in pore throats. However, as shown in Chapter 1, experiments did not agree with the theory: particles smaller than this lower bound may nevertheless be strained.

The hypothesis is that the particles undergoing retention by straining in gaps correspond to the particle sizes whose behavior differed from classic theories in the experiments described in the literature. The size of a particle 3 to 9 times smaller than a pore throat (Hall, 1957; Gruesbeck and Collins, 1982) would be between $0.033R$ and $0.1R$. Particles one order of magnitude smaller than pore throats (Baghdikian et al. 1987) would be approximately $0.03R$ in size and, particles sixteen times smaller than pore throats (Marlow et al., 1991) would have a minimum diameter around $0.02R$.

Straining is a geometric mechanism that will be studied in this project assuming no physicochemical forces are involved. Thus the range of interest for gap sizes in this thesis is going to be close to the size of the particles being strained. In accord with the previous data and the statistical characterization of the models for soils that will be shown in the next chapter, the gap width between $0.03R$ and $0.1R$ have been selected as the range of interest. This range of widths corresponds to gaps between 1% and 5% of the grain size. This agrees with Sakthivadivel (1966) who observed straining for colloids diameters near 5% of the median grain diameter of the porous medium. In this study, gap

sizes bigger than 0.1R are considered part of the pore throat. Even so, ranges of gap width smaller and bigger than the range of interest have also been investigated in this project.

Making an analogy with sands, if the average size (diameter) of a sand grain is 0.2 mm, particle size 0.1R (R=0.1mm) corresponds to 10 microns and particle size 0.03R corresponds to 3 microns.

The tolerance for sphere contact is $10^{-2}R$ for the Finney pack and $10^{-3}R$ for the computer generated packs. Gap widths smaller than those values will be considered point contact and thus are not considered in this study.

Figure 2.6 shows to scale the differences in size between soil grains and particles being strained. Spheres 1, 2 and 3 have equal radius R and represent soil grains. Flow is assumed to be normal to the plane of the paper. The radius of sphere 4 is 0.2R, i.e., the 20% of the radius of soil grains and it is retained in the pore throat. The radius of sphere 5 is 0.05R, i.e., 5% of the grain radius and it is strained in a gap between grains 1 and 3 of size 0.03R. The radius of sphere 6 is 0.03R and it is trapped in a gap of size 0.02R. The radius of sphere 7 is the 0.02R, i.e., 2% of the grain radius and it shown in the pore throat for size comparison. Spheres 5, 6 and 7 are too small to be trapped in the pore throat; nevertheless particles 5 and 6 are strained in gaps in Figure 2.6. Particle 7 is not strained in Figure 2.6. Figure 2.7 shows particles 4, 6 and 7 being strained.

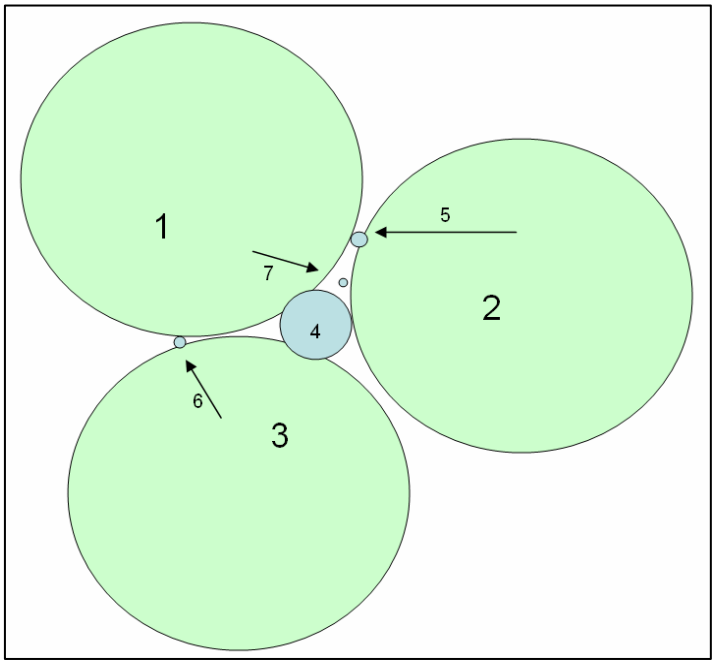

Figure 2.6: Trapping of particles smaller than pore throats. Flow is perpendicular to the plane of the paper.

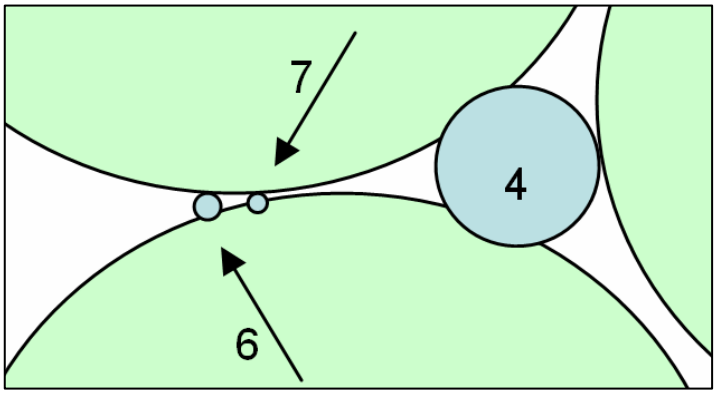

Figure 2.7: Two particles being retained in a gap. Flow is perpendicular to the plane of the paper.

These examples show how particles whose size are 5% or less the size of the soil grains and also smaller than the smallest pore throat (of size 15% of the grains) could nevertheless get trapped in the porous medium by straining.

The previous magnitudes for particle trapping can also be expressed in term of the diameters of the soil grains (D) and strained particles (d). Particles of size $0.03R$ correspond to d/D=0.015 and particle sizes of $0.1R$ correspond to d/D=0.05. These particles will be strained in the smallest part of the gap having the same nominal size, along the line that joins the centers of the two spheres making the gap. Particles bigger than this will be trapped at different points in those gaps.

2.5 RANGE OF CAPTURE

This section discusses how the size of the particle being strained affects the calculation of the specific flow through gaps. As stated before, the gap width is the minimum distance between the spheres' surfaces, at the line joining their centers. A particle of diameter d equal to the gap width will be strained only if the streamline carrying it passes through its minimum constriction. This event has an infinitesimal probability. However, particles whose diameters are bigger than the gap width will be strained if they pass within some finite distance of the minimum constriction. This distance will be called "range of capture" and represented by a. Its value depends on the particle size d and the gap width w_{gap}.

Figure 2.8 shows a scheme of the range of capture. A particle of diameter d can be strained in a gap of width w_{gap} if it passes within a distance a of the narrowest part of the gap.

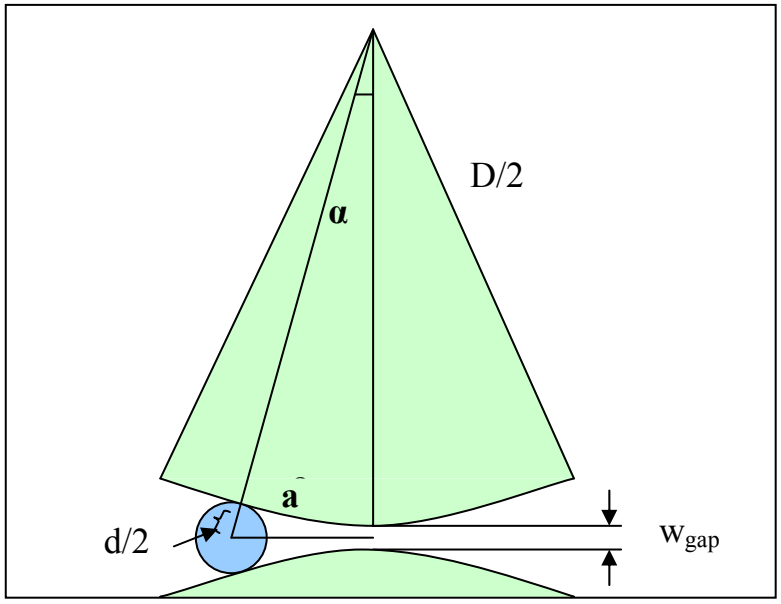

Figure 2.8: Scheme of the range of capture. The particle is moving perpendicular to the plane of the paper. It will be trapped if it enters the gap within a distance *a* of the center.

The following equation derives from the application of Pythagoras theorem to the triangle in Figure 2.8, and it relates range of capture *a*, particle size *d*, gap width w_{gap} and grain diameter *D*.

$$\frac{2a}{D} = \sqrt{\left(\frac{d}{D}\right)^2 - \left(\frac{w_{gap}}{D}\right)^2 + 2\left(\frac{d}{D} - \frac{w_{gap}}{D}\right)} \qquad \text{Eqn. 2.1}$$

Also from Figure 2.8,

$$\cos\alpha = \frac{1 + w_{gap}/D}{1 + d/D} \qquad \text{Eqn. 2.2}$$

and,

$$a = \frac{w + D}{2} \cdot \tan \alpha \qquad \text{Eqn. 2.3}$$

The local flow relevant to the particle can be calculated as:

$$q = 2\, a\, w_{gap}\, u_{gap} \qquad \text{Eqn. 2.4}$$

This approximation is reasonable for angles α up to about 15°. Notice that α is measured at the center of either grain defining a gap.

Large values of a would extend the range of capture into the pore throat, where local flow velocities differ from both the average throat velocity and the gap velocity. Equation 2.3 will be used as a criterion for calculating the maximum extent of the gap when the angle α is equal to 15°. This magnitude will be called l.

The sensitivity of the straining has been tested to the value of α. The results are shown in Chapter 4. Of primary interest are small particles (d/D<0.1) since they exhibit non-classical straining in experiments. It will be shown later whether these particles can be strained within a range corresponding to the maximum extent of the gap, l.

Chapter 3: Statistical Characterization of Pore Space in Sphere Packs

Since straining is a geometric mechanism, it is essential to know the geometry of the media that is causing some particles to be strained. For a dense random packing of spheres, the number, frequency and density of near neighbors and point contacts for every sphere, and the frequency distribution of gap widths describe this geometry. Gaps are defined in Chapter 1 as the void spaces between the centers of two neighboring spheres. The statistics for the Finney packing will be compared with those for the computer-generated packs.

Only the spatial coordinates of the sphere centers and the sphere radii are needed to characterize the geometry of the packings. Commercial code (MATLAB) has been used to perform these calculations.

In Section 3.1 the number of neighbors within different gap width is calculated for every sphere in the Finney and computer-generated packing. The results are shown in histograms of frequency in the number of neighbors. The statistics referent to the point contacts are presented in this section.

Section 3.2 studies the density of gaps of small widths in both packings, and the distribution of gaps in Delaunay cells is shown in section 3.3.

All distances in this chapter have been normalized by sphere radius R.

3.1 DISTRIBUTION OF NEIGHBORS

The number of near neighbors within certain gap width has been calculated for every sphere in both the Finney and computer generated packings. The gap width is calculated as the distance between centers of the spheres less the radius of each sphere. If (x_1,y_1,z_1) and (x_2,y_2,z_2) are the coordinates of the centers of spheres 1 and 2 respectively, the gap width (w_{gap}) is calculated as:

$$w_{gap} = \sqrt{(x_1 - x_2)^2 + (y_1 - y_2)^2 + (z_1 - z_2)^2} - 2 \qquad \text{Eqn. 3.1}$$

Gap widths of 2*R*, 1*R*, 0.03*R*, and intervals of gap width between 0.03*R* to 0.1*R*, 0.05*R* to 0.125*R*, 0.125*R* to 0.25*R*, 0.25*R* to 0.5*R*, and 0.5*R* to 1*R* have been studied. Two spheres in point contact have a gap of width exactly equal to zero, so identifying point contacts computationally requires specifying a tolerance. The occurrence of point contacts and overlap has been tested by setting a tolerance of $|10^{-2}|$ *R* for Finney and $|10^{-4}|$ *R* for the computer generated packs. Zero distance has also been tested.

For every distance or interval studied, plots of the average number of neighbors per sphere and frequency histograms have been created. A complete set of histograms is shown here for the Finney pack and one of the computer generated packings. A table at the end of this section summarizes the statistics for all the packings.

The following figure shows, for every sphere in the Finney packing, the number of neighbors within a gap width of 0.2*R*.

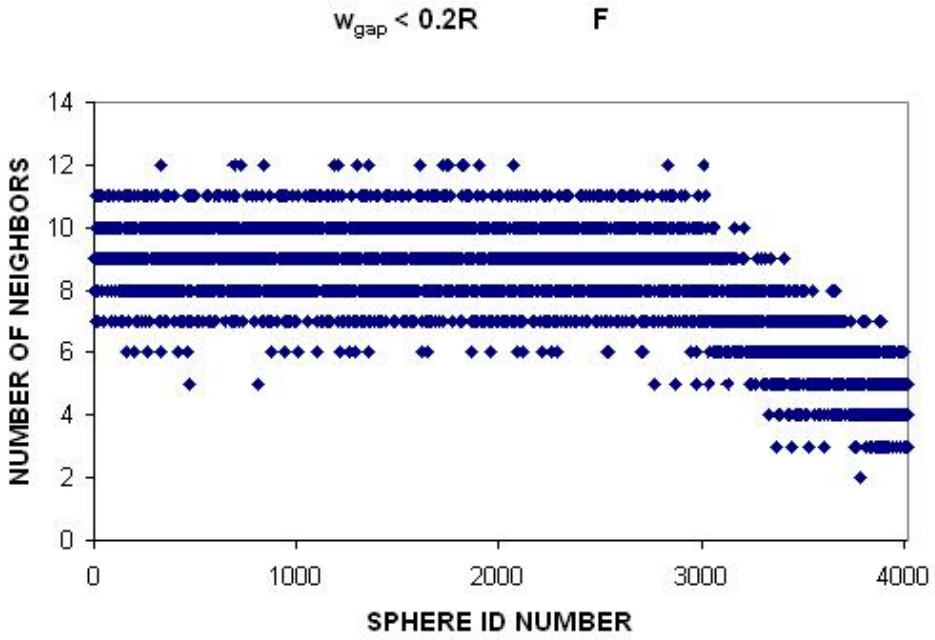

Figure 3.1: Number of neighbors within a gap width of 0.2*R* for spheres 1 to 4021 in the Finney packing (F).

There is a decrease in the number of neighbors starting around sphere 3000. Spheres whose "id number" is bigger than 3000 are close to the packing boundary or edge and therefore they have fewer neighbors than the ones in the middle. To eliminate this edge effect, statistics are gathered only on the 2000 spheres in the center of the packing. This makes the packing to be a sphere with a radius of about 15.6*R*. Figure 3.2 shows number of neighbors within a gap width of 0.2*R* for the center 2000 spheres.

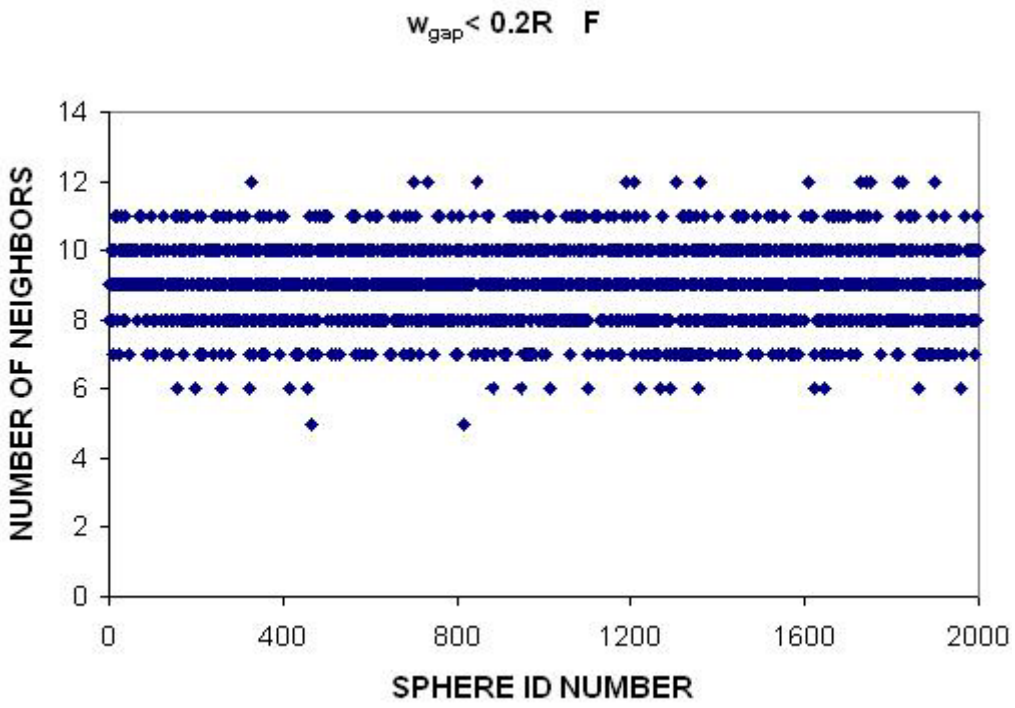

Figure 3.2: Number of neighbors within a gap width of 0.2*R* for spheres 1 to 2000 in Finney packing (F).

For the computer generated packings, as in the case of the Finney pack, the statistics are gathered only for spheres in the center of the packing. In these cases, small cubes of side about 14.6*R,* whose center coincides with the origin of coordinates, have been extracted of the packings for statistical purposes. Table 3.1 shows the number of spheres considered in every packing, together with the side of the small cube that they made and the side of the box containing the cube. The dimensions of the Finney packing are also shown in the table.

Table 3.1: Number of spheres used for statistical purposes in each packing.

Packing	**Used spheres**	**Radius**	**Total spheres**	**Total radius**
Finney	2000	15.6 *R*	4021	36.26R
		Side cube		**Side Box**
Packing 1	459	14.63 *R*	4000	30.11*R*
Packing 2	459	14.60 *R*	4000	30.11*R*
Packing 3	475	14.60 *R*	4000	29.76*R*
Packing 4	475	14.60 *R*	4000	29.75*R*
Packing 5	465	14.60 *R*	4000	30.10*R*
Packing 6	459	14.67 *R*	4000	30.11*R*
Packing 7	472	14.60 *R*	4000	29.73*R*
Packing 8	454	14.80 *R*	4000	30.10*R*
Packing 9	453	14.60 *R*	4000	30.10*R*
Packing 10	110	9.03 *R*	1000	18.79*R*

In order to compare with Finney packing, Figure 3.3 shows number of neighbors within a gap width of 0.2*R* for the center 475 spheres in one of the computer generated packings. The average number of neighbors within that distance in the Finney packing (Figure 3.2) is 9.02 while the average number of neighbors for this computer generated packing is 8.9.

The x-axis in Figure 3.3 ranges from 0 to 4000 since it is the sphere id number what has been plotted. Only the data points correspondent to 475 the spheres inside the small cube are shown in the figure. In Finney packing, the sphere id number varies continuously from 1 to 2000 for the 2000 center spheres. In the computer-generated packings this number is random.

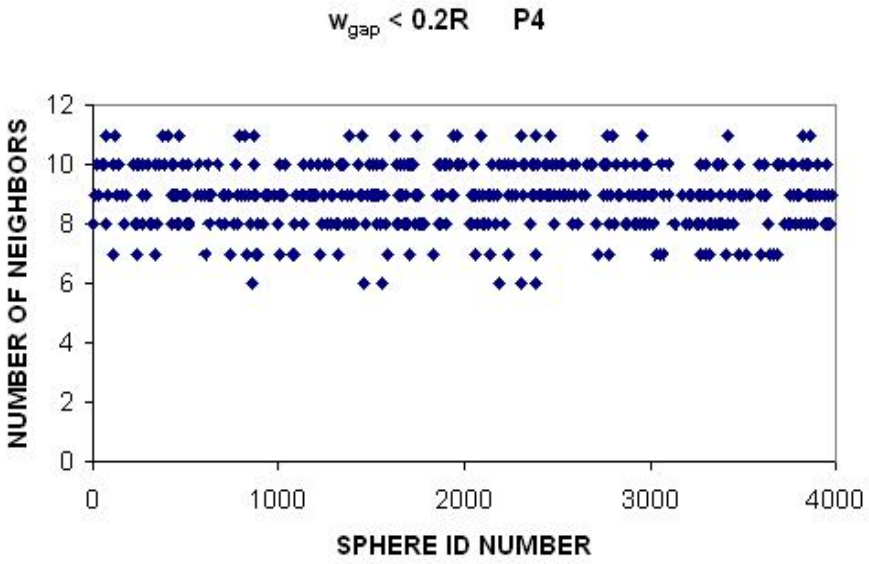

Figure 3.3: Number of neighbors within a gap width less than 0.2*R* for 475 spheres in computer-generated packing 4 (P4).

Figures 3.4, 3.5 and 3.6 show the number of neighbors in the range of widths of interest (0.03*R*-0.1*R*) for the Finney packing and two computer-generated packings respectively.

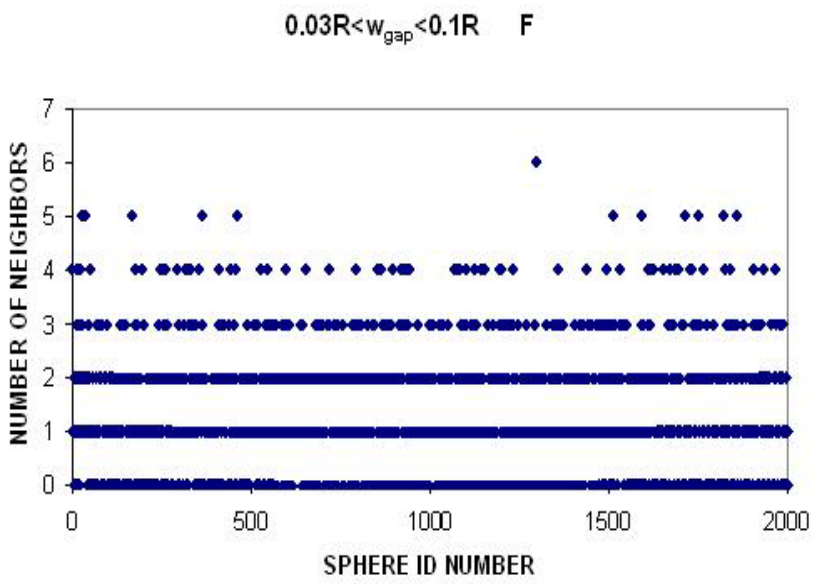

Figure 3.4: Number of neighbors within a gap width between 0.03*R* and 0.1*R* in Finney packing

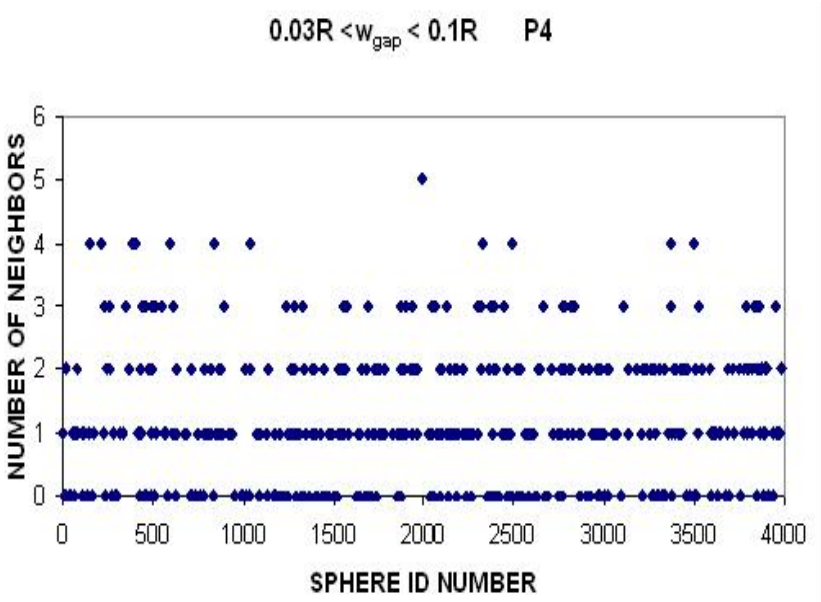

Figure 3.5: Number of neighbors within a gap width between 0.03*R* and 0.1*R* in the computer-generated packing 4.

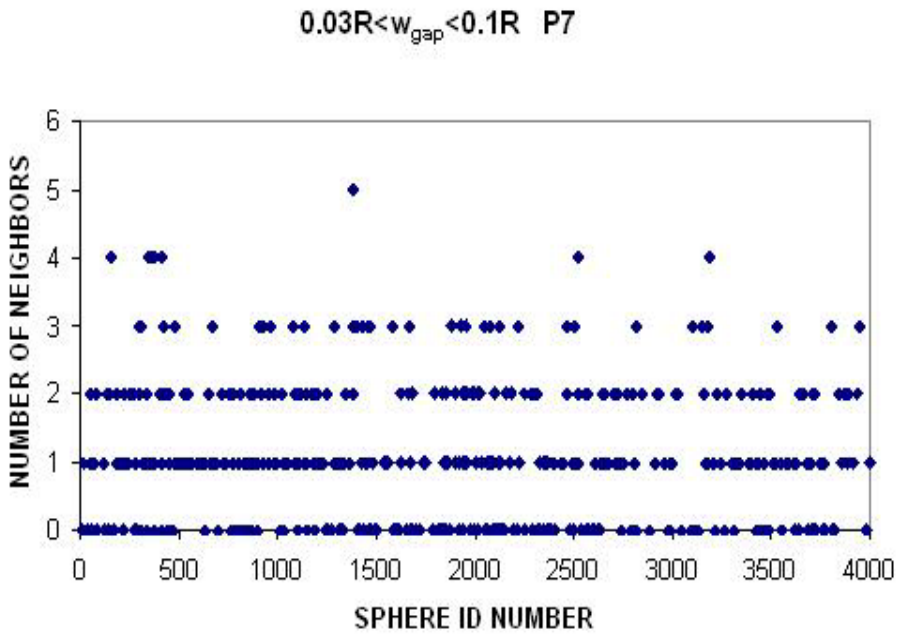

Figure 3.6: Number of neighbors within a gap width between0.03*R* and 0.1*R* in the computer-generated packing 7.

The average number of neighbors in the range of interest is 1.31 in the Finney packing (Figure 3.4), 1.08 in the first computer generated packing (Figure 3.5) and 1.17 in the second computer generated packing (Figure 3.6). Table 3.2 shows the average, minimum and maximum number of neighbors in the range of interest, for the Finney and the computer generated packings. The computer-generated packings have slightly smaller number of gaps in the range of interest than the Finney packing. This can be explained on the basis of the differences in porosity between the packings. These porosities are reported in Table 3.3

Table 3.2: Statistic of the number of neighbors within the range of gap widths of interest for the Finney and computer-generated packings

Packing	Minimum	Maximum	Mode	Average
Finney	0	6	1	1.31
1	0	6	1	0.97
2	0	5	1	1.05
3	0	5	1	1.07
4	0	5	1	1.17
5	0	4	1	0.99
6	0	4	0	0.95
7	0	5	1	1.08
8	0	5	0	0.94
9	0	5	1	0.93
10	0	5	1	1.11

Table 3.3: Porosity of the packings

Packing	Porosity (%)
Finney	36.20
1	38.64
2	38.64
3	36.43
4	36.37
5	38.57
6	38.56
7	36.27
8	38.56
9	38.50
10	36.87

The porosities of the computer-generated packings are always bigger than the porosity of the Finney pack. This means that Finney pack is denser than the computer-generated packings. For this reason the number of neighbors in the range of interest is slightly bigger in the Finney packing.

The information in Figures 3.1 to 3.6 can be illustrated in histograms as follows. The histograms show number of spheres having a given number of neighbors separated by a particular range of gap sizes. Frequency is also shown in the secondary axis for an easier comparison. The histograms in Figures 3.7, 3.8 and 3.9 correspond to the range of gap widths 0.01*R*-0.03*R*, 0.03*R*-0.1*R* and 0.1*R*-0.3*R* for the Finney packing.

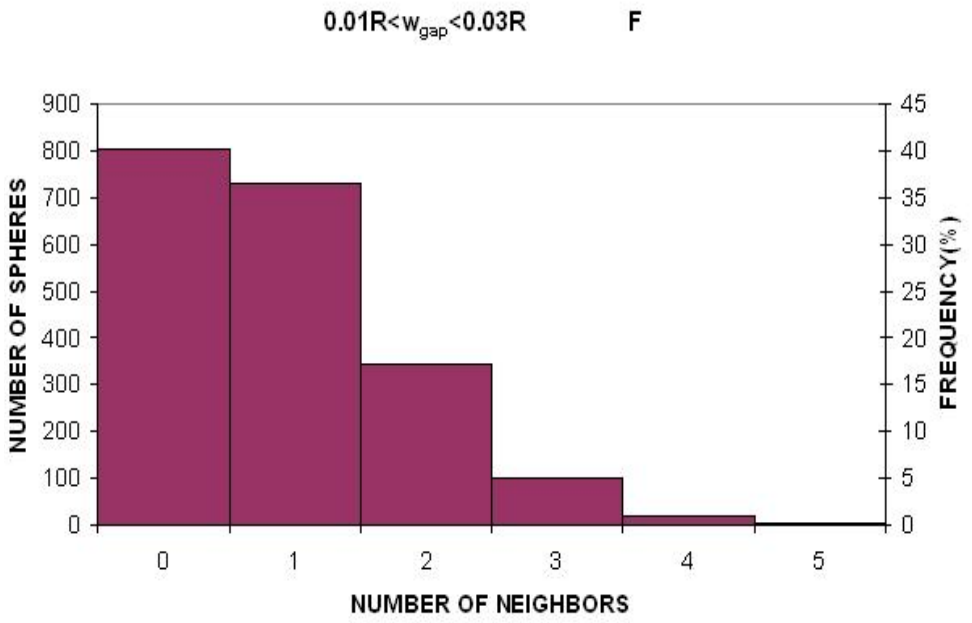

Figure 3.7: Histogram of number of neighbors within a gap width between 0.01*R* to 0.03*R* for the Finney Packing. Average=0.90.

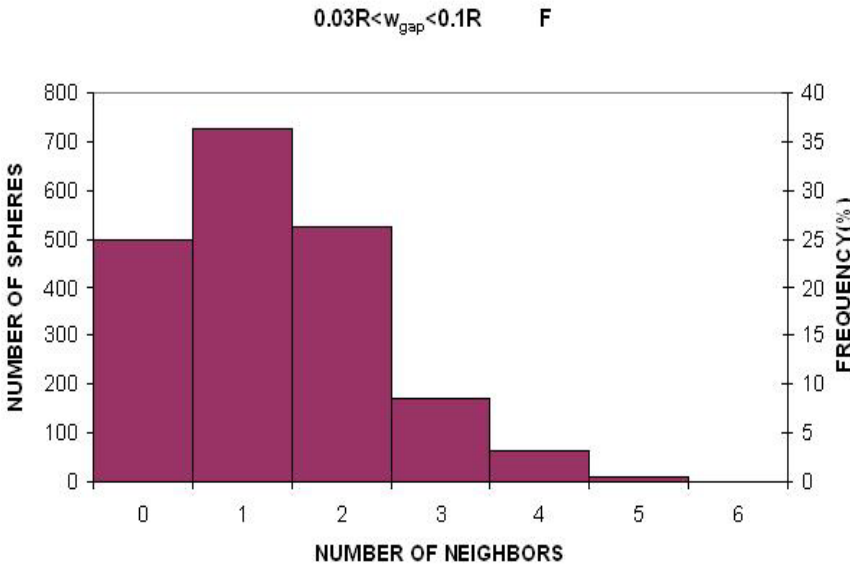

Figure 3.8: Histogram of number of neighbors within a gap width between 0.03*R* to 0.1 *R* for the Finney Packing. Average=1.31.

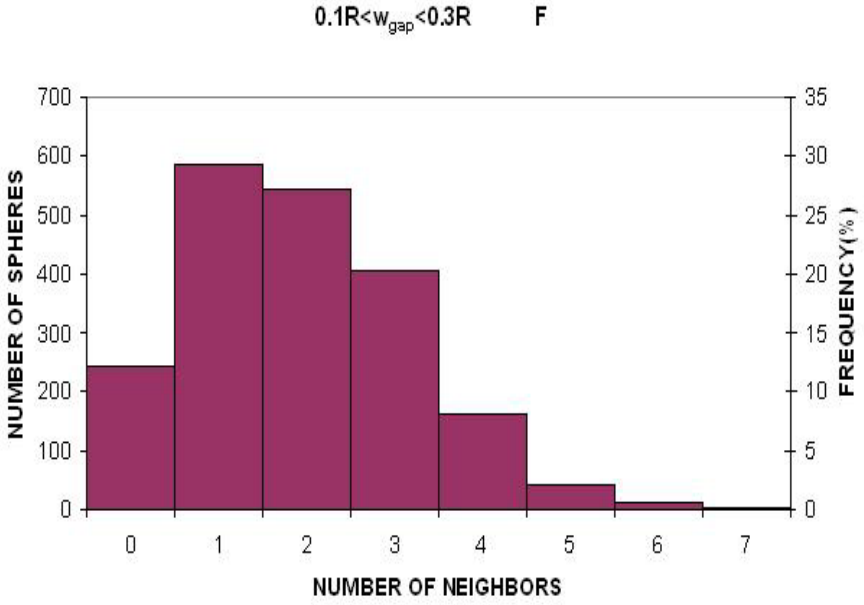

Figure 3.9: Histogram of number of neighbors within a gap width between 0.1 *R* to 0.3 *R* for the Finney Packing. Average=1.93.

There is an increase in the average number of neighbors when the range of gap widths is increased. The average number of neighbors in Figure 3.7 is 0.90 while the average in Figure 3.8 is 1.31 and the average in Figure 3.9 is 1.93. Equivalent histograms are shown next for two computer generated packing. Figures 3.10, 3.11 and 3.12 correspond to packing 4 and Figures 3.13, 3.14 and 3.15 to packing 7.

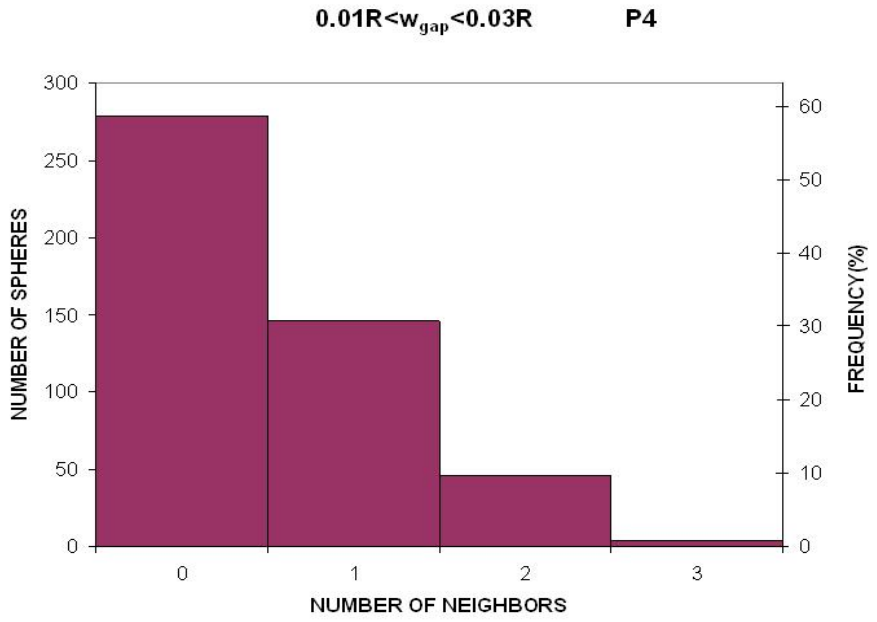

Figure 3.10: Histogram of number of neighbors within a gap width between 0.01 *R* to 0.03 *R* for computer-generated packing 4. Average=0.52.

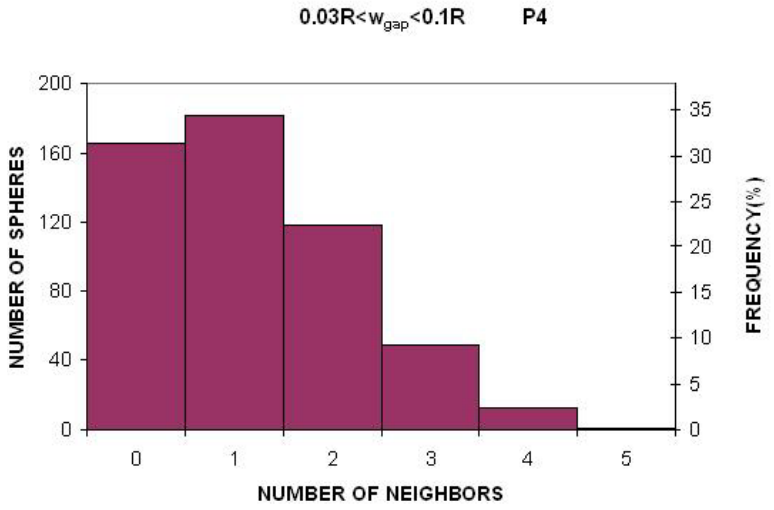

Figure 3.11: Histogram of number of neighbors within a gap width between 0.03 *R* to 0.1 *R* for computer-generated packing 4. Average=1.17.

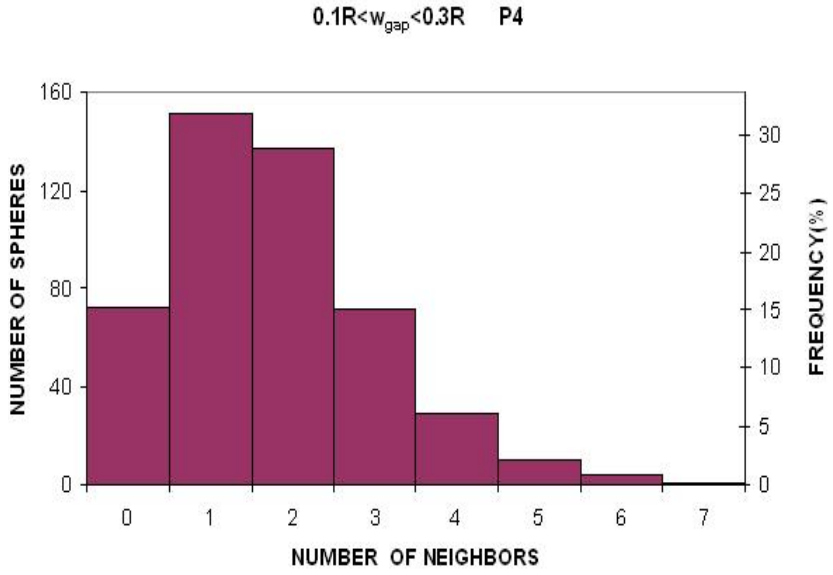

Figure 3.12: Histogram of number of neighbors within a gap width between 0.1 *R* to 0.3 *R* for computer-generated packing 4. Average=1.76.

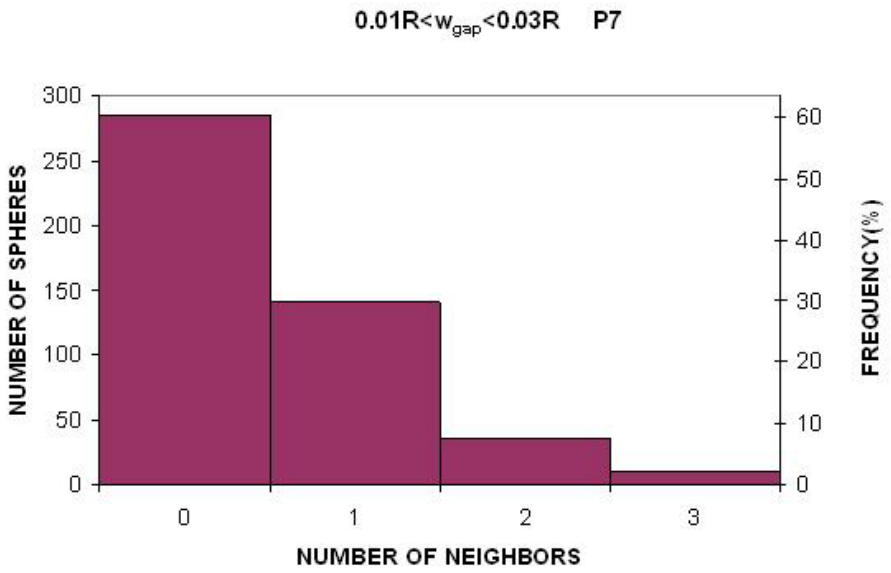

Figure 3.13: Histogram of number of neighbors within a gap width between 0.01*R* to 0.03*R* for computer-generated packing 7. Average=0.51

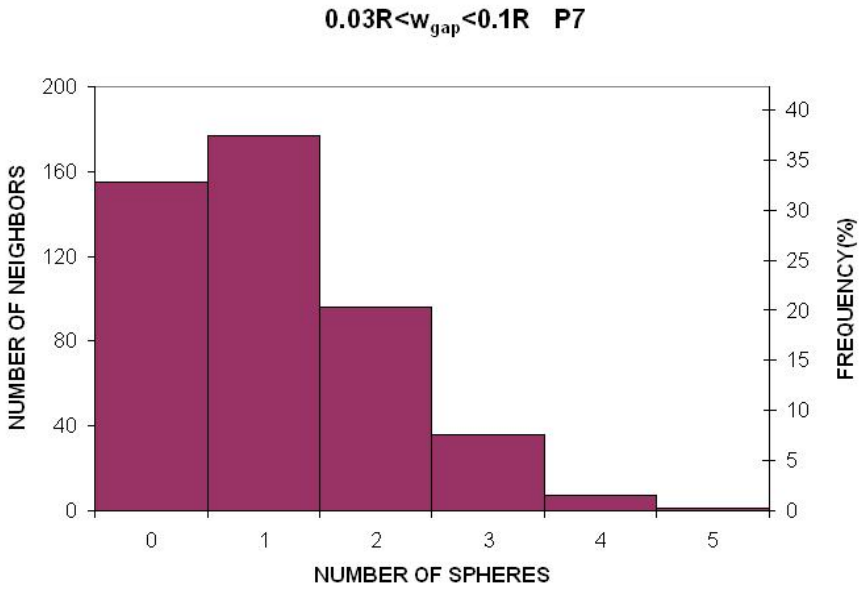

Figure 3.14: Histogram of number of neighbors within a gap width within 0.03*R* to 0.1*R* for computer -generated packing 7. Average=1.08.

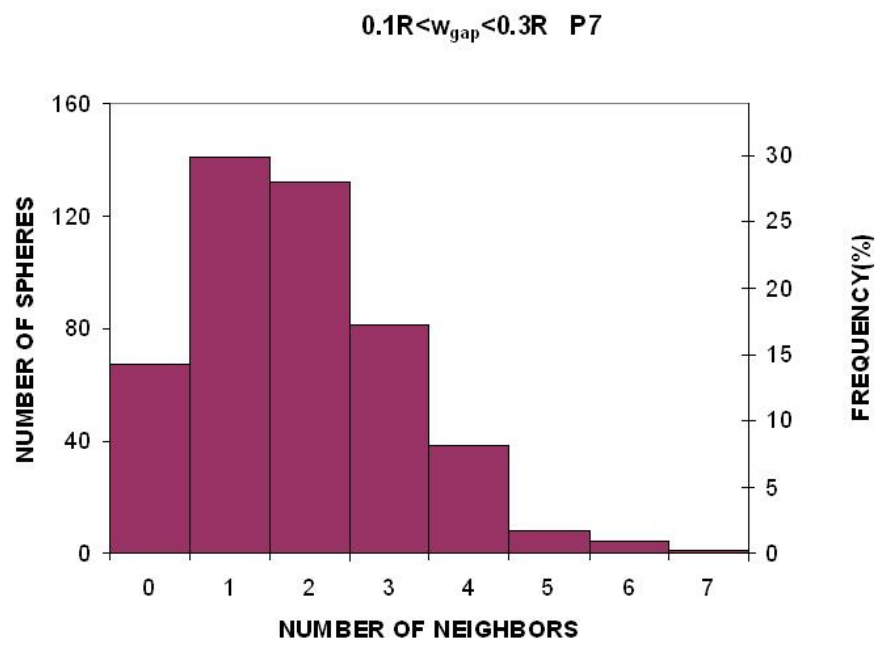

Figure 3.15: Histogram of number of neighbors within a gap width between 0.1*R* to 0.3*R* for computer-generated packing 7. Average=1.85.

The following plots show the cumulative frequency in the number of neighbors for the previous examples. Figure 3.16 plots the cumulative frequency for the Finney packing and Figures 3.17 and 3.18 do the same for computer-generated packings 4 and 7. It is shown how in the three cases the number of neighbors increases as the range of widths increases.

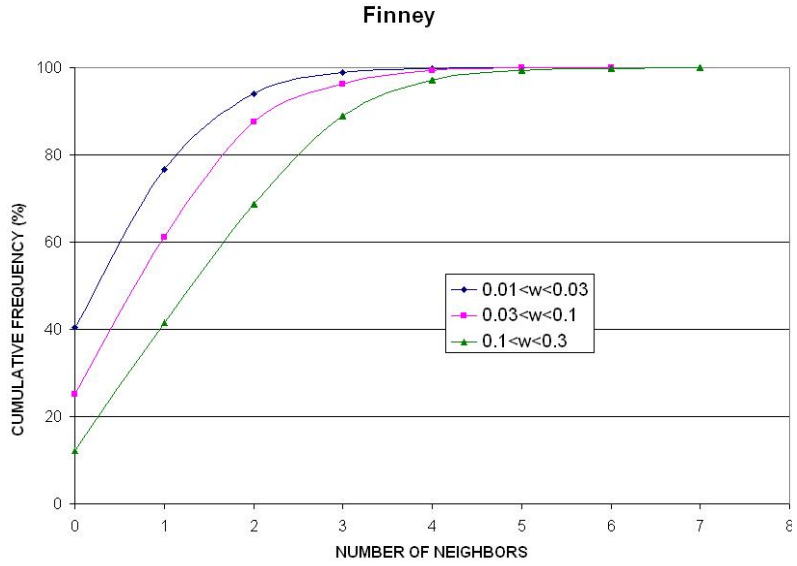

Figure 3.16: Cumulative frequency of number of neighbors within gap widths between 0.01*R* to 0.1*R*, 0.03*R* to 0.1 *R* and 0.1 *R* to 0.3*R* for the Finney packing.

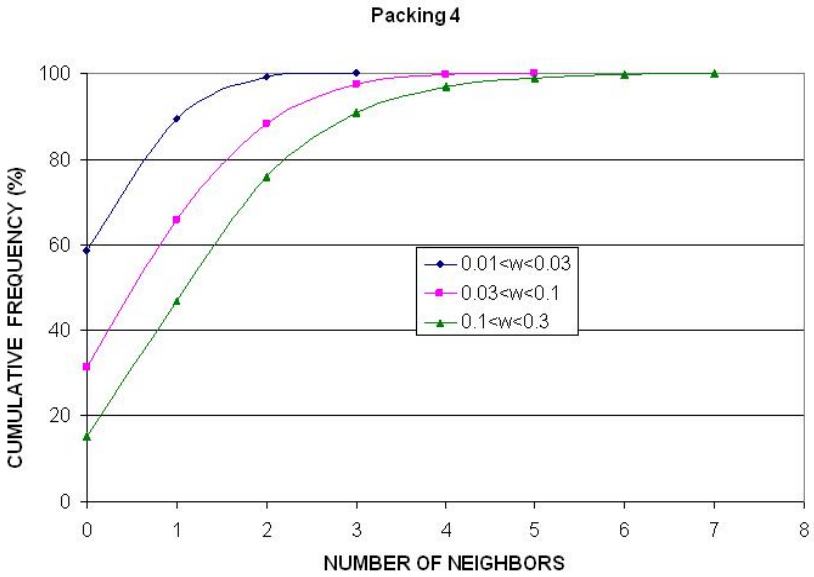

Figure 3.17: Cumulative frequency of number of neighbors within gap widths between 0.01*R* to 0.1*R*, 0.03*R* to 0.1 *R* and 0.1 *R* to 0.3*R* for computer generated packing 4.

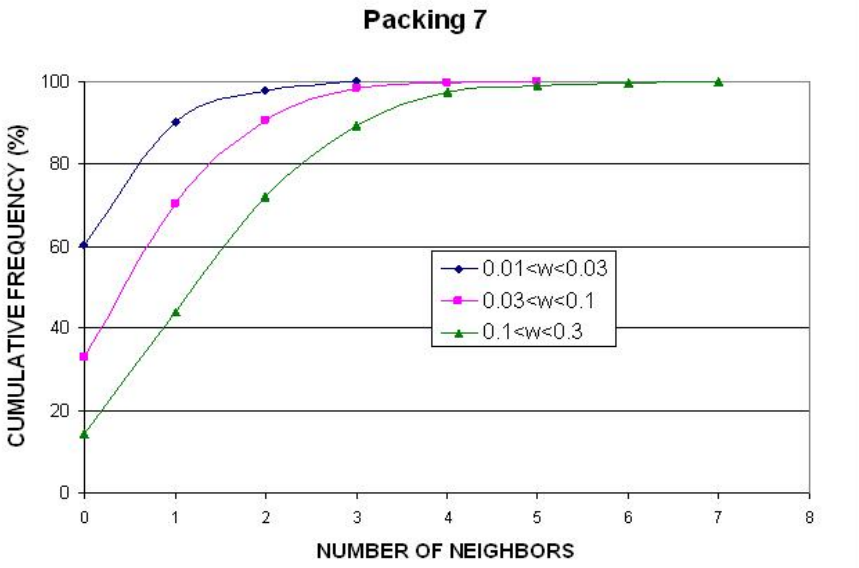

Figure 3.18: Cumulative frequency of number of neighbors within gap widths between 0.01*R* to 0.1*R*, 0.03*R* to 0.1 *R* and 0.1 *R* to 0.3*R* for computer generated packing 7.

The same exercise has been done with a different set of gap widths in order to see how the number and distribution of neighbors change with the considered gap width. The following histograms correspond to the number of neighbors within distances of 0.0625*R*-0.125*R*, 0.125*R*-0.25*R*, 0.25*R*-0.5*R*, and 0.5*R* to 1*R*. The same packings have been used, namely Finney packing and computer generated packings 4 and 7.

Figures 3.19, 3.20, 3.21 and 3.22 correspond to Finney packing, figures 3.23, 3.24, 3.25 and 3.26 correspond to packing 4, and figures 3.27, 3.28, 3.29, and 3.30 correspond to packing 7.

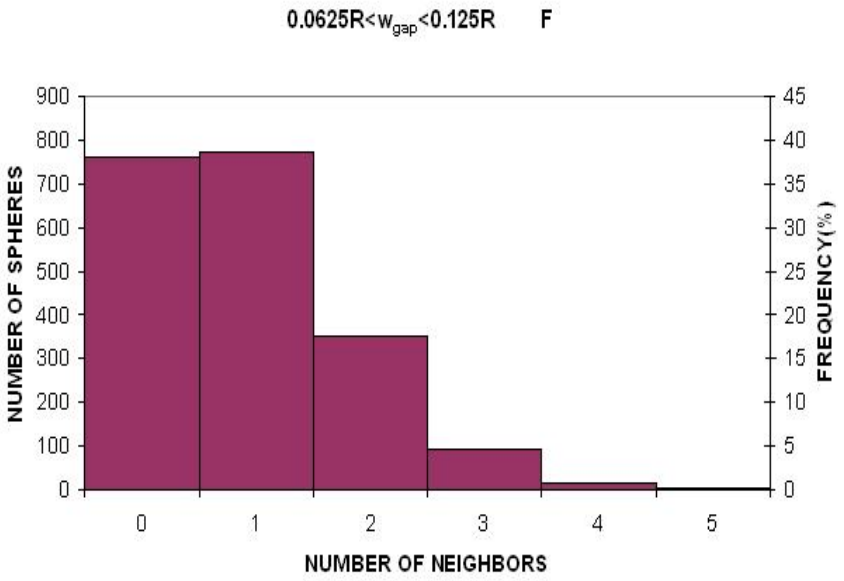

Figure 3.19: Histogram of number of neighbors within a gap width between 0.0625*R* to 0.125*R* for Finney packing. Average=0.92.

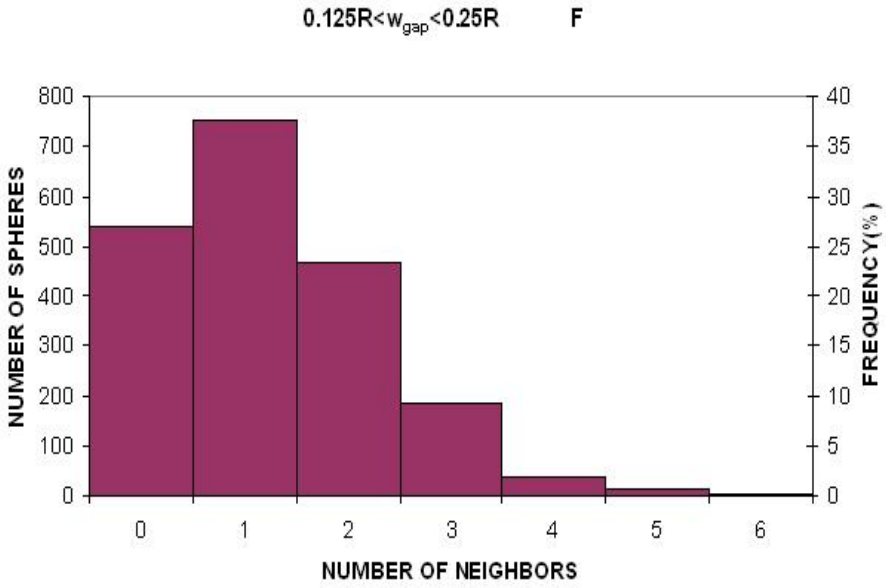

Figure 3.20: Histogram of number of neighbors within a gap width between 0.125*R* to 0.25*R* for Finney packing. Average=1.24.

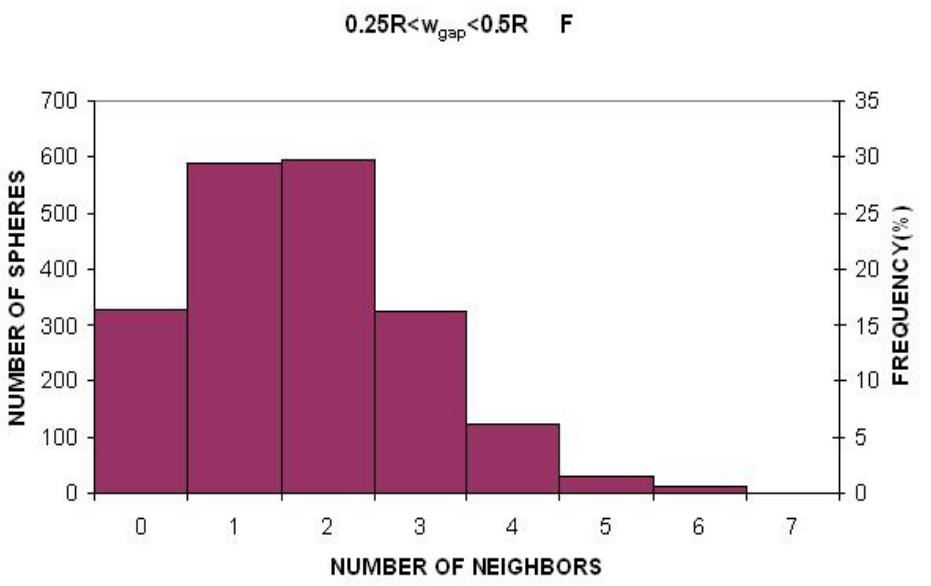

Figure 3.21: Histogram of number of neighbors within a gap width between 0.25*R* to 0.5*R* for Finney packing. Average=1.73

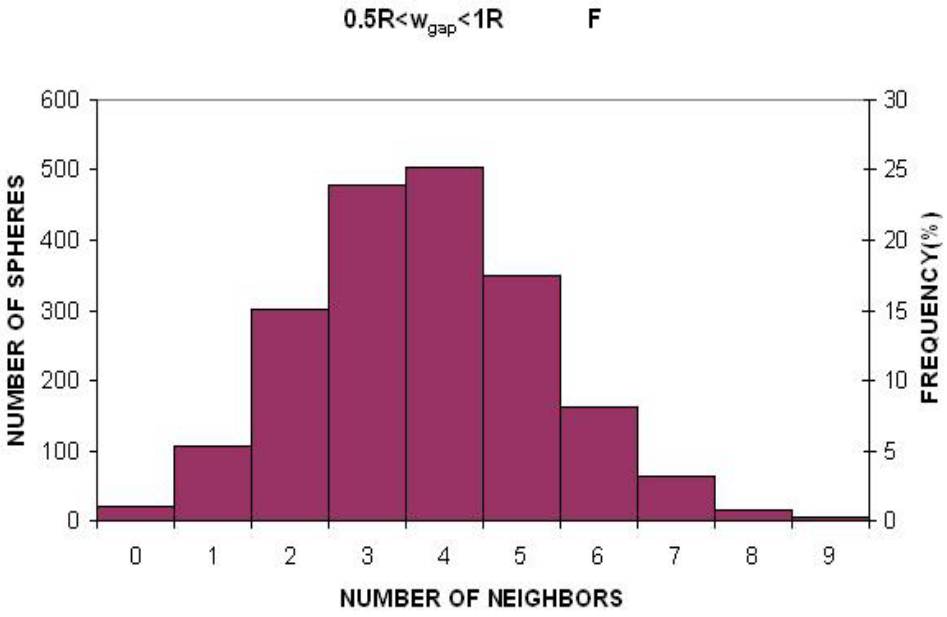

Figure 3.22: Histogram of number of neighbors within a gap width between 0.5*R* to 1*R* for Finney packing. Average=3.73.

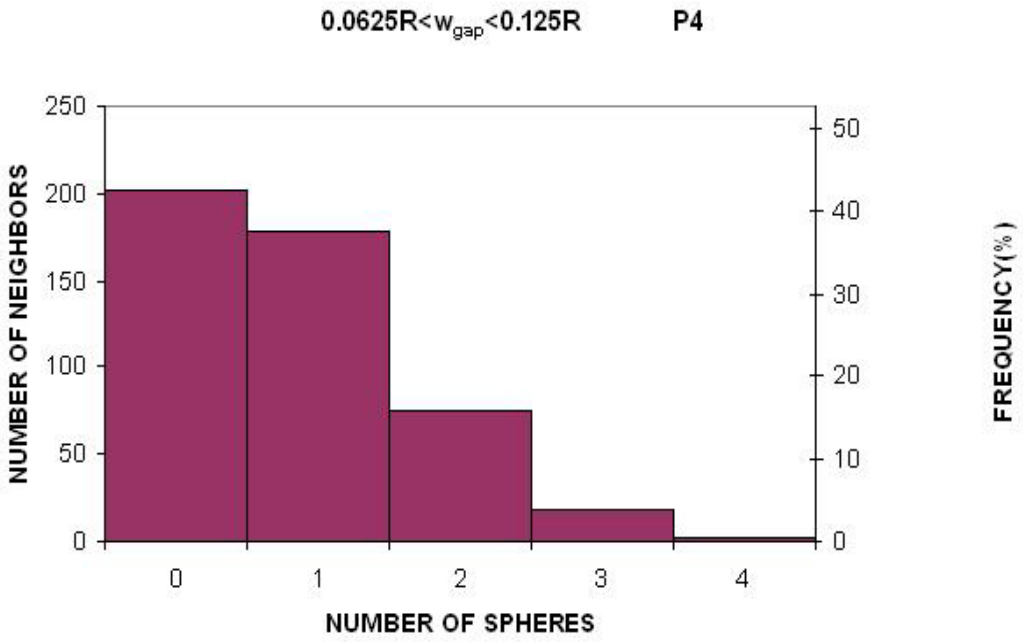

Figure 3.23: Histogram of number of neighbors within a gap width between 0.0625*R* to 0.125*R* for computer-generated packing 4. Average=0.82.

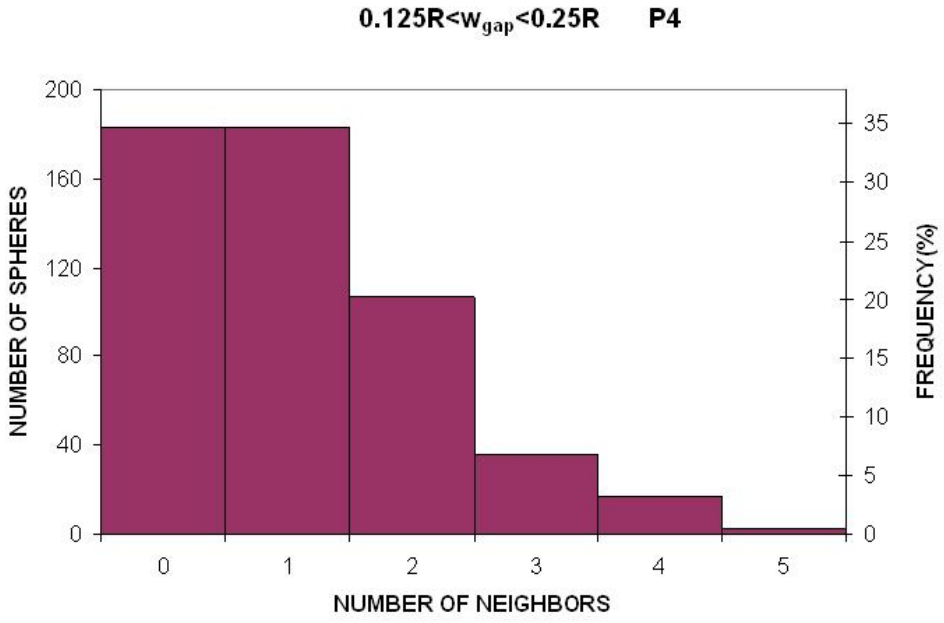

Figure 3.24: Histogram of number of neighbors within a gap width between 0.125*R* to 0.25*R* for computer-generated packing 4. Average=1.10.

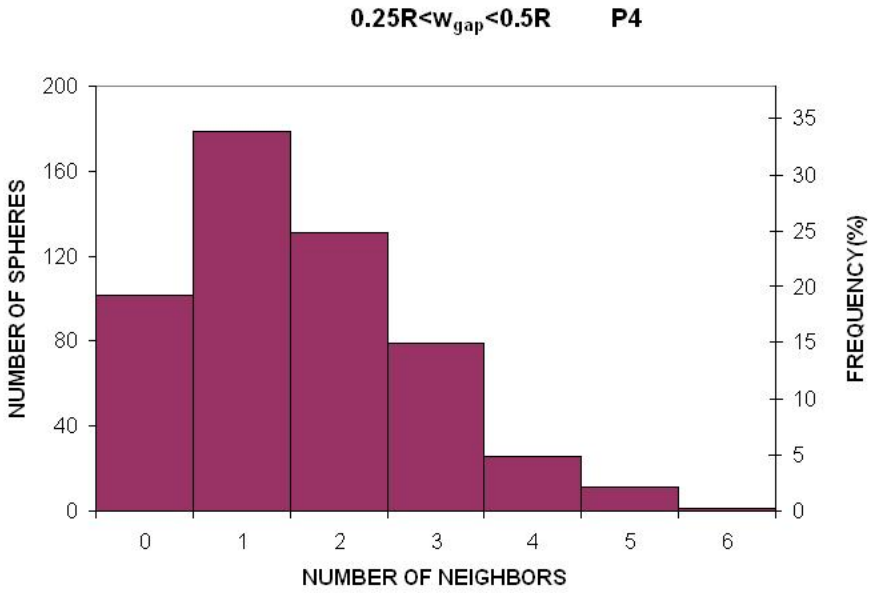

Figure 3.25 Histogram of number of neighbors within a gap width between 0.25*R* to 0.5*R* for computer-generated packing 4. Average=1.59.

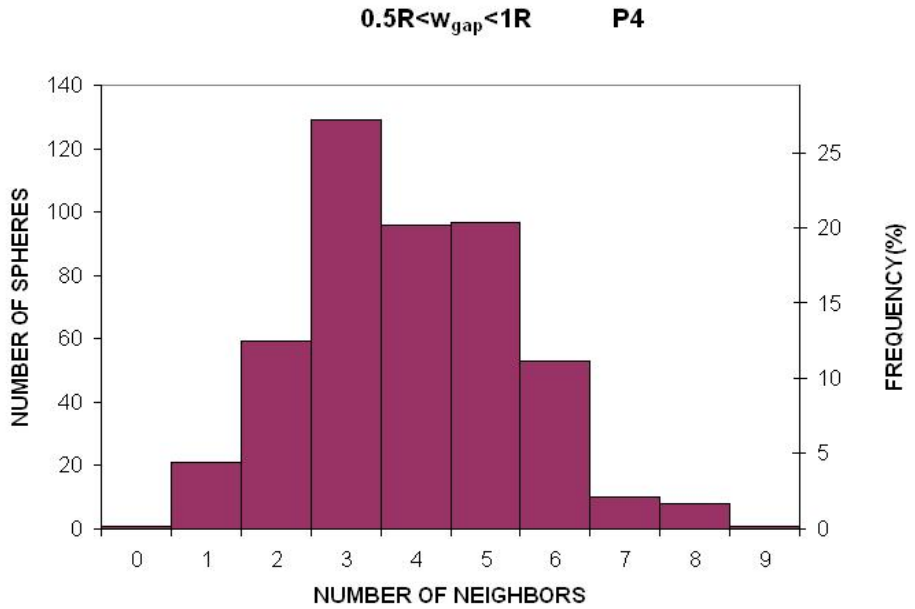

Figure 3.26: Histogram of number of neighbors within a gap width between 0.5*R* to 1*R* for computer-generated packing 4. Average=3.91.

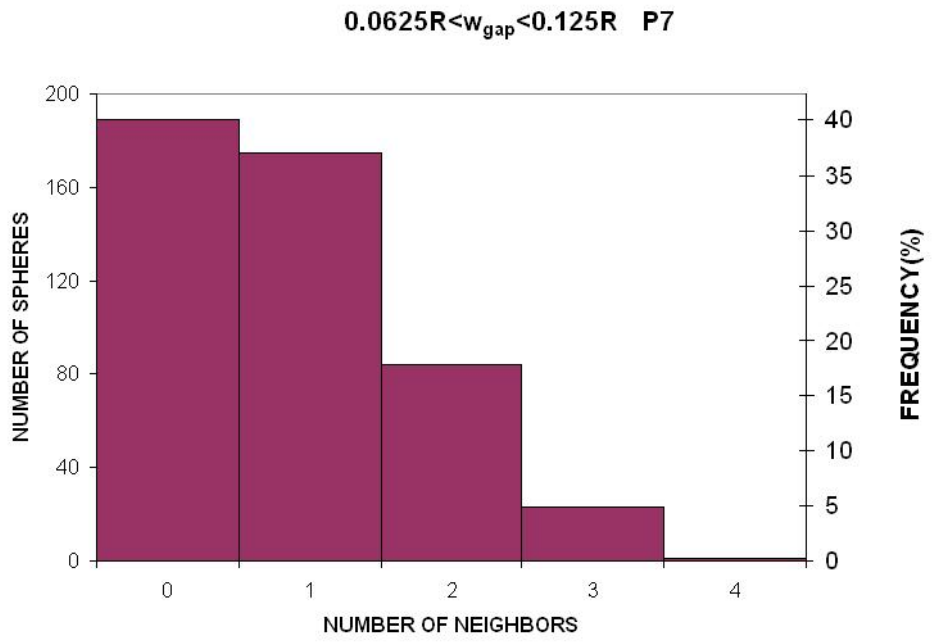

Figure 3.27: Histogram of number of neighbors within a gap width between 0.0625*R* to 0.125 *R* for computer-generated packing 7. Average=0.68.

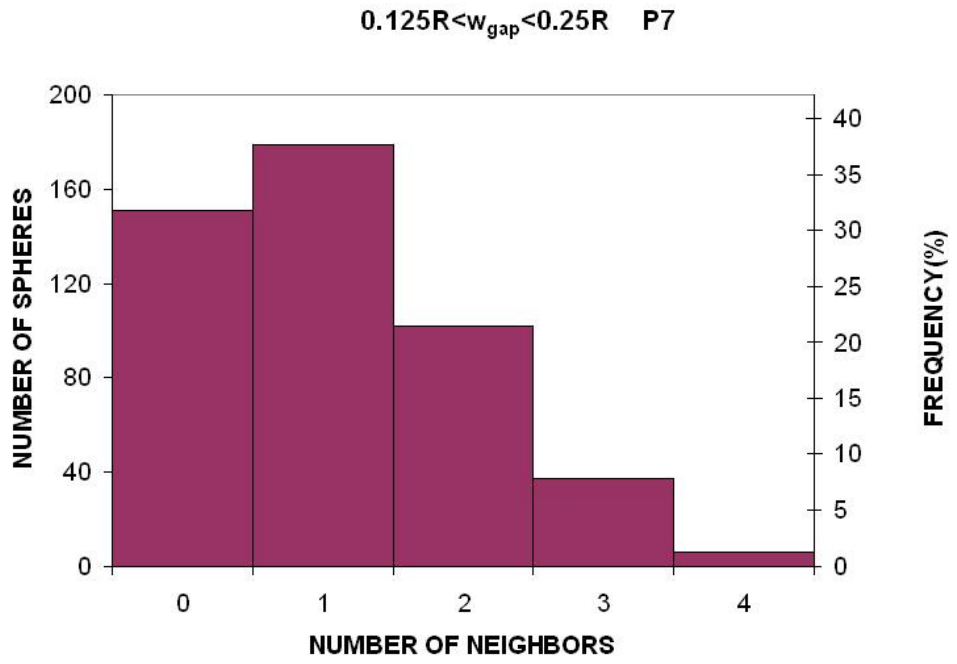

Figure 3.28: Histogram of number of neighbors within a gap width between 0.125 *R* to 0.25*R* for computer-generated packing 7. Average=1.03.

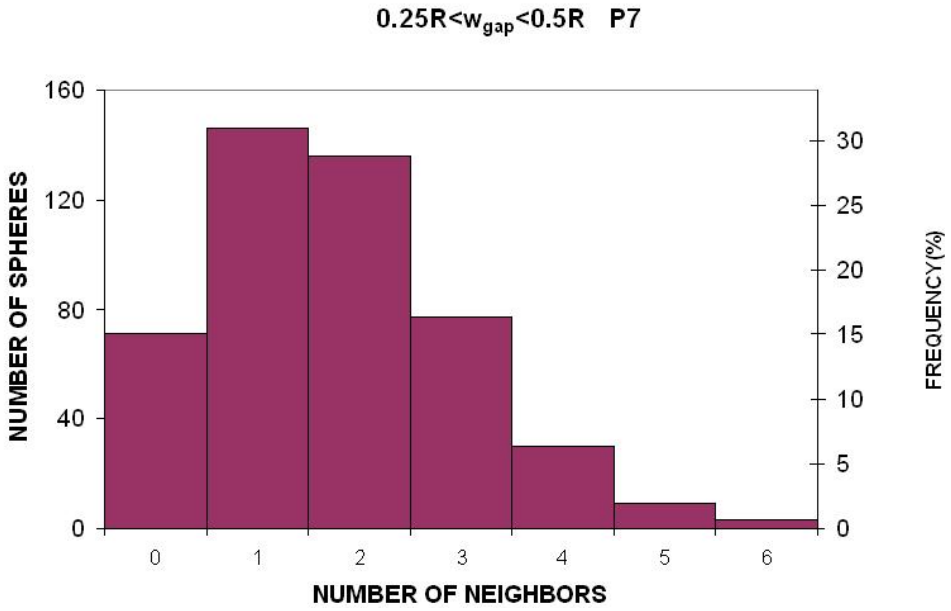

Figure 3.29: Histogram of number of neighbors within a gap width between 0.25 *R* to 0.5 *R* for computer-generated packing 7. Average=1.72.

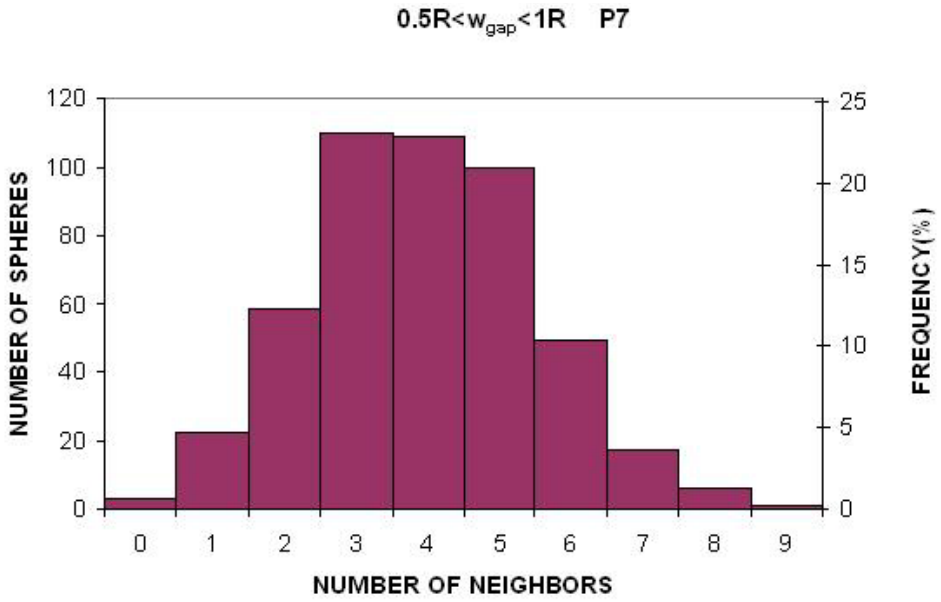

Figure 3.30: Histogram of number of neighbors within a gap width between 0.5 *R* to 1 *R* for computer-generated packing 7. Average=4.23.

For the three packings, as in the previous case (Figures 3.7 to 3.15) the number of neighbors increases when the range of widths increases. The three packings show similar averages values of neighbors for the same ranges of widths considered. Figures 3.31, 3.32, and 3.33 show the cumulative frequency of neighbors the Finney packing, packing 4 and packing 7 respectively. Note the similarity between the three plots.

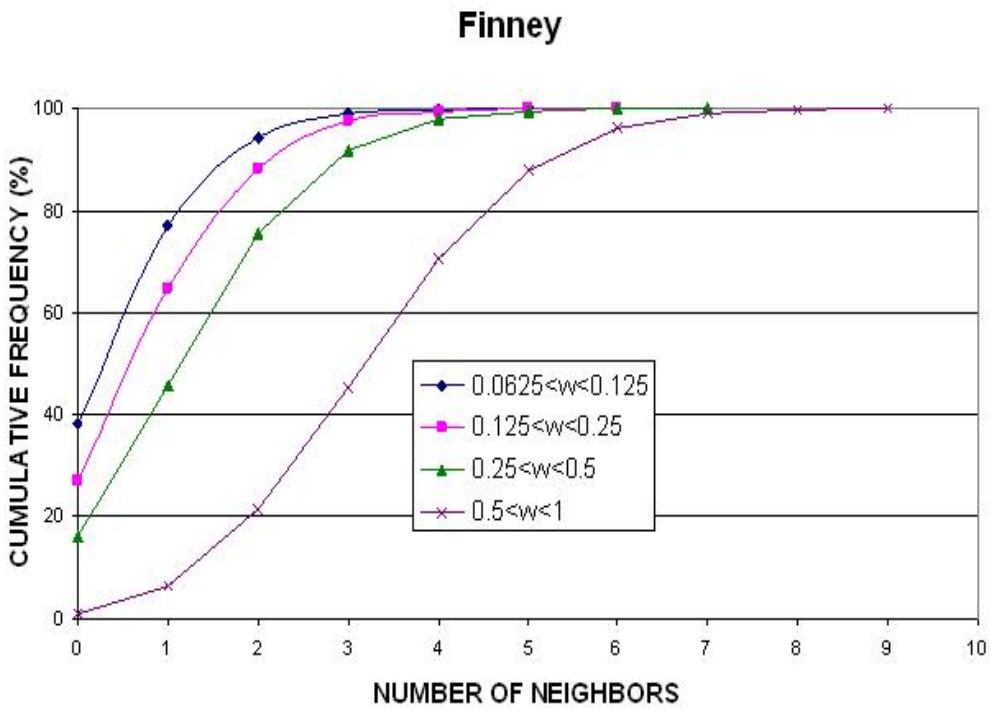

Figure 3.31: Cumulative frequency of number of neighbors within gap widths between 0.0625*R* to 0.125*R*, 0.125 *R* to 0.25 *R*, 0.25 *R* to 0.5 *R*, and 0.5R to 1*R* for Finney packing.

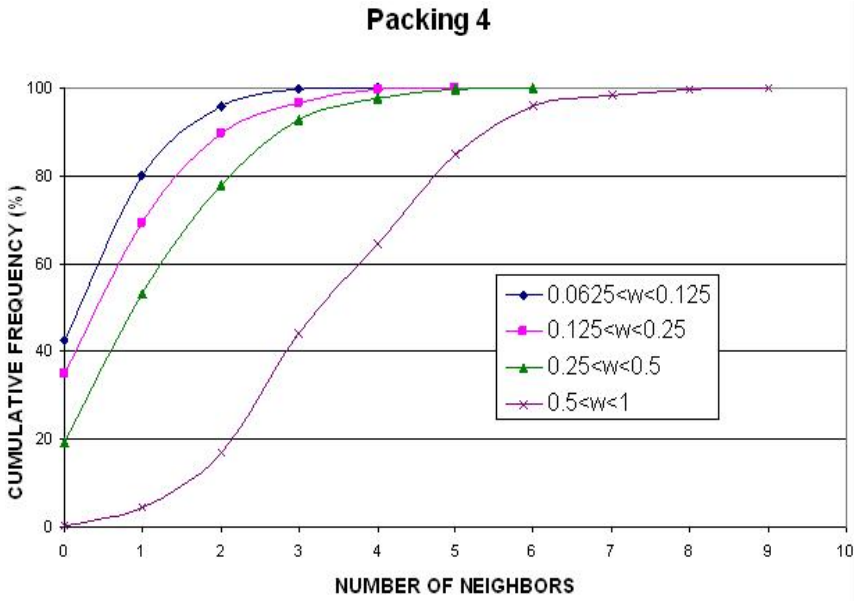

Figure 3.32: Cumulative frequency of number of neighbors within gap widths between 0.0625*R* to 0.125*R*, 0.125 *R* to 0.25 *R*, 0.25 *R* to 0.5 *R*, and 0.5R to 1*R* for computer-generated packing 4.

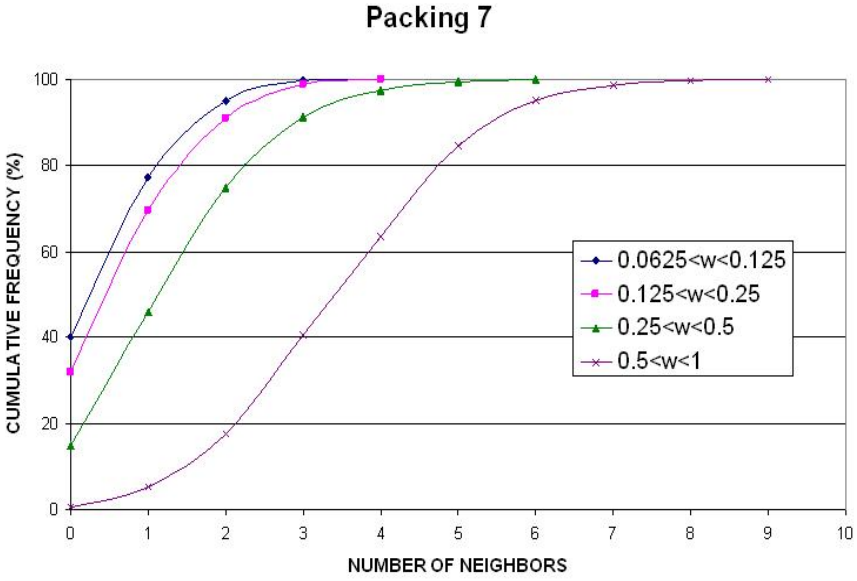

Figure 3.32: Cumulative frequency of number of neighbors within gap widths between 0.0625*R* to 0.125*R*, 0.125 *R* to 0.25 *R*, 0.25 *R* to 0.5 *R*, and 0.5R to 1*R* for computer-generated packing 7.

The number of neighbors within gap widths of 1*R*, 2*R*, 0.03*R*-0.0625*R* and 0.05*R* -0.1*R* has been also studied. Histograms relative to these ranges of gap widths are showed next for the Finney packing and the computer-generated packings 4 and 7. Figures 3.33 to 3.36 correspond to Finney packing, Figures 3.37 to 3.40 correspond to packing 4 and Figures 3.41 to 3.44 correspond to packing 7.

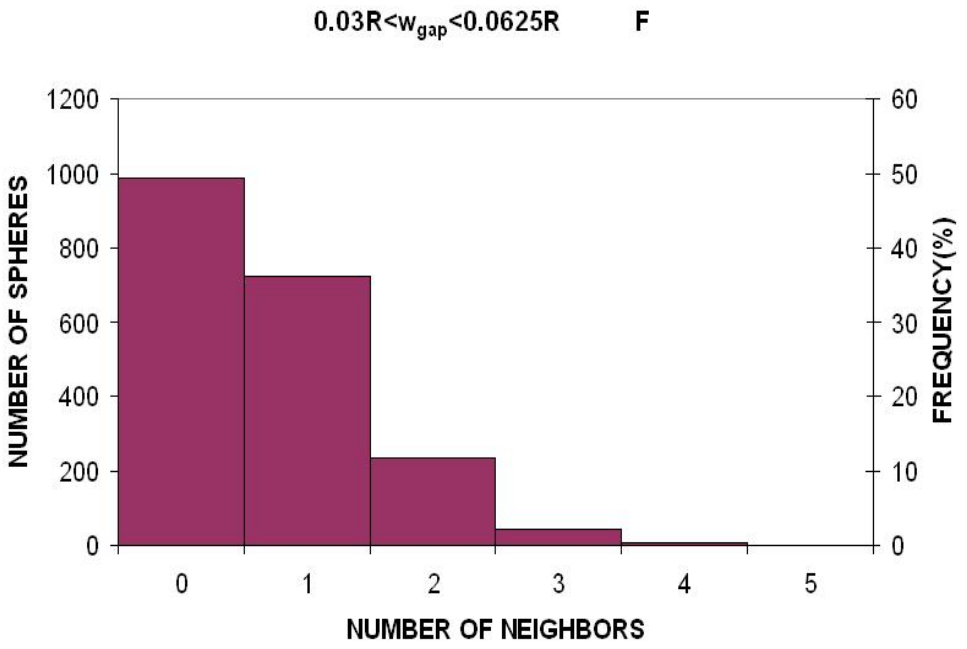

Figure 3.33: Histogram of number of neighbors within a gap width between 0.03 *R* and 0.0625 *R* for Finney packing. Average=0.68.

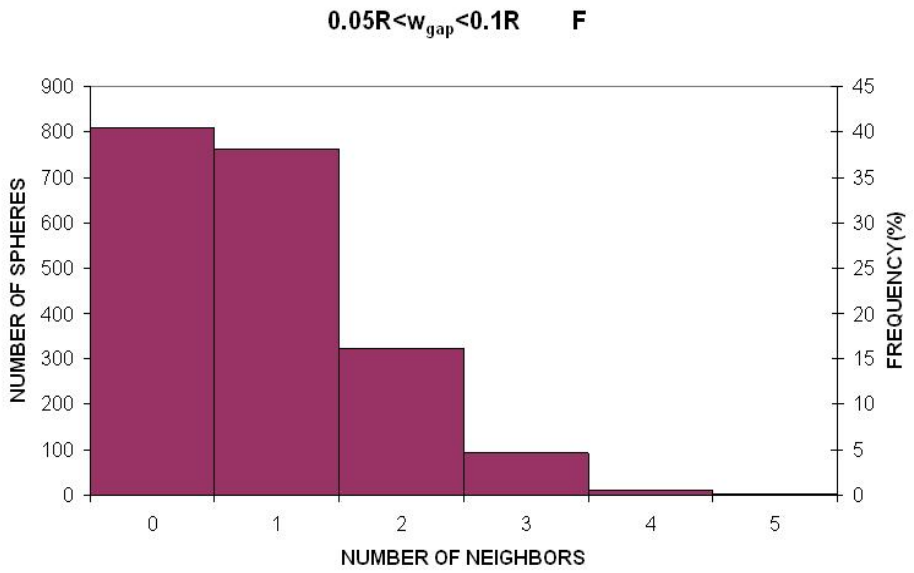

Figure 3.34: Histogram of number of neighbors within a gap width between 0.05 *R* and 0.1*R* for Finney packing. Average=0.87.

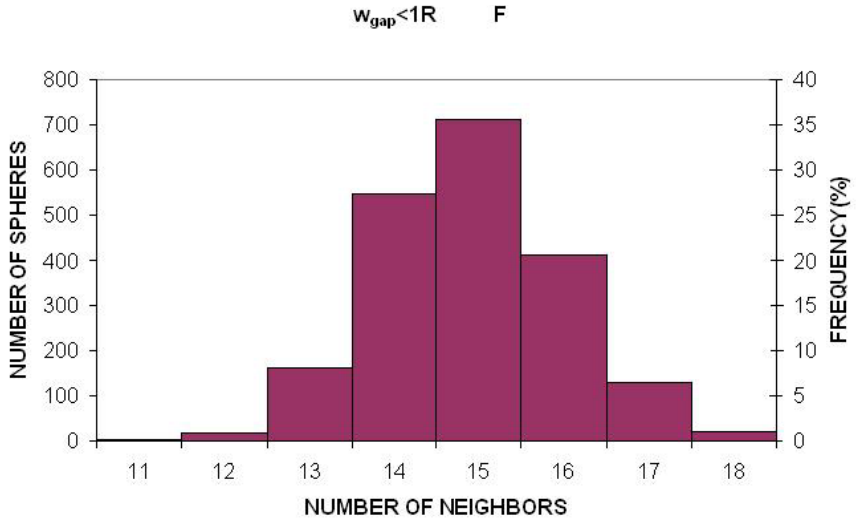

Figure 3.35: Histogram of number of neighbors within a gap width of 1*R* for Finney packing. Average=14.90.

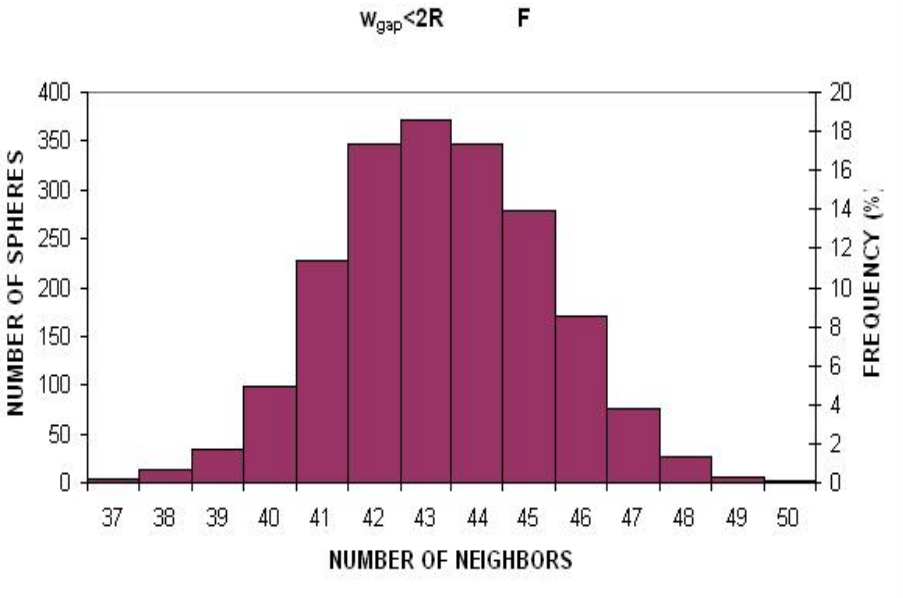

Figure 3.36: Histogram of number of neighbors within a gap width of 2*R* for Finney packing. Average=43.29.

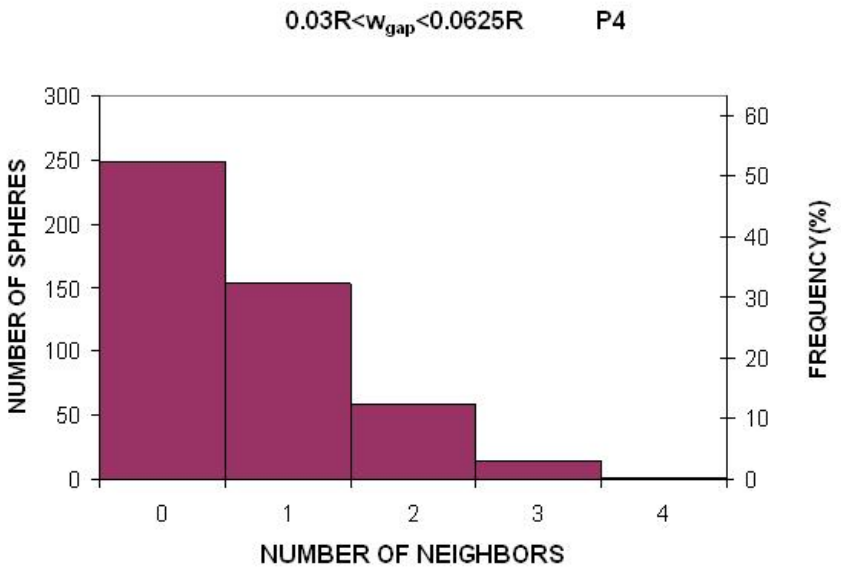

Figure 3.37: Histogram of number of neighbors within a gap width between 0.03 R and 0.0625 *R* for packing 4. Average=0.66.

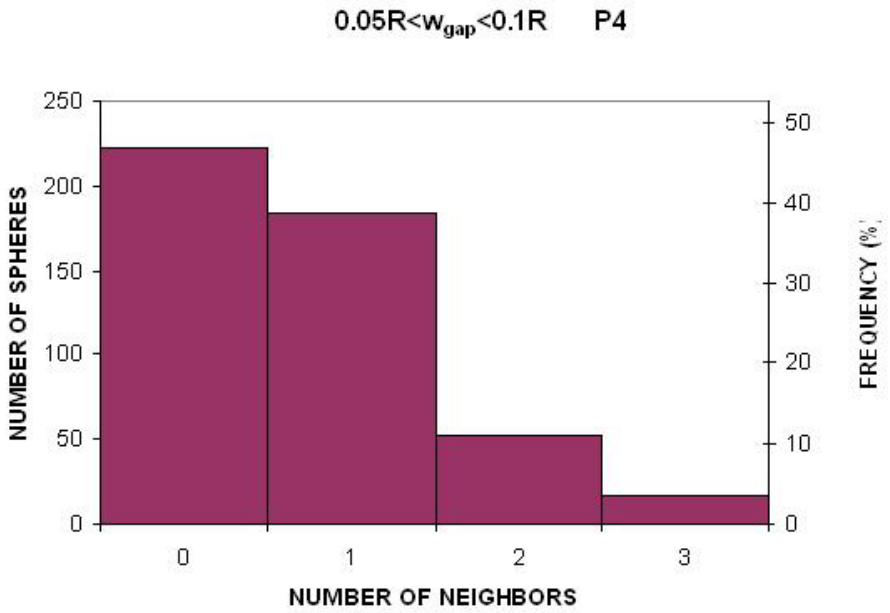

Figure 3.38: Histogram of number of neighbors within a gap width between 0.05 *R* and 0.1*R* for packing 4. Average=0.71.

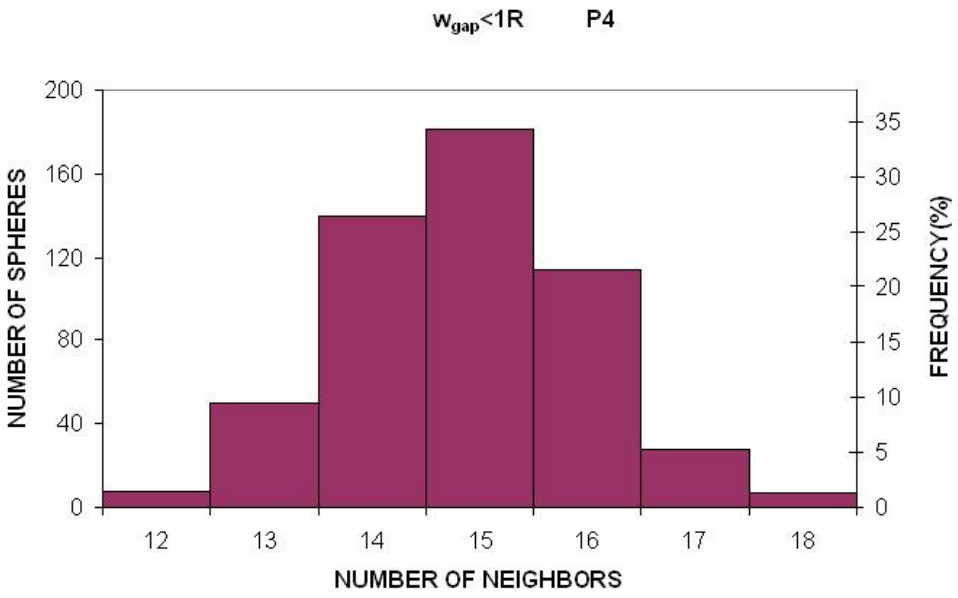

Figure 3.39: Histogram of number of neighbors within a gap width of 1*R* for packing 4. Average=14.86.

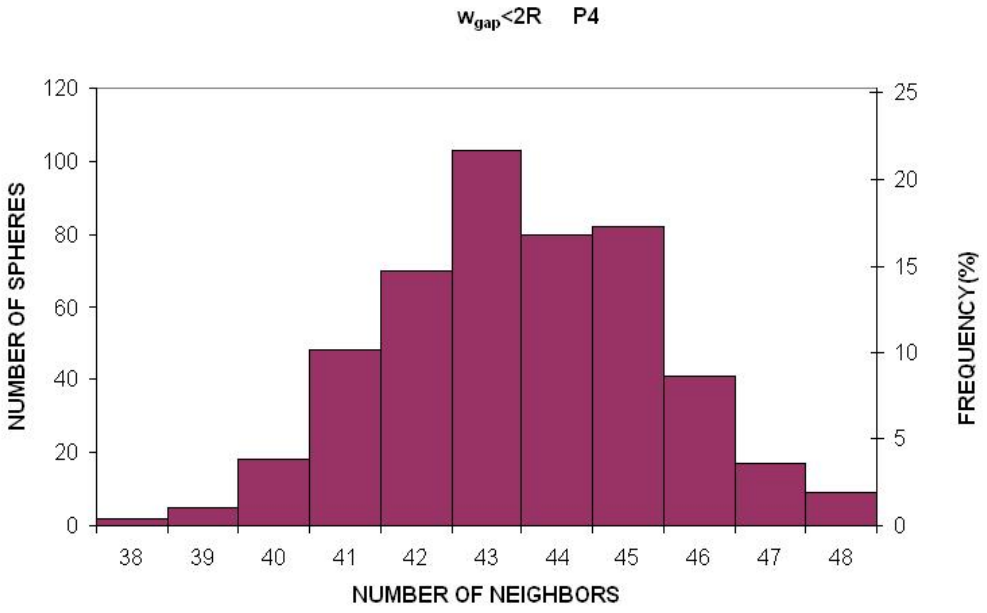

Figure 3.40: Histogram of number of neighbors within a gap width of 2*R* for packing 4. Average=43.48.

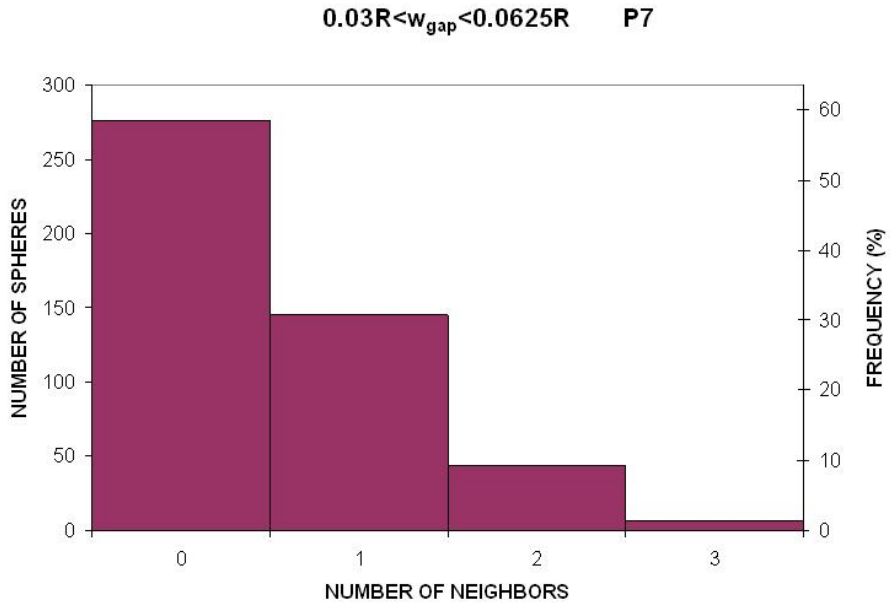

Figure 3.41: Histogram of number of neighbors within a gap width between 0.03 *R* and 0.0625 *R* for packing 7. Average=0.54.

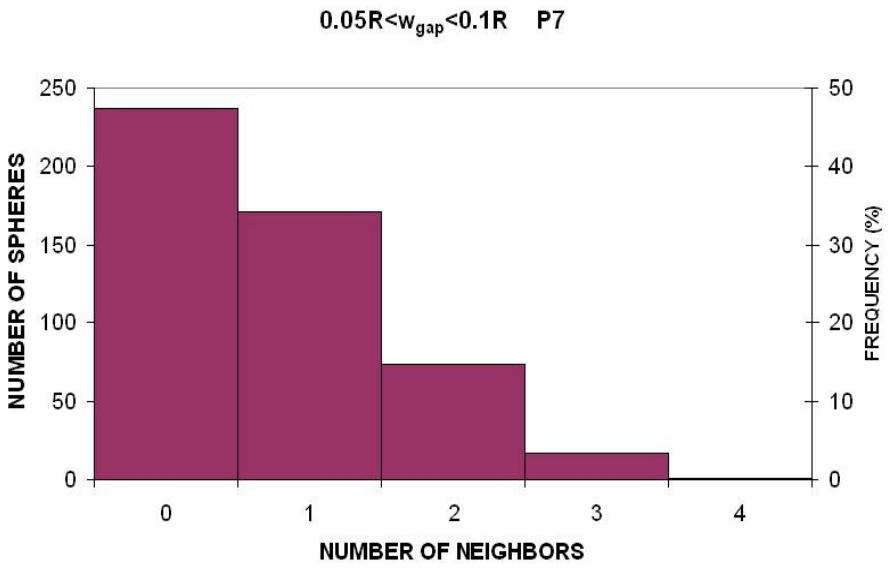

Figure 3.42: Histogram of number of neighbors within a gap width between 0.05 *R* and 0.1*R* for packing 7. Average=0.7.

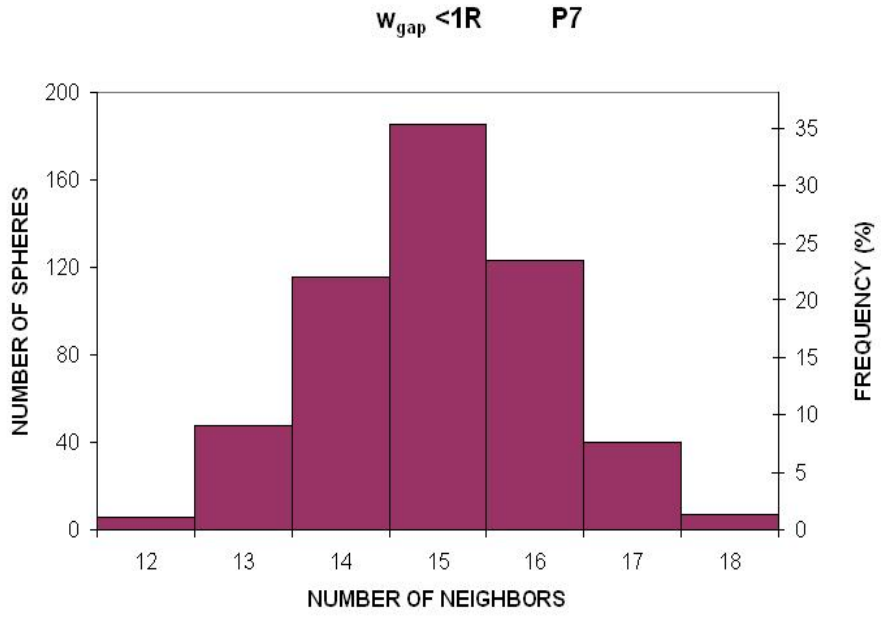

Figure 3.43: Histogram of number of neighbors within a gap width of 1*R* for packing7. Average=14.99.

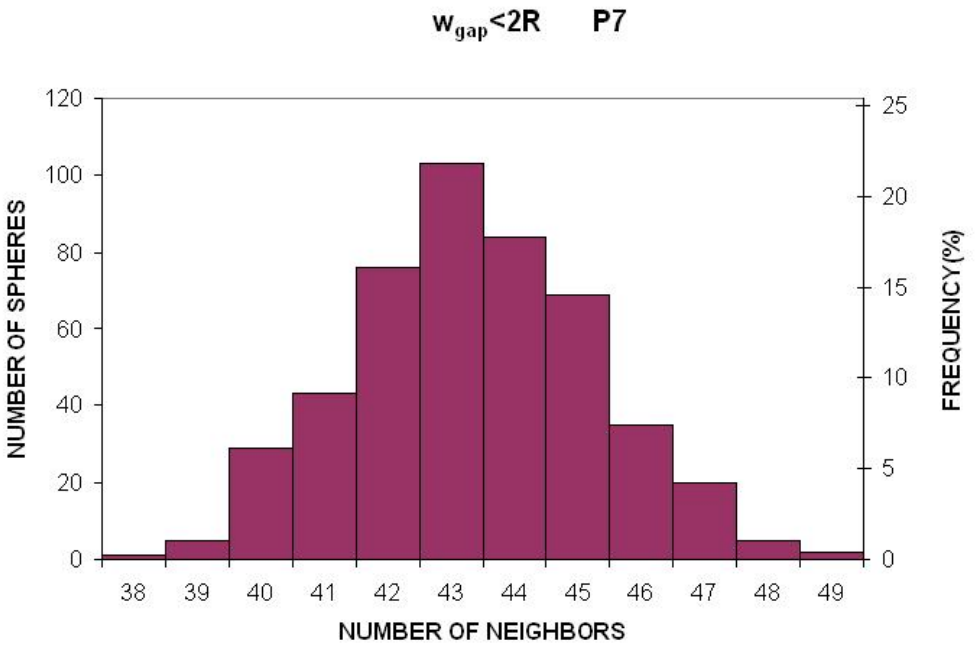

Figure 3.44: Histogram of number of neighbors within a gap width of 2*R* for packing7. Average=43.36.

The similarity between the histograms for the same range of widths is obvious. The computer-generated packings presented in general a smaller number of neighbors than the Finney pack for all the intervals of gap width studied. As stated before, this difference is due to the differences in porosity between the packings. The slightly smaller porosity of the Finney packing when compared with the computer-generated packings make it denser than those and this causes number of neighbors within a given gap width to be bigger. Nevertheless can be concluded that the statistics of the computer-generated packings, referent to the number of neighbors, are the same as the statistics of the Finney packing. Tables 3.5 and 3.6 in section 3.1.2 present the summary of the average number of neighbors within different gap widths for all the packings.

3.1.1 Point contacts

The point contacts have been determined by calculating the number of neighbors within distances of -0.0001*R* and +0.0001*R*, -0.001*R* and +0.001*R*, etc. (Negative values occur when two spheres overlap. This situation is described in more detail later in this section). Figures 3.45 to 3.47 show number of neighbors in the Finney packing within an absolute distance of 0.0001*R*, 0.001*R* and 0.01*R* respectively. The averages for each one of these examples are 0.1, 0.99 and 5.6. These results suggest a criterion of 0.01*R* for two spheres being in contact in the Finney packing. Therefore, 5.6 represents the average number of point contacts for the Finney packing. This value is in reasonable agreement with values obtained in previous studies. Bernal and Mason (1960) reported an average of 6.6 point contacts per sphere, Mellor (1989) reported 5.8 and Bryant and Johnson (2003) reported 5.9 point contacts per sphere.

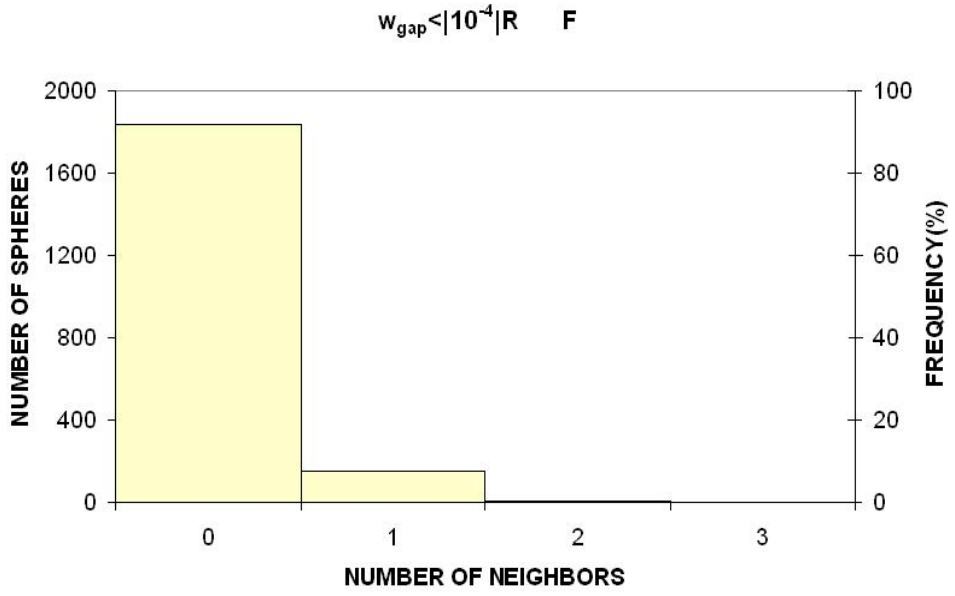

Figure 3.45: Neighbors within an absolute distance of 0.0001*R* for the Finney packing. Average=0.09

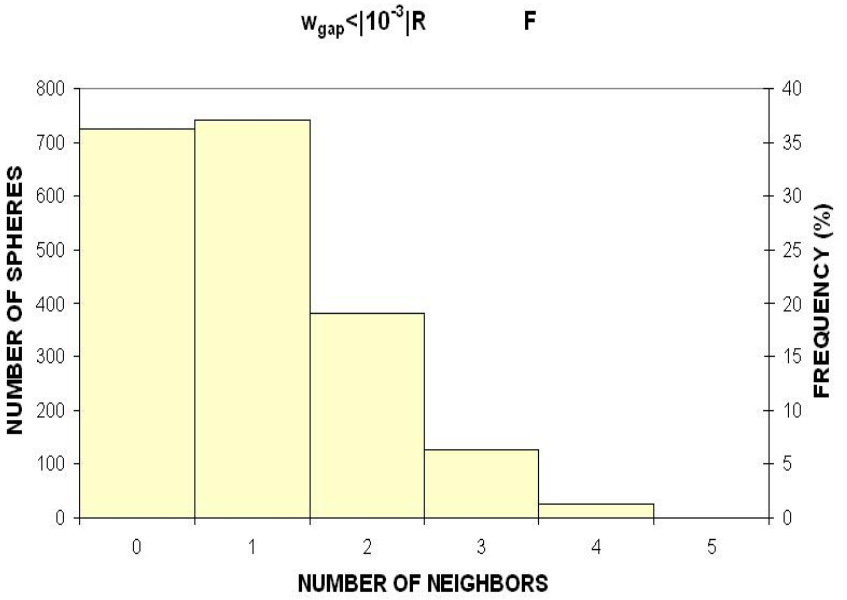

Figure 3.46: Neighbors within an absolute distance of 0.001*R* in Finney packing. Average=1.00.

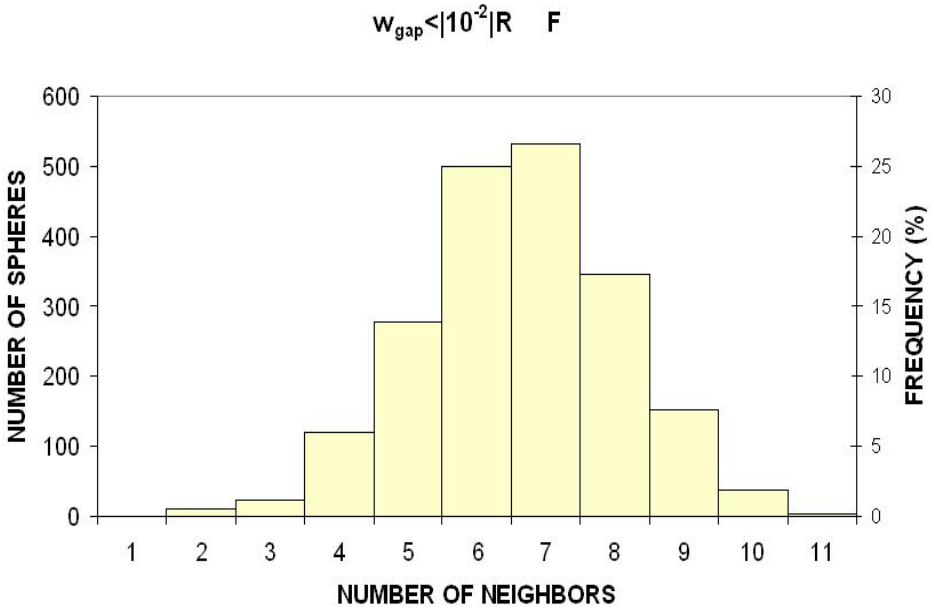

Figure 3.47: Neighbors within an absolute distance of 0.01*R* in Finney packing. Average=5.61.

The same analysis has been done for the computer-generated packings. Figures 3.48 to 3.50 show the number of neighbors within the absolute distances of 0.01R, 0.001R and 0.0001R for packing 7. The average number of point contacts for these cases are 5.21, 5.74 and 6.26 correspondingly. These numbers are bigger than the ones for the same distances in the Finney packing. Decreasing the range of distances to $|10^{-5}|R$ reduces the average number of neighbors to1.84, as it is shown in Figure 3.51.

There are many spheres that have two or fewer neighbors within gap widths of $|10^{-5}|R$ and $|10^{-4}|R$. If either value were taken as the threshold for point contacts, these packings could not be considered dense random packings since those spheres would be loose, floating in space. Thus the criterion for point contacts in the computer-generated packings is taken to be $|10^{-3}|R$. This value is consistent with the overlap tolerance used when creating the packing, which is 10^{-4}. It also yields an average number of contacts very close to the Finney pack.

The criterion for point contacts in the Finney packing, $|10^{-2}|R$, is derived from the precision in the measurement of the spatial coordinates of the ball bearing in the pack. The average number of point contacts in the computer-generated packings is 5.57 (see table 3.4 below) which is very close to the 5.61 point contact obtained for the Finney packing.

The histograms below correspond to packing 7; for the same range of gap widths, the differences between the average number of neighbors in different packings are unimportant. See Table 3.4 after the histograms.

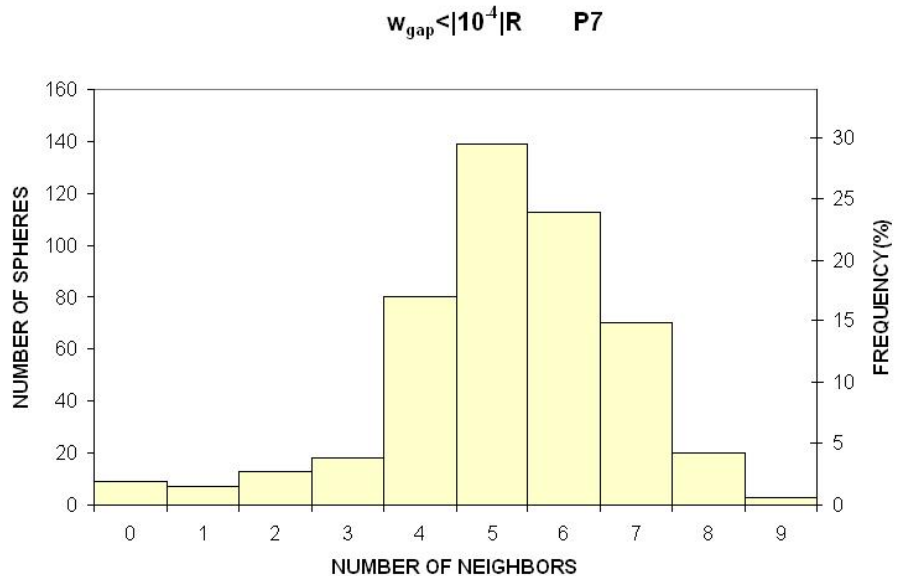

Figure 3.48: Number of neighbors within an absolute distance of $10^{-4}R$ for packing number 7. Average=5.21.

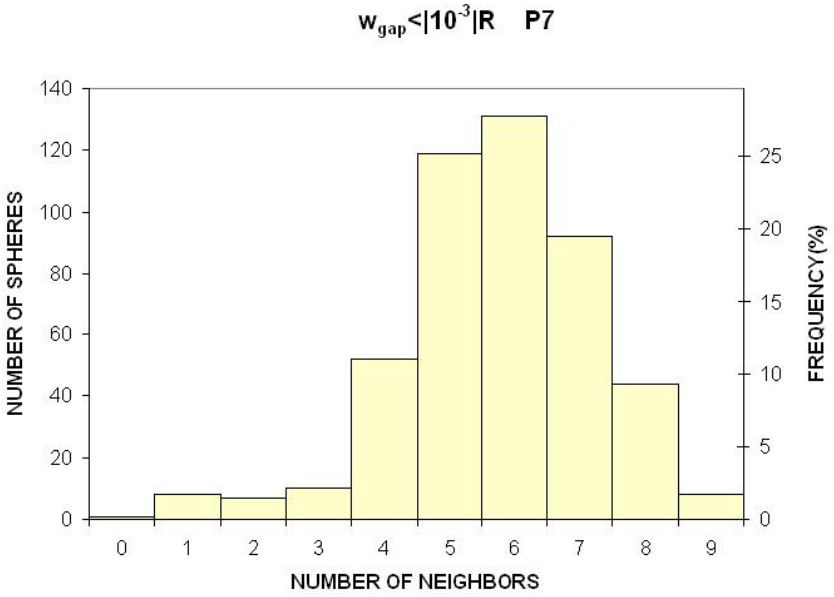

Figure 3.49: Number of neighbors within an absolute distance of $10^{-3}R$ for packing number 7. Average=5.74.

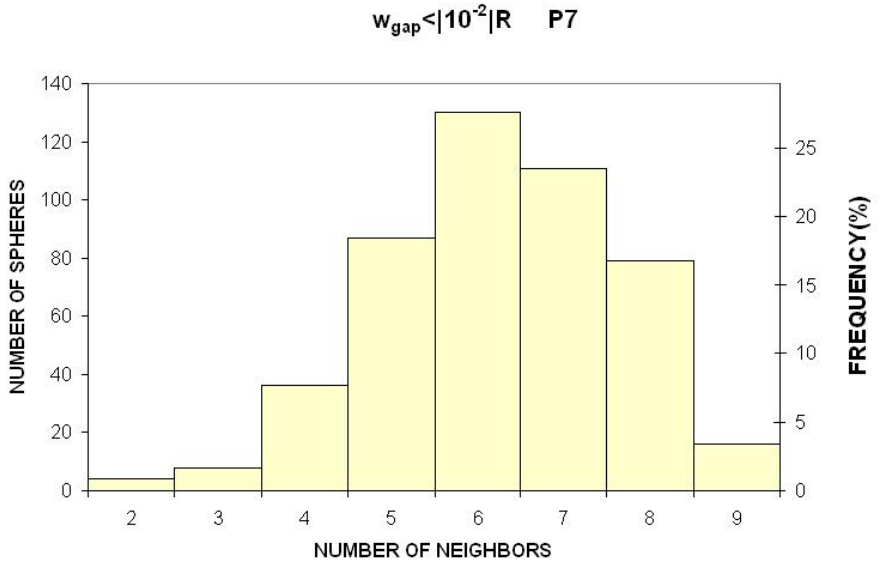

Figure 3.50: Number of neighbors within an absolute distance of $10^{-2}R$ for packing number 7. Average =6.26.

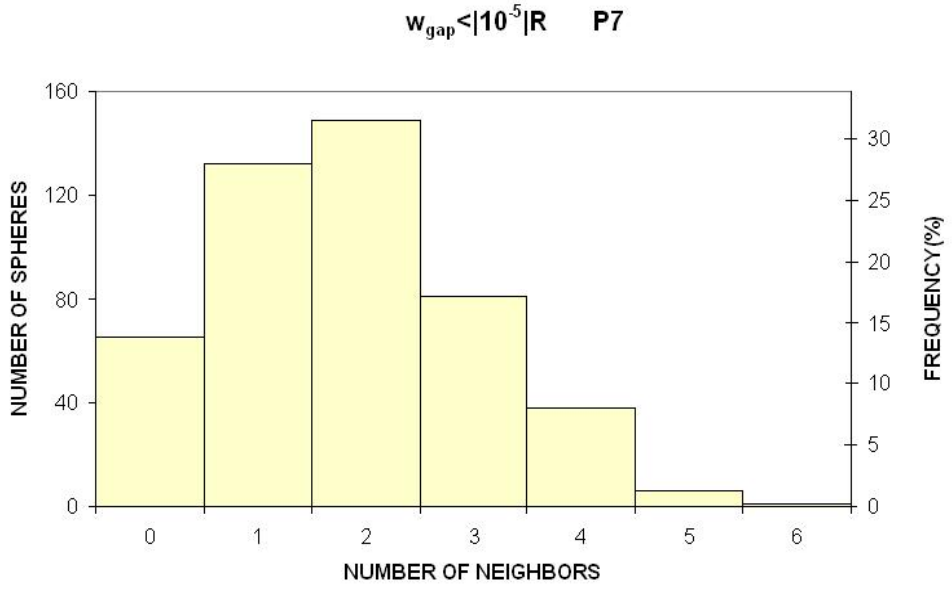

Figure 3.51: Number of neighbors within an absolute distance of $10^{-5}R$ for packing number 7. Average=1.84.

Table 3.4 presents the average number of neighbors within these small distances for the 10 computer generated packings and the Finney packing. All the computer generated packings have similar number of neighbors except for packing 10, which is made of 1000 spheres instead of 4000. Finney packing has a small number of neighbors within these small distances.

The number of neighbors within $10^{-3}R$ for the computer generated packings correspond to the number of point contacts and it is comparable to the number of neighbors within a distance of 0.01 for the Finney packing. Therefore, Finney packing has an average number of point contacts of 5.61 per sphere, while this value for the computer generated packings varies between 5.38 and 5.74.

Table 3.4: Number of neighbors within small gaps for all the packings studied.

	$w_{gap}<\|10^{-5}\|R$	$w_{gap}<\|10^{-4}\|R$	$w_{gap}<\|10^{-3}\|R$	$w_{gap}<\|10^{-2}\|R$	$w_{gap}<0R$
Finney	0.07	0.087	1.00	5.61	2.54
Packing 1	2.17	5.35	5.47	5.84	1.96
Packing 2	2.09	5.3	5.41	5.85	1.92
Packing 3	2.23	5.47	5.74	6.28	2.18
Packing 4	2.00	5.41	5.70	6.24	1.64
Packing 5	2.14	5.45	5.63	6.00	1.98
Packing 6	1.95	5.46	5.58	6.01	2.06
Packing 7	1.84	5.21	5.74	6.26	1.30
Packing 8	2.08	5.31	5.48	5.98	1.94
Packing 9	2.13	5.48	5.6	6.03	2.34
Packing 10	0.05	0.28	5.38	6.06	0.27

The number of neighbors within gaps widths smaller than zero corresponds in part to the point contacts and in part to the overlapping. According to the previous analysis, gap widths between -0.01R and 0R are considered point contacts in the Finney pack. Gap widths smaller than -0.01R are considered overlap. Including this overlap in the number of point contacts in the Finney packing yields an average of 5.7 point contacts. In the computer-generated packings, gap widths between $-10^{-3}R$ and 0R are considered point contacts while gap widths smaller than $-10^{-3}R$ are considered overlap. However the tolerance for overlap in the computer-generated packings is $10^{-4}R$, which in this case makes the overlap to be included with the point contacts. In order to properly compare Finney statistics for contacts with the computer-generated packs all the gaps smaller than 0.01R should be considered point contacts in the former, making 5.7 point contacts in the Finney pack comparable with the values of point contacts given for computer-generated packings in the fourth column of Table 3.4.

3.1.2 Summary

Tables 3.5 and 3.6 summarize the statistics regarding number of neighbors for both types of packings. The number showed in the table represents the average number of neighbor within the interval of gap width (w_{gap}) considered. The gap width is calculated as the distance between centers of spheres less the radius of the spheres:

$$w_{gap} = \sqrt{(x_1 - x_2)^2 + (y_1 - y_2)^2 + (z_1 - z_2)^2} - 2 \qquad \text{Eqn. 3.1}$$

There is a clear similitude between all the computer generated packings and also between the Finney packing and these packings. The Finney packing is slightly denser than the computer generated packings, and thus has slightly more gaps in the range of interest.

In Table 3.5 the gap width has been reduced 50% in each column. The number of neighbors in these cases decreases accordingly.

Table 3.6 shows the statistics for another set of gap widths. The range $0.03R<w_{gap}<0.1R$ is the range of interest for this study, corresponding to the size of particles that are retained in experiments discussed in previous chapters. The range $0.1R<w_{gap}<0.3R$ corresponds to portions of the pore space that are bigger than gaps but smaller than pore throats. Remember the smallest pore throat has a diameter of $0.3R$. The range $0.01R<w_{gap}<0.03R$ correspond to the gaps immediately smaller than the range of interest. Gaps smaller than 0.01 are considered point contacts in the Finney packing.

Figures 3.52 and 3.53 presented after tables 3.5 and 3.6 show histograms of number of neighbors for some of the width intervals studied. Figure 3.52 plots number of neighbors within widths intervals of 0.0625R-0.125R, 0.12R-0.25R, 0.25R-0.5R, and 0.5R-0-1R using the data from Table 3.5 and Figure 3.53 plots number of neighbors within widths intervals of 0.01R-0.03R, 0.03R-0.1R and 0.01R-0.3R with data from Table 3.6.

Table 3.5: Summary of average number of neighbors within gaps of different widths in Finney and computer generated packings (1).

	Range of gap widths					
Packing	**w_{gap}<2R**	**w_{gap}<1R**	**0.5R<w_{gap}<1R**	**0.25R<w_{gap}<0.5R**	**0.125R<w_{gap}<0.25R**	**0.0625R<w_{gap}<0.125R**
Finney	43.29	14.90	3.73	1.73	1.24	0.92
Packing 1	41.09	14.7	4.32	1.73	1.16	0.64
Packing 2	41.08	14.61	4.27	1.74	0.99	0.68
Packing 3	43.32	14.94	3.92	1.84	0.97	0.75
Packing 4	43.48	14.86	3.91	1.59	1.10	0.82
Packing 5	41.23	14.72	4.34	1.67	1.00	0.73
Packing 6	41.66	14.74	4.09	1.85	1.04	0.67
Packing 7	43.36	14.99	3.94	1.76	1.09	0.88
Packing 8	41.17	14.64	4.23	1.72	1.03	0.68
Packing 9	41.34	14.63	4.17	1.78	1.01	0.67
Packing 10	42.63	14.67	3.64	1.96	1.05	0.69

Table 3.6: Summary of number of neighbors within gaps of different widths in Finney and computer generated packings (2)

	Range of gap widths				
Packing	**$0.01R<w_{gap}<0.03R$**	**$0.03R<w_{gap}<0.0625R$**	**$0.03R<w_{gap}<0.1R$**	**$0.05R<w_{gap}<0.1R$**	**$0.1R<w_{gap}<0.3R$**
Finney	0.90	0.68	1.31	0.87	1.93
Packing 1	0.44	0.57	0.97	0.56	1.78
Packing 2	0.51	0.57	1.05	0.68	1.56
Packing 3	0.56	0.61	1.07	0.67	1.69
Packing 4	0.53	0.66	1.17	0.71	1.76
Packing 5	0.43	0.55	0.99	0.62	1.66
Packing 6	0.55	0.53	0.95	0.62	1.67
Packing 7	0.51	0.54	1.08	0.70	1.85
Packing 8	0.45	0.54	0.94	0.60	1.68
Packing 9	0.45	0.51	0.93	0.57	1.64
Packing 10	0.55	0.70	1.11	0.65	1.87

The average number of neighbors in the range of interest ($0.03R<w_{gap}<0.1R$) is 1.31 for the Finney packing and it varies between 0.93 and 1.17 for the other packs. Thus, each grain in a dense random packing of equal spheres will have about one gap that can trap particles in the size range of interest. This presents some preliminary support for the feasibility of the hypothesis of this research. Also from the table, the number of neighbors within a distance from $0.01R$ to $0.1R$ can be calculated by adding the number of neighbors within $0.01R$-$0.03R$ and $0.03R$-$0.1R$. This number is 2.21 for the Finney packing and it varies between 1.38 and 1.7 for the computer-generated packs. Therefore, every sphere in the packings has at least one neighbor within a distance considered *gap*, not *pore throat*.

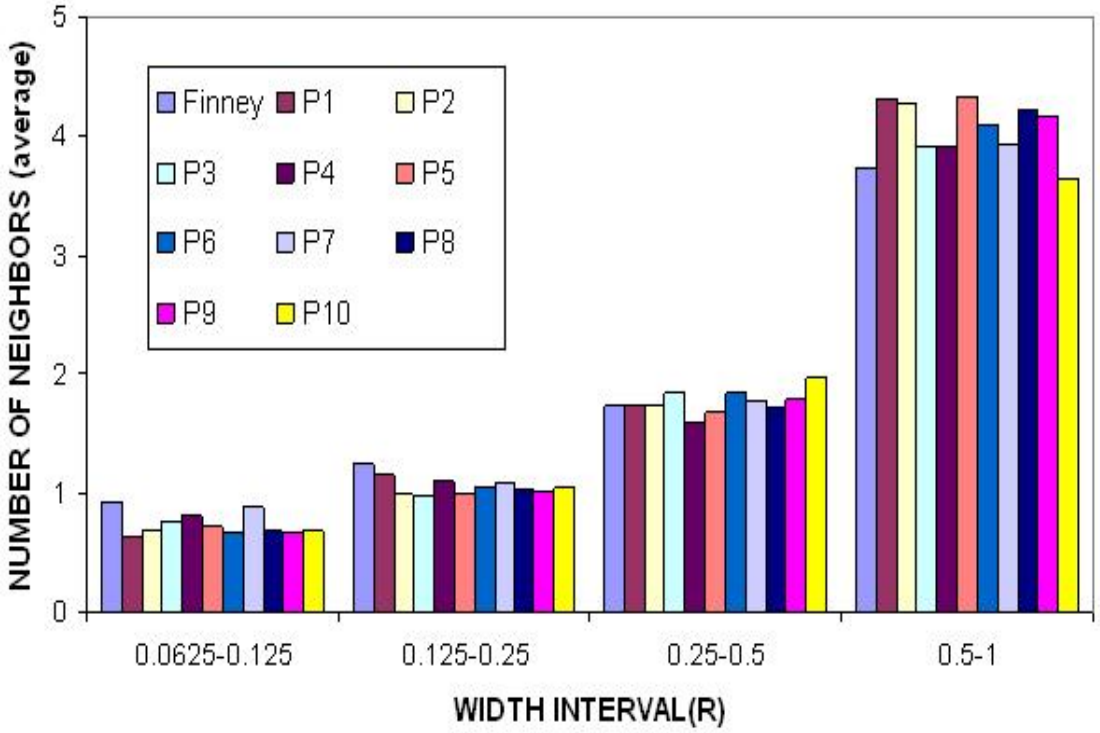

Figure 3.52: Average number of neighbors for different widths intervals for the Finney and computer generated packings (1).

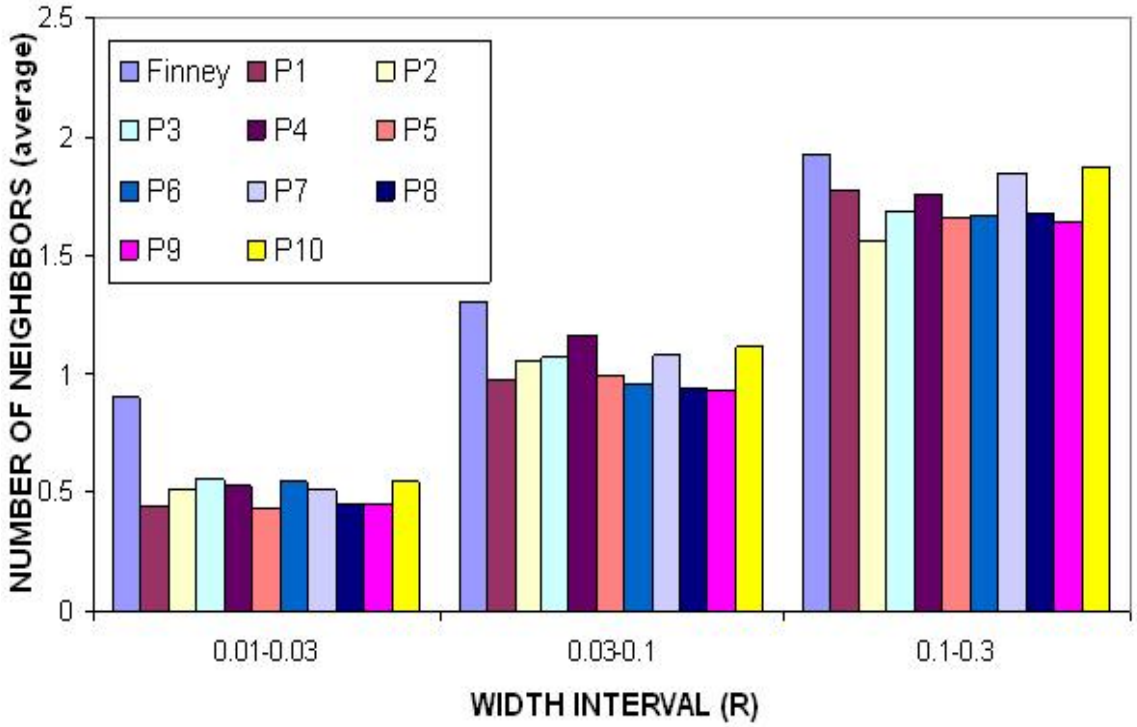

Figure 3.53: Average number of neighbors for different widths intervals for the Finney and computer generated packings (2).

3.2 DISTRIBUTION OF GAP WIDTHS

The influence of a gap in the straining model that will be presented in Chapter 5 depends on its frequency and the flow rate through it. The same code that calculates the number of neighbors for each sphere provides the widths of gaps between spheres. It calculates the distance from the center of one sphere to the centers of all the other ones. The gap width is determined by subtracting the particle diameter from the distance between centers (recall figure 1.1b and equation 3.1).

Also the number of gaps in the packing having a certain width has been calculated. This number divided by the volume of the packing provides the density of gaps.

Table 3.7 summarizes the number of gaps in the Finney packing. Remember that gaps bigger than 0.1 are considered part of the pore throat.

Table 3.7: Number of gaps in the Finney pack

Gap width	**Number of gaps in Finney Pack** (central 2000 spheres)
Point contacts (<0.01R)	6178
0.01R-0.03R	993
0.03R-0.1R*	1449
0.1R-0.5R	3653

*Range of interest for straining small particles

The number of point contacts in the packing is not just the result of multiplying the average number of point contacts per sphere (5.7) by the number of spheres (2000) and then dividing by 2. This is because not all the point contacts between the 2000 spheres involve two spheres within those 2000. Remember that the statistics are gathered around the inner 2000 spheres but a total of 4021 spheres are considered when calculating neighbors. To cite an example, sphere 1048 has 4 point contacts with spheres 1335, 1443, 1573, and 2006. Point contacts with spheres 1335 1443 and 1573, are counted again as a point contact for the latter spheres. But the point contact with sphere 2006 is only counted once, since the number of points contacts for spheres whose id is bigger than 2000 are not considered for the statistics.

The number of gaps shown in table 3.7 and subsequent tables 3.8, 3.9 and 3.10 have also been calculated this way for the inner 2000 spheres.

The portion of the Finney packing considered in this thesis is a sphere of radius about 15.6R. Its volume is then 15,900R^3.

The total number of gaps (between 0.01R and 0.1R) is 2442, which yields a gap density of 0.15 per R^3 bulk volume. The density of gaps in the range of interest is about 0.10 per R^3 bulk volume, which is enough to trap a significant number of particles. The gap densities are comparable to the density of small throats (unambiguously identified via Delaunay tessellation of sphere centers) which is about 0.3 per R^3. Tables 3.8 to 3.10 summarize these calculations for Finney and computer generated packings. The density of gaps shown refers to the total number of gaps (n_T).

Table 3.8: Number of gaps of different sizes and density of gaps for Finney packing.

Range of gap widths	**Number of gaps (n)**
0.01*R*-0.03*R*	993
0.03*R*-0.1*R*	1449
Total (n_T)	2442
Pack Volume (R^3)	15900
Density (gaps/R^3)	**0.15**

Table 3.9: Number of gaps of different sizes and density of gaps for computer generated packings 1 to 5

	Number of gaps (n)				
Range of gap widths	**P1**	**P2**	**P3**	**P4**	**P5**
0.01*R*-0.03*R*	98	113	139	126	98
0.03*R*-0.1*R*	226	240	253	269	240
Total (n_T)	324	353	392	395	338
Pack Volume (R^3)	3131.36	3112.14	3112.14	3112.14	3112.14
Density (gaps/R^3)	**0.10**	**0.11**	**0.13**	**0.13**	**0.11**

Table 3.10: Number of gaps of different sizes and density of gaps for computer generated packings 6 to 10

	Number of gaps (n)				
Range of gap widths	**P6**	**P7**	**P8**	**P9**	**P10**
0.01*R*-0.03*R*	125	125	101	100	31
0.03*R*-0.1*R*	224	258	222	211	59
Total (n_T)	349	383	323	311	90
Pack Volume (R^3)	3150.67	3112.14	3241.79	3112.14	736.31
Density (gaps/R^3)	**0.11**	**0.12**	**0.10**	**0.10**	**0.12**

The volume of the packings is calculated according to the dimensions of the packings given in table 3.1. The average density of gaps in the computer generated packing is 0.11gaps/R^3 which is one third smaller than the density of gaps in the Finney packing (0.15gaps/R^3).

The smaller density of gaps of any size in the computer generated packings may be related to the fact that the tolerance for point contacts in Finney packing is 0.01R while this tolerance for the computer-generated packings is 0.001R. Tables 3.9 and 3.10 present the number of gaps within distances of 0.01R-0.03R and 0.03R-0.1R in the computer-generated packings in order to compare with the values obtained in the Finney packing, shown in Table 3.8. But gap widths between 0.001R and 0.01R, considered point contacts in the Finney packing, are distinguishable as small gaps in the computer generated packings. For example, a gap of width 0.0015R is considered point contact in the Finney packing but not in the computer-generated packings.

Table 3.11 shows the number of gaps whose width is between 0.001R and 0.01R in the computer generated packings, called n*. These values are added to the number of gap widths between 0.01 and 0.03 shown in tables 3.9 and 3.10 yielding a new total number of gaps n_T', and the new density is calculated.

Table 3.11: New gap densities for the computer generated packings.

Packing	**n***	**n_T'**	**gaps/R^3**
P1	85	409	0.13
P2	98	451	0.14
P3	127	519	0.17
P4	128	523	0.17
P5	93	431	0.14
P6	99	448	0.14
P7	130	513	0.16
P8	111	434	0.13
P9	93	401	0.13
P10	39	129	0.17

The average gap density between the ten computer-generated packings, for gap width smaller than 0.1R is now 0.15gaps/R^3, which is the same obtained for the Finney packing.

The density of gaps has been also calculated for the intervals of gap width 0.01R-0.02R, 0.02R-0.03R, 0.03R-0.04R, 0.04R-0.05R, 0.05R-0.06R, 0.06R-0.07R, 0.07R-0.08R, 0.08R-0.09R, and 0.09R-0.1R. The results are shown in tables 3.12 and 3.13.

Table 3.12: Number of gaps (n) for different intervals of gap width

	Gap width interval								
	0.01*R* to 0.02*R*	0.02*R* to 0.03*R*	0.03*R* to 0.04*R*	0.04*R* to 0.05*R*	0.05*R* to 0.06*R*	0.06*R* to 0.07*R*	0.07*R* to 0.08*R*	0.08*R* to 0.09*R*	0.09*R* to 0.1*R*
Packing	n	n	n	n	n	n	n	n	n
Finney	635	358	279	209	217	197	197	177	173
Packing 1	62	36	48	45	32	26	27	29	19
Packing 2	56	57	43	42	37	25	32	38	23
Packing 3	71	68	47	48	46	31	31	21	29
Packing 4	80	46	61	45	37	31	29	30	36
Packing 5	56	42	41	50	35	31	24	36	23
Packing 6	66	59	37	42	37	30	24	26	28
Packing 7	68	57	41	40	39	32	30	38	38
Packing 8	59	42	45	36	37	27	29	23	25
Packing 9	61	39	48	38	25	32	23	20	25
Packing 10	20	11	11	12	11	2	10	6	7

Table 3.13: Density of gaps for different intervals of gap width

	Gap width interval								
	0.01*R* to 0.02*R*	0.02*R* to 0.03*R*	0.03*R* to 0.04*R*	0.04*R* to 0.05*R*	0.05*R* to 0.06*R*	0.06*R* to 0.07*R*	0.07*R* to 0.08*R*	0.08*R* to 0.09*R*	0.09*R* to 0.1*R*
Packing	gaps/R^3	gaps/R^3	gaps/R^3	gaps/R^3	gaps/R^3	gaps/R^3	gaps/R^3	gaps/R^3	gaps/R^3
Finney	0.040	0.023	0.018	0.013	0.014	0.012	0.012	0.011	0.011
Packing 1	0.020	0.011	0.015	0.014	0.010	0.008	0.009	0.009	0.006
Packing 2	0.018	0.018	0.014	0.013	0.012	0.008	0.010	0.012	0.007
Packing 3	0.023	0.022	0.015	0.015	0.015	0.010	0.010	0.007	0.009
Packing 4	0.026	0.015	0.020	0.014	0.012	0.010	0.009	0.010	0.012
Packing 5	0.018	0.013	0.013	0.016	0.011	0.010	0.008	0.012	0.007
Packing 6	0.021	0.019	0.012	0.013	0.012	0.010	0.008	0.008	0.009
Packing 7	0.022	0.018	0.013	0.013	0.013	0.010	0.010	0.012	0.012
Packing 8	0.018	0.013	0.014	0.011	0.011	0.008	0.009	0.007	0.008
Packing 9	0.020	0.013	0.015	0.012	0.008	0.010	0.007	0.006	0.008
Packing 10	0.027	0.015	0.015	0.016	0.015	0.003	0.014	0.008	0.010

Figure 3.54 shows the histogram of gap densities for the Finney packing and 10 computer generated packings. The general trend in Figure 3.54 is a decrease in the density of gaps when the gap width increases.

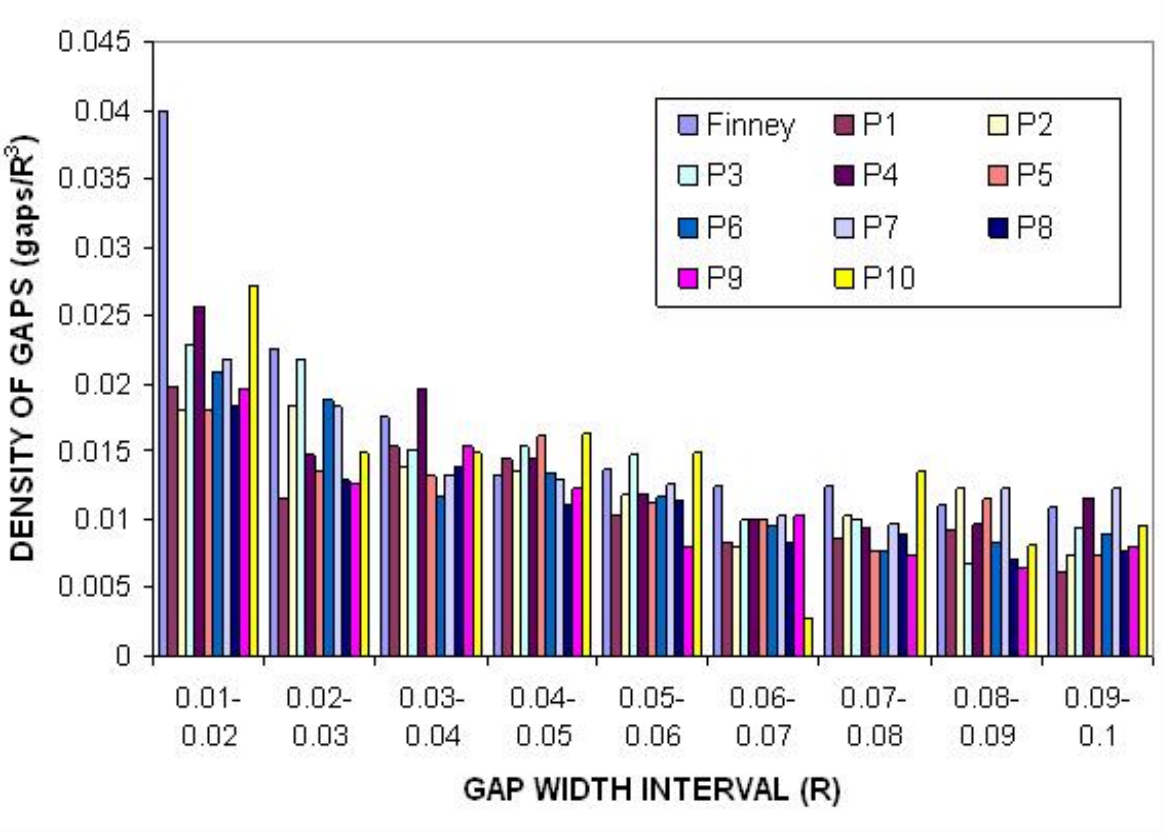

Figure 3.54: Histogram gap density *vs*. gap size for the Finney packing and the 10 computer generated packings.

The results presented in this section show a great similarity between Finney and computer-generated packings. The average number of neighbors within given gap widths and the density of small gaps proved to be comparable in all the packings. Since the statistics concerning these two types of packings are comparable, the computer-generated packings can be used as well as models for ideal soils to test pore-level theories and models.

3.3 DISTRIBUTION OF DELAUNAY CELLS FOR GAPS

Another method to describe the geometry of the pore space is presented in this section. The Delaunay cells surrounding a gap identify the pore bodies and pore throats associated with that gap. Each gap between a pair of grains is associated with a cluster of pores identified by the Delaunay tessellation as shown in figure 3.55. The figure shows that the spheres making the gap AA' are part of at least 5 Delaunay cells.

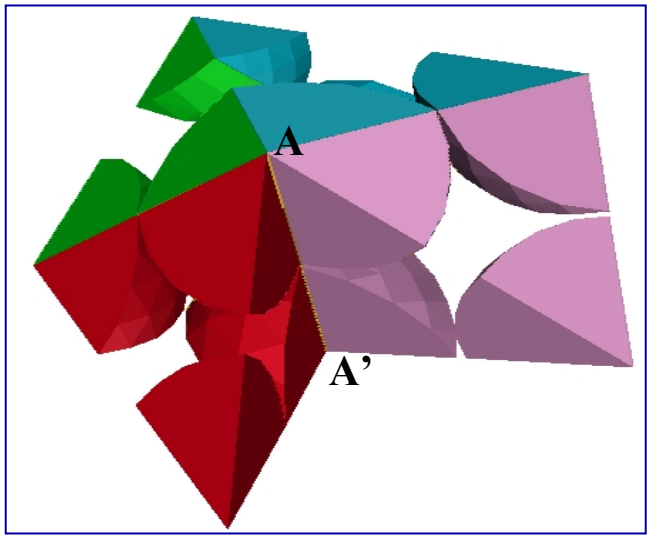

Figure 3.55: Cluster of five pores surrounding a small gap between grains A and A' (from Bryant and Johnson, 2003)

Pictures of the spheres surrounding the spheres defining the gap are shown later in this section. For the Finney and computer-generated packings a list of all Delaunay cells containing those spheres has been generated. Figures 3.56 to 3.59 show histograms of frequency of the number of Delaunay cells in which a gap is contained for the Finney packing.

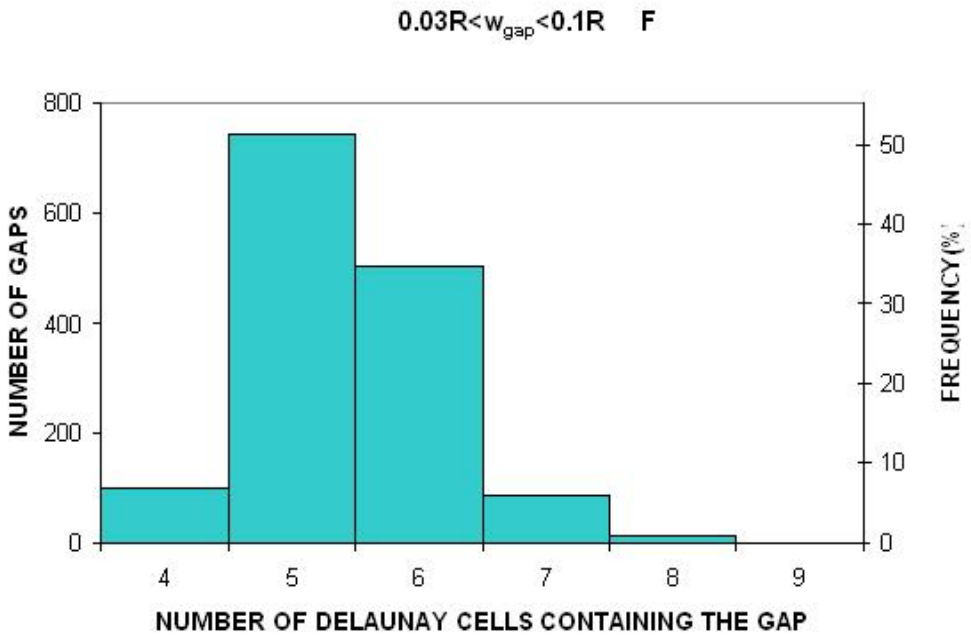

Figure 3.56: Frequency histogram for gap widths within 0.03*R* and 0.1*R* in the Finney packing.

This histogram shows that, for example, approximately 50% of the gaps in the range of interest are part of clusters of 5 Delaunay cells and that approximately 35% of the gaps are included in clusters of 6 Delaunay cells. Figures 3.57 and 3.58 show equivalent histograms for bigger and smaller ranges of gap widths respectively.

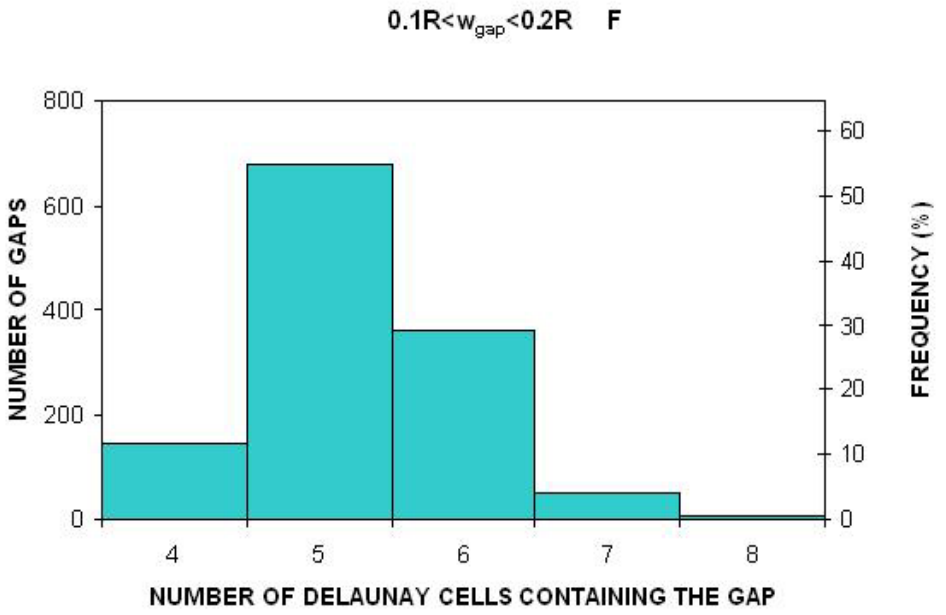

Figure 3.57: Frequency histogram for gap widths within 0.1*R* and 0.2*R* in the Finney packing.

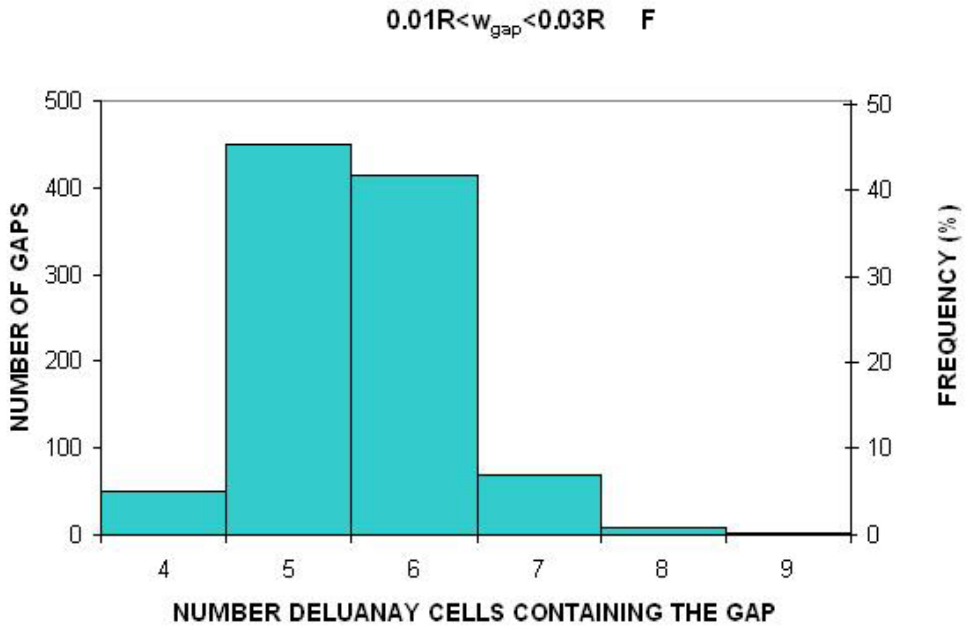

Figure 3.58: Frequency histogram for gap widths within 0.01*R* and 0.03*R* in the Finney packing.

There is a small difference among the number of Delaunay cells containing a gap when the width are between 0.01*R* and 0.2*R*. Figure 3.59 shows the same histogram for bigger gaps. For gaps widths within 0.2*R* and 0.5*R* the difference is slightly bigger. These gaps are already part of the pore throat.

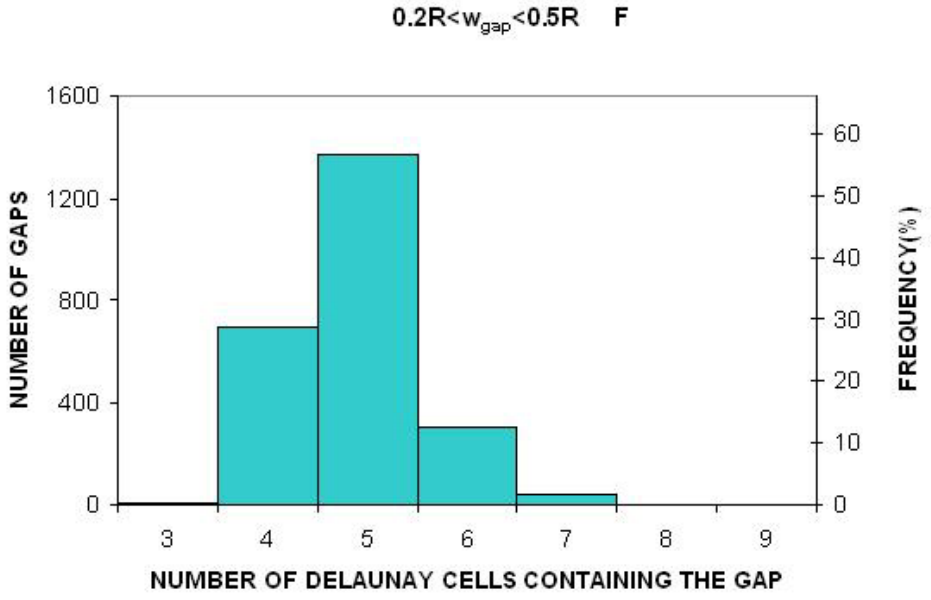

Figure 3.59: Frequency histogram for gap widths within 0.2*R* and 0.5*R* in the Finney packing.

Table 3.14 summarizes the number of Delaunay cells containing gaps of different widths and Figure 3.60 shows the cumulative frequency of number of cells for gap for the previous examples. The average number of Delaunay cells containing a gap slightly decreases with the increase in the gap width.

Table 3.14: Summary of number of Delaunay cells containing a gap

Range of gap widths	Min	Max	Mode	Average
0.01*R*-0.03*R*	4	9	5	5.54
0.03*R*-0.1*R*	4	9	5	5.43
0.1*R*-0.2*R*	4	8	5	5.27
0.2*R*-0.5*R*	3	9	5	4.87

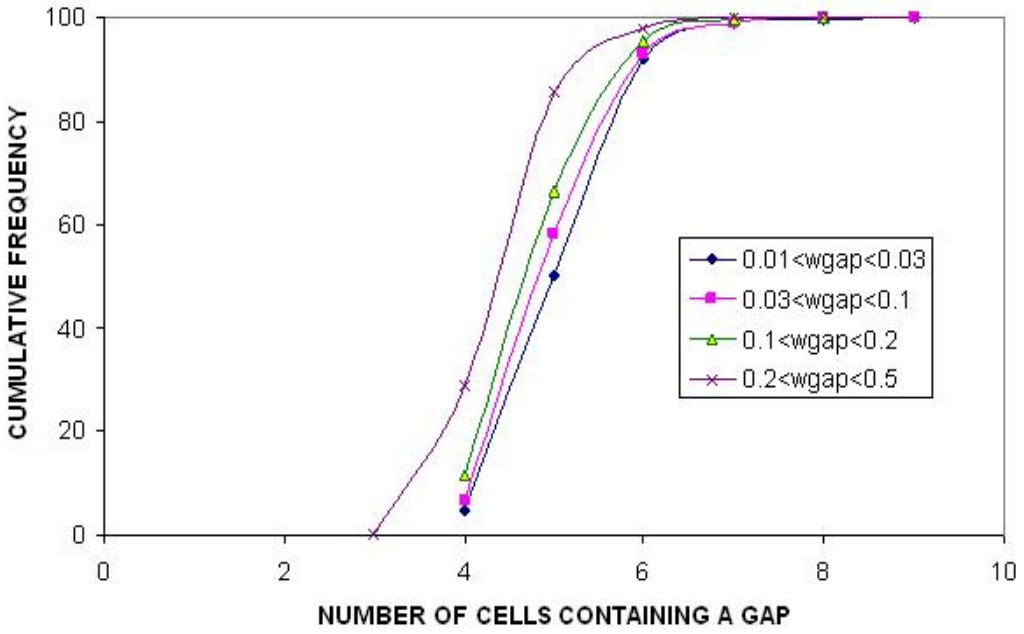

Figure 3.60: Cumulative frequency for the number of cells containing a gap, for gap widths 0.01*R*-0.03*R*, 0.03*R*-0.1*R*, 0.1*R*-0.2*R* and 0.2*R*-0.5*R*.

Figures 3.61 through 3.65 show pairs of spheres having gaps of different width (in dark color) and the surrounding spheres that together make a cluster of Delaunay cells. The same number of spheres can make different numbers of Delaunay cells. For example, there are 7 spheres in Figures 3.62 and 3.63 but they make 5 Delaunay cells in one case and 4 in the other. These four figures correspond to the Finney packing.

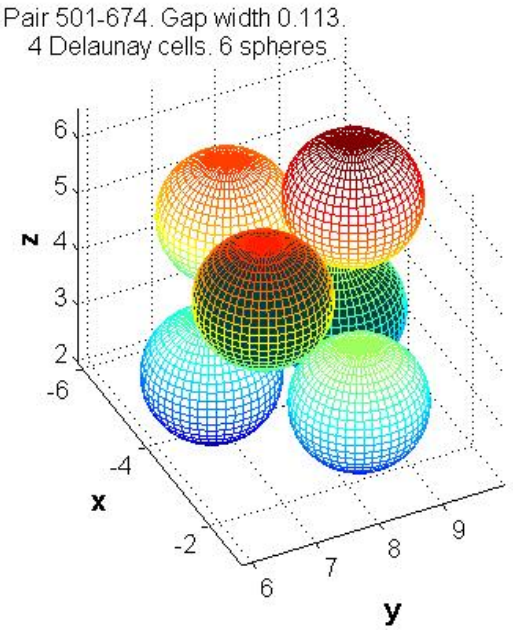

Figure 3.61: Spheres 501 and 674 having a gap between them of 0.113*R* are contained in 4Delaunay cells. The total number of spheres is 6.

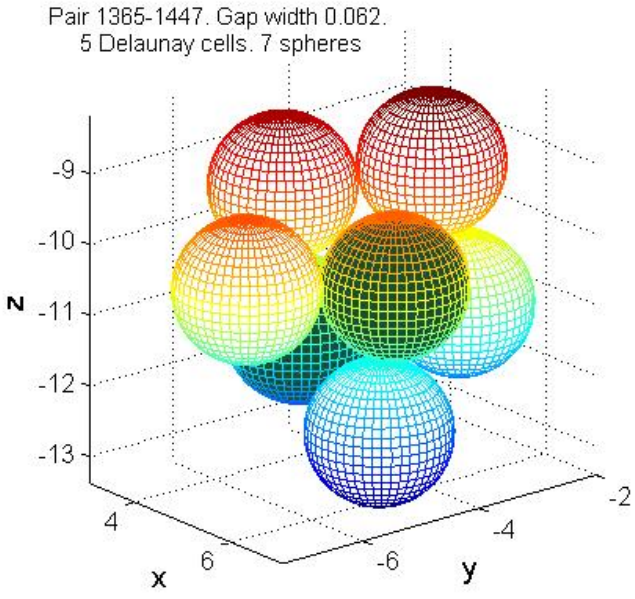

Figure 3.62: Spheres 1365 and 1447 having a gap between them of 0.062 *R* are contained in 5 Delaunay cells. The total number of spheres is 7.

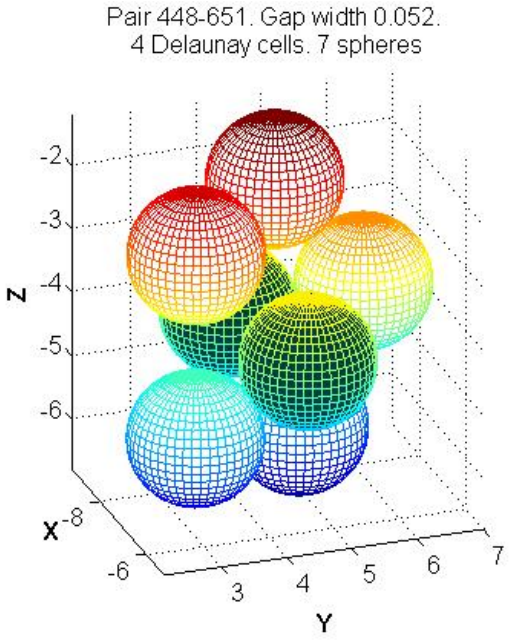

Figure 3.63: Spheres 448 and 651 having a gap between them of 0.052 *R* are contained in 4 Delaunay cells. The total number of spheres is 7.

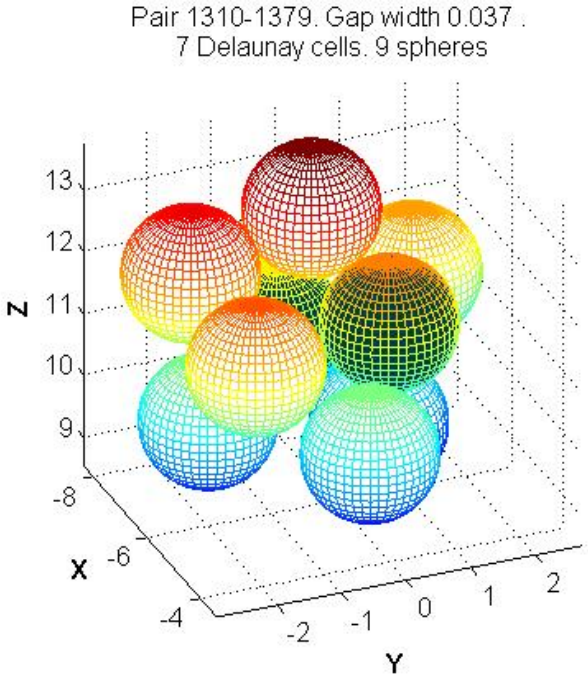

Figure 3.64: Spheres 1310 and 1379 having a gap between them of 0.037 *R* are contained in 7 Delaunay cells. The total number of spheres is 9.

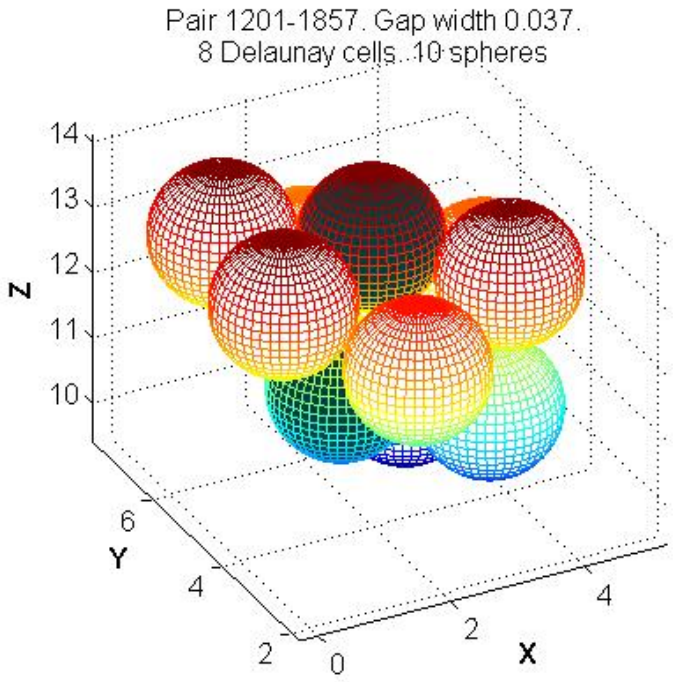

Figure 3.65: Spheres 1201 and 1857 having a gap between them of 0.037 *R* are contained in 8 Delaunay cells. The total number of spheres is 10.

Chapter 4: Physics of Flow Rates through Gaps

A particle must be carried into a gap in order to be strained there. In the theory of Sharma and Yorstos (1987 a,c) it is assumed that the probability of a particle to enter a gap is proportional to the flow rate through the gap.

The possibility of separation in laminar flow around multiple spheres (Davis et al., 1976; Taneda, 1979) will not be considered. Separation of streamlines results in sluggish zones and eddies that would increase the probability of trapping. On the other hand, the streamlines can curve around gaps instead of passing through them, reducing the probability of straining.

The objective of this chapter is to calculate the steady state flow of a single phase fluid through the Finney packing, in pore throats and gaps. The steady state flow through the packing will be calculated first (Section 4.1). This computation provides the volumetric flow rate in each throat and the potential in each pore body. The local potential gradient through each gap will be calculated next (Section 4.2) approximating the flow resistance of the gap by that of a slit having the same width as the gap. A transformation of the spatial coordinates of the spheres in the packing will be made in order to calculate the pressure gradient.

This local potential gradient will be used to finally calculate the volumetric flow rate through the gap appropriate to the particle being strained (Section 4.3).

4.1 STEADY STATE FLOW THROUGH PORE THROATS

The approach of Bryant et al. (1993a), which involves the Delaunay tessellation, will be used to determine flow in pore throats in the Finney pack. After the tessellation of the sphere pack is calculated, the hydraulic conductance of each pore throat can be estimated from the effective throat radius R_{ef} (Eqn. 1.5) and length L:

$$g = \frac{\pi R_{ef}^4}{8\mu L} \qquad \text{Eqn.4.1}$$

where μ is the fluid viscosity. Values of g, R_{ef}, and L have been calculated for each throat in the packing. L is the distance from the center of one Delaunay cell to the center of the neighboring cell.

The volumetric flow rate through the pore throat, q, is the product of its conductance, g, and the difference in potential in the two pores connected by the throat, ΔP.

$$q = g\,\Delta P \qquad \text{Eqn.4.2}$$

The steady state flow field requires mass conservation at each pore:

$$\sum_{j=1}^{4} q_{ij} = 0\,; \qquad \text{Eqn.4.3}$$

where q_{ij} is the flow from the i^{th} pore into its j^{th} neighbor, and flow in (out) of the pore is positive (negative). This sum extends to the four throats (j=1:4) connected to pore i. Since pore bodies correspond to the centers of the Delaunay tethraeda each pore body is contected to another four pore bodies through exactly four pore throats. Expressed in terms of pressures, P_i, in each pore, the former equation transforms into:

$$\sum_{j=1}^{4} g_{ij}(P_i - P_j) = 0 \quad \forall i \qquad \text{Eqn.4.4}$$

where $(P_i – P_j)$ is the difference in pressure between the centers of the pores i and j and g_{ij} is the conductance in the throat that connects those pores.

The solution of this system of equations (4.4) yields the pressures in each pore body. Eqn 4.2 can then be used to compute the flow rate through each face of the Delaunay cells. Therefore each cell will be assigned four conductance values, four flow values and one pressure value.

Inner and outer boundaries were defined in the Finney packing in order to solve the previous system. The inner boundary has a radius of 1.5*R* and the pressure in pores inside this boundary was set to 2. The outer boundary is defined by the incomplete Delaunay cells, i.e., those cells that involve spheres which are not among the 2000 interior spheres of interest. Pressure for pores in that zone was set to one.

Figure 4.1 shows the histogram of conductance in every face of the Delaunay cells. Conductance has been calculated with equation 4.1 using a viscosity of 1 cp. The dimensions of the conductance are $M^{-1}L^{4}T$. Since length scales in this thesis are normalized by the radius *R* of the soil grains, the actual magnitude of the conductance is obtained by multiplying the value shown by R^{4}.

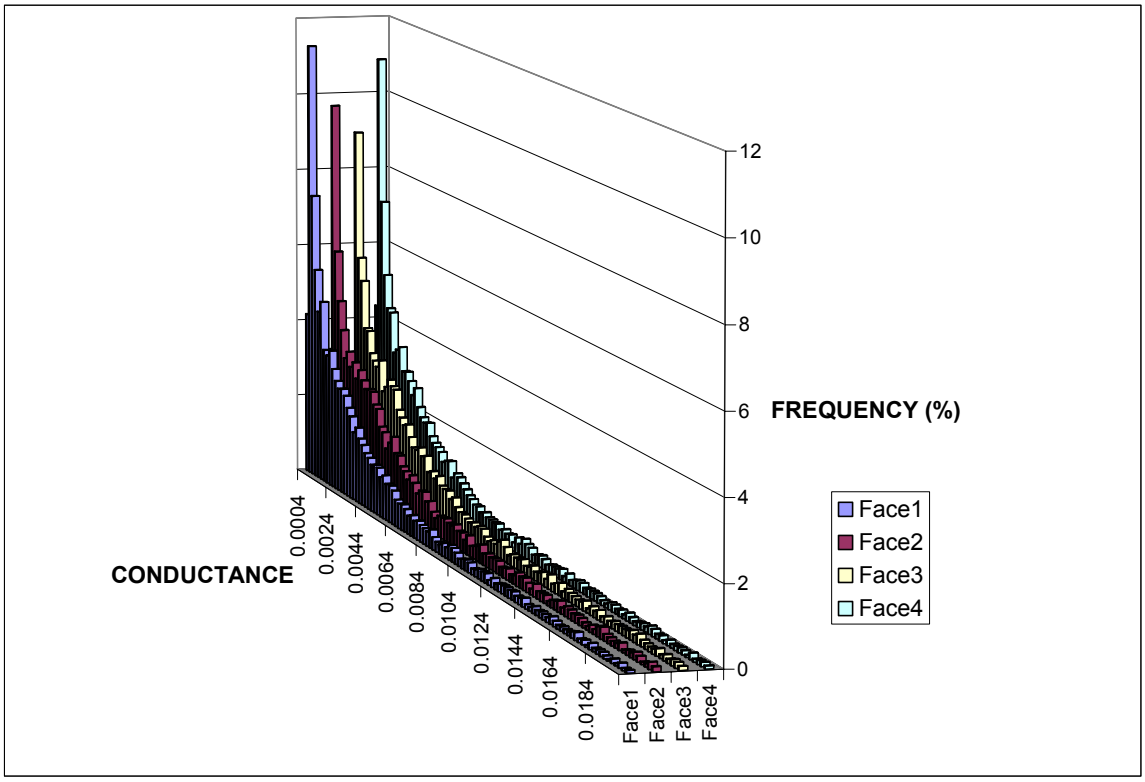

Figure 4.1: Conductance in every face of the Delaunay cells.

A list of unique throats has been generated to best represent the magnitudes of conductance, and consequently velocity and volumetric flow, in the packing. Every Delaunay cell has 4 associated values of conductance, one per face, but every face is shared with a neighboring cell yielding duplicated values of conductance. There are 14871 Delaunay cells in the portion of the Finney packing used for this project therefore there are 59484 conductance values. A sorting of the data to keep only the non repeated values yields 30721 unique throats. 1958 of these throats are in Delaunay cells at the outer boundary of the packing whose 4^{th} face does not have any neighbor; therefore their calculated conductance is zero. Since those 1958 pore throats are not representative of the flow within the packing, they are not going to be included in the calculations. Therefore

the previous number of unique pore throats reduces to 28763 for the calculations. Figure 4.2 shows the histogram of conductance with the non duplicated data.

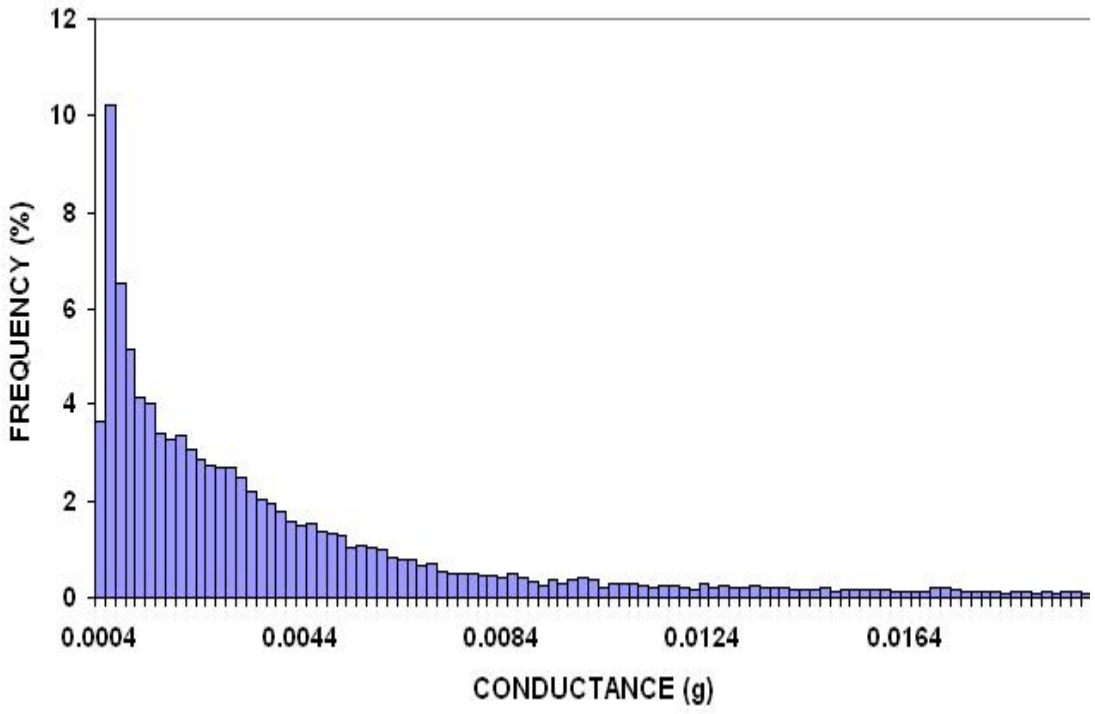

Figure 4.2: Histogram of conductance in pore throats.

Pore throats whose conductance is bigger than 0.02 have a frequency of approximately 12%, but they are not shown in the histogram since they have disperse conductance values that range from 0.02 to 9800. In order to show all the values, Figure 4.3 shows the histogram of conductance in pore throats with logarithmic scale in the conductance axis for a range of conductance from 1 to 10000. The frequency is shown in number of counts.

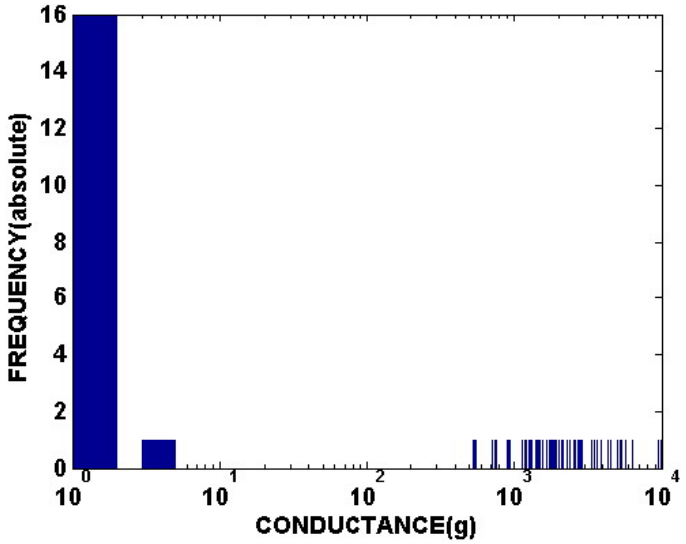

Figure 4.3: Histogram of conductance in pore throats for a range of conductance from1 to 10^4. Frequency is shown in number of counts.

Figure 4.4 shows the volumetric flow, q, in pore throats obtained after solving the system of equations 4.4. Volumetric flow is plotted versus the throat inscribed radius r_c (cf. Chapter 1).

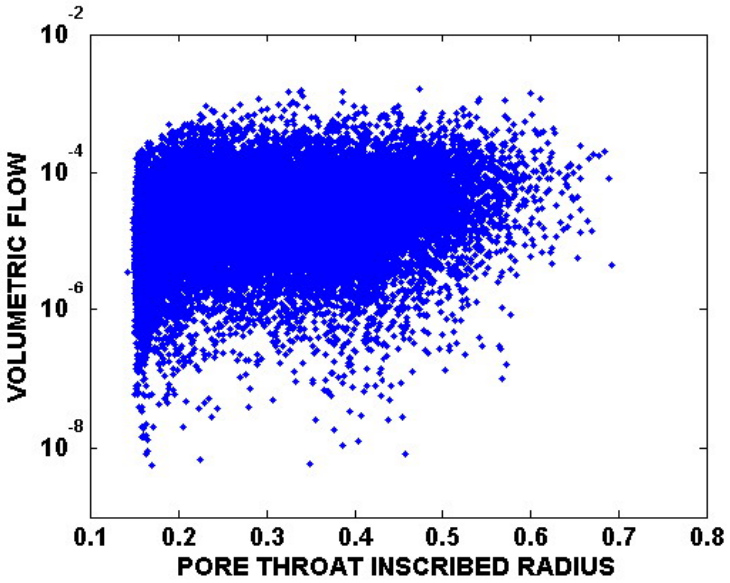

Figure 4.4: Volumetric flow (L^3T^{-1}) in throats vs. pore throat inscribed radius.

Figure 4.4 shows that the volumetric flow in throats ranges from 10^{-8} to 10^{-3} with an average value of $4.5 \cdot 10^{-5}$ (arithmetic average). The dimensions of the volumetric flow are L^3T^{-1}. As in the case of conductance, the length scale in this quantity is normalized by the soil grain radius *R*. Moreover, the units of pressure used to solve the system of equations ($P_{outisde}$ =1 and P_{inside}=2) are arbitrary.

There is a range of values of volumetric flow for a single value of pore throat radius because of the alignment of each pore throat with the macroscopic gradient of pressure varies. Those throats aligned perpendicular to the macroscopic gradient in potential have a negligible flow through them. 1995 pore throats out of the 28763 are aligned perpendicular to the macroscopic gradient and therefore have computed volumetric flow of zero through them. Setting the pressure in the cells within 1.5*R* of the center and in cells at the external surface of the packing causes 1995 of the throats to join

"boundary pores". In these cases, the pressure in the center of each one of the two Delaunay cells connected by the pore throat are the same, thus the flow rate is zero in these throats. They represent the 6.5% of the total number of throats. Besides that, the lower part of the cloud of data points shows an increase in volumetric flow as the radius of the pore throat increases. The geometric average of the flow has been calculated in bins of inscribed radius to see this trend. Figure 4.5 shows the results.

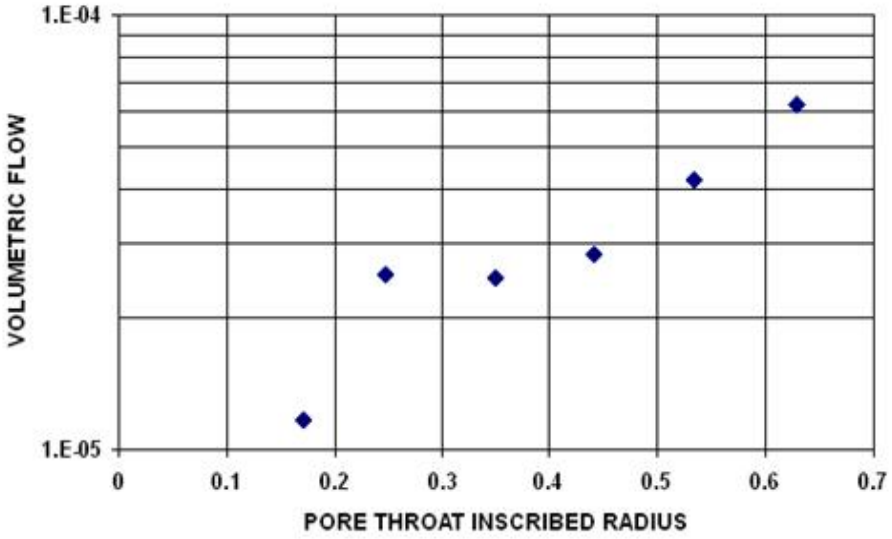

Figure 4.5: Geometric average of volumetric flow in bins of inscribed radius.

The volumetric flow in pore throats has also been plotted versus the distance from the center of the packing to the center of the throat, as shown in Figure 4.6. The volumetric flow rate is constant for steady incompressible flow but since the Finney pack is spherical, there is a decrease in the volumetric flow in pore throats located far from the center of the packing. A normalization of the data to linear flow will be performed in

Chapter 5. The geometric mean of the volumetric flow in bins of distances from the center has also been calculated and it is shown in Figure 4.7. The distance from the center is given in units of soil grain radius *R*. Table 4.1 shows the minimum, maximum and average values of the volumetric flow in pore throats. Pore throats with zero flow have been ignored.

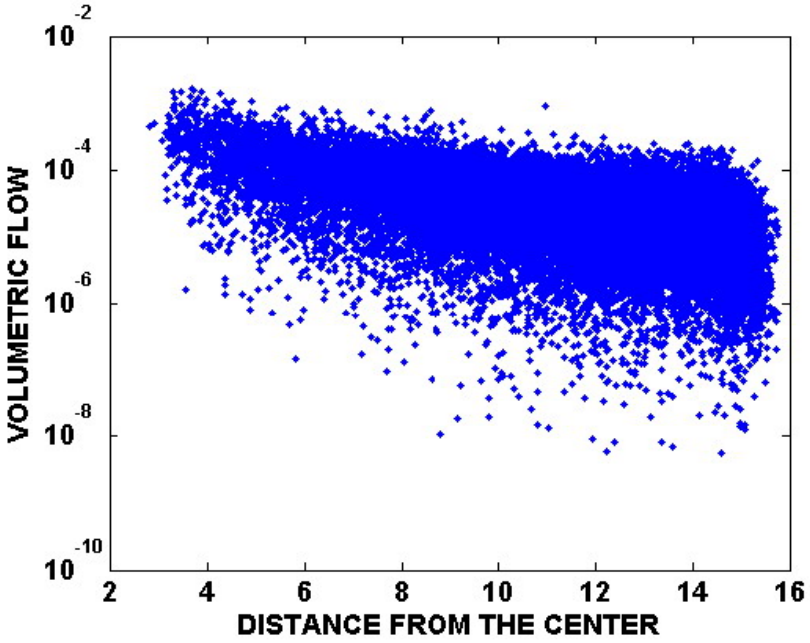

Figure 4.6: Flow in pore throats vs. distance from the center.

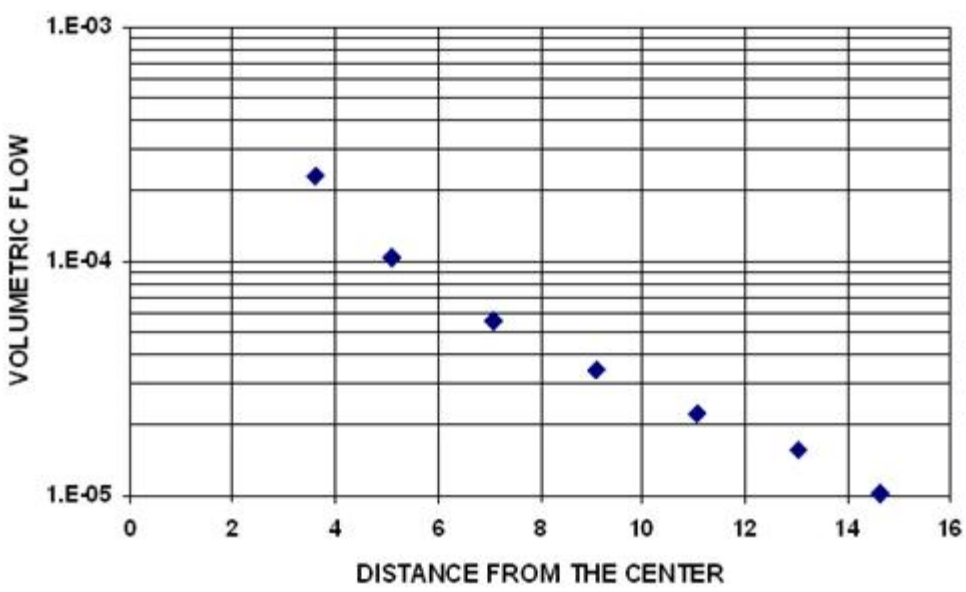

Figure 4.7: Geometric average of volumetric flow in bins of distance from the center.

Table 4.1: Statistics of the volumetric flow in pore throats.

	Volumetric flow, q
Minimum	$5.6 \cdot 10^{-9}$
Maximum	$1.64 \cdot 10^{-3}$
Average (geometric)	$2.13 \cdot 10^{-5}$

4.2 STEADY STATE FLOW THROUGH GAPS

The previous calculation of flow does not provide the detailed distribution of flow within the pore, therefore the flow through the gaps is still unknown. Each gap between a pair of grains is associated with a cluster of pores as shown in Figure 3.55.

The local gradient in potential in the plane normal to the line joining the center of any two spheres drives flow through the gap between the grains (cf. Figure 3.55, line between points A and A'). One of the methods to estimate this gradient is the smooth field approximation, which defines local gradient as the projection of the macroscopic gradient onto the normal plane. However this approximation may overestimate the value of the gradient in potential in gaps (Burganos, 1987). A more refined calculation is needed.

The values of the steady state potentials in the pores surrounding the gap were calculated in section 4.1. These can be used to estimate the local gradient using a variety of numerical methods. An original method has been used in this project.

4.2.1 Conductance in gaps

Two approaches were used to calculate conductance in gaps:

a) **Slit**. The gap is considered as a slit of length equal to twice the range of capture ($2a$) and width equal the gap width (w_{gap}). The equation for flow through a slit is (Bird, 1960):

$$q = \frac{2}{3}\frac{\Delta P \cdot B^3 \cdot W}{\mu \cdot L} \qquad \text{Eqn. 4.5}$$

where μ is the viscosity of the fluid and B,W and L are the dimensions of the slit (see figure 4.8 below). This equation applied to the gap results in:

$$q = \frac{2}{3}\frac{\Delta P}{\mu L}\left(\frac{w_{gap}}{2}\right)^3 2a \qquad \text{Eqn. 4.6}$$

which yields the equation for the conductance in the gaps (g):

$$g = \frac{1}{6}\cdot\frac{a\cdot w_{gap}^3}{\mu L} \qquad \text{Eqn. 4.7a}$$

$$g^* = gL = \frac{1}{6}\frac{a w_{gap}^3}{\mu} \qquad \text{Eqn. 4.7b}$$

and the equation for the velocity in the gaps (u_{gap}):

$$u_{gap} = -\frac{w_{gap}^2}{12}\frac{\nabla P}{\mu} \qquad \text{Eqn. 4.8}$$

The volumetric flow can then be calculated from equations 4.6 and 4.8 as:

$$q = 2a w_{gap} u_{gap} \qquad \text{Eqn. 4.9}$$

Figure 4.8 shows the dimensions of the slit for the original case (Bird, 1960) and for the gap analogy.

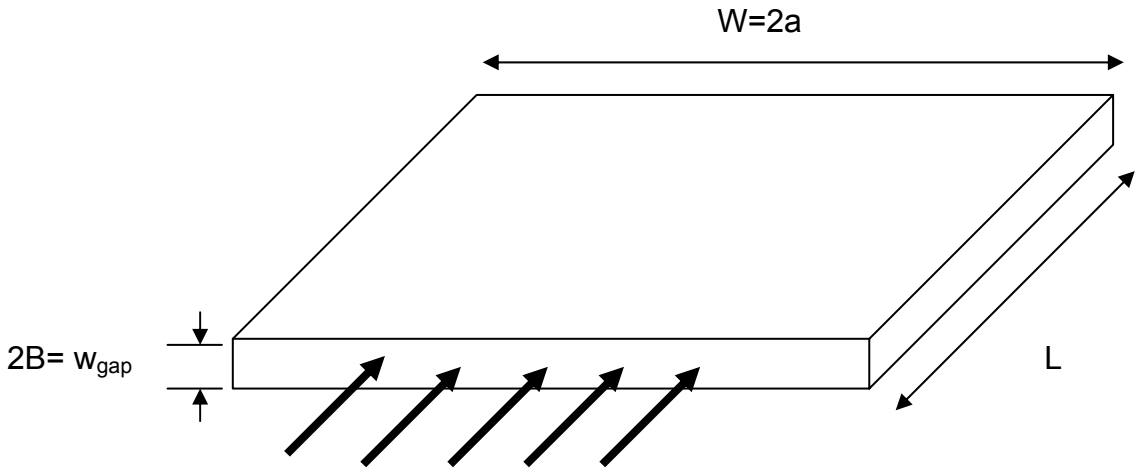

Figure 4.8: Flow through a gap represented by a slit. The black thick arrows represent the direction of the flow.

b) **Hagen-Poiseuille/Hydraulic radius**. The gap is considered a cylinder of radius equal to the hydraulic radius of the gap, R_h, and length L.

$$g = \frac{\pi}{8} \cdot \frac{R_h^4}{\mu L} \qquad \text{Eqn. 4.10}$$

The hydraulic radius of the gap is calculated as the area of the cross section of the gaps divided by the wetted perimeter. Suppose the gap is approximated as a slit with closed sides. According to Figure 4.8 it can be calculated as:

$$R_h = \frac{a \cdot w_{gap}}{\left(2a + w_{gap}\right)} \qquad \text{Eqn. 4.11}$$

$$g = \frac{\pi}{8} \cdot \frac{1}{\mu \cdot L} \cdot \left[\frac{a \cdot w_{gap}}{\left(2a + w_{gap}\right)} \right]^4 \qquad \text{Eqn. 4.12a}$$

$$g^* = gL = \frac{\pi}{8\mu} \left[\frac{a\, w_{gap}}{(2a + w_{gap})} \right]^4 \qquad \text{Eqn. 4.12b}$$

where μ is the viscosity of the fluid.

The methods described above for the calculation of the conductance include the variable L. The magnitude of L is well known in the case of pore throats since it is the distance between the centers of neighboring Delaunay cells. The value of L is ambiguous for the case of the gaps. For example, it can be taken as equal to the gap width, as equal to the range of capture, or as equal to the distance from the center of the gap to the center of a neighboring gap. Because of the uncertainty of the value of L in the case of gaps, the conductance will be expressed as the product of conductance by length. This variable will be called conductance-length product, g^*, and its dimension analysis yields $M^{-1}L^5T$. Both conductance and conductance-length product depend on the cube of the gap width. Equation 4.6 can be expressed in terms of the conductance-length product as follows:

$$q = \frac{\Delta P}{L} \cdot g^* = \nabla P \cdot g^* \qquad \text{Eqn. 4.13}$$

Therefore two quantities, the local gradient in potential and the conductance length product, are needed in order to calculate the volumetric flow through gaps.

4.2.2 Range of capture of the gap

As seen in the previous section, the conductance, and thus the volumetric flow, depends on the range of capture *a* (cf. Chapter 2, section 2.5). The range of capture for every gap is calculated here followed by the calculation of the conductance-length product. After that, only the local gradient of pressure is needed to obtain the volumetric flow in gaps.

Since the range of capture *a* depends on the size of the particle being trapped *d/D* (Eqn. 2.1), the conductance-length product of the gaps g^* depends on this value too. Of primary interest are small particles of relative sizes $d/D<0.05$ since they exhibit non-classical straining in experiments. Particles of relative sizes *d/D* equal to 0.02, 0.025, 0.03, 0.035, 0.04, 0.045 and 0.05 have been used to calculate range of capture and conductance in gaps whose width falls in the range of interest ($0.03R<w_{gap}<0.1R$). The diameter of the grains *D* is equal to 2*R*; therefore the absolute sizes *d* of these particles are 0.04*R*, 0.05*R*, 0.06*R*, 0.07*R*, 0.08*R*, 0.09*R* and 0.1*R* respectively. Depending on the width of the gap that these particles may encounter while carried by the flow, some of them will pass through the gap while other will be strained. For example, a particle of size $d= 0.05R$ ($d/D=0.025$) will pass through a gap of size 0.07*R* but it will be strained in a gap of size 0.04*R*.

The size of the particle that can be strained, *d/D*, has been calculated for every gap whose width falls in the range of interest using different values of the angle α (cf. Figure 2.8). Equation 4.14, derived from equation 2.2 in Chapter 2, relate angle with particle size and is independent of the range of capture.

$$\frac{d}{D} = \frac{1 + w_{gap}/D}{\cos\alpha} - 1 \qquad \text{Eqn. 4.14}$$

The maximum and minimum values of d/D for a given angle α (d/D_{min} and d/D_{max}) correspond to the upper and lower limits in the gap widths considered respectively. These values are shown in Table 4.2 for the gaps in the range of interest (maximum width=0.1R, minimum width=0.03R)

Table 4.2: Minimum and maximum sizes of particles that can be trapped within a given angle for gaps widths in the range of interest.

Angle α	**(d/D) min**	**(d/D) max**
5	0.02	0.05
10	0.03	0.07
15	**0.05**	**0.09**
20	0.08	0.12
25	0.12	0.16
30	0.17	0.21

As shown in the table, angles bigger than 15° can strain particles that are too big for the gaps widths of interest (the biggest size of the strained particle relevant in this thesis is d/D=0.05). Therefore, equation 2.1 will be used in the calculation of the range of capture and the local flow through the gap will be calculated with equation 2.4. Remember that the latter equation is valid for a range of capture extending about 15° from the minimum constrictions. These two equations are shown here again:

$$\frac{2a}{D} = \sqrt{\left(\frac{d}{D}\right)^2 - \left(\frac{w_{gap}}{D}\right)^2 + 2\left(\frac{d}{D} - \frac{w_{gap}}{D}\right)} \qquad \text{Eqn. 2.1}$$

$$q = 2\, a\, w_{gap}\, u_{gap} \qquad \text{Eqn 2.4}$$

Also, for different angle α the range of capture has been calculated with equation 2.3, considering the minimum and maximum gap sizes in the range of interest. The results are shown in table 4.3 for the minimum and maximum gap sizes considered.

$$a = \frac{w + D}{2} \cdot \tan \alpha \qquad \text{Eqn. 2.3}$$

Table 4.3: Maximum range of capture for different angles

Angle α	$\mathbf{a_{max}}$ (w_{gap}=0.03R)	$\mathbf{a_{max}}$ (w_{gap}=0.1R)
5	0.089R	0.092R
10	0.179R	0.185R
15	**0.272*R***	**0.281*R***
20	0.369R	0.382R
25	0.473R	0.490R
30	0.586R	0.606R

The maximum range of capture for 15° angles is between 3 to 9 times bigger than the gap width. It is also about the 28% of the sphere radius. This indicates that it is reasonable to assume that the range of capture does not extend far enough into the void space in the pore throat region where the flow velocities may differ from both the average throat velocity and the gap velocity that will be calculated later.

Finally the range of capture has been calculated with Eqn. 2.1 for the different sizes of strained particles considered. Figure 4.9 shows range of capture a versus gap width w_{gap} for the different particle sizes studied.

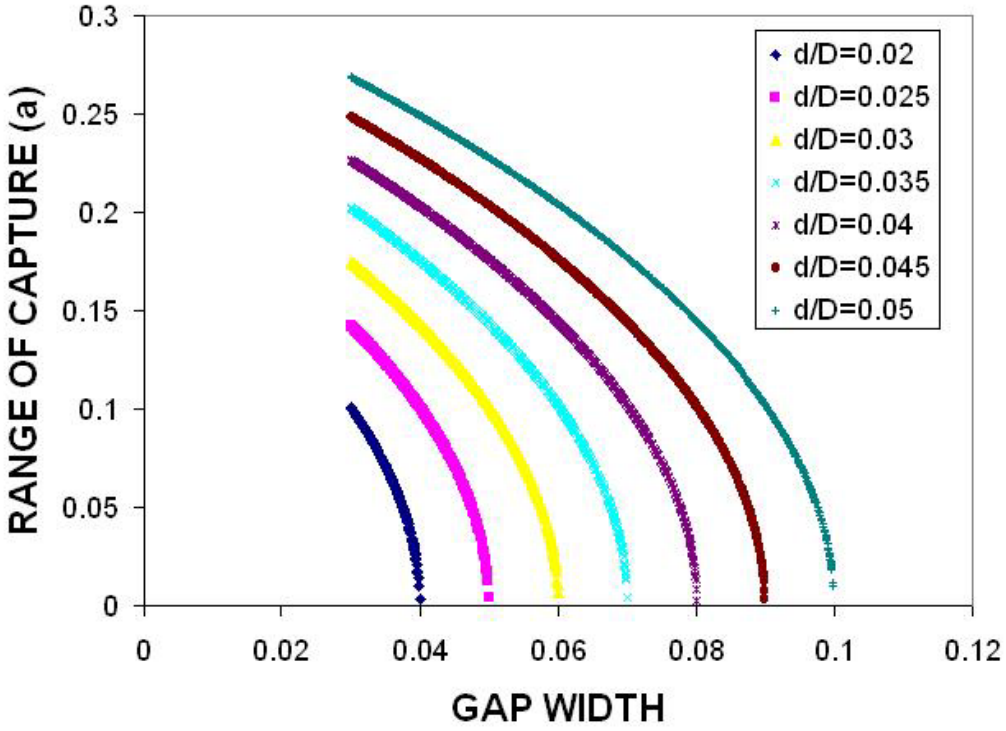

Figure 4.9: Range of capture *vs*. gap width for gaps in the range of interest.

The first thing to be noticed in Figure 4.9 is that, for a given particle size, the range of capture decreases when the gap width increases. A particle big enough will be trapped at some point within a finite distance from the center of the gap. Wider gaps trap the suspended particles of the right size closer to the minimum constriction than the smaller gaps. These small gaps can trap the same particle at the same distance from the gap center as a bigger gap would do and also at longer distance from this minimum constriction. Also shown in Figure 4.9 is that, for a gap of a given width, the range of capture increases as the size of the strained particle increases. The reason for the smaller range of data points for the smaller particle sizes is that these particles are not strained in the bigger gaps.

The range of capture is now used in equation 4.7b (slit approximation for the shape of the gap) to calculate the conductance-length product, g^*. Figure 4.10 shows the conductance-length product (g^*) versus gap width (w_{gap}) for the different sizes of trapped particles studied. All the particle sizes considered show a peak in conductance-length product. Conductance-length product increases with the increase in the gap width, and then it starts decreasing when the particle reaches bigger gaps. Equation 4.7b clearly shows that conductance-length product is directly proportional to the product of the range of capture and the cube of the gap width. Figure 4.9 showed how the range of capture decreases with the increase in the gap width, therefore at some gap width, the weight of the range of capture in equation 4.7b is bigger that the weight of the gap width yielding a peak in the conductance-length product.

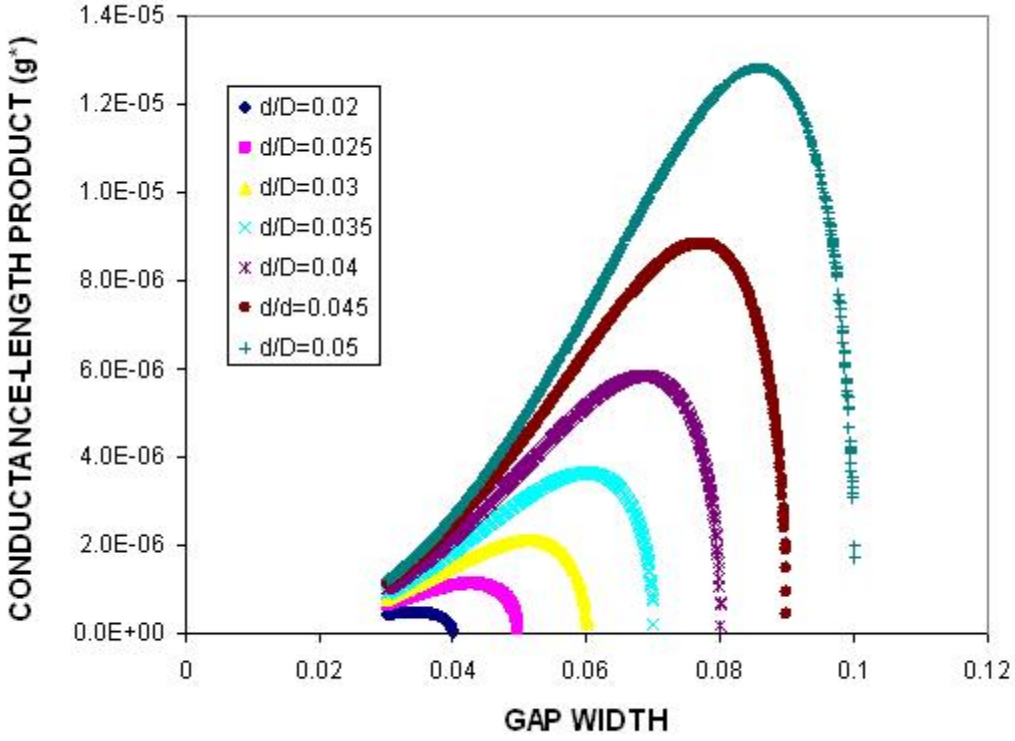

Figure 4.10: Conductance-length product *vs*. gap width for different sizes of particles strained, for gaps in the range of interest.

Figure 4.11 plots the conductance-length product g^* versus range of capture a. There is a complex relation between the conductance-length product g^*, particle size d/D and gap width w_{gap}. Even if equation 4.7b looks simple, the range of capture a also depends on gap width and particle size (equation 2.1). The figure shows that the conductance-length product increases with the size of the particle being strained for the same range of capture. Also a peak in the conductance-length product is shown in this case. Points to the left of the peak correspond to bigger gaps, which for a given particle size have a smaller range of capture. Remember that, for a given particle size d/D, the range of capture decrease with the increase in gap width (Eqn. 2.1 and Figure 4.9).

The conductance in the gaps depends on the cube of the gap width so it is bigger for bigger gaps.

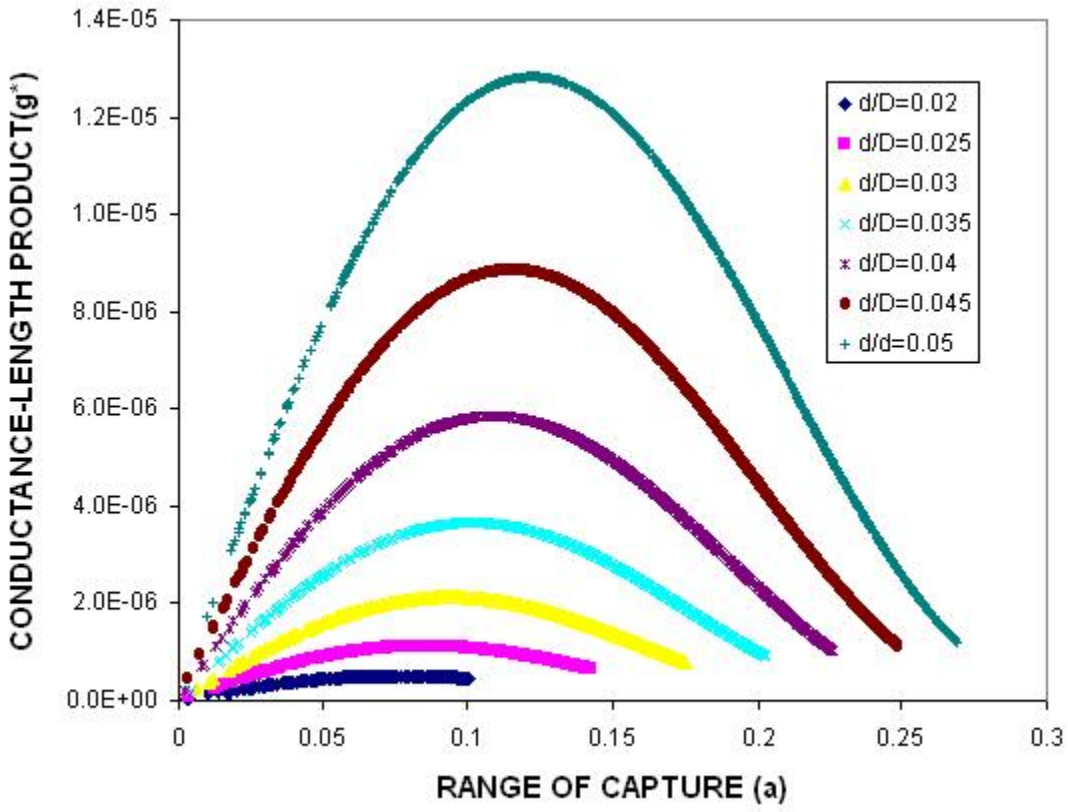

Figure 4.11: Conductance-length product vs. range of capture for gaps in the range of interest.

These calculations were repeated using the Hagen-Poiseuille equation (Eqn. 4.12b) for the calculation of the gap conductance-length product. Bigger values of g^* have been obtained but the trends of g^* with range of capture and gap width remain the same.

The same procedure has been done for gap widths between $0.01R$ and $0.03R$ and between $0.1R$ and $0.2R$ changing the size of the strained particles accordingly. Similar results were observed.

4.2.3 Hydraulic radius of the gap

Velocity can be expressed as a function of the hydraulic radius of the gap, R_h, as follows:

$$u_{gap} = -R_h^2 \cdot c \cdot \frac{\nabla P}{\mu} \qquad \text{Eqn. 4.15}$$

where c is a constant. In section 4.2.1 R_h was determined by approximating the gap as slit with closed sides. Here the hydraulic radius is calculated using the range of capture of the gap for different particle sizes.

If the gap is considered as an open slit, the hydraulic radius R_h in this case is simply calculated as:

$$R_h = \frac{2aw_{gap}}{4a} = \frac{w_{gap}}{2} \qquad \text{Eqn. 4. 16}$$

where a is the range of capture (specific for the size of the particles being strained) and w_{gap} is the gap width. The gap width is not included in the wetted perimeter since the only physically wetted surfaces are those of the soil grains. Figure 4.12 shows the variables a and w_{gap} in the gap.

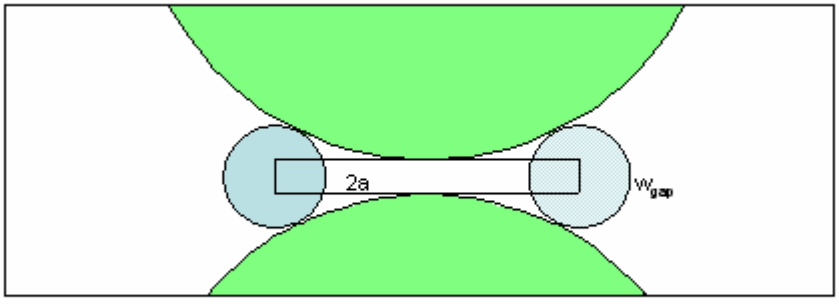

Figure 4.12: Range of capture (a) and gap width (w_{gap}).

Substituting the value of R_h in equation 4.15 by its value in equation 4.16 yields the formula for the velocity in a slit of width w_{gap} when the value of the constant c equal to 1/3.

The other approach for the calculation of R_h uses a formula derived from the calculation of surface areas for pendular rings (Rose, 1958). The area of the gap used for the calculations is the part of the gap within the two tangent points of the soil grain with the particle being strained. This area is shown with downward diagonal lines in Figure 4.13.

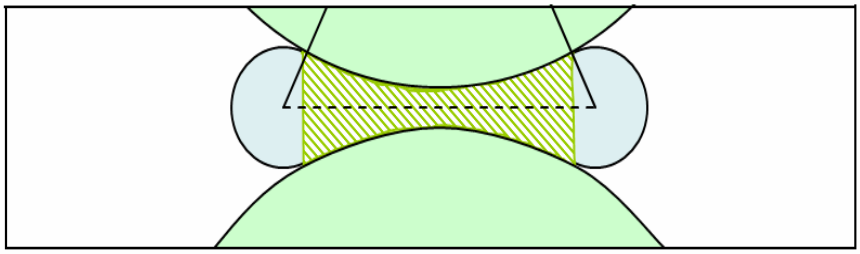

Figure 4.13: Area for the calculation of the pendular ring hydraulic radius.

Figure 4.14 shows the variables needed to calculate the hydraulic radius with the pendular ring method.

a)

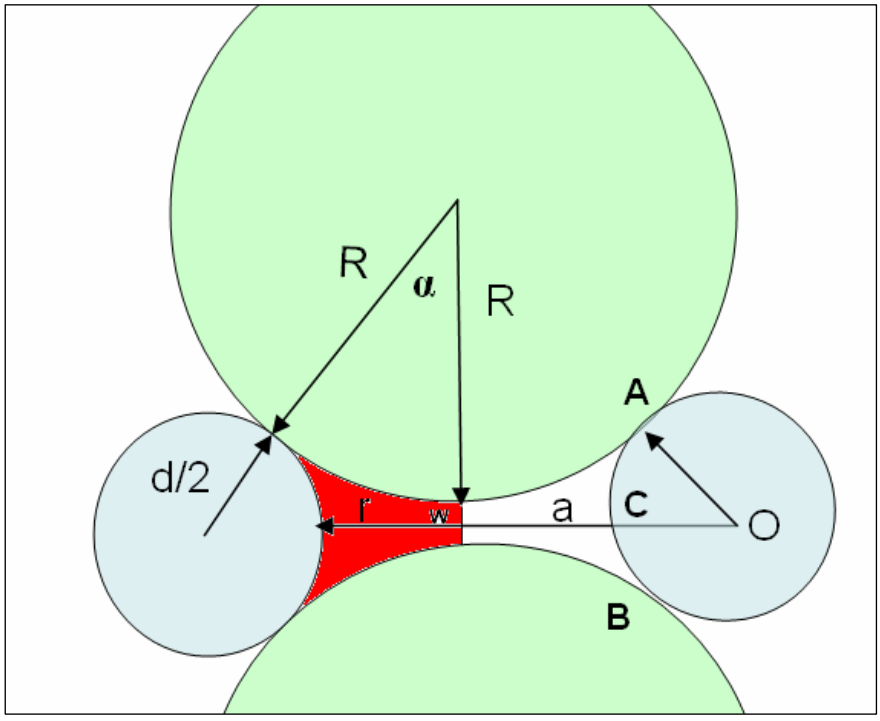

b)

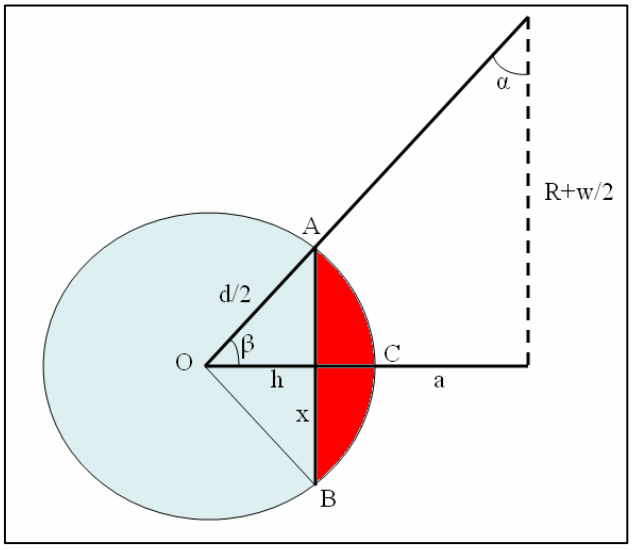

Figure 4.14: Geometric measurements of the gap.

In Figure 4.14:

R=Radius of the soil grains.

d/2= Radius of the trapped particles.

a= Range of capture, distance from the center of the gap to the center of the trapped particle.

w= Gap width.

r= Distance from the center of the gap to the surface of the trapped particle.

O= Center of the trapped particle.

A, B= Point contacts between the soil grain and the trapped particle.

h= Height of the triangle OAB.

x= Distance between points A and B.

α, β = Angles of the triangle defined by the center of the soil grain, the center of the trapped particle and the center of the gap; $\alpha + \beta = 90°$

The hydraulic radius is calculated as the cross sectional area divided by the wetted perimeter of the cross section. The cross sectional area in this case is two times the summation of the red area in figure 4.14a plus the red area in Figure 4.14 b. The red area in Figure 4.14a will be called A_{pen} and it is directly calculated with the pendular ring method as:

$$A_{pen} = \left\{ \left[a\left(R + \frac{w_{gap}}{2} \right) \right] - \alpha R^2 - \frac{d^2}{4}\left(\pi/2 - \alpha \right) \right\} \qquad \text{Eqn. 4.17}$$

where

$$\alpha = \arcsin\left(\frac{a}{d/2 + R} \right) \qquad \text{Eqn. 4.18}$$

The red area in Figure 4.14b is the area of the arc ABC (A_{arc}) which is calculated as the area of the circle sector OABC (A_{sector}) less the area of the triangle OAB (A_{tri})

$$A_{arc}=A_{sector}- A_{tri} \quad \text{Eqn. 4.19}$$

From Figure 4.14b, the area of the sector OACB is calculated as:

$$A_{sector}=0.5*2\beta*(d/2)^2 \quad \text{Eqn. 4.20}$$

where β is the angle made by the line that joins the center of the grain with the center of the particle and the line that joins the center of the particle with the center of the gap.

$$\beta = \arctan(\frac{R + w_{gap} / 2}{a}) \quad \text{Eqn 4.21}$$

The area of the triangle is calculated as:

$$A_{tri} = \frac{1}{2} x \cdot h \quad \text{Eqn. 4.22}$$

where x is the distance from point A to point B and h is the height of the triangle OAB. x is calculated as:

$$x=d \cdot \sin \beta \quad \text{Eqn. 4.23}$$

and h is calculated as:

$$h=d/2 \cdot \cos \beta \quad \text{Eqn. 4.24}$$

The cross section of the gap is then calculated as:

$$A_{gap}=2*(A_{pen}+A_{arc}) \quad \text{Eqn. 4.25}$$

Finally, the hydraulic radius is calculated as the area A_{gap} divided by the wetted perimeter. The wetted perimeter four times the length of the arc defined by the angle α. This length (s) is calculated as:

$$s = R \cdot \alpha \quad \text{Eqn. 4.26}$$

where α is the angle expressed in radians. The hydraulic radius R_h is thus calculated as:

$$R_h = \frac{A_{gap}}{4R\alpha} \qquad \text{Eqn. 4.27}$$

Unlike the hydraulic radius derived from the slit approximation, this hydraulic radius depends of the size of the particle being strained and if introduced in equation 4.15 it will yield a value of velocity in gaps dependent on d/D. The following figure illustrates the differences between the hydraulic radii calculated in these two ways. Figure 4.15 shows the hydraulic radius calculated with the two methods for the gap between spheres 763 and 908. The gap width is 0.064*R*. Every point in the plot corresponds to one size of strained particle. The data are shown in Table 4.4.

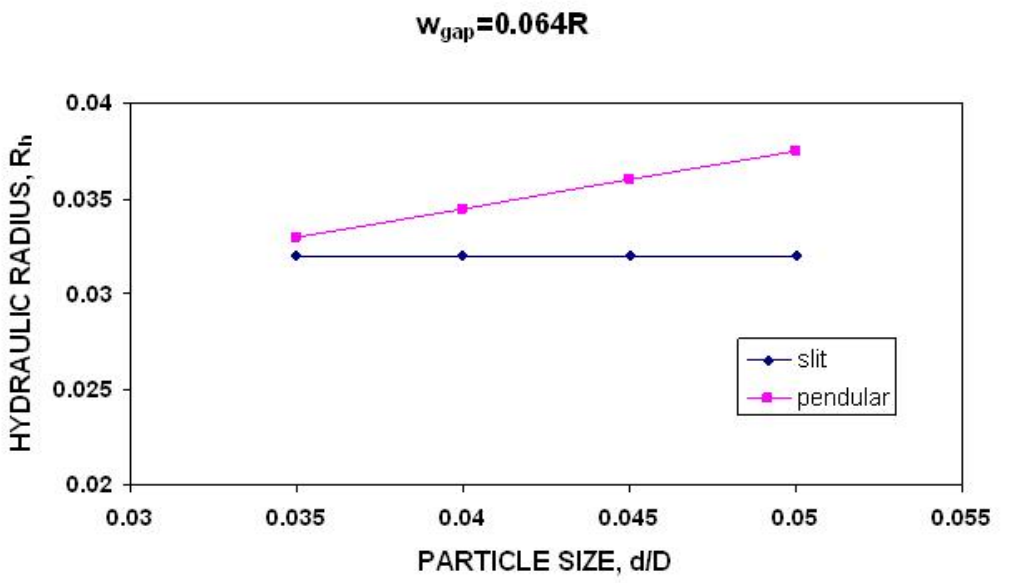

Figure 4.15: Hydraulic Radius calculated with the two approximations for a gap width in the range of interest.

Table 4.4: Hydraulic radius for the gap between spheres 763 and 908 calculated by two different methods.

d/D	R_h, slit	R_h, pendular	Error (%)
0.035	0.032*R*	0.033	2.85
0.040	0.032*R*	0.034	7.18
0.045	0.032*R*	0.036	11.09
0.050	0.032*R*	0.037	14.63

According to Figure 4.15, the hydraulic radius for the given gap calculated with the pendular ring method is bigger than the one calculated with the slit method. Remember that the hydraulic radius calculated for the slit approximation is independent of the size of the particle being strained. In the example in Figure 4.15 there are no points for d/D=0.02, 0.025, and 0.030 since those particles pass through gaps whose width is 0.064*R*. Table 4.4 shows that the error between values obtained with the two methods increases as the size of the strained particle increases. Figure 4.16 shows the differences between the two hydraulic radius, for different gap widths, when the size of the strained particle is d/D=0.045 and d/D= 0.035.

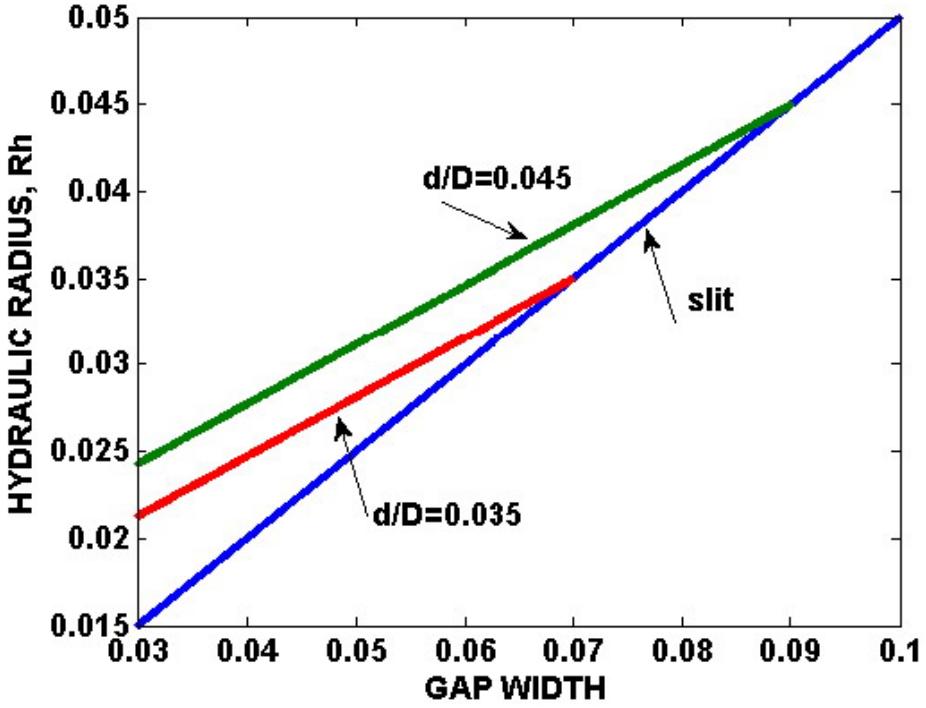

Figure 4.16: Hydraulic radius of gaps straining particles of relative sizes d/D=0.035 and d/D=0.045 *vs*. gap width.

Figure 4.16 shows that the hydraulic radius calculated with the pendular ring method is larger than the one calculated with the slit approximation. For the same particle size, the difference between these two values decreases for bigger gap widths. There are not data points in the range of gap width 0.07R to 0.1R for the particle sizes d/D=0.035, since these will not get trapped in those gaps. The same thing happens with particles of size d/D=0.045 when they encounter gaps whose width range from 0.09R to 0.1R.

For the remainder of this thesis, the slit approximation (equation 4.8) has been used to calculate linear velocities in gaps. This will yield a conservative estimate of the volumetric flow through gaps. The volumetric flow appropriate to the size of the particle being strained is then calculated with equation 4.9.

4.2.4 Local gradient in gaps

After the estimation of the conductance-length product or the hydraulic radius of the gap, the local gradient in potential is necessary in order to estimate the volumetric flow in gaps (cf. equations 4.8 and 4.13).

An original method to calculate the pressure gradient is shown in this section. The Delaunay tessellation divides the central 2000 spheres of the Finney packing in 14871 Delaunay cells. The pressure in the center of each one the Delaunay cells is known from the previous calculation of the steady state flow in pore throats. The geometric analysis of the Finney packing in Chapter 3 revealed that each gap between pair of spheres is part of four and up to nine Delaunay cells, for the gap widths in the range of interest.

The centers of those cells are in the same plane as is the center of the gap. Figure 4.17 shows two spheres in the Finney packing (id numbers 763 and 908) separated by a gap of width 0.064*R*.

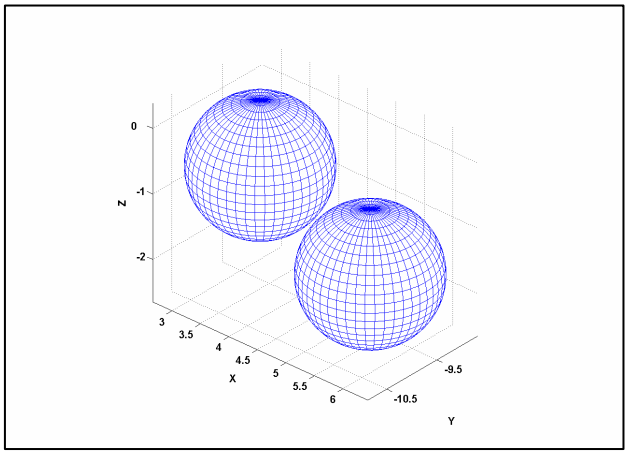

Figure 4.17: Two spheres separated by a gap of width 0.064*R*.

There are 6 Delaunay cells containing that pair of spheres and there are 8 different spheres involved in those 6 Delaunay cells: 491, 578, 731, 763, 908, 962, 1185 and 1326. This is shown in Table 4.5.

Table 4.5: Delaunay cells that contain the pair 763-908

Cell	**Spheres**			
4062	491	578	763	908
4065	491	731	763	908
4698	578	763	908	962
5822	731	763	908	1185
6065	763	908	962	1185
6062	763	908	1185	1326

Figure 4.18 shows a 3D view of those 8 spheres in the space. The two dark spheres are the ones having a gap in the range of interest.

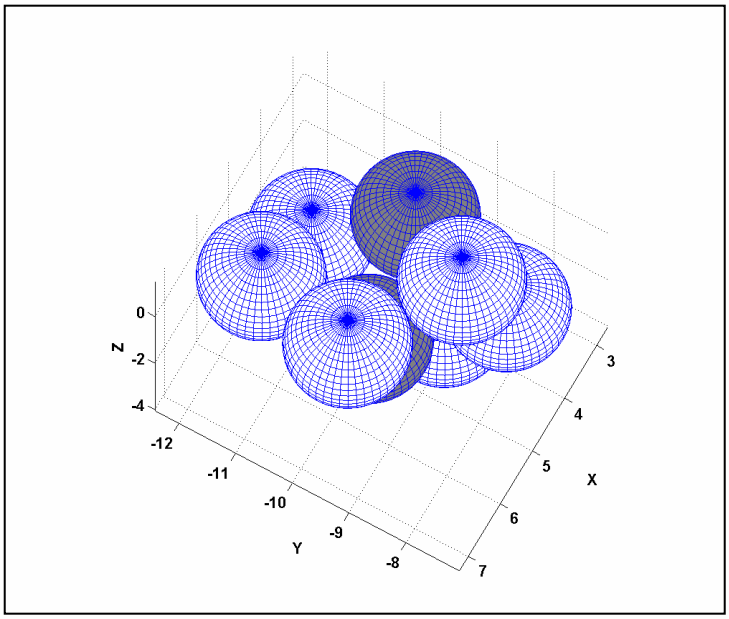

Figure 4.18: 3D view of the 8 different spheres that make 6 Delaunay cells.

Figure 4.19 shows the 6 Delaunay tetrahedra in that set of 8 spheres.

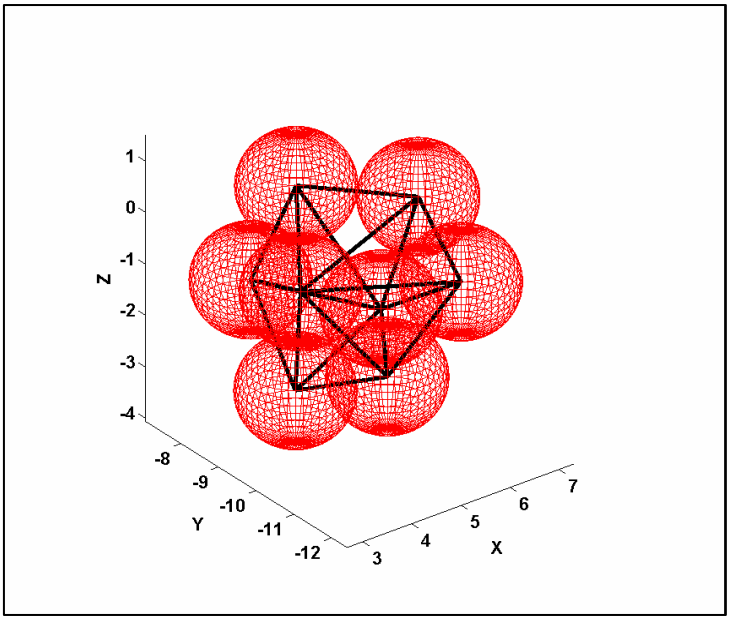

Figure 4.19: Delaunay tetrahedra for the set of spheres.

Figure 4.20a shows the centers of the Delaunay cell and the center of the gap. Part b. shows how these points are in the same plane.

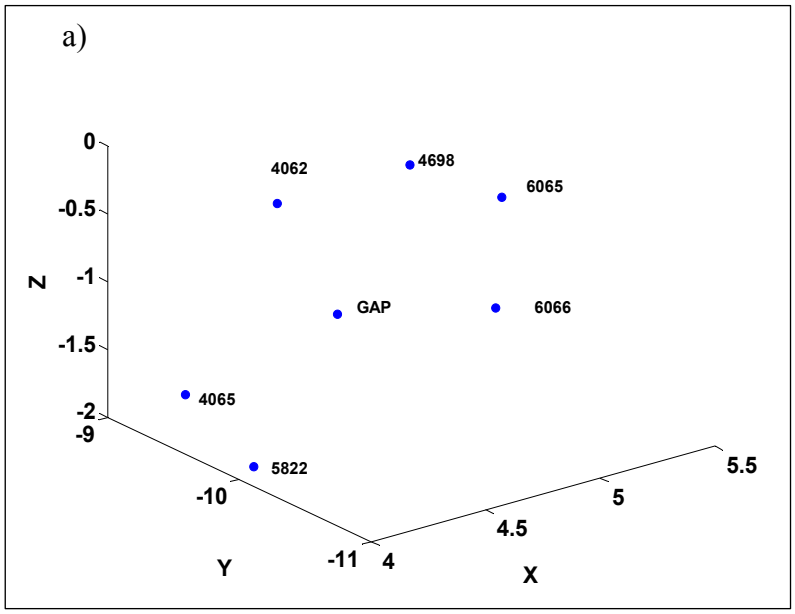

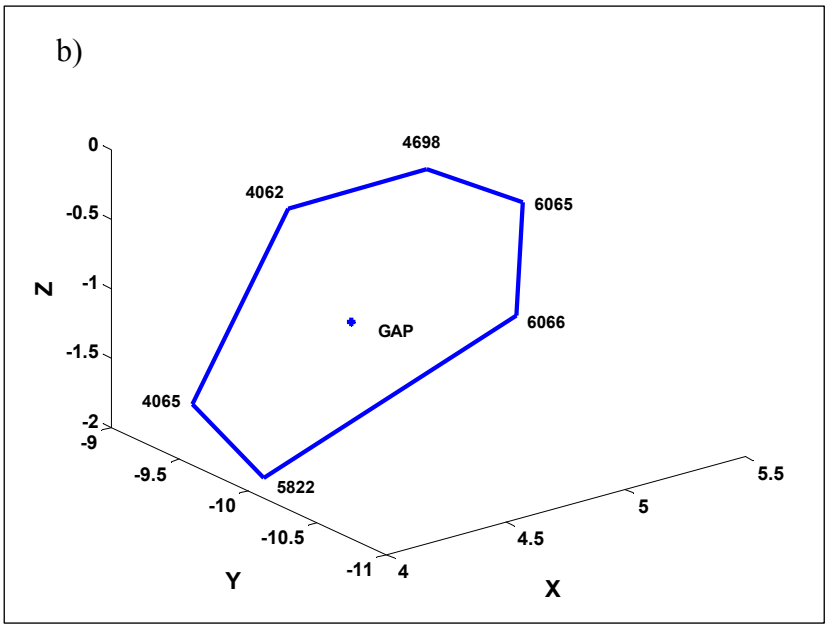

Figure 4.20: a)Centers of the 6 Delaunay cells and center of the gap in the space.
b) Plane made by the 7 center points.

Figure 4.21 shows the two spheres 763 and 908 separated by a gap width of $0.064R$ and the plane defined by the centers of the Delaunay cells which contain that pair of spheres. A line has been drawn joining the centers of the spheres. This line is perpendicular to the plane defined by the Delaunay cells centers and it defines the center of the gap in its intersection with the plane. Why this line is perpendicular to the plane is a issue of classical geometry. Each gap is defined by two spheres whose centers define one edge. This edge is part of several Delaunay cells, 6 in this example, each of which has a geometric center. By definition a cell center is equidistant from the four spheres defining the cell. Therefore each of these cell centers is equidistant from the two spheres defining the gap. Each cell center lies in the plane of all points that are equidistant from those two spheres. That plane is necessarily perpendicular to the line joining the centers of the two spheres.

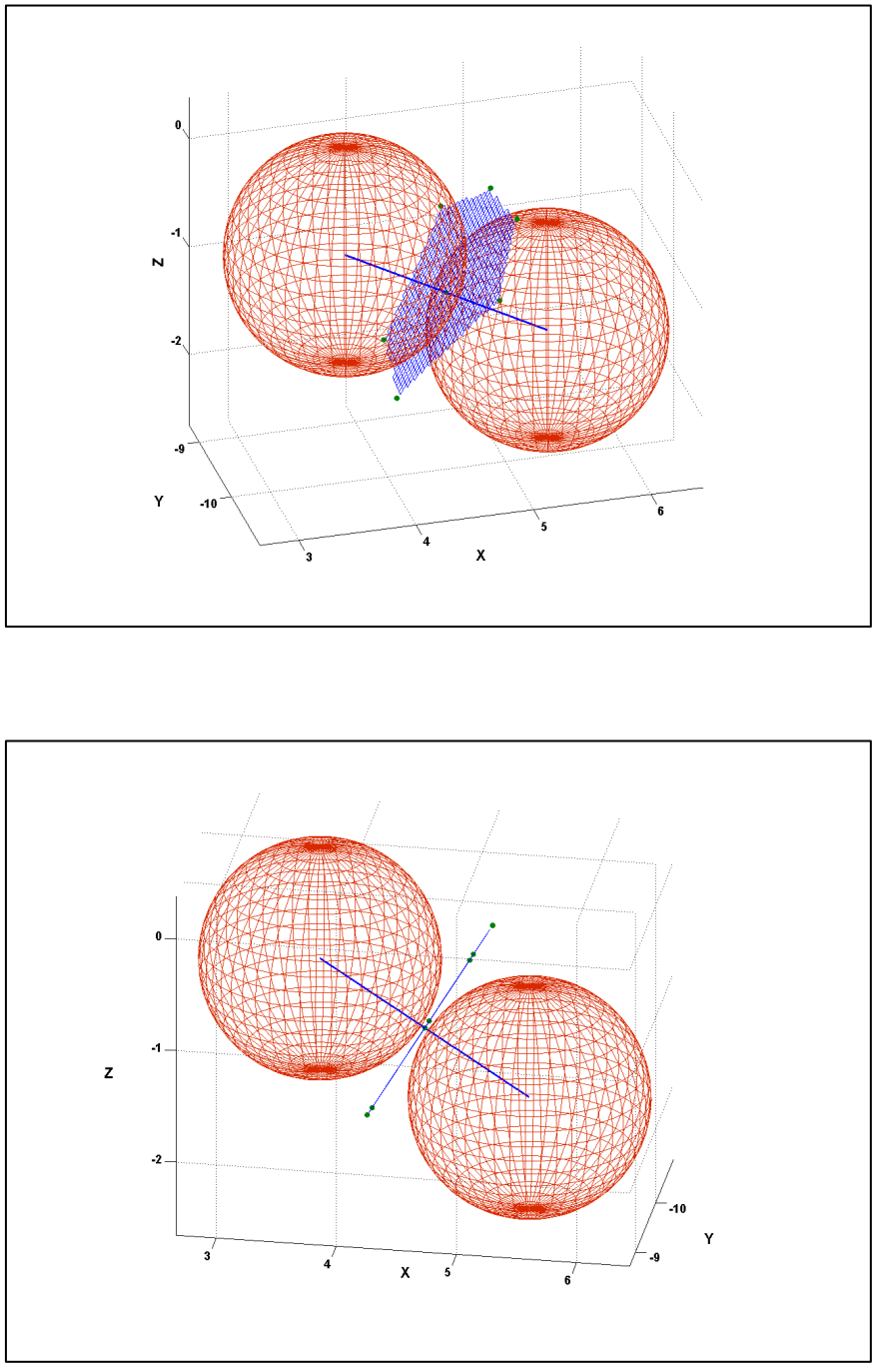

Figure 4.21: Two spatial views of spheres 763 and 908, the plane defined by the centers of the Delaunay cells in which the spheres are contained and the line that joins the sphere centers.

Plane equations of the type AX+BY+CZ=D can be written for every gap. The planes are defined by the centers of each Delaunay cell in the cluster and the center of the gap.

In order to calculate the local gradient of pressure it is necessary to express pressure as a function of spatial coordinates. Hypothetically, the pressure will be a linear function of these coordinates.

Because of the difficulties in finding a good fitting between pressure (P) and x, y and z coordinates, a fit of the pressure to two equivalent coordinates in the plane of the cell centers has been made. A transformation of the planes containing the gaps and the centers of the surrounding Delaunay cells has been performed in order to make those planes coincide with the plane Z_t=0, i.e., the coordinates z of all the points in the planes have been converted to zero (z_t=0), where the subscript *t* indicates transformed plane or coordinate. This way, pressure can be expressed as a function of x_t and y_t. Two steps are needed to achieve this transformation: translation and rotation of the plane.

1) **Translation** of the planes to make them pass through the origin of coordinates. In order to do this, the center coordinates of one Delaunay cell in the cluster are subtracted from the center coordinates of all the other Delaunay cells, including the first one. The new coordinates are called x', y' and z'. The resulting equation for the translated planes is:

$$A'x'+B'y'+C'z'=0 \qquad \text{Eqn. 4.28}$$

Table 4.6 contains the original coordinates of the centers of the Delaunay cells and the gap in the example considered.

Table 4.6: Spatial coordinates of the centers of the Delaunay cells and the center of the gap

CELL	x	y	z
4062	4.712206	-9.048703	-0.738846
4065	4.147898	-9.337939	-1.750930
4698	4.993623	-9.566960	-0.347516
5822	4.085258	-9.961979	-1.964586
6065	5.055728	-10.153978	-0.342051
6066	4.796963	-10.560625	-0.853045
GAP(center)	4.552448	-9.789479	-1.13814

The plane equation for these points is:

$$z = 1.706x + 0.171y - 7.228 \qquad \text{Eqn.4.29}$$

Figure 4.22 shows the original plane made by the centers of the 6 cells and the center of the gap. The plane does not pass through the origin of coordinates (0,0,0) which is represented by (•). Figure 4.23 shows another view of the same plane with the coordinates axis intersecting in the origin of coordinates.

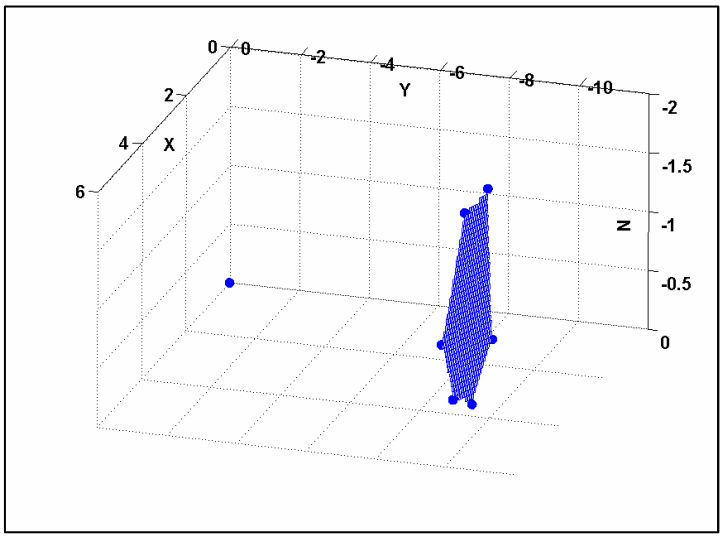

Figure 4.22: Original plane defined by the centers of the Delaunay cells and the center of the gap. The origin of coordinates is shown as well.

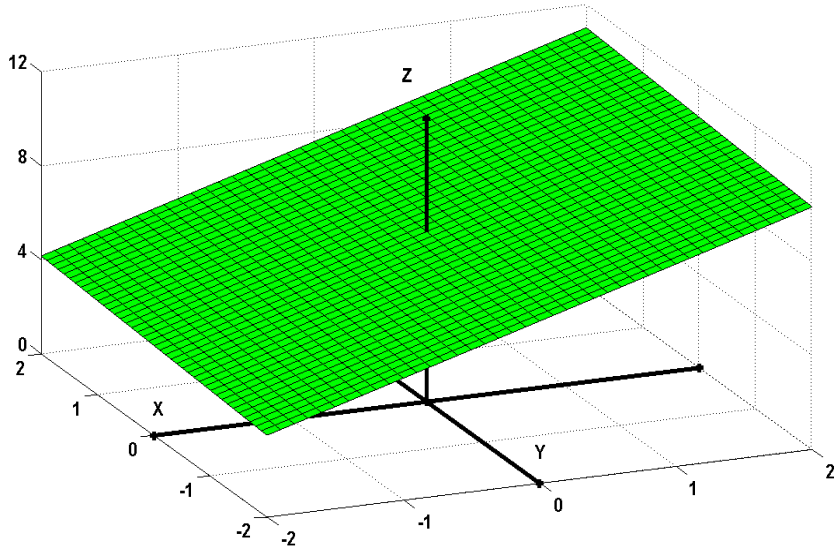

Figure 4.23: Another view of the original plane defined by the centers of the Delaunay cells and the center of the gap. The coordinates axes cross at point (0,0,0).

The coordinates of cell 4062 are subtracted to all the other cells including itself and the gap. Table 4.7 shows the new coordinates.

Table 4.7: Coordinates of Delaunay cells and gap after translation

	x'	y'	z'
4062	0.000000	0.000000	0.000000
4065	-0.564308	-0.289236	-1.012084
4698	0.281417	-0.518257	0.391330
5822	-0.626948	-0.913275	-1.225740
6065	0.343522	-1.105275	0.396795
6066	0.084757	-1.511922	-0.114199
GAP(center)	-0.159758	-0.740776	-0.399298

The new equation is:

$$z' = 1.706x' + 0.171y' \quad \text{Eqn. 4.30}$$

Figure 4.24 shows how, after translation, the plane passes through the origin of coordinates.

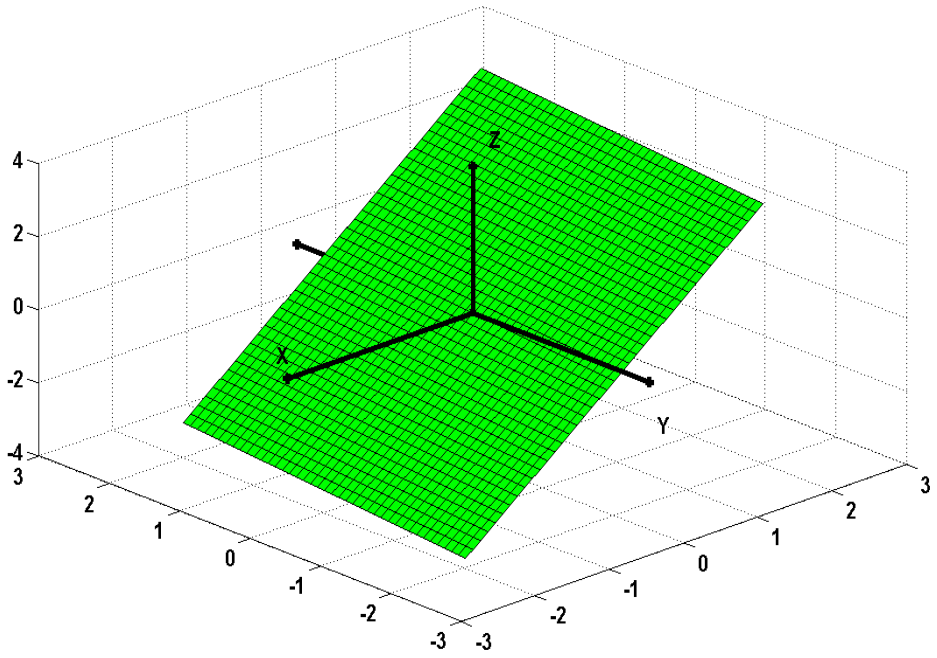

Figure 4.24: Plane passing through the origin after translation.

2) **Rotation** of the translated plane. Looking at Figure 4.24 above, it can be shown that there is not a single rotation that makes the plane coincide with the plane z=0. The plane has angles different than zero with the three coordinate axes. Two rotations are needed, the first one, around *z* axis makes the intersection of the plane with the plane z=0 coincide with the *x* axis, and the second one, around x axis, make the plane coincide with the plane z=0. The *z* coordinates of the points in the plane after these two rotations will equal zero.

Rotation around Z axis

Figure 4.25 shows the line resulting from the intersection of the translated plane with the plane z=0. The arrows indicate the direction in which the plane has to be rotated to make the intersection line coincide with the *x* axis.

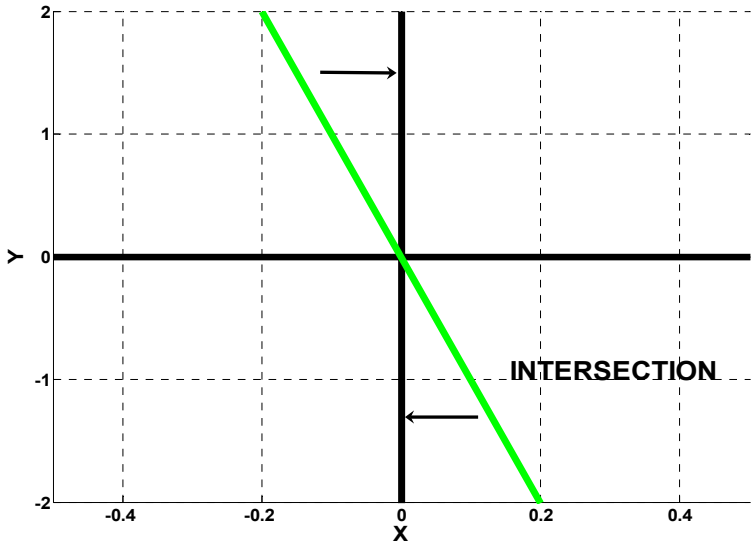

Figure 4.25: Intersection of the translated plane with the plane z=0.

Expressing the equation of the translated planes in step 1 as z'=Ax'+By', the angle for the first rotation depends on the values of A and B:

If (A>0 and B>0) or (A<0 and B<0)

$\theta = \text{atan}(A/B)$ Eqn. 4.31

Else if (A>0 and B<0) or (A<0 and B>0)

$\theta = -\pi/2 - \text{atan}(B/A)$ Eqn. 4.32

This rotation can be performed with the following rotation matrix (R_z):

$$R_Z = \begin{bmatrix} \cos\theta & -\sin\theta & 0 \\ \sin\theta & \cos\theta & 0 \\ 0 & 0 & 1 \end{bmatrix} \qquad \text{Eqn 4.33}$$

This matrix multiplies the matrix (*v'*) containing the coordinates of the points that are going to be transformed (Eqn 4.34) and the resultant matrix (*v"*) has the rotated coordinates.

$$v' = \begin{bmatrix} x_1' & x_2' & x_3' & x_4' & x_5' & x_6' & x_{gap}' \\ y_1' & y_2' & y_3' & y_4' & y_5' & y_6' & y_{gap}' \\ z_1' & z_2' & z_3' & z_4' & z_5' & z_6' & z_{gap}' \end{bmatrix} \qquad \text{Eqn. 4.34}$$

$$v'' = R_Z \cdot v' \qquad \text{Eqn. 4.35}$$

In the example considered, A=1.706 and B=0.071 (Eqn. 4.30), therefore equation 4.32 is used, yielding: θ= 84.3°. Equation 4.31 requires the angle in radians, therefore θ= 1.47. This rotation makes the intersection of the plane with the plane z=0 coincide with the *x* axis as Figure 4.26 shows. Table 4.8 shows the coordinates of the gap and the Delaunay cell centers after first rotation.

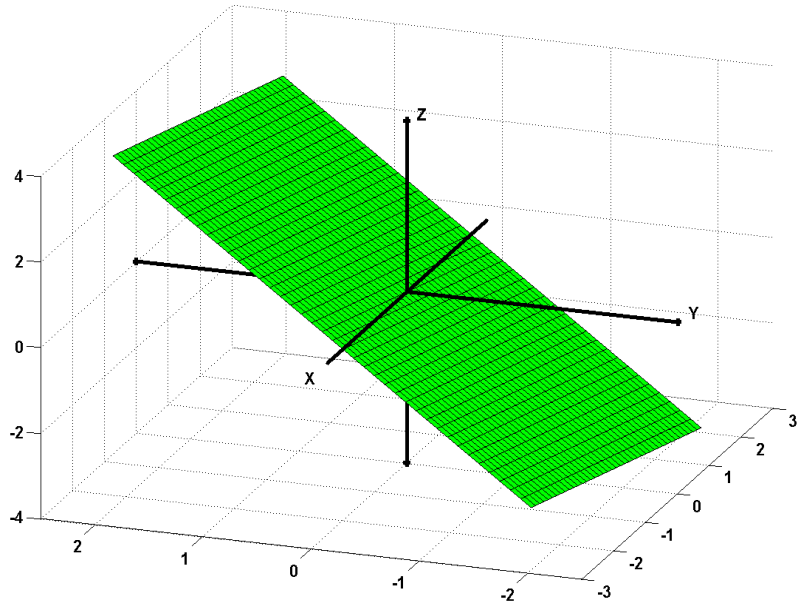

Figure 4.26: Plane after rotation around Z axis.

Table 4.8: Coordinates after rotation around Z axis.

	x''	y''	z''
4062	0	0	0
4065	0.2314	-0.5904	-1.0121
4698	0.5438	0.2283	0.3913
5822	0.8461	-0.715	-1.2257
6065	1.1341	0.2314	0.3968
6066	1.5128	-0.0667	-0.1142
GAP(center)	0.7211	-0.2329	-0.3993

Since the rotated plane contains the *x* axis, the new equations for the plane are of the type z=By; all *A* coefficients are equal to zero. The equation for the plane in the example is:

$$z'' = 1.71y'' \qquad \text{Eqn. 4.36}$$

Rotation around X axis

Figure 4.27 shows the *zy* projection of the plane after rotation around the *z* axis. The arrows show the direction in which the plane has to be rotated now to make it coincide with the plane z=0.

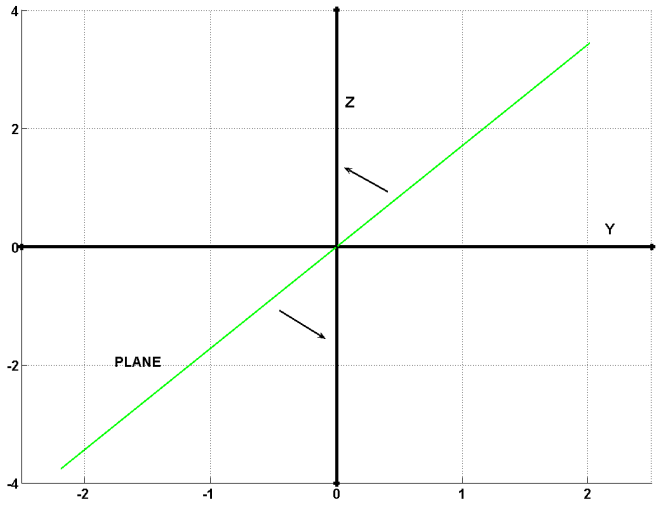

Figure 4.27: yz projection of the plane. The plane is the diagonal green line.

The angle needed for the second rotation is:

$$\alpha = \text{atan}(-B) \qquad \text{Eqn. 4.37}$$

In the example considered, α= -59.7 °, or -1.04 radians for the rotation matrix. In this case, the rotation matrix R_x corresponds to:

$$R_X = \begin{bmatrix} 1 & 0 & 0 \\ 0 & \cos\alpha & -\sin\alpha \\ 0 & \sin\alpha & \cos\alpha \end{bmatrix} \qquad \text{Eqn 4.38}$$

which is going to be multiplied by the matrix *v''* containing the coordinates of the points after the rotation around *z* axis:

$$v'' = \begin{bmatrix} x_1'' & x_2'' & x_3'' & x_4'' & x_5'' & x_6'' & x_{gap}'' \\ y_1'' & y_2'' & y_3'' & y_4'' & y_5'' & y_6'' & y_{gap}'' \\ z_1'' & z_2'' & z_3'' & z_4'' & z_5'' & z_6'' & z_{gap}'' \end{bmatrix} \qquad \text{Eqn 4.39}$$

The resulting matrix v_t contains the final transformed coordinates of the points

$$v_t = R_X \cdot v'' \qquad \text{Eqn. 4.40}$$

$$v_t = \begin{bmatrix} x_{1t} & x_{2t} & x_{3t} & x_{4t} & x_{5t} & x_{6t} & x_{gap\,t} \\ y_{1t} & y_{2t} & y_{3t} & y_{4t} & y_{5t} & y_{6t} & y_{gap\,t} \\ z_{1t} & z_{2t} & z_{3t} & z_{4t} & z_{5t} & z_{6t} & z_{gap\,t} \end{bmatrix} \qquad \text{Eqn. 4.41}$$

Figure 4.28 shows how the rotated plane coincides with the plane z=0.

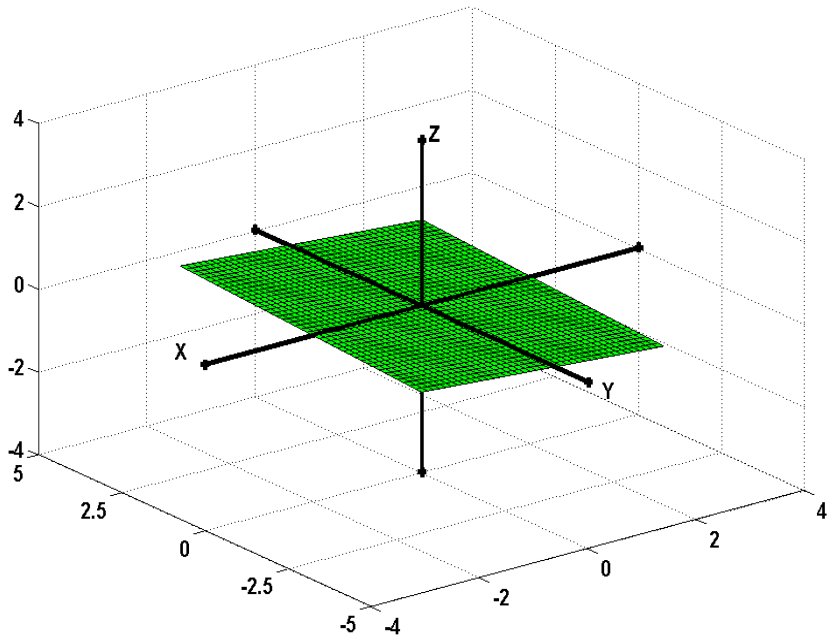

Figure 4.28: Plane after second rotation around *x* axis.

Table 4.9 shows the transformed coordinates. Now z_t coordinates are all equal to zero and the equation for the plane is $\mathbf{z_t=0.}$

Table 4.9: Coordinates after rotation around Z axis.

	$\mathbf{x_t}$	$\mathbf{y_t}$	$\mathbf{z_t}$
4062	0	0	0
4065	0.2314	-1.1717	-0.0032
4698	0.5438	0.453	0.0012
5822	0.8461	-1.419	-0.0039
6065	1.1341	0.4593	0.0013
6066	1.5128	-0.1323	-0.0003
GAP(center)	0.7211	-0.4623	-0.0013

Pressure can be now expressed as a function of the new coordinates x_t and y_t for every gap (notice every gap needs its own rotations). Table 4.10 shows, for every Delaunay cell in this example, the transformed coordinates and the pressures in the center of the cells (from the steady state calculation) and figure 4.29 plots pressure as a function of the transformed coordinates.

Table 4.10: Transformed coordinates and pressure in Delaunay cells

Cell	**x_t**	**y_t**	**P**
4062	0	0	1.104094
4065	0.2314	-1.1717	1.105602
4698	0.5438	0.453	1.098336
5822	0.8461	-1.419	1.101616
6065	1.1341	0.4593	1.087927
6066	1.5128	-0.1323	1.083915

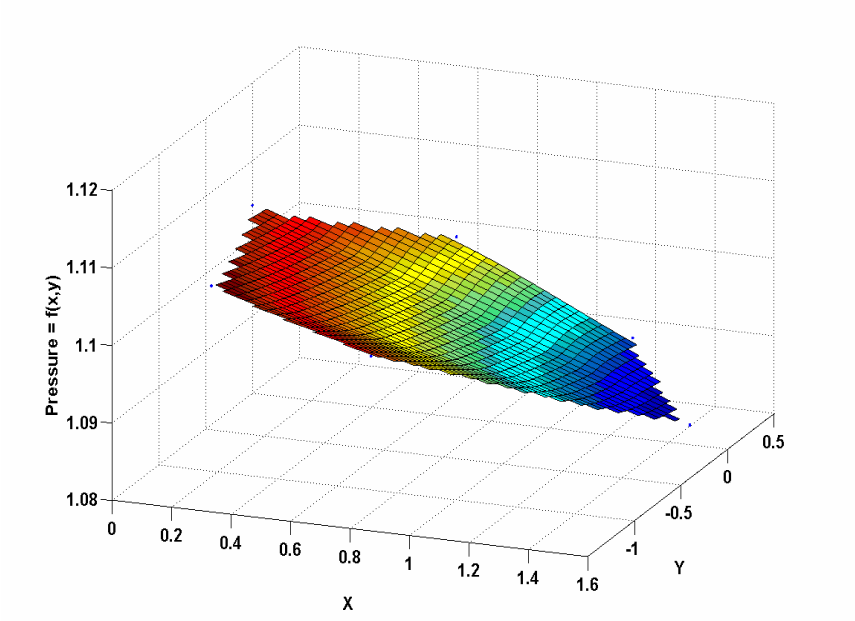

Figure 4.29: Pressure *vs*. transformed coordinates x_t and y_t

Figure 4.29 suggest a linear relationship between these three parameters. For each gap, the pressures have been fitted to plane equations such as

$$P= AX_t+BY_t+C \qquad \text{Eqn. 4.42}$$

For the example considered:

$$P=-0.0134X_t-0.0041Y_t+1.1052 \qquad \text{Eqn. 4.43}$$

Table 4.11 compares the real values of pressure in the centers of the cells with the values calculated with equation 4.43. The percentage of error has been calculated as:

$$Error\,(\%) = \frac{P - P^*}{P} \times 100 \qquad \text{Eqn. 4.44}$$

Table 4.11 Actual (P) and calculated (P*) pressures in the centers of the Delaunay cells. Linear correlation.

Cell	P	P*	Error (%)
4062	1.104094	1.1052	-0.100
4065	1.105602	1.106903	-0.118
4698	1.098336	1.096056	0.208
5822	1.101616	1.09968	0.176
6065	1.087927	1.08812	-0.018
6066	1.083915	1.085471	-0.145

The correlation coefficient for this fitting is R^2=0.9643.

A fit including the cross product term has also been tried. In this case the fitting equation corresponds to:

$$P= AX_t+BY_t+CX_tY_t+D \qquad \text{Eqn. 4.45}$$

The corresponding equation for the considered example is:

$$P = -0.014X_t - 0.0017Y_t - 0.0036X_tY_t + 1.1058 \quad \text{Eqn. 4.46}$$

The calculated values of pressure are shown in Table 4.12 and plotted in Figure 4.30.

Table 4.12: Actual (P) and calculated (P*) pressures in the centers of the Delaunay cells. Cross product correlation.

Cell	P	P*	Error (%)
4062	1.104094	1.1058	-0.154
4065	1.105602	1.105528	0.007
4698	1.098336	1.09653	0.164
5822	1.101616	1.100689	0.084
6065	1.087927	1.087267	0.061
6066	1.083915	1.085566	-0.152

The correlation coefficient for this fitting is R^2=0.9746.

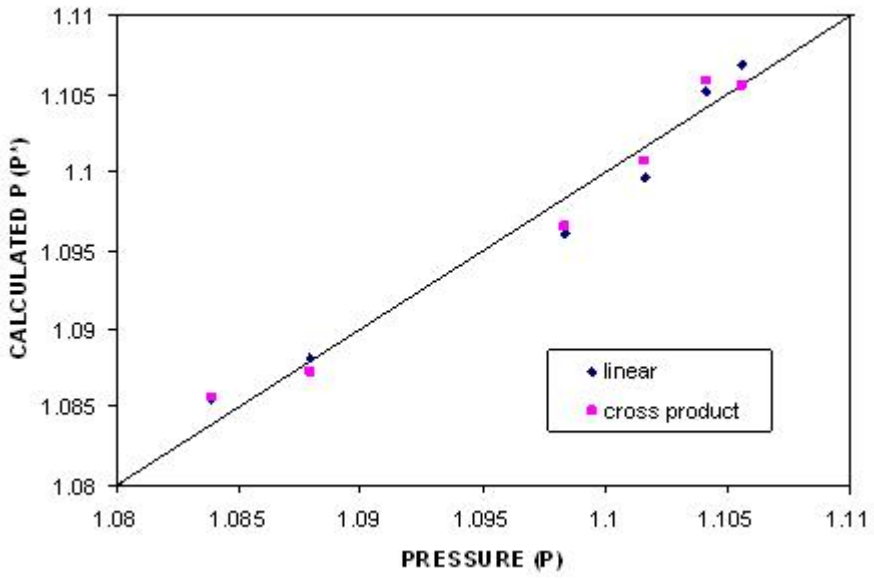

Figure 4.30: Calculated pressure *vs.* real pressure by two different fitting equations.

The correlation coefficients are similar for both methods. The linear method is going to be used in this thesis for the rest of the calculations.

Since a relationship between pressure and spatial coordinates has been obtained, the pressure in the gap can be easily calculated by substituting X_t and Y_t for the transformed coordinates of the center of the gap.

Figure 4.31 is a XY projection of Figure 4.29 where the center of the gap and each Delaunay cell are shown. The lines correspond to contours of pressure.

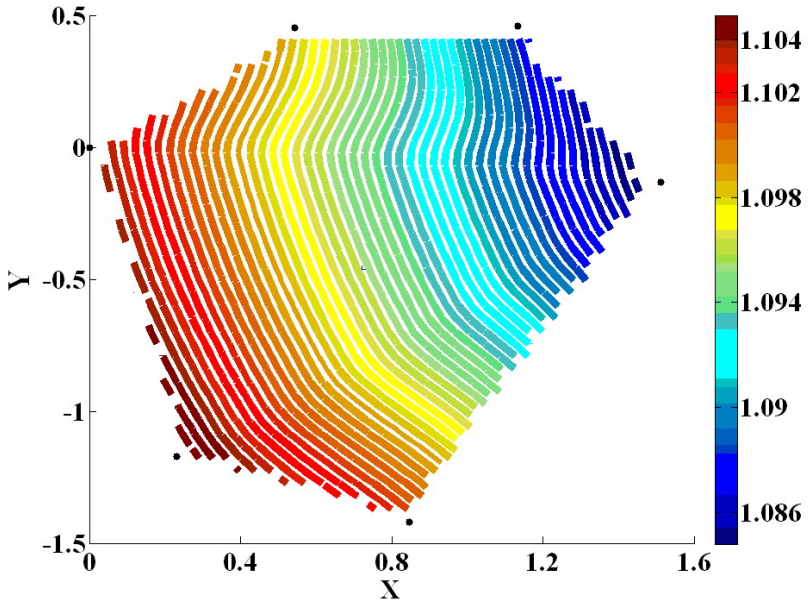

Figure 4.31: Contours of pressure in the plane defined by the centers of the Delaunay cells and the center of the gap.

The gradient of pressure (∇P) necessary to estimate velocity and flow in gaps is calculated from equation 4.42 as follows:

$$\nabla \vec{P} = \frac{\partial P}{\partial X}\vec{i} + \frac{\partial P}{\partial Y}\vec{j} \qquad \text{Eqn. 4.47}$$

which allows the calculation of the pressure gradient modulus as:

$$\left\|\nabla P\right\| = \sqrt{A^2 + B^2} \qquad \text{Eqn. 4.48}$$

Table 4.13 shows the minimum, maximum and average values of the calculated pressure gradient and Figure 4.32 plots the modulus of the pressure gradient in every gap in the range of interest versus the distance of the gap from the center of the packing. Figure 4.33 plots the modulus of the pressure gradient in every gap versus the gap width. A crude estimate average gradient follows from the boundary conditions: *P* in the pore space is P=2 at distances smaller than 1.5*R* and P=1 at distances bigger than or equal to 15*R*:

$$\nabla P = \frac{1}{r}\frac{dP}{dr} \approx \frac{\Delta P}{(r_{out} - r_{in})(r_{out} - r_{in})} \qquad \text{Eqn. 4.49}$$

From where:

$$\nabla P \approx \frac{2-1}{(15-1.5)^2} = 0.005$$

Table 4.13: Minimum, maximum and average values for the modulus of the pressure gradient in gaps.

	$\|\| \nabla \mathbf{P} \|\|$
Minimum	$1.9 \cdot 10^{-5}$
Maximum	0.340
Average	0.037

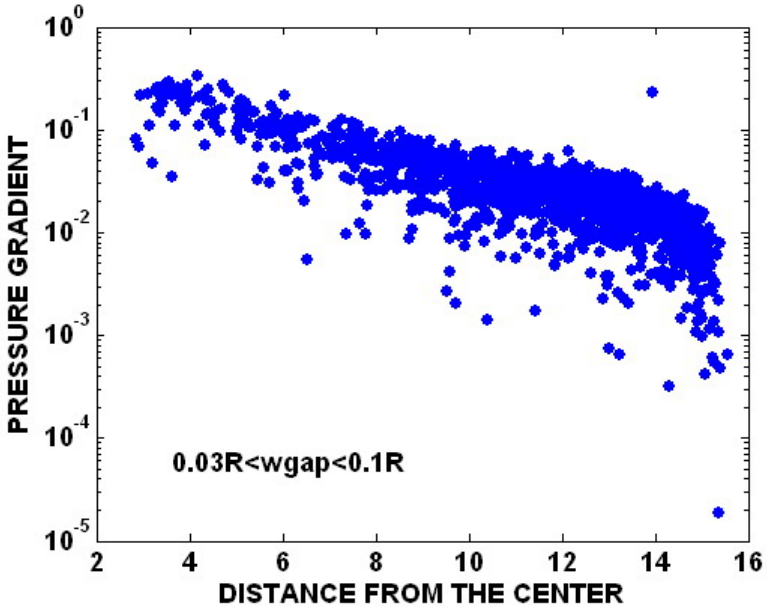

Figure 4.32: Pressure gradient in gaps *vs.* distance from the center of the packing to the gaps in the range of interest.

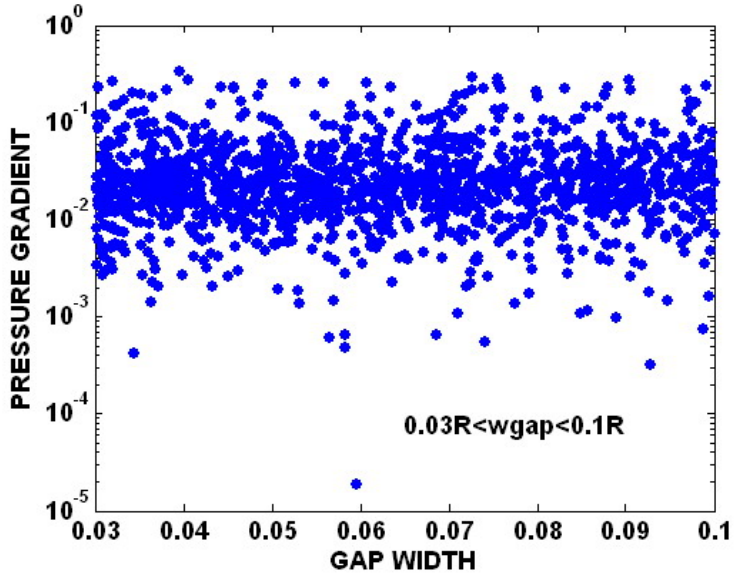

Figure 4.33: Pressure gradient in gaps *vs.* distance from the center of the packing to the gaps in the range of interest.

Table 4.14 shows the values of the pressure gradient from one pore to its neighbor for the Delaunay cells containing the pair of spheres used as example in this section (763-908). The value of the pressure gradient in the gap has been calculated with the method outlined above.

Table 4.14: Example of pressure gradient in the pore throats surrounding a gap.

Pore throat	**ΔP**	**Distance between centers**	**∇P**
4062-4065	0.001508	1.194331	0.001263
4065-5822	0.003986	0.662581	0.006016
5822-6066	0.012214	1.449256	0.084278
6066-6065	0.004012	0.702481	0.005711
6065-4698	0.010409	0.590235	0.017635
4698-4062	0.005758	0.707762	0.008135
Gap			**0.014**

Note that the value of the pressure gradient in the gap is between the minimum and maximum values of the pressure gradients for the throats surrounding the gap (cf. Figure 4.31 for the pressure contours).

Of particular interest are gaps between grains whose centers are aligned approximately with the macroscopic gradient in potential. Flow through such gaps should be negligible, and thus they will not contribute to straining. The number of gaps rendered ineffective in this way could be an important factor when considering the entire packing. For the gaps in the range of interest ($0.03R<w_{gap}<0.1R$), only 23 out of 1449 (1.6% of the gaps) have zero flow through them. These gaps are not associated with boundary Delaunay cells since those cells were not considered from the beginning for this calculation. When considering all the gaps in the packing, i.e., gaps whose width is between $0.01R$ and $0.1R$, this number is 35 out of 2442 (1.4% of the gaps).

A flow chart summarizing the steps described above for calculation of the pressure gradient in gaps is shown next (Figure 4.34).

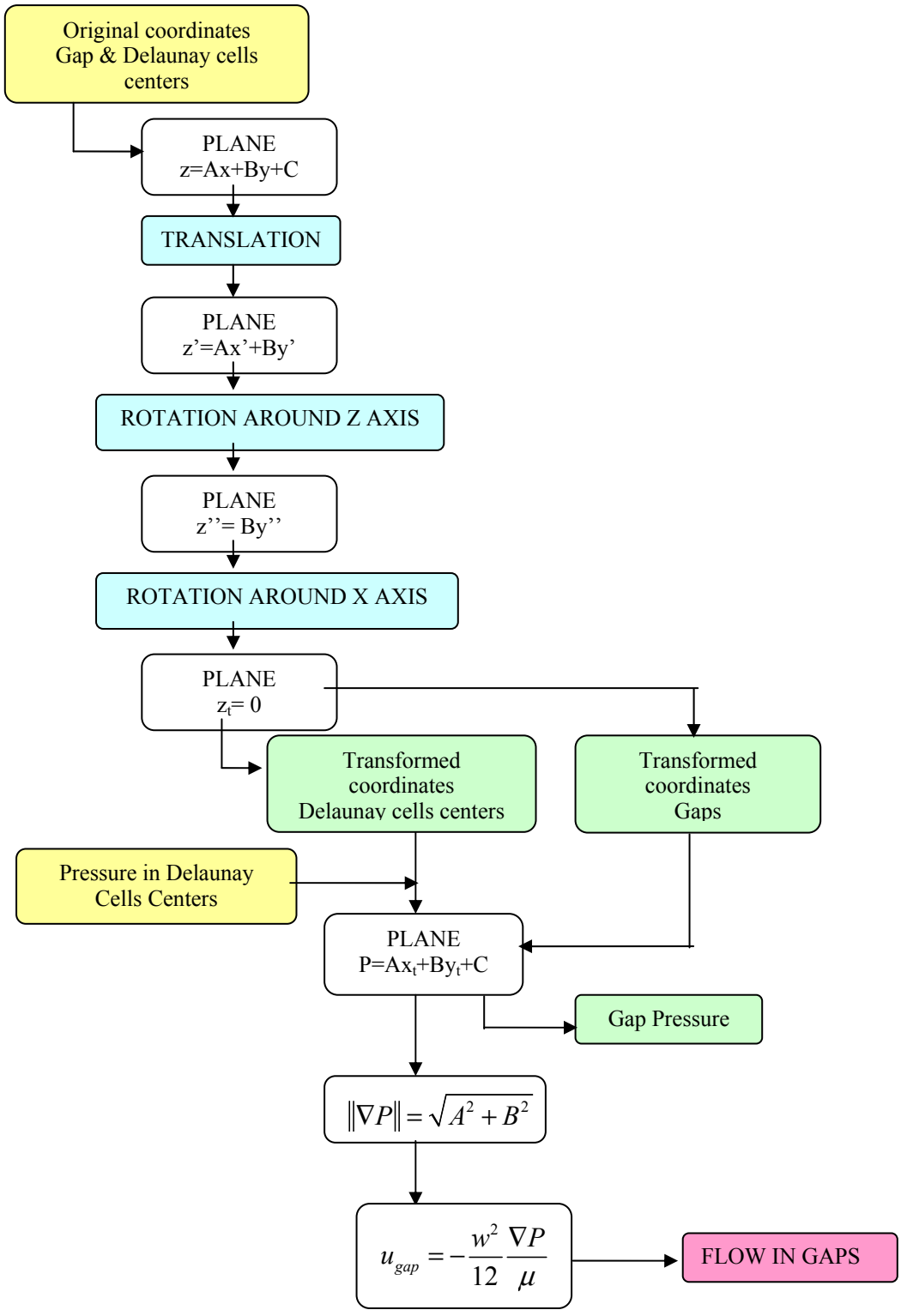

Figure 4.34: Flow chart for the calculation of the pressure gradient in gaps.

4.2.5 Results: Particle specific flow through gaps

The previous section provides an estimation of the local gradient in potential. The velocity in gaps has been calculated with equation 4.8, using the gradient of pressure calculated in the previous section. Figure 4.35 plots velocity in gaps vs. gap width.

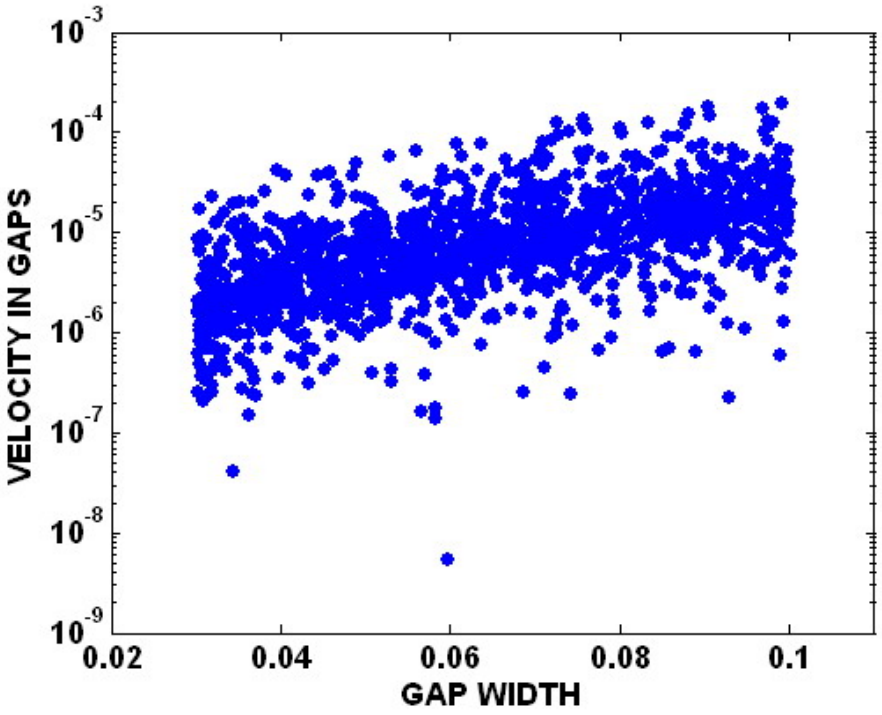

Figure 4.35: Linear velocity (LT^{-1}) in gaps *vs.* gap width.

This equation calculated velocity in gaps independently of the size of the suspended particles.

Next, there are Figures showing the variation of volumetric flow in gaps with the distance from the center, the gap width or radius and the size of the particles being retained. The flow in gaps has also been compared with the flow in pore throats.

First of all, Figure 4.36 shows the variation of volumetric flow in gaps with the gap size for strained particles of size d/D=0.03, figure 4.37 shows this variation for particles of size d/D=0.04 and Figure 4.38 does the same with particles of sizes d/D=0.05. In order to compare with the magnitude for pore throats, the gap size is represented now by half its width, and this magnitude is called *gap radius*.

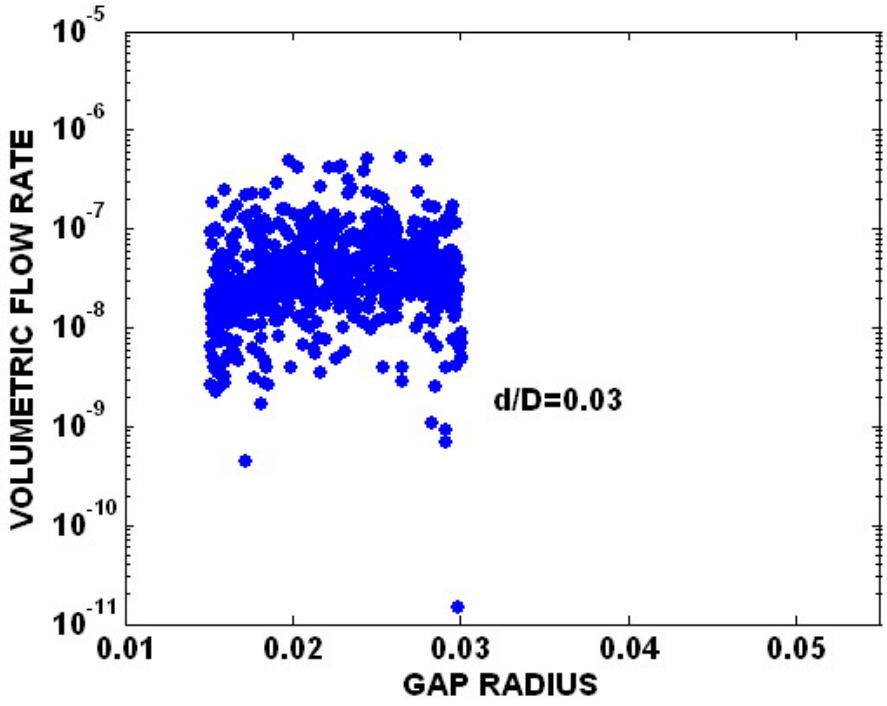

Figure 4.36: Volumetric flow vs. gap radius for particle size d/D=0.03.

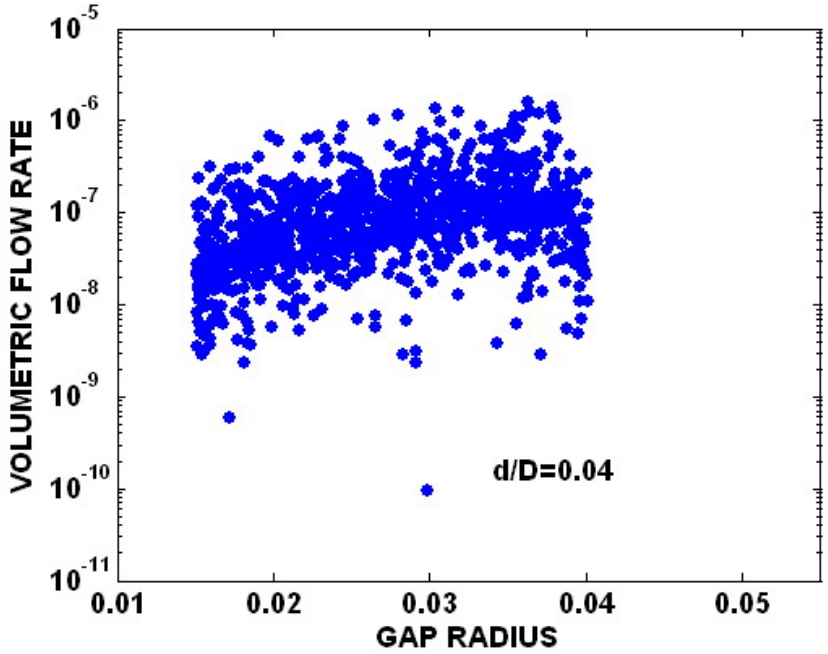

Figure 4.37: Volumetric flow vs. gap radius for particle size *d/D*=0.04.

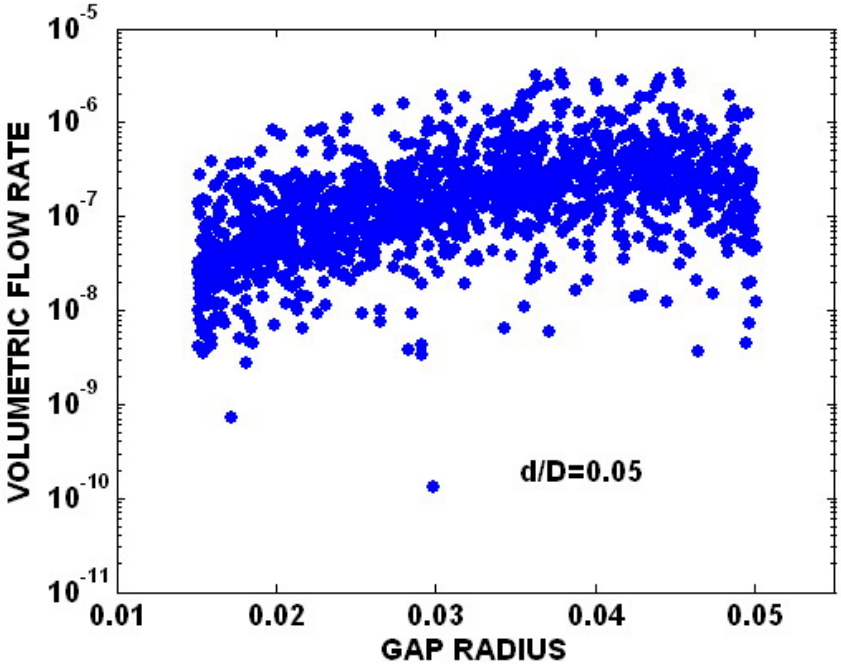

Figure 4.38: Volumetric flow vs. gap radius for particle size *d/D*=0.050.

In Figure 4.36 there are no data points for gap radius bigger than 0.03*R* since the particles whose size is *d/D*=0.03 will not be strained in those gaps. Particles of relative size *d/D*=0.030 will get strained in the gaps in the range of interest whose radii (half width) are between 0.015*R* and 0.03 *R*. They will pass through the gaps whose radii are within 0.03*R* and 0.05*R*. Particles of size *d/D*=0.04 shown in Figure 4.37 will pass through the gaps whose radii are bigger than 0.04*R*. On the other hand, the particles of size *d/D*=0.05, shown in Figure 4.38, will get strained in all the gaps whose size is within the range of interest. Both figures show how the volumetric flow slightly increases with the radius of the gap but starts decreasing when the particle reach gaps whose radii are close to the particle size. As in the case of the conductance-length product, Figure 4.10, the variables range of capture and gap width affects the value of the volumetric flow. Moreover, in equation 4.9 for the volumetric flow calculation, those factors are also included in the value of the linear velocity u_{gap}.

Table 4.15 summarizes the average volumetric flows for particles of different sizes. Geometric and arithmetic averages have been calculated. In this case, since the volumetric flows do not add together to produce a total, the geometric mean is more relevant. The flow increases as the particle size increases. Table 4.15 shows that the flow in gaps is about two to three orders of magnitude smaller than the flow in pore throats.

Table 4.15: Average flow in gaps for different particle sizes.

Particle size (d/D)	**Volumetric flow (geometric mean)**	**Volumetric flow (arithmetic mean)**
0.02	$1.02 \cdot 10^{-8}$	$1.65 \cdot 10^{-8}$
0.025	$2.11 \cdot 10^{-8}$	$3.39 \cdot 10^{-8}$
0.03	$3.40 \cdot 10^{-8}$	$5.44 \cdot 10^{-8}$
0.035	$5.16 \cdot 10^{-8}$	$8.51 \cdot 10^{-8}$
0.04	$7.42 \cdot 10^{-8}$	$1.33 \cdot 10^{-7}$
0.045	$1.01 \cdot 10^{-7}$	$1.89 \cdot 10^{-7}$
0.05	$1.34 \cdot 10^{-7}$	$2.63 \cdot 10^{-7}$
Throats	$2.13 \cdot 10^{-5}$	$4.54 \cdot 10^{-5}$

Figures 4.39, 4.40 and 4.41 show the variation of the flow in gaps with the distance from the center of the packing for particles of sizes *d/D* equal to 0.03, 0.04 and 0.05 respectively. In the three cases the flow decreases with the increase in distance due to the spherical flow field through the Finney packing. This same trend was observed for the pore throats (cf. Figure 4.6).

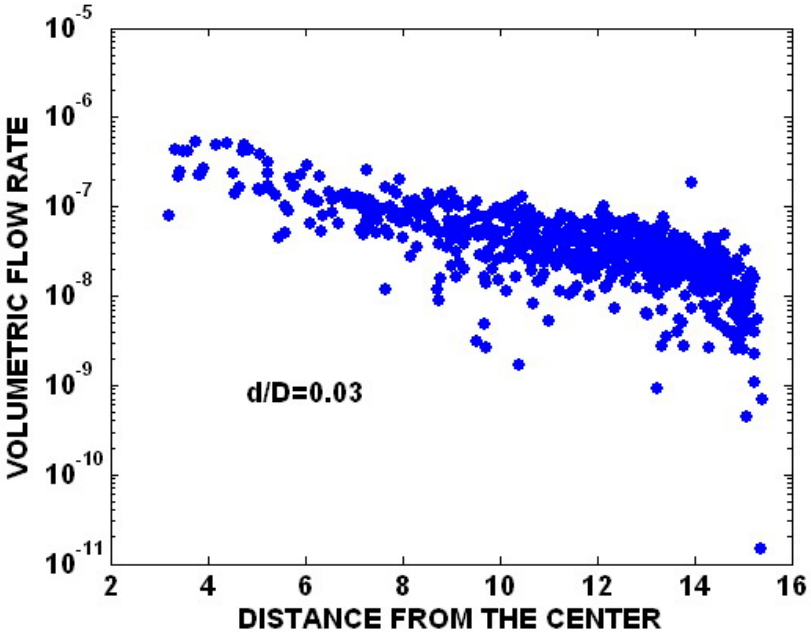

Figure 4.39: Volumetric flow in gaps vs. distance from the center for particle size *d/D*=0.03.

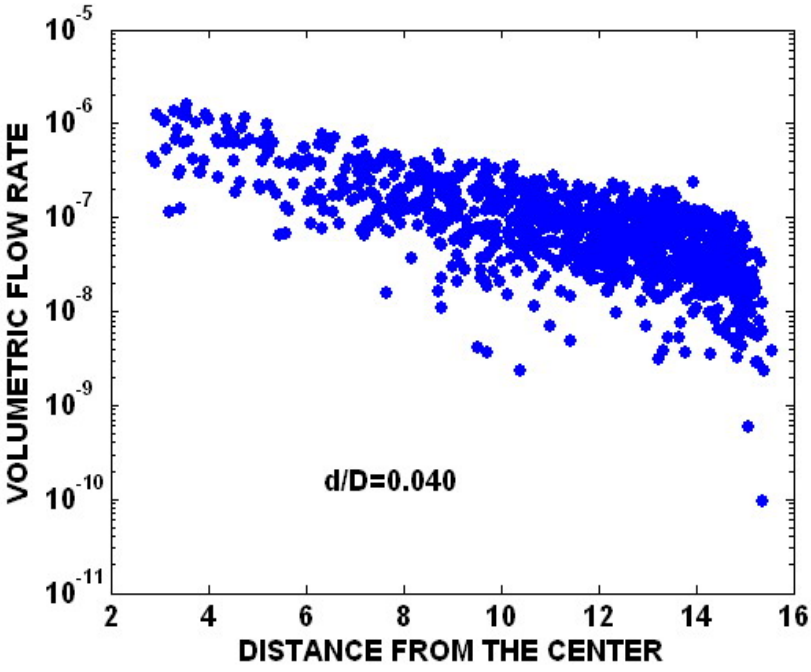

Figure 4.40: Volumetric flow in gaps vs. distance from the center for particle size *d/D*=0.04.

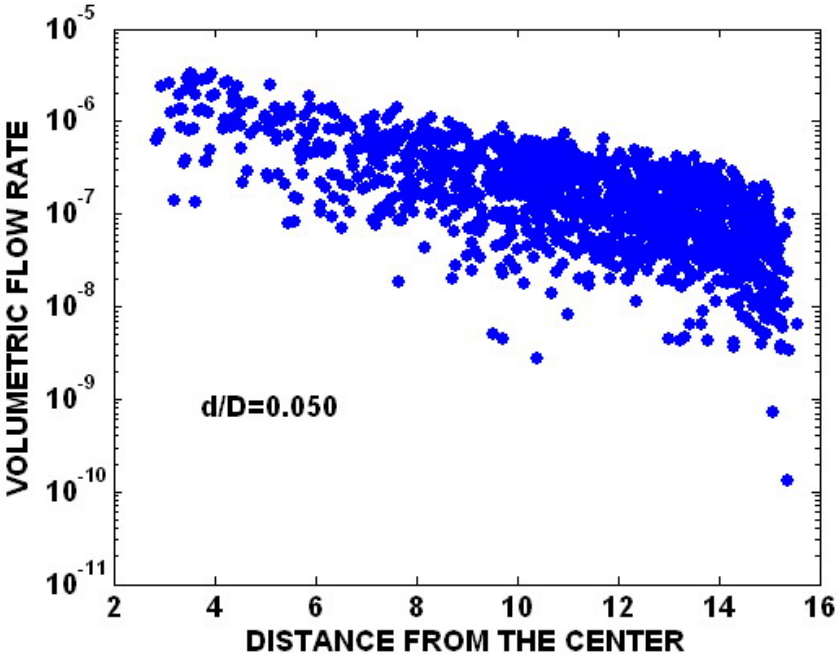

Figure 4.41: Volumetric flow in gaps vs. distance from the center for particle size *d/D*=0.05.

Those gaps with volumetric flow equal to zero have not been included in the calculations. The spherical flow field emphasizes the contribution of gaps near the center. A correction for this artifact will be described in Chapter 5.

4.2.6. Average flow in throats around gaps

To compare the flow in the gaps to the flow in the pore throats, an average value of flow for the throats surrounding a gap has been calculated. Every gap in the range of interest is contained in 4 to 9 Delaunay cells, therefore for every gap there are 4 to 9 throats. The average of the absolute values of the flows in the surrounding throats and the average of their inscribed radius have been calculated. In this fashion, there is one value of flow in throats corresponding to each of the 1449 gaps in the range of interest. Figure 4.42 shows volumetric flow versus radius for gaps and corresponding throats. The data for the gaps corresponds to the particles of size d/D=0.05. Similar to previous results, the flow in the gaps is about two to three orders of magnitude smaller than the average flow in adjacent throats. Figure 4.43 shows flow in gaps and equivalent throats vs. distance from the center. The data for the gaps also corresponds to the particle size d/D=0.05. The equivalent flow in throats around gaps also decreases in pores that are far from the center of the packing. The geometric average of all the average flows around gaps in the range of interest is $2.53 \cdot 10^{-5}$ which is only slightly bigger than the value reported in Table 4.15 as the average flow of all the throats in the packing.

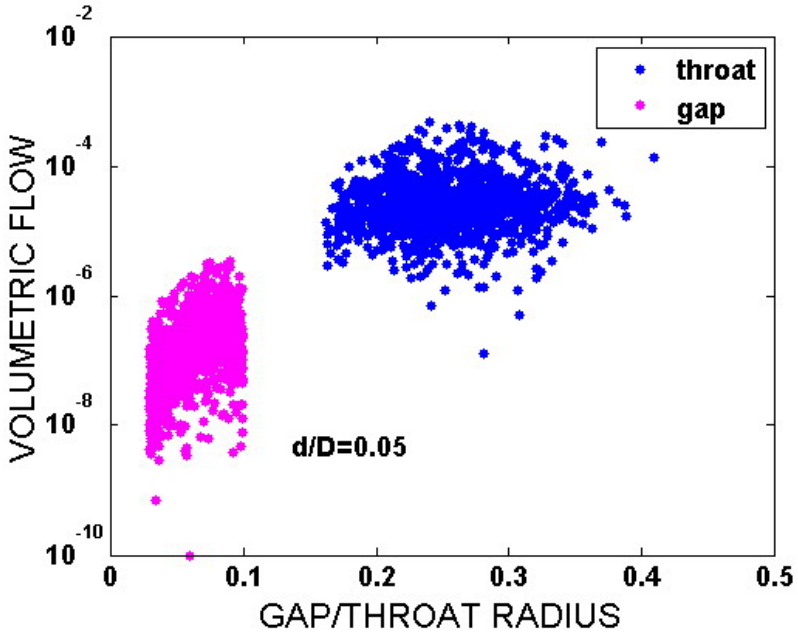

Figure 4.42: Volumetric flow in gaps and equivalent pore throats *vs*. radius. Particle size *d/D*=0.05.

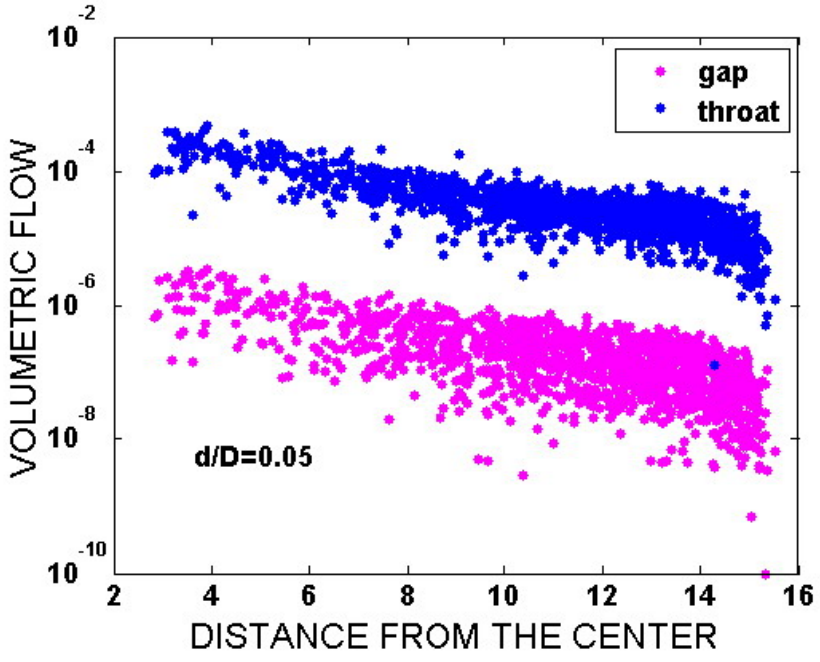

Figure 4.43: Volumetric flow in gaps and equivalent pore throats *vs*. distance from the center of the packing. Particle size *d/D*=0.05.

4.3 REVIEW

The steady state flow velocity has been calculated for each gap in the range of interest assuming the gap is a slit of length equal to twice the range of capture and width equal to the gap width. The volumetric flow through the gap is calculated then by multiplying the velocity in the gap by its cross sectional area. This step introduces the dependence of the volumetric flow on the size of the particle being strained, since this dependence is embodied in the range of capture.

The local gradient in potential in gaps needed to calculate velocities and therefore flows in gaps. Because of the complex spatial distribution of gaps in the pore space this calculation is not straightforward. A transformation of the spatial coordinates of the centers of the gaps and the centers of the Delaunay cells containing the gaps was performed in order to find a correlation between spatial coordinates and pressure that allows an estimation of the pressure gradient.

The results showed that the flow in gaps is about three orders of magnitude smaller than the flow in the gaps.

Chapter 5: Model for particle straining in gaps

The objective of this chapter is to forecast the macroscopic consequences of straining in gaps between pair of grains. The results will be compared to the experiments reported in the literature, particularly to the correlations between straining rate and the ratio of colloid to grain sizes (Eqn.1.2 and Eqn.1.3).

An appropriate support for these predictions is the theory of Sharma and Yortsos (1987c). This theory establishes a mechanistic connection between pore scale straining events and macroscopic behavior considering size exclusion as the dominant mechanism for particle trapping. In the process considered in this theory the size of the fine particles (strained particles) is comparable to the pore size. Continuum scale population balances have been formulated in terms of frequency distributions of pore throat sizes and particle sizes. The dimensional form of the population balance equation for single size particles is expressed as follows:

$$\frac{\partial C}{\partial t}+\frac{\partial C}{\partial x}=-\frac{1}{\mu}\frac{I(r_s)}{I(\infty)}C \qquad \text{Eqn. 5.1}$$

where μ is the ratio of typical pore throat length l_p to length of granular medium L, r_s is the size of suspended particles, C is the concentration of suspended particles in number of particles by volume of injected carrier fluid, x is the distance along the length of the porous medium, and I is a cumulative local flow rate distribution. The right hand side of Eqn. 5.1 corresponds to a particle trapping rate that is first order in particle concentration.

The cumulative flow rate distribution I is expressed as a function of the pore throat radius, r_p in a previous paper by the same authors (Sharma and Yortsos, 1987a). In this case:

$$I(r) = \int_0^r r_p^2 u_R f_p dr_p \qquad \text{Eqn. 5.2}$$

where u_R is the fluid velocity through a throat of radius r_p, and $f_p\ dr_p$ is the fraction of pore throats of radius r_p. The volumetric flow rate through a throat is proportional to $r_p^2 u_R$.. Therefore, the previous equation can be expressed as a function of the volumetric flow through a throat, q_R:

$$I(r) = \int_0^r q_R f_p dr_p \qquad \text{Eqn. 5.3}$$

In this theory the influence of pore scale geometry enters the rate constant for straining as the ratio of cumulative flow distributions in the particle balance equation (Eqn. 5.1)

The frequency distribution of gaps between grains calculated in Chapter 3 for the Finney packing and the flow rates through each gap appropriate for a given particle size calculated in Chapter 4 enter the continuum model via the local flow distribution $I(r)$ defined in equation 5.2. In this work the flow distribution includes only gaps. The inclusion of the pore throats will be the next step in future work after testing the theory for gaps.

The straining rate constant in the Sharma and Yortsos theory, derived from a dimensionless form of equation 5.1, is:

$$\frac{1}{\mu}\frac{I(1/A)}{I(\infty)} \qquad \text{Eqn. 5.4}$$

where A is the ratio of the average size of pore throats r_p to the average size of suspended particles r_s.

After extending the theory to include gaps, the primary validation will be to determine how the straining rate constant scales with the size of particle being strained. For the purpose of this thesis, the diameter of the strained particle, d, is identified as d_s, which is equal to $2 \cdot r_s$. The diameter of the soil grains, D, is identified as D_p, which is equal to $2 \cdot r_p$. Therefore, d/D is equivalent to r_s/r_p denoted $1/A$ in Sharma and Yortsos theory. Hence the dependence of the straining rate constant on the size of the strained particle will be:

$$\frac{1}{\mu}\frac{I(d/D)}{I(\infty)} \qquad \text{Eqn. 5.5}$$

which expressed in a dimensional form leads to :

$$\frac{I(r_s)}{I(\infty)} \qquad \text{Eqn. 5.6}$$

Since μ is a constant only the ratio between the two cumulative flows is going to be used in order to study the scaling of the straining constant with the particle size. The cumulative flow distribution $I(r)$ expresses the assumption that the probability of a particle entering a constriction is proportional to the flow rate into that constriction. A second validation of the extension of the theory to include gaps will be the case in which straining is taken to be independent of local flow velocity. This assumption reduces the integral I to the frequency distribution of the constrictions, and it will be called $I_c(r)$:

$$I_c(r) = \int_0^r f_p dr_p \qquad \text{Eqn. 5.7}$$

If the straining constant calculated this way scales correctly with *d/D*, it would provide a geometric basis for straining models that would be easier to measure and apply than the flow-weighted theory.

5.1 NORMALIZATION OF THE FLOW

Since the Finney packing is a spherical, the calculated flow in gaps and pore throats decreases when the pores or gaps are further away from the center of the packing. Figures 4.6 and 4.38 in Chapter 4 presented this tendency. At constant flow rate, the spherical flow velocity is inversely proportional to the square of the distance as indicated by the shape of the Laplace operator (∇^2) that calculates radial flow:

$$\nabla^2 = \frac{1}{r}\frac{d}{dr}\left(r\frac{d}{dr}\right) = \frac{d^2}{dr^2} + \frac{1}{r}\frac{d}{dr} \qquad \text{Eqn. 5.8}$$

where r is the distance from the center. Thus gaps near the center of the packing will influence $I(r)$ disproportionately. A normalization of the spherical flow field is performed in this section in order to balance the influence of all gaps.

A first approach for the normalization will be to multiply the flow in every gap and pore throat by the square of the distance from the center. For the purpose of this chapter, the volumetric flow has been calculated in all the gaps in the portion of the Finney packing considered, that is, gaps whose width is between $0.01R$ and $0.1R$. The lower bound is given by the point contact threshold and the upper bound is given by the assumption that gap widths bigger than $0.1R$ are part of the pore throat.

Figure 5.1 shows the results for the case of d/D=0.045 before multiplication by the square of the distance from the center, and Figure 5.2 shows the results for the same particle size after multiplication. Notice how the amount of data for the gaps in the

figures increases with respect to the figures shown in Chapter 4, since now the range of gaps considered has increased.

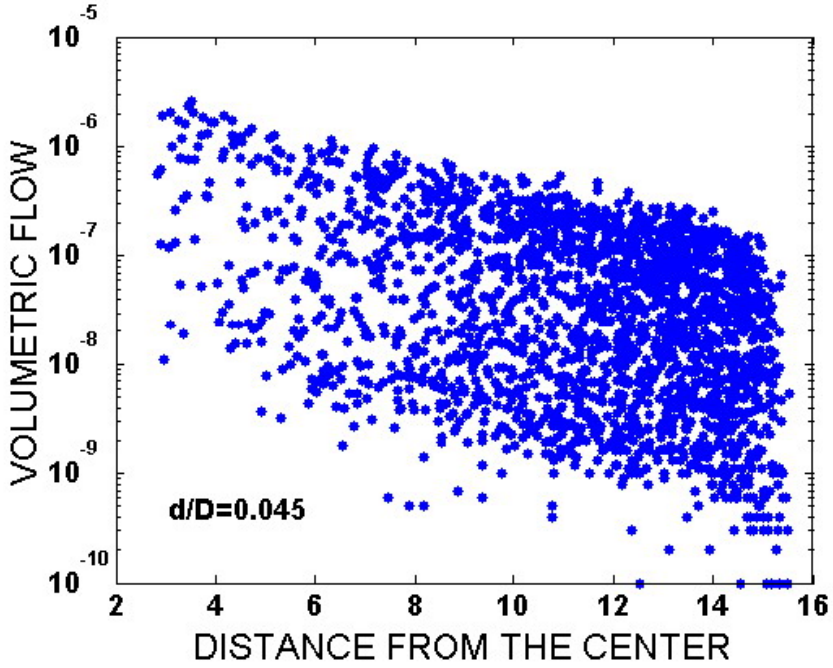

Figure 5.1: Volumetric flow (L^3T^{-1}) in gaps *vs.* distance from the center. The data corresponds to particle size d/D=0.045.

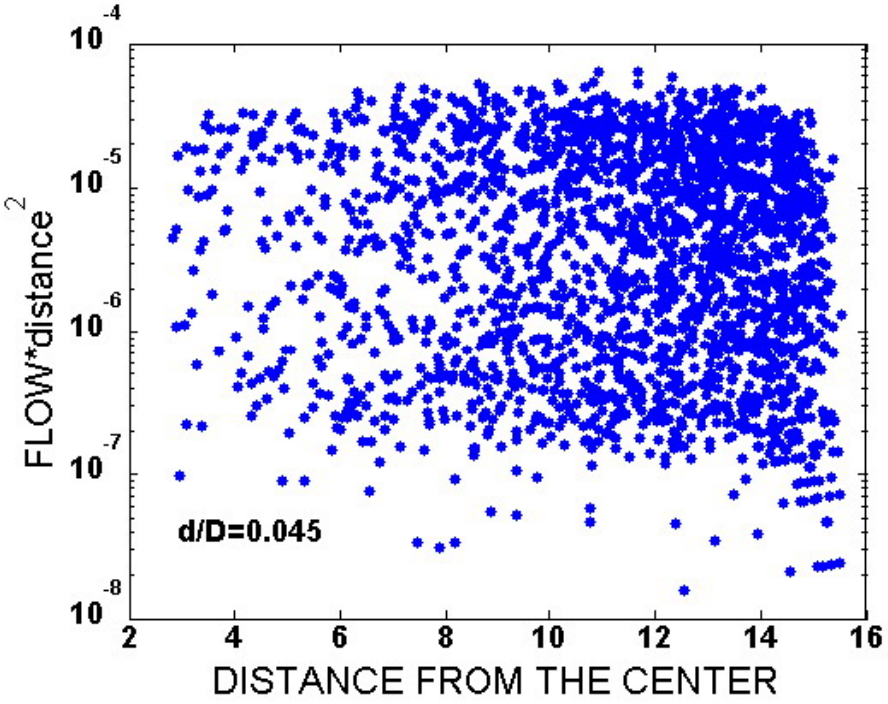

Figure 5.2: Flow times distance squared *vs.* distance from the center in gaps for particle size d/D=0.045.

Figure 5.2 shows that volumetric flow in gaps is constant with the distance from the center when the former is multiplied by the square of this distance. Figure 5.3 compares the flows in gaps before and after the transformation for particle size d/D=0.03 and Figure 5.4 does the same for the pore throats.

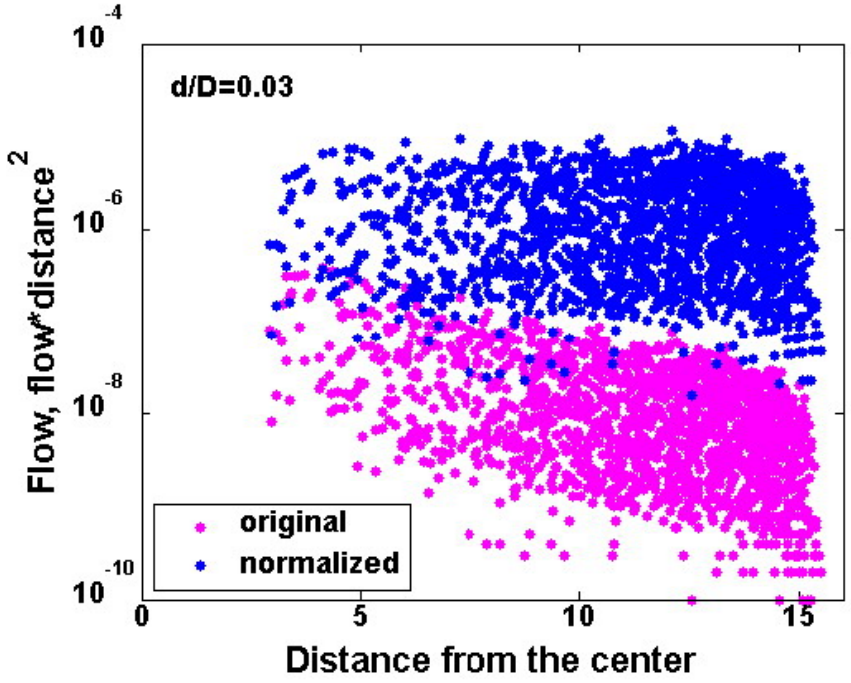

Figure 5.3: Flow in gaps *vs.* distance from the center before and after transformation, for particle size d/D=0.03.

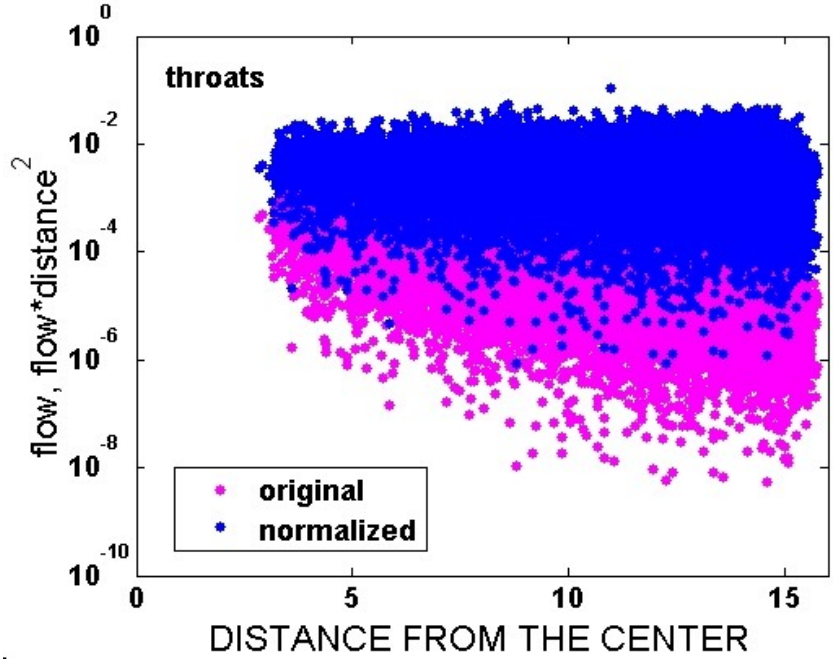

Figure 5.4: Flow in throats *vs.* distance from the center before and after transformation.

An alternative normalization calculates the logarithmic mean of the flow in intervals of distance and then fits the data to an equation of the type:

$$log(q)=log(q_o)+c \cdot distance \qquad \text{Eqn. 5.9}$$

where c is the slope of the plot of the logarithm of the velocity versus the distance from the center. For every gap and pore throat, the constant c will be multiplied by the gap or throat distance from the center and then added to the logarithm of their volumetric flow, in order to compensate for the effect of spherical flow. This procedure is shown next.

Figure 5.5 shows the logarithmic mean of the flow in every interval of distance versus the average value of the distance in such interval, for the seven particle sizes considered. The same procedure has been done for the pore throats and it is shown in Figure 5.6. The fitting equations for every case are presented in table 5.1.

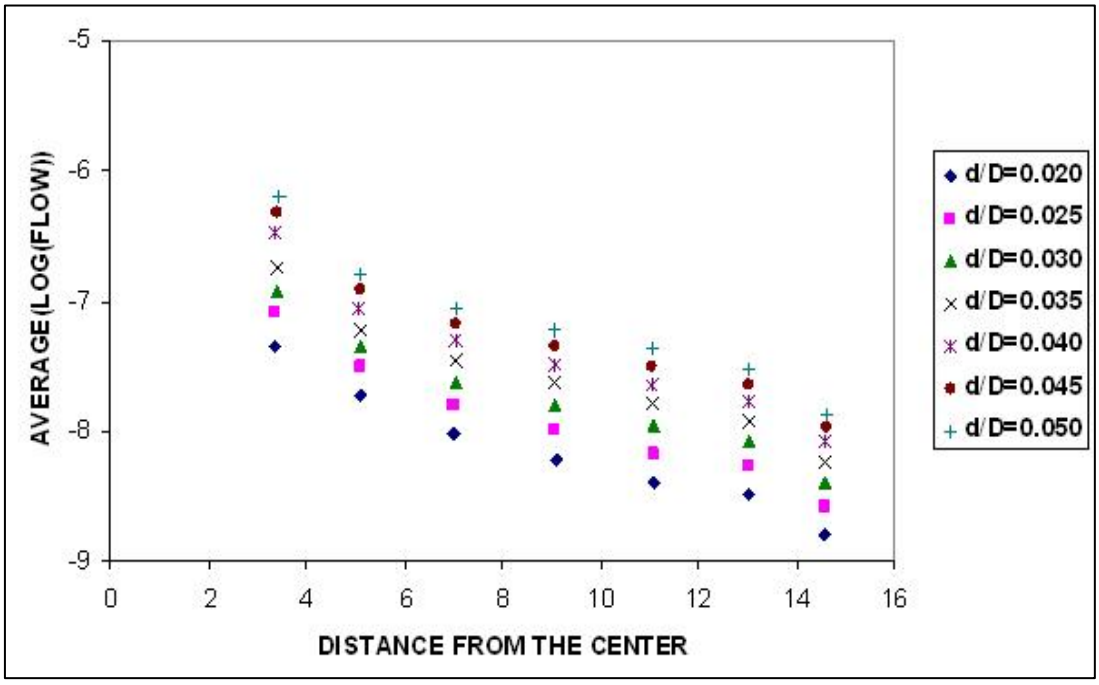

Figure 5.5: Logarithmic mean of flow in gaps *vs.* distance from the center. Data for different particle sizes are shown.

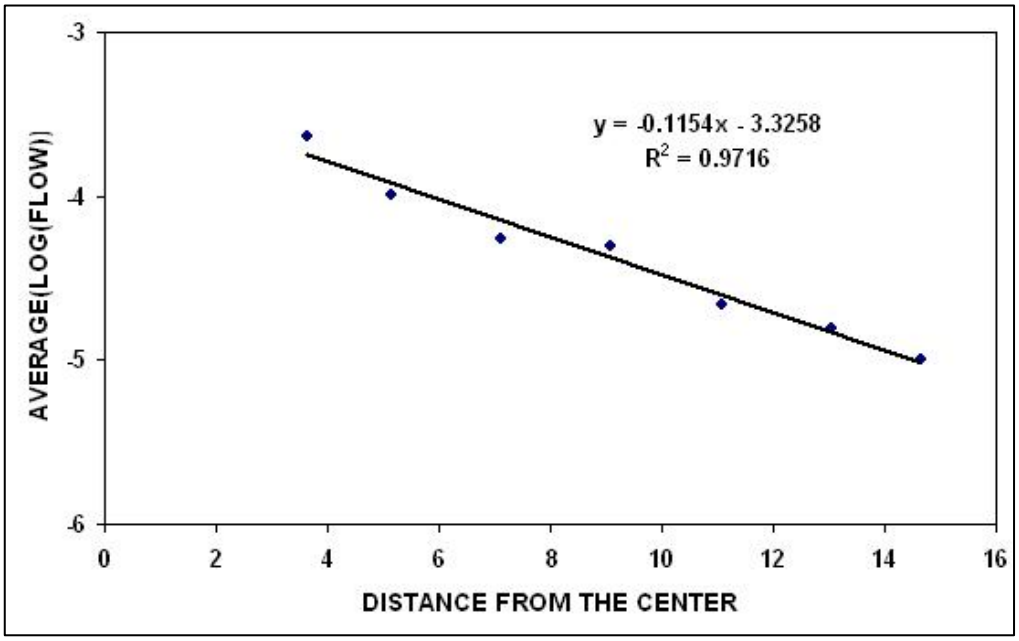

Figure 5.6: Logarithmic mean of flow in throats *vs.* distance from the center.

Table 5.1: Fitting equations

d/D	Equation	R^2
0.020	log(q)= -7. 0945-0.1161·dis	0.9670
0.025	log(q)= -6.8489 -0.1183·dis	0.9564
0.030	log(q)=-6.6965 -0.115·dis	0.9583
0.035	log(q)= -6.5230-0.116·dis	0.9529
0.040	log(q)= -6.3006-0.1223·dis	0.9318
0.045	log(q)= -6.1337-0.1255·dis	0.9269
0.050	log(q)= -6.0029-0.1265·dis	0.9303
Throats	log(q)= -3.3258 -0.1154·dis	0.9716

The absolute value for $\log(q_o)$ decreases with the increase in the particle size while the absolute value of the constant c slightly increases. The normalized values of

flow are calculated adding the product of the constant *c* by the distance from the center of every gap or pore throat to the logarithm of their original volumetric flow value and then calculating the anti logarithm of the resultant value. Figures 5.7 and 5.8 present the normalized volumetric flows for particle size *d/D*=0.03 and pore throats respectively.

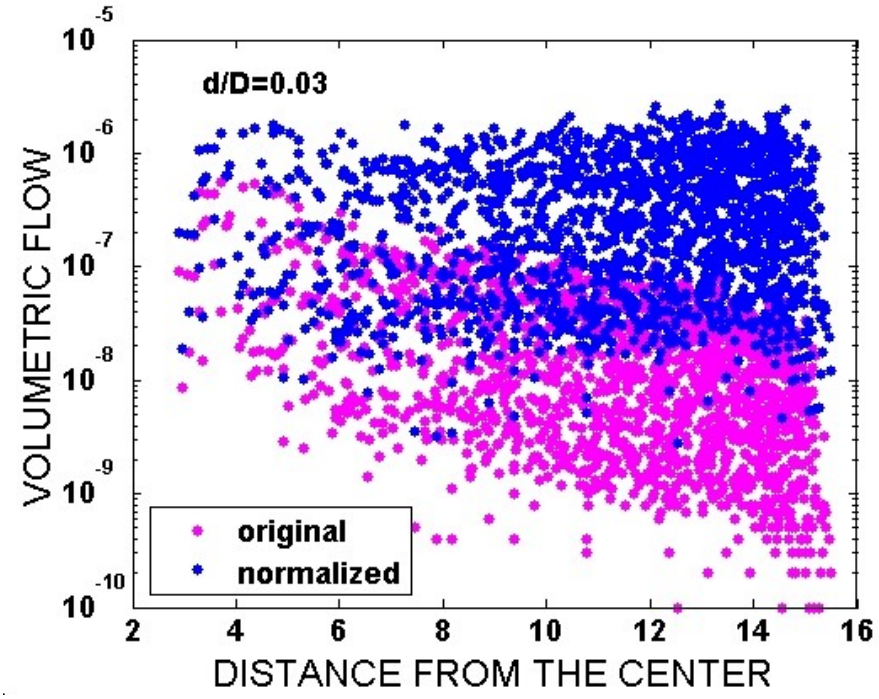

Figure 5.7 Original and normalized values of volumetric flow in gaps *vs.* distance from the center, for particle size *d/D*=0.03. Logarithmic mean method.

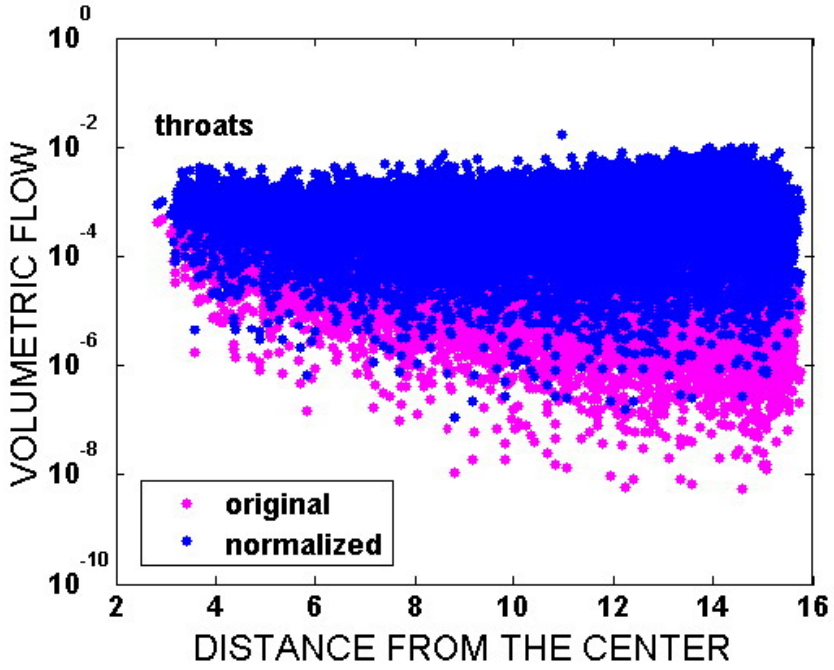

Figure 5.8: Original and normalized values of volumetric flow in throats vs. distance from the center. Logarithmic mean method.

The same procedure has been performed for all the different particle sizes considered. When comparing these data with the data obtained multiplying the flows by the square of the distance to the center (Figure 5.3), this method provides a more uniform weighting values of the flow. The flow values for gaps closer to the center do not increase as much as when multiplying by the square of the distance from the center. These normalized values of volumetric flow are going to be used in the evaluation of the integral $I(r)$ (Eqn. 5.3).

Figure 5.9 shows the average volumetric flow values in the gaps, for the different particle sizes considered, and in the pore throats, before and after the normalization. In all cases the average volumetric flow increased after normalization. Notice that the flow in

pore throats is calculated independently of the size of the particle being strained. The data are shown in table 5.2.

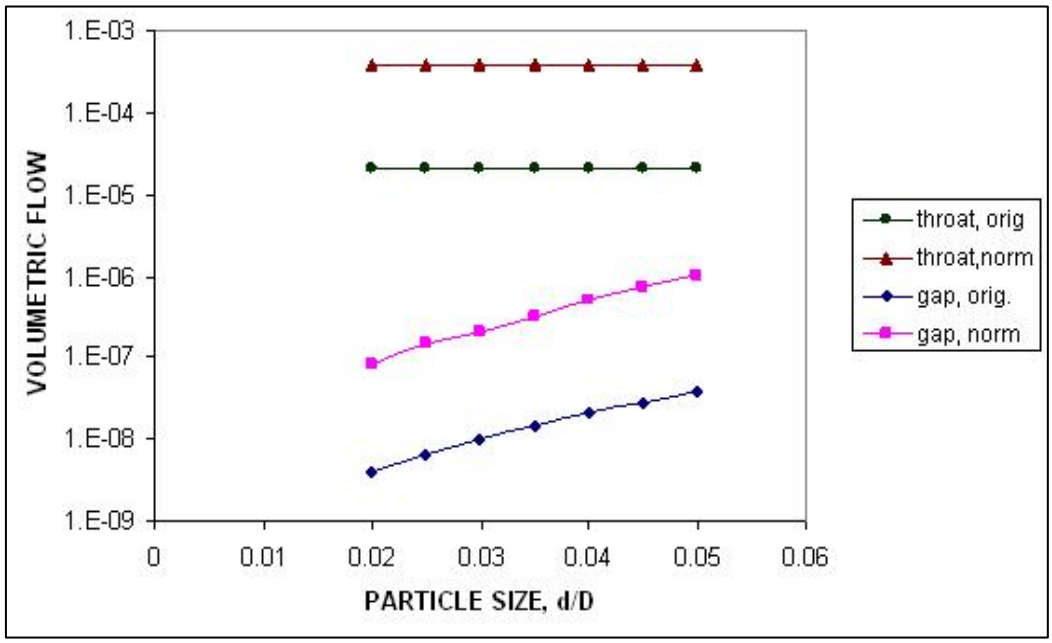

Figure 5.9: Average flow in gaps and pore throats before and after normalization, for different particle size.

Table 5.2: Average flow in gaps and pore throats for different particle sizes.

	Original		Normalized	
d/D	**Gap**	**Pore throat**	**Gap**	**Pore throat**
0.020	$3.96 \cdot 10^{-9}$	$2.13 \cdot 10^{-5}$	$8.20 \cdot 10^{-8}$	$3.77 \cdot 10^{-4}$
0.025	$6.55 \cdot 10^{-9}$	$2.13 \cdot 10^{-5}$	$1.45 \cdot 10^{-7}$	$3.77 \cdot 10^{-4}$
0.030	$1.01 \cdot 10^{-8}$	$2.13 \cdot 10^{-5}$	$2.05 \cdot 10^{-7}$	$3.77 \cdot 10^{-4}$
0.035	$1.47 \cdot 10^{-8}$	$2.13 \cdot 10^{-5}$	$3.08 \cdot 10^{-7}$	$3.77 \cdot 10^{-4}$
0.040	$2.09 \cdot 10^{-8}$	$2.13 \cdot 10^{-5}$	$5.15 \cdot 10^{-7}$	$3.77 \cdot 10^{-4}$
0.045	$2.84 \cdot 10^{-8}$	$2.13 \cdot 10^{-5}$	$7.57 \cdot 10^{-7}$	$3.77 \cdot 10^{-4}$
0.050	$3.77 \cdot 10^{-8}$	$2.13 \cdot 10^{-5}$	$1.03 \cdot 10^{-6}$	$3.77 \cdot 10^{-4}$

The original values of volumetric flow were already presented in Table 4.14. The geometric (logarithmic) average is shown.

5.2. CUMULATIVE FLOW RATE DISTRIBUTION

The cumulative local flow rate distribution $I(r)$ will be calculated with equation 5.3:

$$I(r) = \int_0^r q_R f_p dr_p \qquad \text{Eqn. 5.3}$$

where q_R is the volumetric flow in both gaps and pore throats.

Only the volumetric flow in gaps will be used in solving this integral, although some calculations for the pore throats are shown in this section. The flow in the gaps for different sizes has been calculated in Chapter 4. In this chapter, the gaps are characterized by half their width, in order to compare on the same basis as the strained particle radius. This magnitude will be called *gap radius*.

The frequency of radius for gaps between $0.005R$ and $0.05R$ ($0.01R<w_{gap}<0.1R$) and pore throats has been calculated. Note that the limit zero in the integral corresponds to $0.005R$ since gaps with radius smaller that $0.005R$ are considered point contacts in the Finney pack. The histogram in Figure 5.10 shows the frequencies distribution. The part correspondent to the gaps is shown in more detail in Figure 5.11. Independent histograms of frequency of pore throat radius and gap radius are shown in Figures 5.12 and 5.13 respectively.

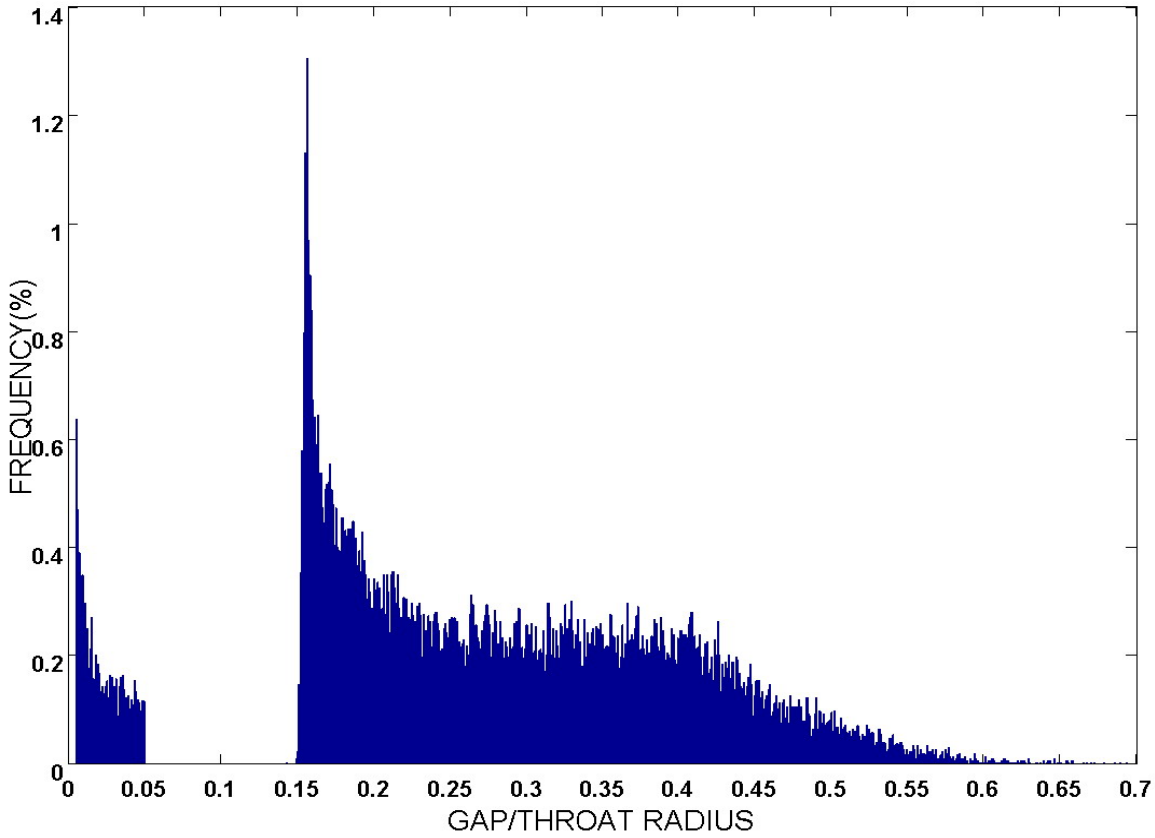

Figure 5.10: Frequency distribution of gap and throat radius in the Finney packing.

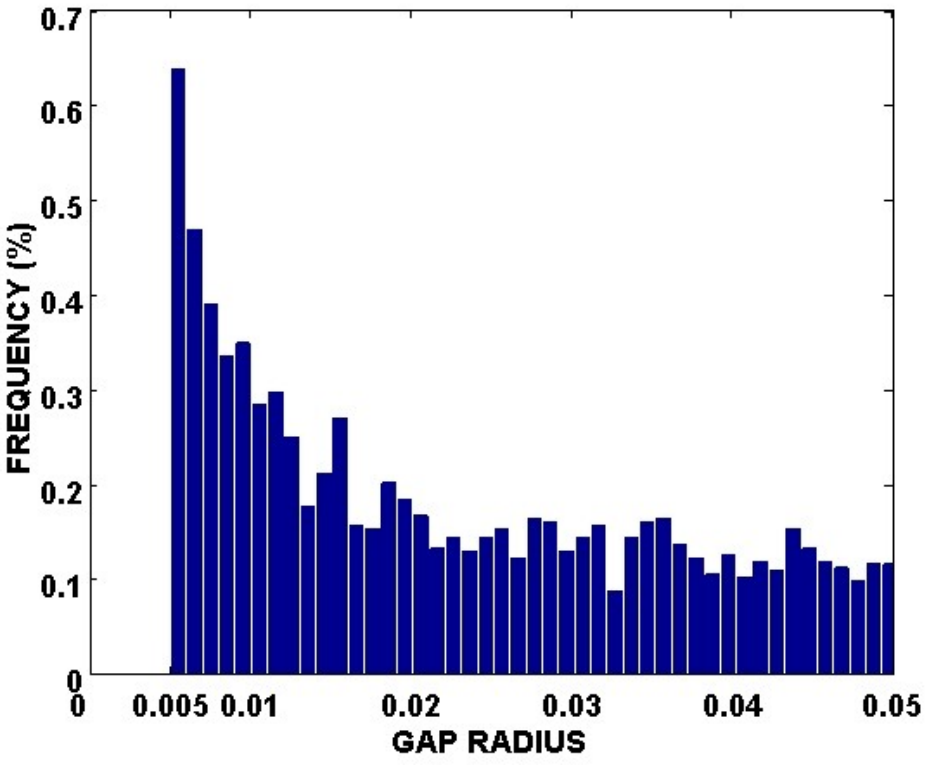

Figure 5.11: Zoom of the frequency distribution of radius correspondent to the gaps.

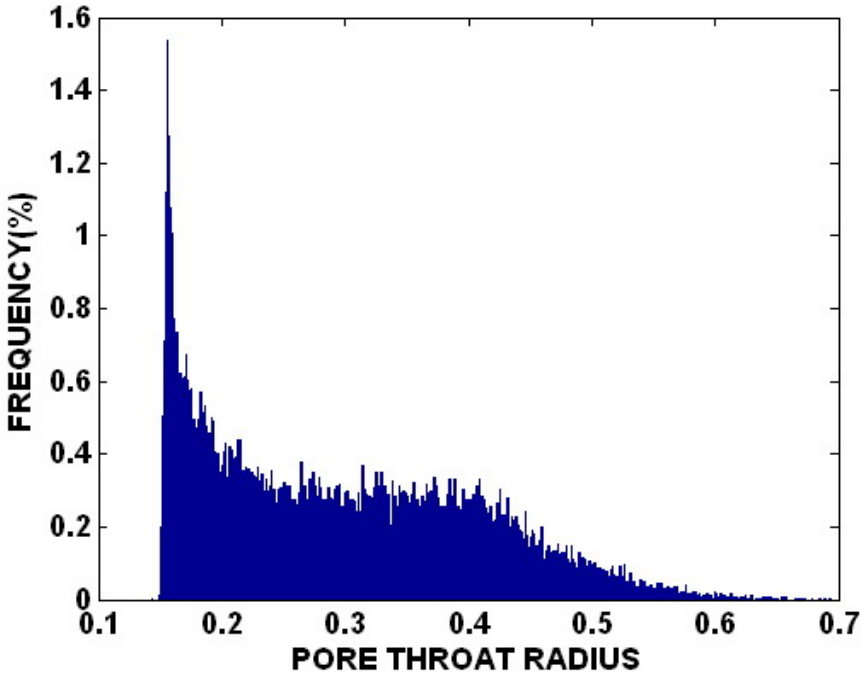

Figure 5.12: Frequency distribution of pore throats radius in the Finney packing.

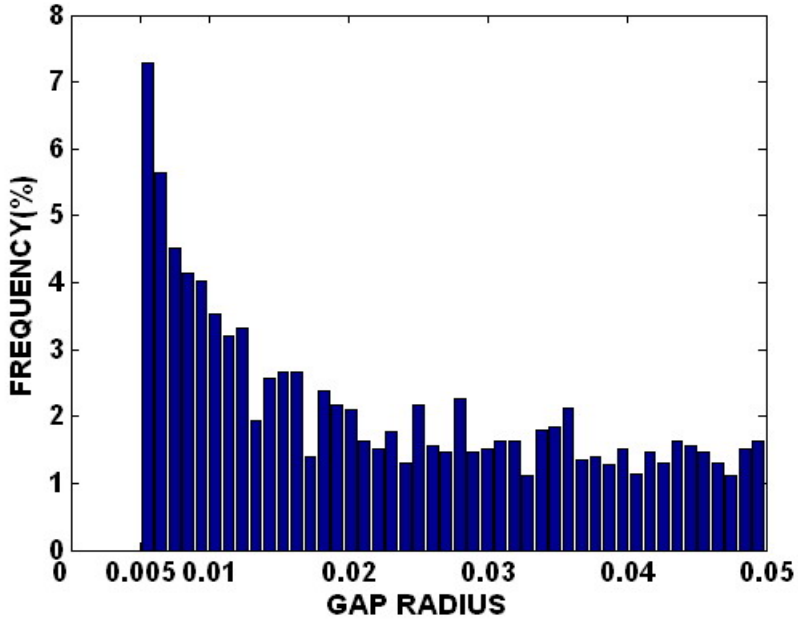

Figure 5.13: Frequency distribution of gaps radius in the range of interest for straining the Finney packing.

Pore throat radii range from 0.15*R* to 0.7*R*. Gap radii in the range of interest for straining particles smaller than throats vary from 0.005*R* to 0.05*R* (corresponding to the range of gap widths being considered which is 0.01*R* to 0.1*R*). The flow is known for every gap and pore throat in the packing. The average value of the volumetric flow has been calculated for every bin in the frequency histogram (685 bins of width 0.001*R*). Figures 5.14 and 5.15 show the normalized values of the volumetric flow versus the radius for gaps and unique throats respectively.

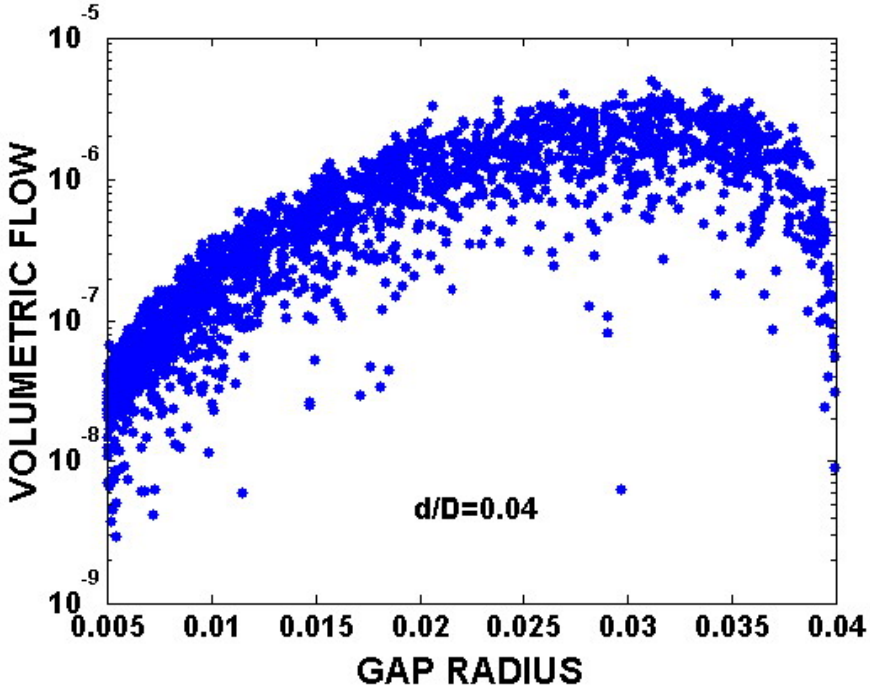

Figure 5.14: Normalized flow in gaps *vs.* gap radius, for particle size *d/D*=0.04.

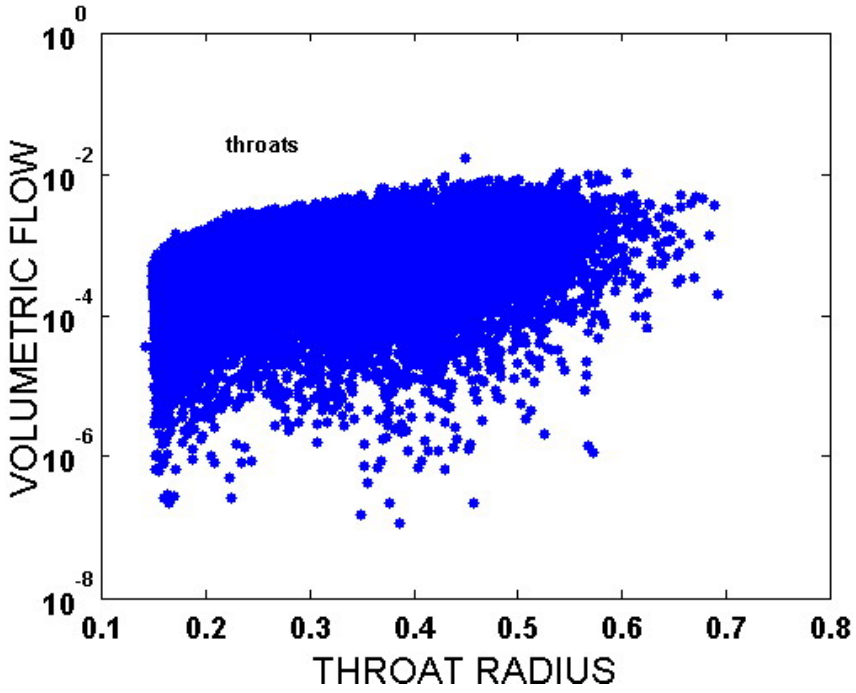

Figure 5.15: Normalized flow in throats *vs.* throat radius.

The volumetric flow in both gaps and pore throats increase with the increase in radius of the gap or pore throat.

From now on, only the data referent to the gaps is going to be used in order to calculate the cumulative flow distribution. Figures 5.16 and 5.17 show flow versus radius for gaps, once the average value in every one of the bins for radius has been calculated. The average was calculated using the geometric average of the flows in every bin. The data in Figure 5.16 correspond to particle size d/D=0.03 and the data in Figure 5.17 correspond to particle size d/D=0.04.

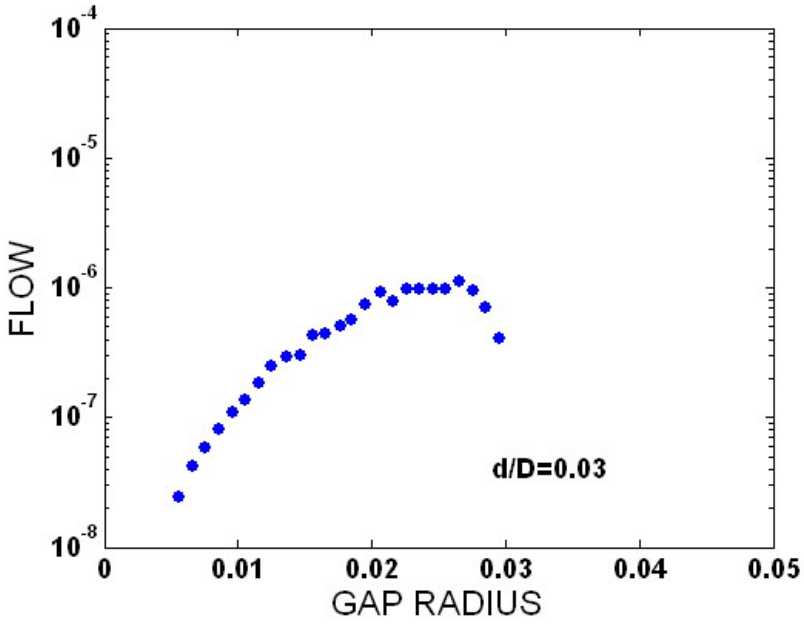

Figure 5.16: Average flow in gaps in bins of radius, for particle size *d/D*=0.03.

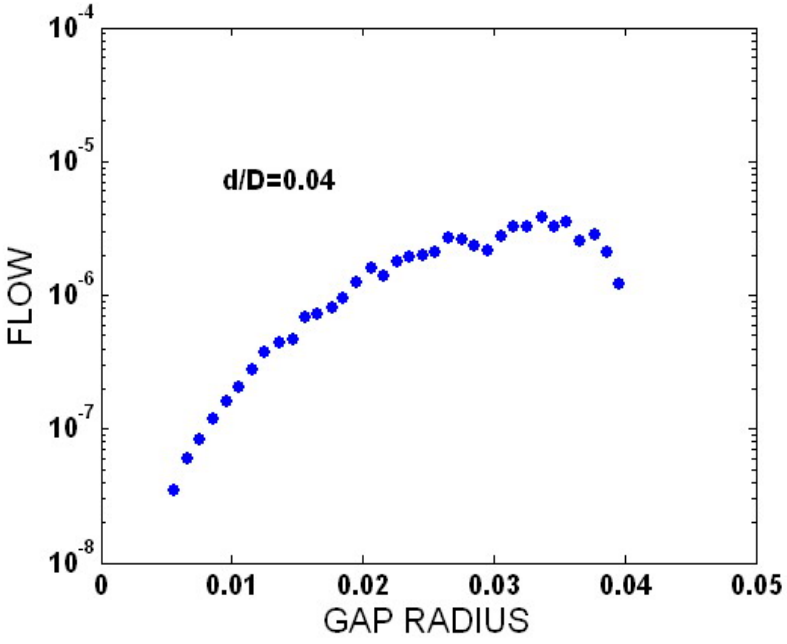

Figure 5.17: Average flow in gaps in bins of radius, for particle size *d/D*=0.04.

In order to solve the integral, the value of flow in every bin has been multiplied by the correspondent value of frequency shown in the histogram in Figure 5.13 (the "per one" value has been used). Figures 5.18 and 5.19 show the values of flow times frequency for the two particle sizes considered in this example. Those are the values of q_R f_p that will be used to calculate the cumulative flow distribution *I(r)* with equation 5.3. The integral has been solved by the trapezoidal method. Finally, Figure 5.20 shows the value *I(r)* for the gaps.

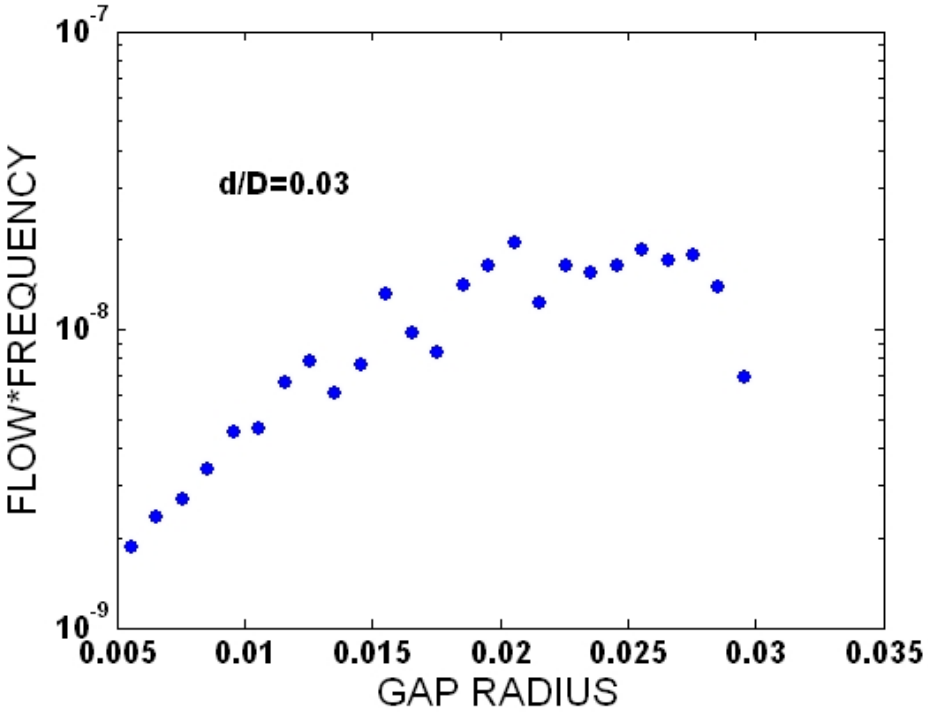

Figure 5.18: Product of frequency and flow in every bin *vs*. gap radius, for particle size *d/D*=0.03.

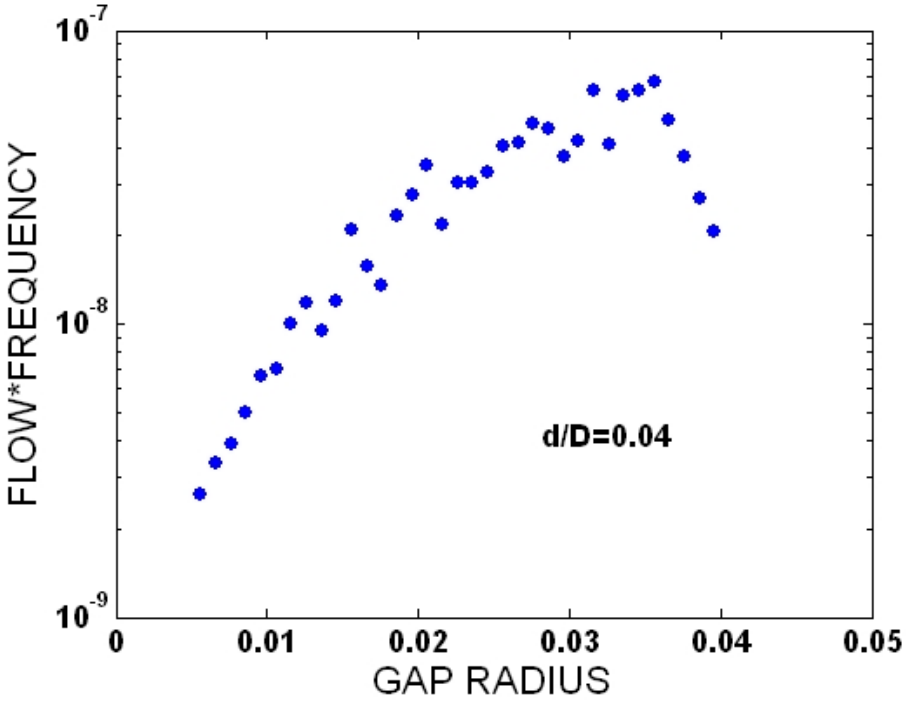

Figure 5.19: Product of frequency and flow in every bin vs. gap radius, for particle size d/D=0.04.

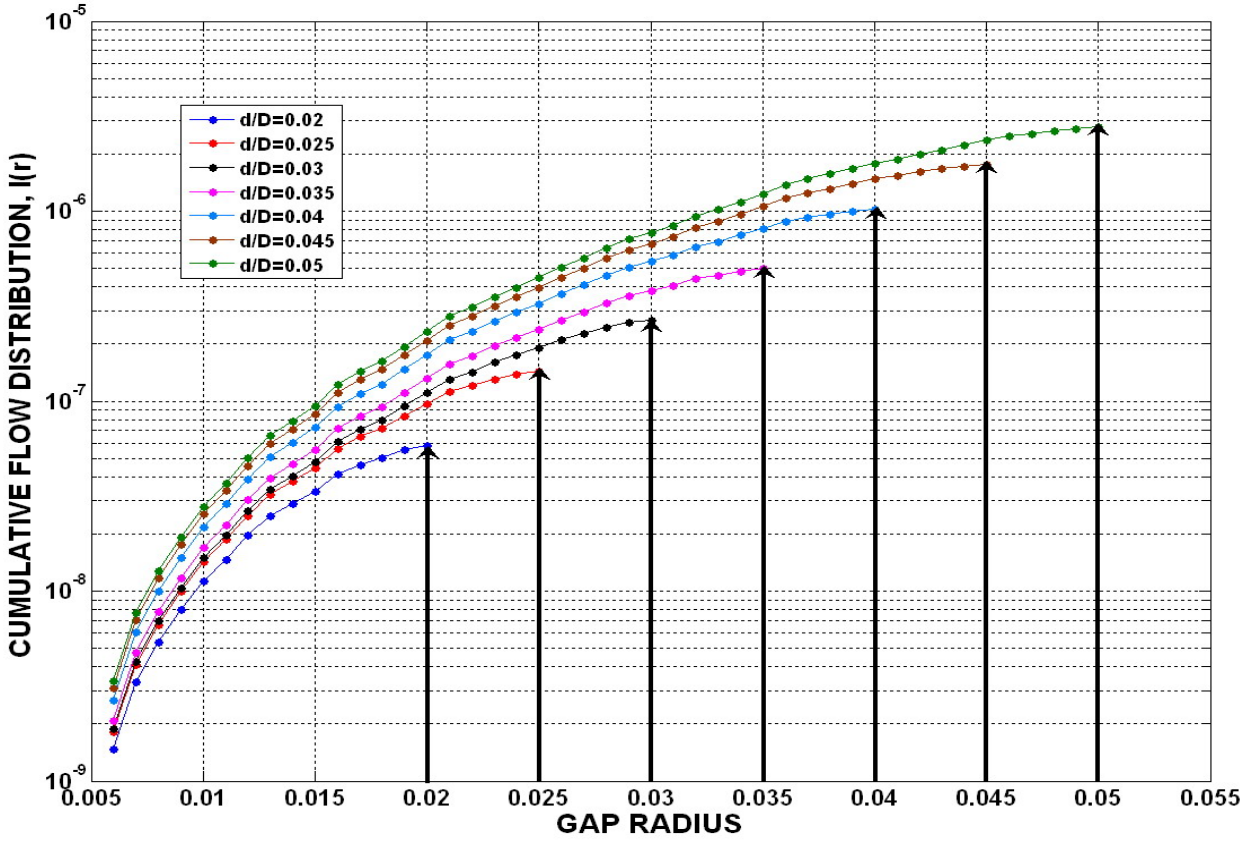

Figure 5.20: Cumulative flow distribution in the gaps region. The arrows indicate the value of *I(r)* for different values of radius of strained particles (r_s).

In order to calculate the constant for straining (Eqn. 5.6) the values of $I(r_s)$ for the different sizes of strained particles and $I(\infty)$ are needed. $I(\infty)$ is the value of the integral for the biggest gap radius, in this case around $0.05R$. The value of $I(0.05R)$ for particles of size $0.05R$ has been taken as the reference value $I(\infty)$. $I(r_s)$ is the value of the cumulative flow given by the radius of the particle being strained. Table 5.3 shows the radius of the strained particles that have been considered in this thesis.

Table 5.3: Radius of the strained particles (r_s)

d/D	**r_s**
0.020	$0.020R$
0.025	$0.025R$
0.030	$0.030R$
0.035	$0.035R$
0.040	$0.040R$
0.045	$0.045R$
0.050	$0.050R$

The values of $I(r_s)$ have been extracted from the integral calculation whose output is shown in Figure 5.20. The arrows point to the value of $I(r_s)$ for the different sizes of strained particles. Table 5.4 shows the numerical values.

Table 5.4: Values of $I(r_s)$ and $I(\infty)$ for different particle sizes.

r_s	**$I(r_s)$**	**$I(\infty)$**
$0.020R$	$5.88 \cdot 10^{-8}$	$2.77 \cdot 10^{-6}$
$0.025R$	$1.44 \cdot 10^{-7}$	$2.77 \cdot 10^{-6}$
$0.030R$	$2.67 \cdot 10^{-7}$	$2.77 \cdot 10^{-6}$
$0.035R$	$4.99 \cdot 10^{-7}$	$2.77 \cdot 10^{-6}$
$0.040R$	$1.02 \cdot 10^{-6}$	$2.77 \cdot 10^{-6}$
$0.045R$	$1.76 \cdot 10^{-6}$	$2.77 \cdot 10^{-6}$
$0.050R$	$2.77 \cdot 10^{-6}$	$2.77 \cdot 10^{-6}$

Recall that the constant for straining according Sharma and Yortsos theory is:

$$\frac{I(r_s)}{I(\infty)} \qquad \text{Eqn. 5.6}$$

Remember that since the parameter μ (the ratio of typical pore length to length of granular media) shown in the previous equation 5.5 is a constant, it has been ignored for the comparative purpose of this thesis. Only the part $I(r_s)/I(\infty)$ will be considered as the straining constant, k_{str} . Its value is shown in Table 5.5.

Table 5.5: Straining constant for different sizes of strained particles.

$\mathbf{r_s}$	$\mathbf{k_{str}}$
0.020*R*	$2.12 \cdot 10^{-2}$
0.025*R*	$5.20 \cdot 10^{-2}$
0.030*R*	$9.53 \cdot 10^{-2}$
0.035*R*	$1.80 \cdot 10^{-1}$
0.040*R*	$3.68 \cdot 10^{-1}$
0.045*R*	$6.53 \cdot 10^{-1}$
0.050*R*	1

Figure 5.21 shows the constant of straining (k_{str}) vs. the radius of the strained particles.

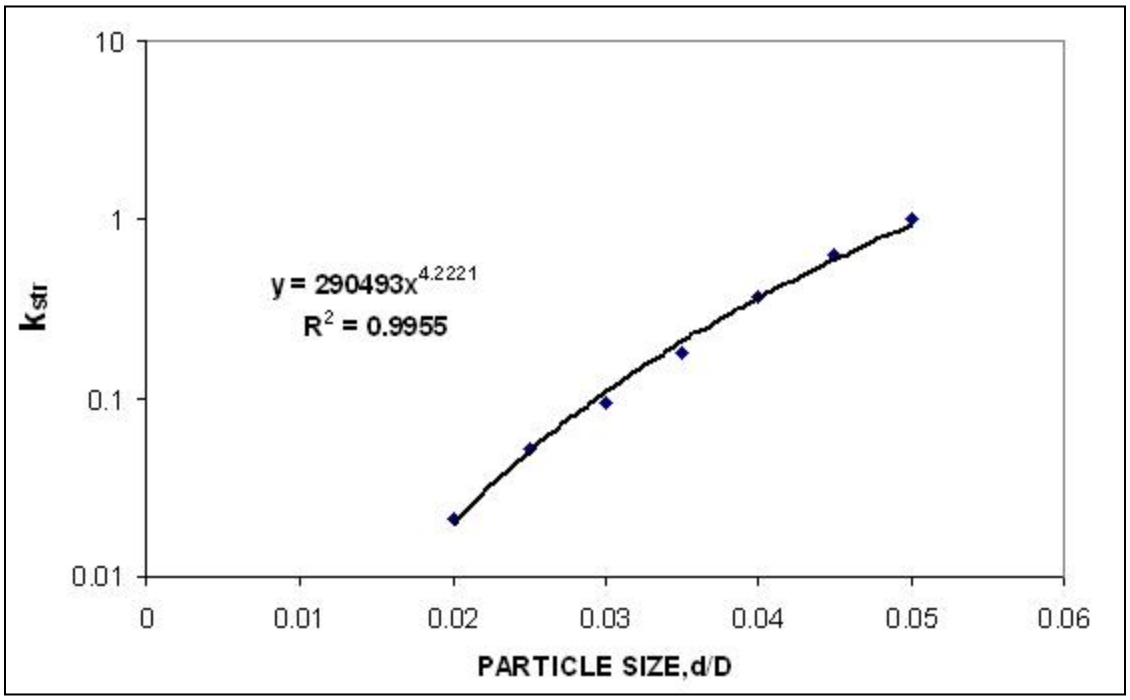

Figure 5.21: Straining constant (k_{str}) for different particle sizes.

In order to compare with the correlation in Bradford (2003), the predicted values of k_{str} have been fitted to a power trend line, yielding:

$$k_{str} = 2.9 \cdot 10^{5} \left(\frac{d}{D} \right)^{4.22} \qquad r^2=0.9955 \qquad \text{Eqn. 5.10}$$

The exponent is about 3 times bigger than the one reported from Bradford in the following equation:

$$k_{str} = 269.7 \left(\frac{d}{D} \right)^{1.42} \qquad \text{Eqn. 5.11}$$

Note that the comparison of the k_{str} value calculated with equation 5.10 with an actual straining constant as the one in equation 5.11 has no physical meaning since the term μ has been ignored.

The discrepancy in scaling between equations 5.10 and 5.11 suggests that the flow rate through a gap may be overestimating the probability of a particle being strained in a gap. Because of this, in the next section, the Sharma and Yortsos theory is going to be approached in a way that does not include the volumetric flow rate through gaps.

5.3 CUMULATIVE CONSTRICTION DISTRIBUTION

Since the results in section 5.2 indicated the possibility of overestimating straining rates when considering flow through gaps, the limiting case in which straining is assumed independent of local flow velocity is presented next. In this case the integral *I* reduces to the frequency distribution of the constrictions and it can be calculated with equation 5.7. As for the flow-weighted distribution, trapezoidal method has been used to evaluate the integral I_C (r). Figure 5.22 shows the cumulative frequency distribution.

$$I_C(r) = \int_0^r f_p dr_p \qquad \text{Eqn. 5.7}$$

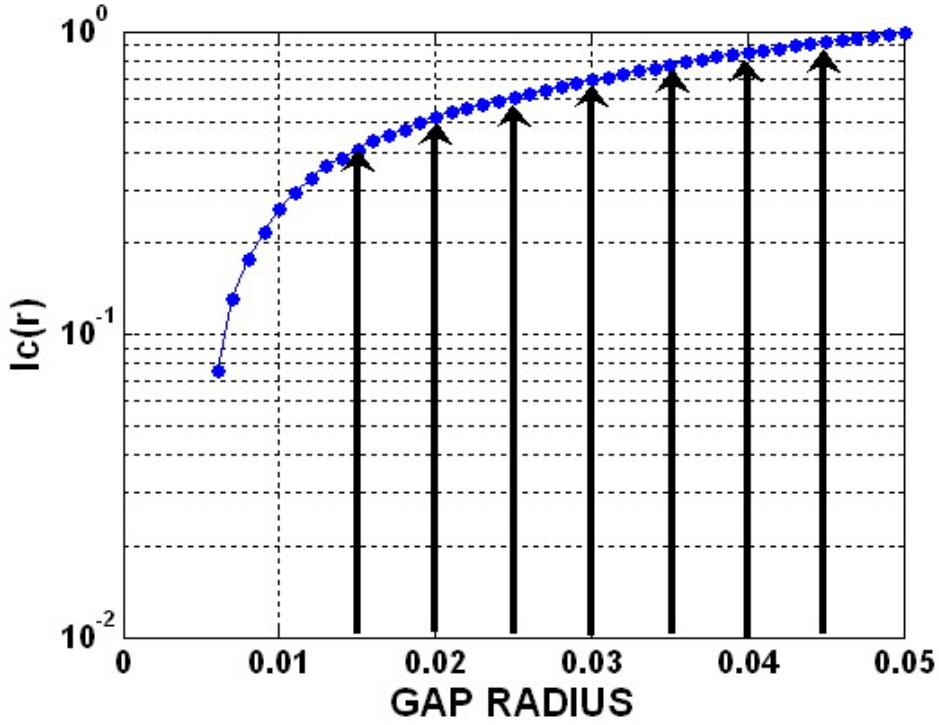

Figure 5.22: Cumulative frequency distribution chart for gaps showing the values of $I_C(r)$ for different particle radius.

The value of $I_C(r)$ is independent of the size of the particle being strained, unlike the cumulative flow distribution where the flow in gaps was dependent on the size of the strained particle. In this case there is only one line in the cumulative frequency distribution plot. The value of $I_C(r)$ has been calculated for different particle sizes and its value is indicated by the arrows in Figure 5.22. Table 5.6 presents the values of $I_C(r)$ and $I_C(\infty)$ and the straining constant k_{str}.

Table 5.6: Straining constant for different particle sizes calculated with the cumulative distribution of constrictions.

r_s	$I_C(r_s)$	$I_C(\infty)$	k_{str}
0.020	0.521	1	0.521
0.025	0.606	1	0.606
0.030	0.695	1	0.695
0.035	0.776	1	0.776
0.040	0.857	1	0.857
0.045	0.929	1	0.929
0.050	1	1	1

Figure 5.23 presents the value of the straining constant for the different particle sizes considered. The calculated values have been fitted to a power trend line in order to compare with the previous correlations (equations 5.10 and 5.11).

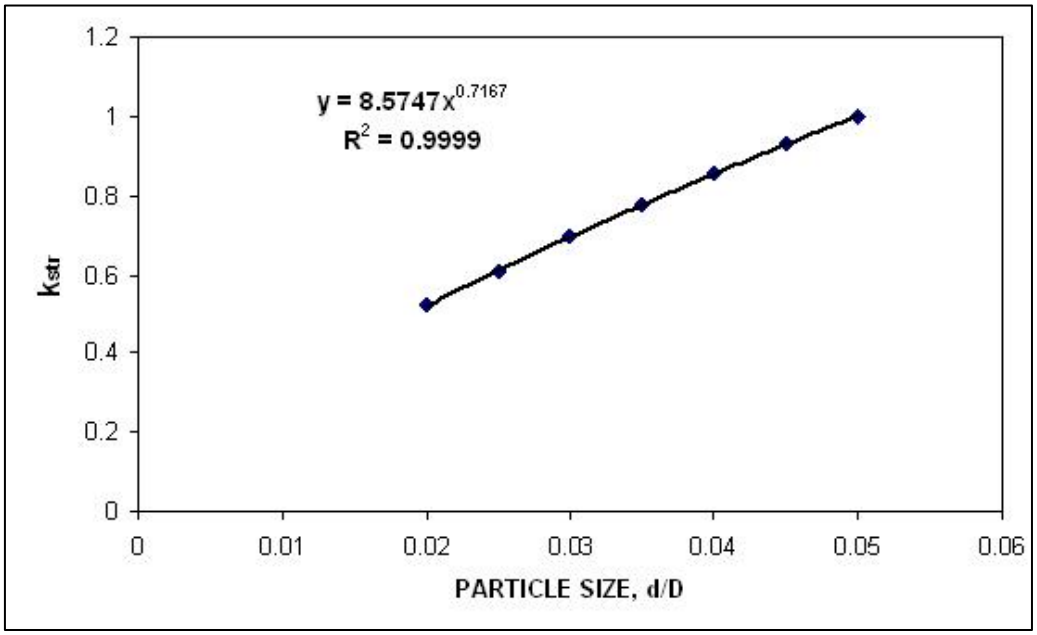

Figure 5.23: Correlation between straining constant and particle size calculated with the cumulative distribution of constrictions.

The correlation between straining constant and the size of the strained particle is:

$$k_{str} = 8.57\left(\frac{d}{D}\right)^{0.72} \qquad r^2 = 0.9999 \qquad \text{Eqn.5.12}$$

In this case the exponent is about 2 times smaller than the coefficient in Bradford's correlation.

Table 5.7 presents the value of k_{str} calculated with Bradford's correlation (equation. 5.11) and with the two correlations presented here (equations 5.10, and 5.12). For comparative purposes, only the value of the exponents has a physical meaning. This value is also shown in Table 5.7 (Exp.). In Figure 5.24 the straining constant value is plotted versus the particle size for the three different methods. In this plot the slopes of the lines are comparable, but not the value of k_{str} itself.

Table 5.7: Straining constant calculated with four different methods.

d/D	**k_{str} (Bradford)**	**k_{str} (flow-weighted)**	**k_{str} (only constrictions)**
0.020	$3.868 \cdot 10^{-3}$	$6.77 \cdot 10^{-8}$	0.0598
0.025	$5.310 \cdot 10^{-3}$	$1.74 \cdot 10^{-7}$	0.0702
0.030	$6.879 \cdot 10^{-3}$	$3.74 \cdot 10^{-7}$	0.0801
0.035	$8.562 \cdot 10^{-2}$	$7.18 \cdot 10^{-7}$	0.0895
0.040	$1.035 \cdot 10^{-2}$	$1.26 \cdot 10^{-6}$	0.0985
0.045	$1.223 \cdot 10^{-2}$	$2.07 \cdot 10^{-6}$	0.1072
0.050	$1.421 \cdot 10^{-2}$	$3.23 \cdot 10^{-6}$	0.1157
Exp.	1.42	4.22	0.72

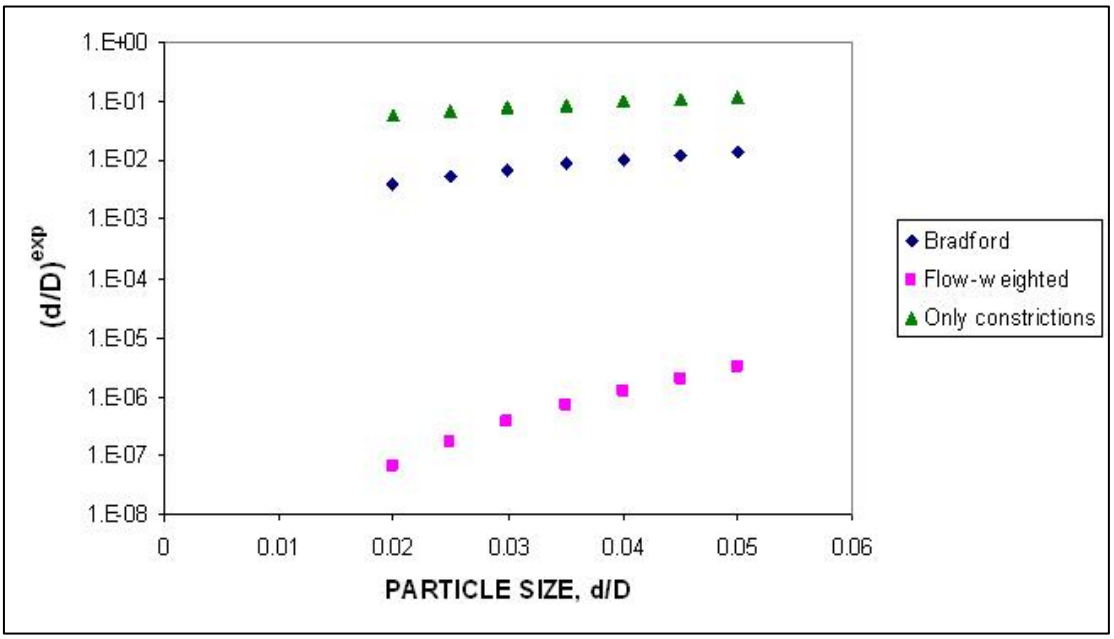

Figure 5.24: Straining constant *vs.* particle size calculated with three different methods.

The biggest difference between the scaling of these parameters when comparing with Bradford's formula is obtained in the case of the flow-weighted distribution (3.98 *vs.* 1.42).

When only the frequency distribution of the constrictions in pore space is considered the exponent is smaller than the value reported by Bradford (0.72 vs.1.42)

5.4 REVIEW

It appears that the work shown in this chapter does not explain the experimental observations. Since no adjustment of the geometric parameters in the model is possible it is necessary to determine if simplified phenomena in the first phases of this research should be considered more thoroughly.

A reason for the discrepancy in the scaling exponent may be derived from the use of the gap range of capture in the flow calculation. The range of capture is taken as the maximum range at which a particle of a given size can be strained. There is small chance that the particles get trapped at exactly the maximum range of capture. Probably the range of capture is smaller than the one considered in this work.

Nevertheless, the two limiting cases described above provide useful insight. On one hand, the assumption that the rate of particle straining is proportional to the flow rate through the gaps yields a greater sensitivity to particle size than observed experimentally. On the other hand, the assumption that the rate of straining is independent of flow rate through gaps, and depends only on the frequency of gaps of the appropriate size, yields a weaker sensitivity to particle size than observed. This suggests that the straining rate does depend on flow rate through gaps, but the dependence is weaker than first order.

Chapter 6: Conclusions and Future Directions

6.1 CONCLUSIONS

The focus of this project has been the influence of the small constrictions naturally present between grains in porous media in the trapping of particles of colloidal size. A hypothesis was proposed that the straining of small particles in gaps between grains explains experimental observations in which the retention by straining exceeds the level predicted by existing theories.

An independent description of the distribution of gap widths in simple but realistic granular materials, dense random packings of spheres, has been made in Chapter 3. The well known Finney packing and several computer-generated packings have been used in this task. The model soils used consist only of smooth mono-dispersed spheres. This type of model describes geometric features of well-sorted sands and sandstones well, but the distribution of narrow gaps in a packing of angular grains might differ qualitatively from those shown in this thesis. The geometric analysis of the packings indicated a similar number and distribution of near neighbors between the computer-generated packings and the Finney pack, making the former suitable as models for ideal soils.

The contribution of small gaps to single-phase flow has been shown in Chapter 4. The volumetric rate through gaps has been calculated by means of a slit approximation of the gap shape. The volumetric flow in gaps in the Finney packing, appropriate to the particle being strained, was found to be about three orders of magnitude smaller than the volumetric flow in pore throats obtained from a steady state flow calculation. To date, the local flow rates have not been calculated in the computer-generated packings.

A direct measurement of the distribution of gap widths and the volumetric flow through them had not been reported before. This information will be useful in evaluating transport phenomena influenced by these constrictions.

A quantitative test of whether particles can be strained in small gaps at rates consistent with experiments reported in the literature was made in Chapter 5. The approach of Sharma and Yortsos (1987a), which establishes a mechanistic connection between pore-scale straining events and macroscopic behavior, has been used as a framework to predict the consequences of straining in gaps between grains. The modeling of gap widths and straining is predictive, and in this case the predictions obtained by the application of the Sharma and Yortsos theory to the transport with straining of mono-dispersed colloids did not explain the geometric observations reported by Hall (1957) and the recent experiments by Bradford et al. (2003).

A reassessment of the assumptions made in this project is indicated. A number of self-imposed restrictions have been made in this work in order to study the new mode for straining. The scope of the assumptions includes the neglect of flow separation near gaps and the dependence of particle straining on local velocity. A re-evaluation will be an effective way to gain insight. As elaborated below, the local flow velocity dependence has a significant effect on the scaling exponent.

Important simplifications have been made when computing the local flow distribution in gaps. Foremost, the use of ideal soils is not a drawback when testing the straining model against experiments, since many of those experiments where the non-classical straining behavior was observed were done in sand columns which are qualitatively identical to bead packs. Polydisperse packings are not expected to introduce qualitatively different straining behavior either.

A principal approximation was that only an average velocity obtained from approximating gaps as slits has been considered. The estimated velocity in gaps is a lower bound on the actual velocity. Therefore, it provides a conservative estimate of the contribution of gaps to particle straining. Using the slit approximation for flow through a gap also means that point contacts between grains are not included as potential locations for straining.

It was assumed that the probability of a particle entering a gap is proportional to the flow rate through the gap. This assumption avoided the calculation of detailed flow fields in the vicinity of the gaps but at the same time yielded a greater sensitivity to particle size than observed experimentally. The actual streamlines will curve around the point of minimum separation in a gap, rather than pass straight through, and possibly, the angle at which a particle approaches a gap between two spheres will influence the probability of straining. When the rate of straining was assumed to be independent of flow rate through gaps, and dependent only on the frequency of gaps of the appropriate size, the sensitivity to particle size was weaker than observed. Hall's geometric model considered crevices (between spheres in point contact, analogous to the gaps in this work), to be associated with the pore throats, while in this thesis the gaps are considered independently of throats. Moreover, the model that assumed straining depends only on the frequency distribution of gaps was implemented in such a way that the probability of a gap straining a particle was independent of particles size (as long as the particle was larger than the gap width). Thus this model establishes a lower bound on the scaling behavior of the straining rate with particle size.

These observations suggest that the straining rate does depend on flow rate through gaps, but the dependence is weaker than first order.

The solution to all these simplifications is a more detailed calculation of the local flow field. The velocity that brings a particle to the region of capture of a gap will vary for each of these situations.

Neglecting the effect of previously strained particles brings another limitation when comparing the predicted results with the experimental observations. This phenomenon will change the geometry of the gaps, and, therefore, affect the local flow field. On the other hand, if experiments involve dilute suspensions of particles, this limitation should not be important at early times. Thus meaningful comparison of model predictions to experiments will be possible, but the model will require revision to be applicable to long-term flows.

6.2. FUTURE DIRECTIONS

In general a re-evaluation of the assumptions is needed in order to gain insight into the straining mechanism. If after this revision the model succeeds, then it motivates further testing and more careful modeling, e.g. model soils with a distribution of grain sizes, or with angular grains.

In Chapter 3 it was shown that the Finney pack has accuracy in distances about $0.01R$. This is not a trivial fraction of the sizes in the range of interest which is $0.03R$ to $0.1R$. Since flow rates vary with the cube of the gap width, this accuracy can strongly affect the computed flow rates in gaps. A next step will be to do the theoretical calculation of the volumetric flow in gaps in the computer-generated packings. There are two clear advantages in this case. First, the flow field through these packings is linear, not spherical, so no normalization is needed; second, since the accuracy in distance in those packings is one order of magnitude better than in the Finney pack the assessment of flow

rates in gaps will be much more accurate. Also, there is a clear distinction between point contacts, very narrow gaps, and gaps in the size range of interest.

Even if mono-dispersed packings of spheres capture the random spatial arrangements of grains in soils, they are an oversimplification of grains naturally occurring in soils. Therefore these packings are not always representative of a physical system. A next step would be to calculate the distribution of gaps and its contribution to the single phase flow in bi-dispersed model soils or in packings with normal distribution of grain sizes.

In this project, gaps were defined as the void distances between the centers of two spheres and they were characterized by half of their width for the purposes of Chapter 5. Pore throats were characterized by the radius of the biggest inscribed circumsphere between triplets of spheres for the calculation of the steady state flow through the packing.

The biggest gap of interest in a mono-dispersed packing has been assumed to have a radius of $0.05R$. This upper bound is driven by the size range of particles that is of interest, i.e. particles that are too small to be trapped in smallest throats yet are retained in experiments. The smallest pore throat has a size of $0.15R$. Any gap, constriction or crevice bigger than $0.05R$ is considered part of the pore throat, therefore the calculation of the flow in gaps was limited to gaps smaller than $0.05R$. Calculating local velocities in gaps between $0.05R$ and $0.15R$ will overestimate the flow in the packing when considering gaps and pore throats together. Consequently there is a discontinuity in the size of the constrictions (gaps and throats) in the pore space. A redefinition of the size of the gap needs to be done in order to better account for gaps and throats in the straining model. Trapping is not limited to the center of the gap since they have a range of capture in which they can capture particles.

When assuming straining rate to be dependent only on the frequency distribution of gaps in pore space, the effect of gap on straining is determined only by its width. This ignores the range of capture, a distance specific to a given particle size and that would introduce a dependence on the size of the particle being strained in this assumption. Accounting for range of capture would define a new cumulative distribution I_R in Sharma and Yortsos theory that will depend in the size of the strained particle. Moreover, the dependence between the straining constant and the particle size predicted by Hall (1957), which is based in purely geometric considerations yet agrees with experimental observations, uses the ratio between the area for straining and the total area of the constriction. Thus it automatically accounts for the effect of a range of capture.

The flow in gaps has been calculated appropriate to the size of the particle being strained. If the particle was smaller than the considered gap, no flow was calculated for that gap, though obviously flow through that gap was not zero. On the other hand, the flow in throats has been calculated independent of the size of the strained particle. A modification in the calculation of the steady state flow in pore throats should be made to account for the size of the particle in order to be consistent when calculating the cumulative flow distribution with the Sharma and Yortsos theory. A natural extension would be to explicitly test Hall's (1957) assumption that the probability of trapping in crevices (gaps) depended on the flow rate through the pore throat associated with each set of crevices. Figure 6.1 shows the idealized cross section through a constriction according to Hall.

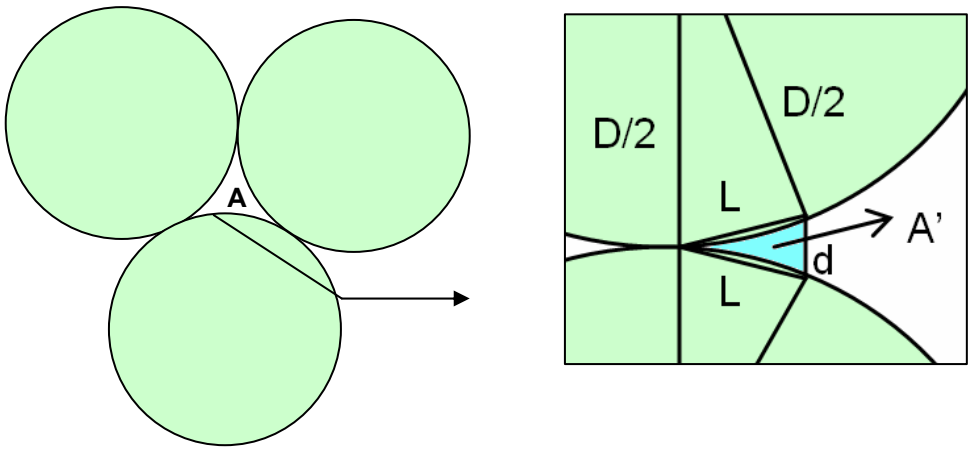

Figure 6.1: Idealized geometry of a cross section of a pore space according to Hall (1957).

In Figure 6.1, *A* is the total area of the constriction between three touching grains. The area of the constriction with a dimension smaller than the particle size *d* is three times the area *A'*. The rate of straining is proportional to the ratio of these two areas times a constant that include the effects of velocity and non-symmetry of grains.

Another way to predict the consequences of straining may be derived from the Effective Medium Theory (EMT, Kirkpatrick, 1973). This theory relates local flow velocity (u_R) to local geometry and does not require calculating the entire flow field. Sharma and Yortsos obtained the following equation for a network of pore throats:

$$u_R = \frac{q}{8k} r_p^2 \left[1 + \frac{r_m^4 - r_p^4}{r_p^4 + \left(\frac{Z}{2} - 1 \right) r_m^4} \right] \qquad \text{Eqn. 6.1}$$

where q is the steady-state macroscopic volumetric flow rate, k is the permeability of the medium, Z is the average number of pore throats connected to each pore body, r_p is the pore throat radius and r_m is a mean pore throat radius. This formula shows that the hydraulic conductance of a pore throat varies with r_p^4. In order to adapt EMT to the straining in gaps, the above formula must be revised because volumetric flow rate through gaps varies with w^3_{gap}.

The cumulative flow distribution can be directly evaluated from the calculated local flow distribution, so that the contribution of each pore and gap is physically representative. Comparing the experimental straining behavior with the results of using EMT will determine if the level details about grain space geometry and local flow velocities shown in Chapters 3 and 4 is necessary.

The neglected possibility of separation of flow in the vicinity of gaps may be a serious pitfall. Experiments by Davis et al. (1976) and Taneda (1979) showed that the separation of flow occurs even in the Stokes' regime for flow past two spheres in the direction of the line of their centers. Kitanidis and Dykaar (1997) also observed separation of flow and eddy formation a model pore of varying cross-section. The flow through the gaps does not occur in the direction assumed for the straining model if eddies form in the vicinity of grain near contacts. On the other hand, eddies may trap particles, so a qualitative agreement with experiments may be observed.

Appendix A

MATLAB CODES

Some of the Matlab codes used in this thesis are showed in this appendix. Many of these codes refer to specific data files. Contact the author at email elenarpin@gmail.com for more information.

1. Gap widths

```
%This code calculates gap widths as the void distance between center of
%spheres. Range has to be selected. The output prints sphere 1 & its
%coordinates, sphere 2 & its coordinates and gap width.

load X.txt;
load Y.txt;
load Z.txt;

fid=fopen('widths.txt','w');
for i=1:4021
    Sphere(i).x=X(i);
    Sphere(i).y=Y(i);
    Sphere(i).z=Z(i);
end
for i=1:2000
    for j=1:4021
        if  i<j
        w(i,j)=sqrt((Sphere(i).x-Sphere(j).x)^2+...
            (Sphere(i).y-Sphere(j).y)^2+...
            (Sphere(i).z-Sphere(j).z)^2)-2;
        % Select range
        if  w(i,j) >= 0.03 && w(i,j) <= 0.1
        fprintf(fid,'%6.0f\t',i);
        fprintf(fid,'%6.6f\t',X(i));
        fprintf(fid,'%6.6f\t',Y(i));
        fprintf(fid,'%6.6f\t',Z(i));
        fprintf(fid,'%6.0f\t',j);
        fprintf(fid,'%6.6f\t',X(j));
        fprintf(fid,'%6.6f\t',Y(j));
        fprintf(fid,'%6.6f\t',Z(j));
        fprintf(fid,'%6.6f\t',w(i,j));
        fprintf(fid,'\n');
        end
        end
    end
```

```
end
```
fclose(fid);

2. Neighboring spheres

```
% This code prints the id's of the neighboring spheres of a sphere
%within a given width

load X.txt
load Y.txt
load Z.txt
size(X)
size(Y)
size(Z)
m=0;

fid=fopen('neighbors.txt','w');

for i=1:size(X) %4021
    Sphere(i).x=X(i);
    Sphere(i).y=Y(i);
    Sphere(i).z=Z(i);
end
for i=1:2000
    fprintf(fid,'%6.0f',i);
    for j=1:4021
        if i~=j
        w(i,j)=sqrt((Sphere(i).x-Sphere(j).x)^2+...
            (Sphere(i).y-Sphere(j).y)^2+...
            (Sphere(i).z-Sphere(j).z)^2)-2;
        %select interval
        if w(i,j)>=0.03 && w(i,j)<=0.1
            m=m+1;
            Sphere(i).Neighbor(m)=j;
            fprintf(fid,'%6.0f\t',j);
        end
        end
        Sphere(i).NoNeighbor=m;
    end
    fprintf(fid,'\n');
    m=0;
end
fclose(fid);
```

3. Delaunay cells containing a gap

```
% This code prints the Delaunay cells containing each gap (for the 1449
gaps
%that are between 0.03 and 0.1
```

```
clear all
load cells.txt; %14871 Delaunay cells with their spheres
load spheres.txt; %4021 spheres in the Finney packing
load widths.txt;  % pair of spheres having certain width

dc= cells (:,1);
s1= cells (:,2);s2= cells (:,3);
s3= cells (:,4);s4= cells (:,5);

s= spheres (:,1);
x= spheres (:,2);y= spheres (:,3);z= spheres (:,4);

s5= widths (:,1);
s6= widths (:,5);
w = widths (:,9);

size (cells)
size (spheres)
size (widths)

for i=1:size(spheres)
    Sphere(i).s=s(i);
    Sphere(i).x=x(i); Sphere(i).y=y(i); Sphere(i).z=z(i);
end

for i=1:size(widths)
    Sphere(i).s5=s5(i); Sphere(i).s6=s6(i);
    width(i).w=w(i);
end
for i=1:size(cells)
    Cell(i).dc=dc(i);
    Sphere(i).s1=s1(i); Sphere(i).s2=s2(i);
    Sphere(i).s3=s3(i);Sphere(i).s4=s4(i);
End

dcellsgaps=zeros(1449,9);
fid=fopen('dcellsgap.txt','w');

k1=1;
for i=1:size(widths)  %
    k2=0;
         for j=1:14871  % Delaunay cells
        switch (Sphere(i).s5)
            case (Sphere(j).s1)
                switch (Sphere(i).s6)
                    case (Sphere(j).s2)
                        k2=k2+1;
                        dcellsgaps(k1,k2)=j;
                        fprintf(fid,'%6.0f\t',j);
                    case (Sphere(j).s3)
                        k2=k2+1;
```

```
            dcellsgaps(k1,k2)=j;
            fprintf(fid,'%6.0f\t',j);
        case (Sphere(j).s4)
            k2=k2+1;
            dcellsgaps(k1,k2)=j;
            fprintf(fid,'%6.0f\t',j);
        otherwise
            continue
    end
case(Sphere(j).s2)
    switch (Sphere(i).s6)
        case (Sphere(j).s1)
            k2=k2+1;
            dcellsgaps(k1,k2)=j;
            fprintf(fid,'%6.0f\t',j);
        case (Sphere(j).s3)
            k2=k2+1;
            dcellsgaps(k1,k2)=j;
            fprintf(fid,'%6.0f\t',j);
        case (Sphere(j).s4)
            k2=k2+1;
            dcellsgaps(k1,k2)=j;
            fprintf(fid,'%6.0f\t',j);
        otherwise
            continue
    end
case (Sphere(j).s3)
    switch (Sphere(i).s6)
        case (Sphere(j).s1)
            k2=k2+1;
            dcellsgaps(k1,k2)=j;
            fprintf(fid,'%6.0f\t',j);
        case (Sphere(j).s2)
            k2=k2+1;
            dcellsgaps(k1,k2)=j;
            fprintf(fid,'%6.0f\t',j);
        case (Sphere(j).s4)
            k2=k2+1;
            dcellsgaps(k1,k2)=j;
            fprintf(fid,'%6.0f\t',j);
        otherwise
            continue
    end
case(Sphere(j).s4)
    switch (Sphere(i).s6)
        case (Sphere(j).s1)
            k2=k2+1;
            dcellsgaps(k1,k2)=j;
            fprintf(fid,'%6.0f\t',j);
        case (Sphere(j).s2)
            k2=k2+1;
            dcellsgaps(k1,k2)=j;
            fprintf(fid,'%6.0f\t',j);
```

```
                    case (Sphere(j).s3)
                        k2=k2+1;
                        dcellsgaps(k1,k2)=j;
                        fprintf(fid,'%6.0f\t',j);
                    otherwise
                        continue
                end
            otherwise
                continue
        end
    end
    fprintf(fid,'\n');
    k1=k1+1;
end
fclose(fid);
save dcellsgaps.out dcellsgaps -ASCII
```

4. Range of capture, conductance and hydraulic radius

```
% This code calculates range of capture (a) for a determined particle
%size (d/D) in a determined gap width and then uses that value to
%calculate conductance times  length (gL or g*) and the hydraulic
%radius (rh)of the gap using the slit approximation. The range goes
%from the center of the gap to one end.

clear all
pack
load X.txt;
load Y.txt;
load Z.txt;
load dD.txt; % This file has the different particles sizes according to
%the range of widths considered
size(X)
size(Y)
size(Z)
size(dD)
wi=sparse(2000,1);
D=2;
alpha=15;
mu=1;
for i=1:4021
    Sphere(i).x=X(i);
    Sphere(i).y=Y(i);
    Sphere(i).z=Z(i);
end

for i=1:size(dD) %this is a column
    particle(i).dD=dD(i);
end
```

```
fid=fopen('aglrhsm.txt', 'w');
for i=1:2000
    for j=1:4021
        if i~=j && i<j
            W(i,j)=sqrt((Sphere(i).x-Sphere(j).x)^2+...
                (Sphere(i).y-Sphere(j).y)^2+...
                (Sphere(i).z-Sphere(j).z)^2)-2;

            % Select range of gaps widths here
            if  W(i,j)>=0.03 && W(i,j)<=0.1

                wi(i)=W(i,j);

                for k=1:size(dD)
                    a(i,k)=sqrt(dD(k)^2-(wi(i)/D)^2 + 2*(dD(k)-
wi(i)/D));
                    rh(i,k)= wi(i)/2;
                    gL(i,k)=wi(i)^3*a(i,k)/(6*mu);
                    fprintf(fid,'%6.6f\t', a(i,k));
                    fprintf(fid,'%6.10f\t',gL(i,k));
                    fprintf(fid,'%6.10f\t',rh(i,k));
                end
                fprintf(fid,'\n');
            end
        end
    end
end
fclose(fid);
```

5. Sphere simulation

```
function spheresim (x,y,z,r)

theta = pi*(-24:1:24)/24;
phi = pi*(0:1:24)'/24;
X=x+r*sin(phi)*cos(theta);
Y=y+r*sin(phi)*sin(theta);
Z=z+r*cos(phi)*ones(size(theta));

mesh(X,Y,Z);
hold on
COLORMAP([0,0,1]);
ALPHA('clear');
%ALPHA('color');
axis equal;
```

6. Translation

```
%This code translates the center coordinates of the Delaunay cells to
%make one of them pass through (0,0,0). Then the plane passes through
%the origin
%Center coordinates are: xc, yc, zc
%Translated coordinates are: xct, yct, zct

load coordinates.out; %This file has, for every gap, the cells that
contain that gap followed by its center coordinates
size (coordinates)

%c1= coordinates (:,1);    c5= coordinates (:,17);    c9= coordinates
(:,33);
xc1= coordinates (:,2);   xc5= coordinates (:,18);   xc9= coordinates
(:,34);
yc1= coordinates (:,3);   yc5= coordinates (:,19);   yc9= coordinates
(:,35);
zc1= coordinates (:,4);   zc5= coordinates (:,20);   zc9= coordinates
(:,36);

%c2= coordinates (:,5);    c6= coordinates (:,21);
xc2= coordinates (:,6);   xc6= coordinates (:,22);
yc2= coordinates (:,7);   yc6= coordinates (:,23);
zc2= coordinates (:,8);   zc6= coordinates (:,24);

%c3= coordinates(:,9);    c7= coordinates (:,25);
xc3= coordinates (:,10);  xc7= coordinates (:,26);
yc3= coordinates (:,11);  yc7= coordinates (:,27);
zc3= coordinates (:,12);  zc7= coordinates (:,28);

%c4= coordinates (:,13);   c8= coordinates (:,29);
xc4= coordinates (:,14);  xc8= coordinates (:,30);
yc4= coordinates (:,15);  yc8= coordinates (:,31);
zc4= coordinates (:,16);  zc8= coordinates (:,32);

%There are up to 9 Delaunay cells containing a certain gap.
tcoor=zeros(1449,27);


k1=1;
for i=1:size(coordinates)
    k2=0;

    xct1(i)= xc1(i)-xc1(i); yct1(i)= yc1(i)-yc1(i); zct1(i)= zc1(i)-
zc1(i);
    if (xct1(i)== -xc1(i) && yct1(i)==-yc1(i) && zct1(i)==-zc1(i))
        tcoor(k1,k2+1)=0; tcoor(k1,k2+2)=0; tcoor(k1,k2+3)=0;
```

```
    else
        tcoor(k1,k2+1)=xct1(i); tcoor(k1,k2+2)=yct1(i);
tcoor(k1,k2+3)=zct1(i);
    end

    xct2(i)=xc2(i)-xc1(i);  yct2(i)= yc2(i)-yc1(i); zct2(i)= zc2(i)-
zc1(i);
    if (xct2(i)== -xc1(i) && yct2(i)==-yc1(i) && zct2(i)==-zc1(i))
        tcoor(k1,k2+4)=0; tcoor(k1,k2+5)=0; tcoor(k1,k2+6)=0;
    else
        tcoor(k1,k2+4)=xct2(i); tcoor(k1,k2+5)=yct2(i);
tcoor(k1,k2+6)=zct2(i);
    end

    xct3(i)=xc3(i)-xc1(i);  yct3(i)= yc3(i)-yc1(i); zct3(i)= zc3(i)-
zc1(i);
    if (xct3(i)== -xc1(i) && yct3(i)==-yc1(i) && zct3(i)==-zc1(i))
        tcoor(k1,k2+7)=0; tcoor(k1,k2+8)=0; tcoor(k1,k2+9)=0;
    else
        tcoor(k1,k2+7)=xct3(i); tcoor(k1,k2+8)=yct3(i);
tcoor(k1,k2+9)=zct3(i);
    end

    xct4(i)=xc4(i)-xc1(i);  yct4(i)= yc4(i)-yc1(i); zct4(i)= zc4(i)-
zc1(i);
    if (xct4(i)== -xc1(i) && yct4(i)==-yc1(i) && zct4(i)==-zc1(i))
        tcoor(k1,k2+10)=0; tcoor(k1,k2+11)=0; tcoor(k1,k2+12)=0;
    else
        tcoor(k1,k2+10)=xct4(i); tcoor(k1,k2+11)=yct4(i);
tcoor(k1,k2+12)=zct4(i);
    end

    xct5(i)=xc5(i)-xc1(i);  yct5(i)= yc5(i)-yc1(i); zct5(i)= zc5(i)-
zc1(i);
    if (xct5(i)== -xc1(i) && yct5(i)==-yc1(i) && zct5(i)==-zc1(i))
        tcoor(k1,k2+13)=0; tcoor(k1,k2+14)=0; tcoor(k1,k2+15)=0;
    else
        tcoor(k1,k2+13)=xct5(i); tcoor(k1,k2+14)=yct5(i);
tcoor(k1,k2+15)=zct5(i);
    end

    xct6(i)=xc6(i)-xc1(i);  yct6(i)= yc6(i)-yc1(i); zct6(i)= zc6(i)-
zc1(i);
    if (xct6(i)== -xc1(i) && yct6(i)==-yc1(i) && zct6(i)==-zc1(i))
        tcoor(k1,k2+16)=0; tcoor(k1,k2+17)=0; tcoor(k1,k2+18)=0;
    else
        tcoor(k1,k2+16)=xct6(i); tcoor(k1,k2+17)=yct6(i);
tcoor(k1,k2+18)=zct6(i);
    end
```

```
    xct7(i)=xc7(i)-xc1(i);  yct7(i)= yc7(i)-yc1(i); zct7(i)= zc7(i)-
zc1(i);
    if (xct7(i)== -xc1(i) && yct7(i)==-yc1(i) && zct7(i)==-zc1(i))
        tcoor(k1,k2+19)=0; tcoor(k1,k2+20)=0; tcoor(k1,k2+21)=0;
    else
        tcoor(k1,k2+19)=xct7(i); tcoor(k1,k2+20)=yct7(i);
tcoor(k1,k2+21)=zct7(i);
    end

    xct8(i)=xc8(i)-xc1(i);  yct8(i)= yc8(i)-yc1(i); zct8(i)= zc8(i)-
zc1(i);
    if (xct8(i)== -xc1(i) && yct8(i)==-yc1(i) && zct8(i)==-zc1(i))
        tcoor(k1,k2+22)=0; tcoor(k1,k2+23)=0; tcoor(k1,k2+24)=0;
    else
        tcoor(k1,k2+22)=xct8(i); tcoor(k1,k2+23)=yct8(i);
tcoor(k1,k2+24)=zct8(i);
    end

    xct9(i)=xc9(i)-xc1(i);  yct9(i)= yc9(i)-yc1(i); zct9(i)= zc9(i)-
zc1(i);
    if (xct9(i)== -xc1(i) && yct9(i)==-yc1(i) && zct9(i)==-zc1(i))
        tcoor(k1,k2+25)=0; tcoor(k1,k2+26)=0; tcoor(k1,k2+27)=0;
    else
        tcoor(k1,k2+25)=xct9(i); tcoor(k1,k2+26)=yct9(i);
tcoor(k1,k2+27)=zct9(i);
    end

k1=k1+1;
end
save tcoor.out tcoor -ASCII
```

7. Equation of a plane

```
%This code calculates the equations of the planes that pass through the
%center of 5, 6... neighboring Delaunay cells. Since the center
%coordinates have been translated to pass through the origin, the term
% "D" in the plane equation is going to be zero.

load tcoor.out; % Translated coordinates. It's the output of
translation.m

size (tcoor)

% xct1, yct1 & zct1 are zero
xct1=tcoor(:,1);  yct1=tcoor(:,2);  zct1=tcoor(:,3);
xct2=tcoor(:,4);  yct2=tcoor(:,5);  zct2=tcoor(:,6);
xct3=tcoor(:,7);  yct3=tcoor(:,8);  zct3=tcoor(:,9);
xct4=tcoor(:,10); yct4=tcoor(:,11); zct4=tcoor(:,12);
xct5=tcoor(:,13); yct5=tcoor(:,14); zct5=tcoor(:,15);
xct6=tcoor(:,16); yct6=tcoor(:,17); zct6=tcoor(:,18);
```

```
xct7=tcoor(:,19); yct7=tcoor(:,20); zct7=tcoor(:,21);
xct8=tcoor(:,22); yct8=tcoor(:,23); zct8=tcoor(:,24);
xct9=tcoor(:,25); yct9=tcoor(:,26); zct9=tcoor(:,27);


fid=fopen('abc.txt', 'w');

for i=1:size(tcoor)
    %fprintf(fid,'%6.0f\t',i);
    ex=[xct2(i); xct3(i); xct4(i); xct5(i); xct6(i); xct7(i); xct8(i);
xct9(i)];
    wy=[yct2(i); yct3(i); yct4(i); yct5(i); yct6(i); yct7(i); yct8(i);
yct9(i)];
    zed=[zct2(i); zct3(i); zct4(i); zct5(i); zct6(i); zct7(i); zct8(i);
zct9(i)];
    A=[ex(:) wy(:) ones(length(ex(:)), 1)];
    c=A\zed(:);
    fprintf(fid,'%6.6f\t',c);
    fprintf(fid,'\n');
end
fclose(fid);
```

8. Rotation around z axis

```
% This code performs the rotation of the planes that make the
%intersection of the planes with the plane z=0 to coincide with the x
%axis of coordinates. After this rotation the plane need to be rotated
%around z axis to make it coincide with the plane Z=0.

load abc.txt; %This  is the output of "planes.m"
load tcoor.out;

size(abc)
size (tcoor)

a=abc(:,1);  % Z = aX + bY
b=abc(:,2);
% d=coefs(:,3); ,
% Coefficient "d" is zero because planes pass through the origin

xct1=tcoor(:,1);  yct1=tcoor(:,2);  zct1=tcoor(:,3);
xct2=tcoor(:,4);  yct2=tcoor(:,5);  zct2=tcoor(:,6);
xct3=tcoor(:,7);  yct3=tcoor(:,8);  zct3=tcoor(:,9);
xct4=tcoor(:,10); yct4=tcoor(:,11); zct4=tcoor(:,12);
xct5=tcoor(:,13); yct5=tcoor(:,14); zct5=tcoor(:,15);
xct6=tcoor(:,16); yct6=tcoor(:,17); zct6=tcoor(:,18);
xct7=tcoor(:,19); yct7=tcoor(:,20); zct7=tcoor(:,21);
xct8=tcoor(:,22); yct8=tcoor(:,23); zct8=tcoor(:,24);
xct9=tcoor(:,25); yct9=tcoor(:,26); zct9=tcoor(:,27);
```

```
fid=fopen('zcoor.txt', 'w');

for i=1:1449
    switch (a(i) && b(i))
        case (a(i)>0 && b(i)>0)
            zeta(i) = atan(a(i)/b(i));
        case (a(i)<0 && b(i)<0)
            zeta(i) = atan(a(i)/b(i));
        case (a(i)>0 && b(i)<0)
            zeta(i) = -0.5*pi-atan(b(i)/a(i));
        case (a(i)<0 && b(i)>0)
            zeta(i) = -0.5*pi-atan(b(i)/a(i));
        otherwise
            continue
    end

    %Translated vector

    u=[ xct1(i) xct2(i) xct3(i) xct4(i) xct5(i) xct6(i) xct7(i) xct8(i)
xct9(i);
        yct1(i) yct2(i) yct3(i) yct4(i) yct5(i) yct6(i) yct7(i) yct8(i)
yct9(i);
        zct1(i) zct2(i) zct3(i) zct4(i) zct5(i) zct6(i) zct7(i) zct8(i)
zct9(i)];

    % Rotation around axis "z". z coordinate will not change

    Rz = [ cos(zeta(i)) -sin(zeta(i))  0;
          sin(zeta(i))  cos(zeta(i))  0;
           0  0  1 ];

    % Vector 'u' rotated
    v = Rz*u;

    fprintf(fid,'%6.6f\t',v);
    fprintf(fid,'\n');
end
fclose(fid);
```

(The code that calculate the planes is run again with the new coordinates)

9. Rotation around x axis

```
% This code performs the second rotation of the planes that make the
%centers of the Delaunay cells once they have been translated to pass
%through(0,0,0).
% After this rotation the plane will coincide with the plane Z=0. The
% coordinate "z" will be zero in every vector.
```

```
load abcx.txt; %This  is the output of "planesz.m"
load zcoor.txt; % This are the coordinates after rotation around "z"
load pressures.out;

size(abcx) % Z = aX + bY
size (zcoor)
size(pressures)

a=abcx(:,1);
b=abcx(:,2);
% d=coefsx(:,3); ,
% Coefficient "d" is zero because planes pass through the origin

xz1=zcoor(:,1);   yz1=zcoor(:,2);    zz1=zcoor(:,3);
p1=pressures(:,1);
xz2=zcoor(:,4);   yz2=zcoor(:,5);    zz2=zcoor(:,6);
p2=pressures(:,2);
xz3=zcoor(:,7);   yz3=zcoor(:,8);    zz3=zcoor(:,9);
p3=pressures(:,3);
xz4=zcoor(:,10);  yz4=zcoor(:,11);  zz4=zcoor(:,12);
p4=pressures(:,4);
xz5=zcoor(:,13);  yz5=zcoor(:,14);  zz5=zcoor(:,15);
p5=pressures(:,5);
xz6=zcoor(:,16);  yz6=zcoor(:,17);  zz6=zcoor(:,18);
p6=pressures(:,6);
xz7=zcoor(:,19);  yz7=zcoor(:,20);  zz7=zcoor(:,21);
p7=pressures(:,7);
xz8=zcoor(:,22);  yz8=zcoor(:,23);  zz8=zcoor(:,24);
p8=pressures(:,8);
xz9=zcoor(:,25);  yz9=zcoor(:,26);  zz9=zcoor(:,27);
p9=pressures(:,9);

fid=fopen('vp_rotated.txt', 'w');

for i=1:1449
    %fprintf(fid,'%6.0f\t',i);

    alpha(i)=atan(-b(i));

    %Translated vector plus pressures

    u=[ xz1(i) xz2(i) xz3(i) xz4(i) xz5(i) xz6(i) xz7(i) xz8(i) xz9(i);
        yz1(i) yz2(i) yz3(i) yz4(i) yz5(i) yz6(i) yz7(i) yz8(i) yz9(i);
        zz1(i) zz2(i) zz3(i) zz4(i) zz5(i) zz6(i) zz7(i) zz8(i) zz9(i);
        p1(i)  p2(i)  p3(i)  p4(i)  p5(i)  p6(i)  p7(i)  p8(i)  p9(i)];

    % Rotation around axis "x" and printing pressure after every set of
    % coordinates
      Rx = [ 1  0  0  0;
             0  cos(alpha(i))  -sin(alpha(i)) 0;
```

```
            0      sin(alpha(i))  cos(alpha(i)) 0;
            0 0 0 1;];

    % Vector 'u' rotated
    v = Rx*u;

    fprintf(fid,'%6.6f\t',v);
    fprintf(fid,'\n');
end
fclose(fid);
```

10. Rotation, picture

```
figure
x=-2:0.1:2;
y=x;
[X Y]=meshgrid (x,y);
a=1.706;
b=0.171;
Z=(X.*a+Y.*b); % Plane equation Ax+By+ZC=0

surf (X, Y, Z)
colormap([0 0 1])
hidden off
h=surf (X, Y, Z); % Define object h
%shading flat
%beta=67.77
%rotate (h, [0 1 0], beta, [0 0 0]) % rotation around Y axis
zeta=84.3;
rotate (h, [0 0 1], zeta, [0 0 0]) % rotation around Z axis
alpha=-59.7;
rotate (h, [1 0 0], alpha, [0 0 0]) % rotation around X axis

hold on
% plot coordinates axis
x1=[-4,4]; y1=[0,0]; z1=[0,0];
plot3(x1,y1,z1, '+')
hold on
x2=[0,0]; y2=[-5,5]; z2=[0,0];
plot3(x2,y2,z2, '+')
hold on
x3=[0,0]; y3=[0,0]; z3=[-4,4];
plot3(x3,y3,z3, '+')
xlabel ('X')
ylabel ('Y')
zlabel ('Z')
hold off
```

11. Pressure in neighboring cells

```
% This code prints for the Delaunay cells containing a gap,
%the pressure in the center

load datap.txt;
load spheres.txt;
load widths.txt;

s1= datap (:,1);s2= datap (:,2);s3= datap (:,3);s4= datap (:,4);
p= datap(:,5);

s= spheres (:,1);
x= spheres (:,2);y= spheres (:,3);z= spheres (:,4);

s5= widths (:,1);
s6= widths (:,5);
w = widths (:,9);

size (datap)
size (spheres)
size (widths)
pressures=zeros(1449,9);

k1=1;
for i=1:1449  % every gap between
    k2=0;
    for j=1:14871  % delaunay cells
        switch s5(i)
            case s1(j)
                switch s6(i)
                    case s2(j)
                        k2=k2+1;
                        pressures(k1,k2)=p(j);
                    case s3(j)
                        k2=k2+1;
                        pressures(k1,k2)=p(j);
                    case s4(j)
                        k2=k2+1;
                        pressures(k1,k2)=p(j);
                    otherwise
                        continue
                end
            case(s2(j))
                switch s6(i)
                    case s1(j)
                        k2=k2+1;
```

```
                    pressures(k1,k2)=p(j);
                case s3(j)
                    k2=k2+1;
                    pressures(k1,k2)=p(j);
                case s4(j)
                    k2=k2+1;
                    pressures(k1,k2)=p(j);
                otherwise
                    continue
            end
        case s3(j)
            switch (s6(i))
                case s1(j)
                    k2=k2+1;
                    pressures(k1,k2)=p(j);
                case s2(j)
                    k2=k2+1;
                    pressures(k1,k2)=p(j);
                case s4(j)
                    k2=k2+1;
                    pressures(k1,k2)=p(j);
                otherwise
                    continue
            end
        case s4(j)
            switch (s6(i))
                case s1(j)
                    k2=k2+1;
                    pressures(k1,k2)=p(j);
                case s2(j)
                    k2=k2+1;
                    pressures(k1,k2)=p(j);
                case s3(j)
                    k2=k2+1;
                    pressures(k1,k2)=p(j);
                otherwise
                    continue
            end
        otherwise
            continue
    end
end
    k1=k1+1;
end
save pressures.out pressures -ASCII
```

12. Pressure gradient

```
load abcp.txt %coefs a and b from the equation P=ax+by+c
size (abcp)
a=abcp(:,1);
```

```
b=abcp(:,2);
c=abcp(:,3);


fid=fopen('gradp.txt', 'w');
for i=1:size(abcp)
    %fprintf(fid,'%6.0f\t',i);
    %modulus of grad_p
    grad_P(i)= sqrt(a(i)^2+b(i)^2);
    fprintf(fid,'%6.6f\t',grad_P(i));
    fprintf(fid,'\n');
end
fclose(fid);
```

13. Pressure contours, picture

```
figure
x=[0    0.2314  0.5438  0.8461  1.1341  1.5128];
y=[0    -1.1717 0.453   -1.419  0.4593  -0.1323];
p=[1.104094 1.105602    1.098336    1.101616    1.087927    1.083915];

[X, Y]= meshgrid(linspace(min(x), max(x),40), linspace(min(y), max(y),
40));
P=griddata(x, y, p, X, Y, 'cubic');
%mesh(X, Y, P);
hold on;
plot3(x, y, p, '.','markersize',10);
xlabel('x'); ylabel('y'); zlabel('Pressure = f(x,y)');
%contour3 (P,30)
%[c,h] = contour(X,Y,P);
contour3 (X, Y, P, 50)
hold on
%plot gap center
plot (0.7211, -0.4623,'+')
```

14. Velocity and flow in gaps

```
% This code calculates velocity and flow in gaps for Rh calculated with
% the slit approximation
% It depends on d/D
clear all
% load aglrh.txt;
load aglrhsm.txt;
load gradp.txt;
load widths.txt;
load distances.txt;

size(aglrhsm)
```

```
size(gradp)
size(widths)
size(distances)

a20=aglrhsm(:,1);
a25=aglrhsm(:,4);
a30=aglrhsm(:,7);
a35=aglrhsm(:,10);
a40=aglrhsm(:,13);
a45=aglrhsm(:,16);
a50=aglrhsm(:,19);

rhs=aglrhsm(:,3);
gp=gradp(:,1);
w=widths(:,9);
dis=distances(:,1);

u=zeros(1449,1);
q20=zeros(1449,1);q25=zeros(1449,1);q30=zeros(1449,1);q35=zeros(1449,1)
;q40=zeros(1449,1);q45=zeros(1449,1);q50=zeros(1449,1);

fid=fopen('velocityandflowsm.txt', 'w');

for i=1:size(aglrhsm)

    %fprintf(fid,'%6.0f\t',i);

    u(i)=rhs(i)^2*gp(i)/3;

    q20(i)=2*u(i)*a20(i)*w(i);q25(i)=2*u(i)*a25(i)*w(i);
    q30(i)=2*u(i)*a30(i)*w(i);q35(i)=2*u(i)*a35(i)*w(i);
    q40(i)=2*u(i)*a40(i)*w(i);q45(i)=2*u(i)*a45(i)*w(i);
    q50(i)=2*u(i)*a50(i)*w(i);

    fprintf(fid,'%6.10f\t',dis(i));
    fprintf(fid,'%6.10f\t',w(i));
    fprintf(fid,'%6.10f\t',u (i));
    fprintf(fid,'%6.10f\t',q20(i));
    fprintf(fid,'%6.10f\t',q25(i));
    fprintf(fid,'%6.10f\t',q30(i));
    fprintf(fid,'%6.10f\t',q35(i));
    fprintf(fid,'%6.10f\t',q40(i));
    fprintf(fid,'%6.10f\t',q45(i));
    fprintf(fid,'%6.10f\t',q50(i));
    fprintf(fid,'\n');
end
fclose(fid);


figure(5)
```

```
semilogy(dis,q40,'or')
title('d/D=0.040');
xlabel('DISTANCE FROM THE CENTER');
ylabel('VOLUMETRIC FLOW RATE');

figure(7)
semilogy(dis,q50,'*k')
title('d/D=0.050');
xlabel('DISTANCE FROM THE CENTER');
ylabel('VOLUMETRIC FLOW RATE');
```

15. Unique throats

```
  %This code sorts the data for the Delaunay cells, neighbors, flows
%and radius  of the throats for the unique throats
clear all
load topor.txt;
load flowsthroats.txt;
load data.txt;
size(data)
size(topor)
size(flowsthroats)

n1=topor(:,1);n2=topor(:,2);n3=topor(:,3);n4=topor(:,4);
r1=topor(:,5);r2=topor(:,6);r3=topor(:,7);r4=topor(:,8);
f1=flowsthroats(:,1);f2=flowsthroats(:,2);f3=flowsthroats(:,3);
f4=flowsthroats(:,4);

x=data(:,5);
y=data(:,6);
z=data(:,7);

fid=fopen('uniquethroats.txt','w');
for i=1:14871
    if n1(i)> i
    fprintf(fid,'%6.0f\t', i);
    fprintf(fid,'%6.0f\t', n1(i));
    fprintf(fid,'%6.10f\t', f1(i));
    fprintf(fid,'%6.6f\t', r1(i));

d(i)=sqrt((0.5*(x(i)+x(n1(i))))^2+(0.5*(y(i)+y(n1(i))))^2+(0.5*(z(i)+z(
n1(i))))^2);
    fprintf(fid,'%6.6f\t', d(i));
    fprintf(fid,'\n');
    else
    end
    if  n2(i)> i
    fprintf(fid,'%6.0f\t', i);
    fprintf(fid,'%6.0f\t', n2(i));
    fprintf(fid,'%6.10f\t', f2(i));
    fprintf(fid,'%6.6f\t', r2(i));
```

```
d(i)=sqrt((0.5*(x(i)+x(n2(i))))^2+(0.5*(y(i)+y(n2(i))))^2+(0.5*(z(i)+z(
n2(i))))^2);
    fprintf(fid,'%6.6f\t', d(i));
    fprintf(fid,'\n');
    else
    end
    if n3(i)> i
    fprintf(fid,'%6.0f\t', i);
    fprintf(fid,'%6.0f\t', n3(i));
    fprintf(fid,'%6.10f\t', f3(i));
    fprintf(fid,'%6.6f\t', r3(i));

d(i)=sqrt((0.5*(x(i)+x(n3(i))))^2+(0.5*(y(i)+y(n3(i))))^2+(0.5*(z(i)+z(
n3(i))))^2);
    fprintf(fid,'%6.6f\t', d(i));
    fprintf(fid,'\n');
    else
    end
    if n4(i)> i
    fprintf(fid,'%6.0f\t', i);
    fprintf(fid,'%6.0f\t', n4(i));
    fprintf(fid,'%6.10f\t', f4(i));
    fprintf(fid,'%6.6f\t', r4(i));

d(i)=sqrt((0.5*(x(i)+x(n4(i))))^2+(0.5*(y(i)+y(n4(i))))^2+(0.5*(z(i)+z(
n4(i))))^2);
    fprintf(fid,'%6.6f\t', d(i));
    fprintf(fid,'\n');
    else
    end
end
fclose(fid);
```

16. Flow in pore throats

```
%This code calculates flows in pore throats (all), from the difference
in
%pressures between centers of Delaunay Cells and conductance. For every
%Delaunay cell there are 4 flows because every cell has 5 neighbors.
The
%absolute value is printed.

load topopg.txt;
size(topopg)
for i=1:14871
    n1=topopg(:,1);   %neighbor 1
    n2=topopg(:,2);   %neighbor 2
    n3=topopg(:,3);   %neighbor 3
    n4=topopg(:,4);   %neighbor 4
    pc=topopg(:,5);   %pressure in the center of the cell
    g1=topopg(:,6);   %conductance between cell and n1
```

```
    g2=topopg(:,7);   %conductance between cell and n2
    g3=topopg(:,8);   %conductance between cell and n3
    g4=topopg(:,9);  %conductance between cell and n4
end
fid=fopen('flowsthroats.txt','w');
for i=1:14871
        p(i,1)=pc(n1(i));
        p(i,2)=pc(n2(i));
        p(i,3)=pc(n3(i));
        switch (n4(i))
            case (0)
        p(i,4)=0;
            otherwise
           p(i,4)=pc(n4(i));
        end
end

for i=1:14871
    delta_p(i,1)=p(i,1)-pc(i);
    delta_p(i,2)=p(i,2)-pc(i);
    delta_p(i,3)=p(i,3)-pc(i);
    delta_p(i,4)=p(i,4)-pc(i);
end
for i=1:14871
    q(i,1)=delta_p(i,1)*g1(i);
    fprintf(fid,'%6.10f\t',abs(q(i,1)));
    q(i,2)=delta_p(i,2)*g2(i);
    fprintf(fid,'%6.10f\t',abs(q(i,2)));
    q(i,3)=delta_p(i,3)*g3(i);
    fprintf(fid,'%6.10f\t',abs(q(i,3)));

    switch (p(i,4))
        case(0)
            q(i,4)=nan;
        otherwise
    q(i,4)=delta_p(i,4)*g4(i);
    end
    fprintf(fid,'%6.10f\t',abs(q(i,4)));
%     if(q(i,1)~=nan && q(i,2)~=nan && q(i,3)~=nan && q(i,4)~=nan);
%     sum(i)=q(i,1)+q(i,2)+q(i,3)+q(i,4);
%     fprintf(fid,'%6.10f\t',sum(i));
%     else
%     end
    fprintf(fid,'\n');
end
fclose(fid);
```

17. Average flow in bins

```
 % This code calculates the average flow (geometric mean) in bins of
% gap/throat radius. Example for one particle size
clear all
load datos % This file has radius , flow and bin information
check=[];
flow=data(:,2);
radius=data(:,1);
format long
average_rad=[];

for i=1:max(size(bins))
    a=bins(i,:);
    ind=find( radius<=a(2) & radius>= a(1));
    check=[check size(ind,1)*size(ind,2)];

    if (size(ind,1)*size(ind,2))~=0
        average_rad=[average_rad   mean(radius(ind))];
        average_flow=[average_flow geomean(flow(ind))];
    else
        average_rad=[average_rad   0.5*(a(1)+a(2))];
        average_flow=[average_flow 0];
    end
end
figure(1)
semilogy(average_rad,average_flow,'o');
xlabel('GAP/THROAT RADIUS');
ylabel('FLOW');
title ('d/D=0.0X');

avflow=(average_flow);
avrad=(average_rad);

save avflow2.out avflow -ASCII
save avrad2.out avrad -ASCII

%(multiply average flow by frequency next)
%(solve integral, cumtrapz,trapz)
```

Bibliography

1. Baghdikian, S.Y., M.M. Sharma, and L.L. Handy, Flow of clay suspensions through porous media, Paper SPE 16257, SPE Intl. Symp. Oilfield Chem., San Antonio, Feb, 4-6, 1989.

2. Bernal, J.D., and G. Mason, Packing of spheres, co-ordination of randomly packed spheres, *Nature*, 188, p910, 1960.

3. Bhattacharjee, S., J. Ryan, and M. Elimelech, Virus transport in physically and geochemically heterogeneous subsurface porous media, *Journal of Contaminant Hydrology*, **57**, 161-187, 2002.

4. Bird, R., W. Steward, and E. Lightfoot, Transport Phenomena, Wiley and Sons, New York, 1960.

5. Bitton, G., and R.W. Harvey, Transport of pathogens through soil, *in* New Concepts in Environmental Microbiology, edited by R. Mitchell, 103-104, John Wiley, New York, 1992.

6. Bradford, S., and M. Bettahar, Concentration dependent transport of colloids in saturated porous media, *Journal of Contaminant Hydrology*, 82, 99-117, 2006.

7. Bradford, S., M. Bettahar, J. Simunek, and M.T Van Genutchen, Straining and attachment of colloids in physically heterogeneous porous media, *Vadose Zone Journal*, 3, 384-394, 2004.

8. Bradford, S., J. Simunek, M. Bettahar, M.T. Van Genutchen, and S. Yates, Modeling colloid attachment, straining and exclusion in saturated porous media, *Environmental Science and Technology,* 37, 2242-2250, 2003.

9. Bradford, S., S. Yates, M. Bettahar, and J. Simunek, Physical factors affecting the transport and fate of colloids in saturated porous media, *Water Resources Research*, 38(12), 1327, paper 63, 2002.

10. Bryant, S., and M. Blunt, Prediction of relative permeability in simple porous media, *Physical Review A*, 46(4), 2004-2011, 1992.

11. Bryant, S., and A. Johnson, Wetting phase connectivity and irreducible saturation in simple granular media, *Journal of Colloid and Interface Science*, 263(2), 572-579, 2003.

12. Bryant, S., P.R. King, and D.W. Mellor, Network model evaluation of permeability and spatial correlation in a real random sphere packing, *Transport in Porous Media*, 11, 53-70, 1993a.

13. Bryant, S., D.W. Mellor, and C. Cade, Physically representative network models of transport in porous media, *AIChE Journal*, 39(3), 387-396, 1993b.

14. Burganos, V.N. and S.V. Sotirchos, Diffusion in Pore Networks: Effective medium theory and smooth field approximation, *AIChE Journal*, 33(10), 1678-1689, 1987.

15. Cargill, G, Radial distribution functions and microgeometry of dense random packings of hard spheres, *in* Physics and Chemistry of Porous Media, AIP Conf. Proc. No 107, D. Johnson and P. Sen, eds., American Institute of Physics, New York, pp. 20-36, 1984.

16. Davis, A., M. O'Neill, J. Dorrepal, and K. Ranger, Separation from the surface of two equal spheres in Stokes flow, *Journal of Fluid Mechanics* 77(4), 625-644, 1976.

17. Elimelech, M., Effect of particle size on the kinetics of particle deposition under attractive double-layer interactions, *Journal of Colloid and Interface Science*, 164(1), 190-199, 1994.

18. Elimelech, M., and C.R. O'Melia, Kinetics of deposition of colloidal particles in porous media, *Environmental Science and Technology,* 24, 1528-1536, 1990.

19. Finney, J., Random packings and the structure of simple liquids. I. The geometry of random close packing, *Proceedings of The Royal Society of London. Series A. Mathematical, Physical and Engineering Sciences*, 319, 479-493, 1970.

20. Fontes, D. E., A.L. Mills, G.M. Hornberger, and J.S. Herman, Physicall and chemical factors influencing transport of microorganisms through porous media. *Applied and Environmental Microbiology*, 57(9), 2473-2481, 1991.

21. Foppen, J.W.A., A. Mporokoso, and J.F. Schijven, Determining straining of *Escherichia coli* from breakthrough curves, *Journal of Contaminant Hydrology*, 76, 191-210 2005.

22. Gao, B., J.E. Saiers, and J. Ryan, Pore-scale mechanisms of colloid deposition and mobilization during steady and transient flow through unsaturated granular media, *Water Resources Research*, 42, W01410, 2006.

23. Geilikman, M.B., D.E. Dria, and D.R. Stewart, Bean-up guidelines for Sand-Control completions. Paper SPE 95870, SPE ATCE, Dallas, Oct, 9-12, 2005.

24. Gruesbeck, C. and R.E. Collins, Entrainment and deposition of fine particles in porous media, *Society of Petroleum Engineering Journal*, 847-856, 1982.

25. Gschwend, P.M., and M.D.J. Reynolds, Monodispersed ferrous phosphate colloids in an anoxic groundwater plume, *Journal of Contaminant Hydrology*, 1, 309-327, 1987.

26. Hall, W.A., An analysis of sand filtration, *Proceedings, American Society of Civil Engineers (Sanitary Engineering Division)*, SA3, paper 1276, 1-9, 1957.

27. Harris, J.W., and H. Sotcker, Handbook of Mathematics and Computational Science. Springer, New York, 1998.

28. Herzig, J.P., D.M. Leclerc, and P. Le Goff. Flow of suspensions through porous media-application to deep filtration. *Industrial and Engineering Chemistry*, 62(5), 8-35, 1970.

29. Khilar, K.C., and H.S. Fogler, Migration of fines in porous media. Kluwer Academic, Dordrecht, 1998.

30. Khilar, K.C., H.S. Fogler, and J.S. Ahluwalia, Sandstone water sensitivity: Existence of a critical rate of salinity decrease for particle capture, *Chemical Engineering Science*, 38(5), 789-800, 1983.

31. Kim, J.I., Actinide colloid generation in groundwater, *Radiochimica Acta*, 52/53, 71-81, 1991.

32. Kitanidis, P. and B. Dykaar. Stokes flow in a slowly varying two-dimensional periodic pore. *Transport in Porous Media*, 26, 89-98, 1997.

33. Logan, B.E., D. G. Jewett, R.G. Arnold, E. J. Bower, and C.R. O'Melia. Clarification of clean-bed filtration models. *Journal of Environmental Engineering*, 121(12), 869-873, 1995.

34. MacLeod, F.A., H.M. Lappin-Scott, and J.W. Costerton, Plugging of a model rock system by using starved bacteria. *Applied and Environmental Microbiology*, 54, 1365-1372, 1988.

35. Magee, B.R., L.W. Leon, and A.T. Lemley. Transport of dissolved organic macromolecule and their effect in the transport of Phenanthrene in porous media. *Environmental Science and Technology*, 25, 323, 1991.

36. Marlow, H.J., K.L. Duston, M.R. Wiesner, M.B.Tomson, J.T. Wilson and C.H. Ward, Microbial transport through porous media: The effects of hydraulic conductivity and injection velocity. *Journal of Hazardous Materials*, 28, 65-74, 1991.

37. Matthess, G., and A. Pekdeger, Survival and transport of pathogenic bacteria and viruses in ground water, in Ground Water Quality, Ward, C.H., Giger, W., McCarty, P., eds., John Wiley, New York, pp. 472-482, 1985.

38. McCarthy, J.F., and J.M. Zachara, Subsurface transport of contaminants. *Environmental Science and Technology,* 23(5), 496-502, 1989.

39. Mellor, D., Random close packing (RCP) of equal spheres: structure and implications for use as a model porous medium, PhD thesis, Open University, Milton Keynes, UK, 1989.

40. Rose, W., Volumes and surface areas of pendular rings, *Journal of Applied Physics*, 29 (4), 687-691, 1958.

41. Ryan, J.N., and M. Elimelech, Colloid mobilization and transport in groundwater, *Colloids and Surfaces A: Physicochemical and Engineering aspects*, 107, 1-56, 1996.

42. Ryan, J.N., and P.M. Gschwend, Colloid mobilization into two Atlantic coastal plan aquifers: Field studies, *Water Resources Research*, 26, 307-322, 1990.

43. Ryan, J.N., and P.M. Gschwend, Effects of ionic strength and flow rate on colloid release: Relating kinetics to intersurface potential energy, *Journal of Colloid and Interface Science*, 164(1), 21-34, 1994.

44. Sharma M.M., and Y.C. Yortsos, Transport of particulate suspensions in porous media: Model formulation, *AIChE Journal*, 33(10), 1636-1643, 1987a.

45. Sharma M.M., and Y.C. Yortsos, A network model for deep bed filtration processes, *AIChE Journal*, 33(10), 1644-1653, 1987b.

46. Sharma M.M., and Y.C. Yortsos, Fines migration in porous media, *AIChE Journal*, 33(10), 1654-1662, 1987b.

47. Schechter, R.S., Oil well stimulation, Prentice Hall, Englewood Cliffs, NJ, 1992.

48. Thane, C., Geometry and topology of model sediments and their influence in sediment properties, M.S. Thesis, The University of Texas at Austin, USA, 2006.

49. Tobiason, J.E., and C.R. O'Melia, Physicochemical aspects of particle removal in depth filtration, *Journal of the American Water Works Association*, 80, 54-64, 1988.

50. Tufenkji, N., G.F. Miller, J.N. Ryan, R.W. Harvey, and M. Elimelech, Transport of *Cryptosporidium* Oocysts in porous media: Role of straining and physicochemical filtration, *Environmental Science and Technology*, 38, 5932-5938, 2004.

51. Yao, K., M.T. Habibian, and C.R. O'Melia, Water and waste water filtration: Concept and applications, *Environmental Science and Technology*, 5(11), 1105-1112, 1971.

The vita has been removed from the reformatted version of this document.